Hot Corrosion of the B2 Nickel Aluminides

David L. Ellis
Case Western Reserve University
Cleveland, Ohio

March 1993

N/\S/
National Aeronautics and
Space Administration

Hot Corrosion of the B2 Nickel Aluminides

David L. Ellis
Case Western Reserve University
Cleveland, Ohio

March 1993

NASA
National Aeronautics and
Space Administration

Hot Corrosion of the B2 Nickel Aluminides

David L. Ellis
Case Western Reserve University
Cleveland, Ohio 44106

Abstract

The hot corrosion behavior of the B2 nickel aluminides was
studied to determine the inherent hot corrosion resistance of the
beta nickel aluminides and to develop a mechanism for the hot
corrosion of the beta nickel aluminides. The effects of the prior
processing of the material, small additions of zirconium,
stoichiometry of the materials, and preoxidation of the samples
were also examined. Additions of 2, 5, and 15 w/o chromium were
used to determine the effect of chromium on the hot corrosion of
the beta nickel aluminides and the minimum amount of chromium
necessary for good hot corrosion resistance.

The results indicate that the beta nickel aluminides have
inferior inherent hot corrosion resistance despite their excellent
oxidation resistance. Prior processing and zirconium additions had
no discernible effect on the hot corrosion resistance of the
alloys. Preoxidation extended the incubation period of the alloys
only a few hours and was not considered to be an effective means of
stopping hot corrosion. Stoichiometry was a major factor in
determining the hot corrosion resistance of the alloys with the
higher aluminum alloys having a definitely superior hot corrosion
resistance. The addition of chromium to the alloys stopped the hot
corrosion attack in the alloys tested.

From a variety of experimental results, a complex hot corrosion
mechanism was proposed. During the early stages of the hot
corrosion of these alloys the corrosion is dominated by a local

sulphidation/oxidation form of attack. During the intermediate
stages of the hot corrosion, the aluminum depletion at the surface
leads to a change in the oxidation mechanism from a protective
external alumina layer to a mixed nickel-aluminum spinel and nickel
oxide that can occur both externally and internally. The material
undergoes extensive cracking during the later portions of the hot
corrosion.

ACKNOWLEDGEMENTS

TABLE OF CONTENTS

viii

1 INTRODUCTION

Hot corrosion can be broadly defined as a form of accelerated attack at elevated temperatures in the presence of a condensed salt. Normally hot corrosion is more closely associated with the accelerated attack on gas turbine components in or near a marine environment due to the presence of condensed sodium sulphate deposits.

Hot corrosion can be particularly damaging because of its catastrophic nature. Parts are corroded in extremely short times to large extents. Over the years since the identification of hot corrosion as a major problem large outlays of time, man power, and money have been made to understand and stop hot corrosion. Methods have been found for stopping hot corrosion, but a true understanding of the hot corrosion process and mechanisms involved have not been achieved.

A prime use envisioned for the B2 nickel aluminides is gas turbine applications. As can be seen in Figure 1, the beta phase melt congruently at a high temperature. To address the possible problem of hot corrosion of beta nickel aluminides in a marine gas turbine system, this study was undertaken to gather basic data on the hot corrosion resistance of the B2 nickel aluminides and to determine the hot corrosion mechanism in the system for the test conditions. The roles of processing, stoichiometry, and third element additions were also investigated.

2 LITERATURE REVIEW

Hot corrosion was first described in 1945 (1) in high pressure steam boilers. Since then many studies have been made into the hot corrosion resistance of metals, hot corrosion mechanisms, and the roles of coating in stopping hot corrosion. The results are often indeterminate, contradictory, or not applicable to other systems. There are also problems with the reproducibility of the results. Nonetheless, the available literature does offer insights into the hot corrosion phenomena.

The literature review section is divided into five sections in an effort to better organize the available literature. In the first section some of the various proposed mechanisms will be presented. The major mechanisms will be discussed in detail with supporting and contradicting evidence presented for each mechanism. Since the method of testing the material has a major influence on the hot corrosion process and results, the second section will deal with the various hot corrosion test methods. The advantages, disadvantages, and relationship to the actual gas turbine environment for each test method will be discussed. The third section will deal with the work done with pure nickel and the superalloys. Since the superalloys have such a wide variation in chemistries, the superalloys as such will not be reviewed. Rather the role of the various major elements used for a base element or an alloying addition will be examined. The fourth section will deal with the problem of hot corrosion with respect to aluminide coatings. Finally, the fifth section will deal with the limited amount of work done prior to this study on the hot corrosion of the nickel aluminides.

2.1 HOT CORROSION MECHANISMS

Through the years many models for the hot corrosion mechanism

have been proposed. Several researchers have also sought to explain the roles of various elements in both the metal and the environment. One important and fundamental change has occurred since the original work was done on hot corrosion. The purity of the fuels has been significantly increased. Problem elements such as vanadium which promote their own forms of attack have been all but eliminated. As a result, several problems addressed by researchers prior to about 1960 no longer exist. Mechanisms that are based on conditions that include highly aggressive elements that have been removed from the present day systems will not be addressed here. It should be noted that with the increased interest in the use of lower grade fuels and the potential for the recurrence of these types of problems in coal gasification processes these models may become important again.

The major mechanisms proposed for hot corrosion can be described as either fluxing models or sulphidation models. Fluxing models are based on the assumption that the protective oxide layer is dissolved into the liquid salt and reprecipitates at the outer surface of the salt layer as a porous, nonprotective oxide layer. Fluxing models are generally subdivided into acidic and basic fluxing depending on the operative chemical reactions and the acidity/basicity of the liquid salt layer. Sulphidation models assume that sulphides are created in the metal by the diffusion of sulphur through the oxide layer which are then oxidized by oxygen diffusing through the oxide layer, resulting in a sustained sulphidation/oxidation type of attack.

Before investigating the hot corrosion mechanisms, it is useful to first determine which phases can be present given the alloy compositions and the oxygen and sulphur activities. Several investigators have used a presentation of the thermodynamic data similar to the Porbaix diagrams of aqueous corrosion based on some measure of the oxygen activity and the sulphur activity. Figure 2

presents a diagram for the sodium-oxygen-sulphur system. The results
for nickel, aluminum, chromium, and cobalt appear in Figures 3
through 6. Since temperature is a variable, the true presentation of
the figures is a three dimensional figure. Of the systems of
interest, only the nickel and cobalt diagrams were available. The
other diagrams presented are for specific temperatures.

In 1972 J. Stringer (2) did an extensive review of the various
proposed hot corrosion reactions, mechanisms, and research work. In
1980 Kawakami, Goto, and Rapp (3) updated Stringer's work. The
following sections draw heavily on the references of these two
papers.

2.1.1 SULPHIDATION MODELS OF HOT CORROSION

The sulphidation model is based on the observations of
sulphides in materials subject to hot corrosion, often immediately
ahead of the advancing corrosion interface. Figure 7 schematically
shows the sulphidation hot corrosion attack for a hypothetical high-
chromium nickel-based alloy as given by Sims (4). The steps to the
sulphidation model are as follows.

In the initial stage of sulphidation hot corrosion, the alloy
forms a protective oxide layer, predominately chromia, Cr_2O_3,
between the alloy and the salt. The oxide layer is enriched in
chromium due to the higher affinity of chromium for oxygen. The
underlying alloy is thus depleted to some extent in chromium. The
oxygen for the reaction to form the oxide layer is supplied by the
salt. If the rate of the use of oxygen for the growth of the oxide
layer exceeds the rate of diffusion of oxygen to the interface, a
chemical potential gradient is established in the salt. The gradient
for oxygen will have the maximum oxygen potential at the
salt/atmosphere interface while the minimum activity will be at the

salt/oxide interface. Since the salt is supplying the oxygen, the composition of the salt and hence the sulphur activity in the salt will also be changed according to the chemical equation

(1) $$SO_4^{2-} = S^{2-} + 2\ O_2$$

As the oxygen activity is decreased, the sulphur activity will increase. This leads to a high sulphur activity at the salt/oxide interface. These two potential gradients supply the driving forces for the transport of sulphur into the metal.

Eventually the protective oxide layer fails. Seybolt (5) has proposed that the reaction of the salt with the oxide layer forms double oxides with sodium, i.e. Na_2CrO_4. The sulphur released by the formation of these oxides diffuses inward into the metal where it reacts with the metal to form sulphides. The transport of the sulphur is accomplished either through the diffusion of sulphur through chromia or SO_2 through NiO. It has been shown that the diffusivities in both cases are high (6). In the case of the high chromium alloy assumed in this example, the sulphur reacts preferentially with the chromium to form CrS_x. Several forms of chromium sulphide are possible, and the exact stoichiometry is dependant on the sulphur and chromium activity levels, the temperature, and other internal and external factors. In other systems the sulphide may be aluminum sulphide, AlS_x, in aluminum rich alloys or nickel sulphide, NiS_x, in pure nickel or depleted nickel-based alloys. As with chromium, the nickel and aluminum can form a variety of sulphides with a wide variation in stoichiometry.

As the chromium is lost through the formation of the double oxides and sulphidation, the oxide layer changes to either a spinel, $NiCr_2O_4$, or a nickel oxide rich oxide layer. These layers are not as protective as the chromia layer, and the oxidation rate increases.

The diffusion of oxygen through the oxide layer also increases. Since the oxides of the metals are more stable than the sulphides, the sulphides are oxidized at low partial pressures of oxygen. The reaction liberates sulphur which is forced deeper into the material by the activity gradient. The sulphur again reacts with the metal to form sulphides which in turn are oxidized releasing sulphur. The process continues as long as oxygen can diffuse to the sulphides.

Eventually the sodium sulphate comes into direct contact with the metal as the oxide layer fails. The mechanism for the failure of the oxide layer can be one of several, but the fluxing mechanisms to be discussed in sections 2.2 and 2.3 are both highly probable causes. The intimate contact of the liquid salt and chromium depleted metal allows for the rapid transport of the external reactants to the reaction site and prevents the formation of an effective protective oxide layer. The depletion of the chromium near the interface aggravates the problem as a protective chromia layer can not be formed due to the low level of chromium available. Another problem caused by the chromium depletion is the possible formation of a liquid eutectic, either $Ni-Ni_2S_3$ or $NiO - NiS$, which would also tend to inhibit or stop the formation of a dense, protective oxide layer.

While sulphidation could theoretically continue until all the material is affected, the test results tend to indicate a leveling off of the rate of attack. This is taken to indicate that the porous oxide layer becomes so thick that the transport of oxygen is slowed by the tortuous path it must take. Also, the sodium sulphate may have been used up in supplying sulphur for the reaction so that the liquid phase that allows the rapid transport of the oxygen is no longer present.

Many examples are available in literature showing the presence

of sulphides in the metal beneath an oxide layer (7,8,9). These sulphides have been conclusively identified as the ones predicted by the sulphidation model, i.e. chromium sulphide in high-chromium alloys. It has also been shown that the sulphides can be present for thousands of hours without any accelerated attack of the material (10). From this it must be concluded that the presence of sulphides alone will not cause hot corrosion.

Other work has also shown contradictory evidence that sulphur may or may not be necessary for hot corrosion. Seybolt (11) showed in crucible tests that sodium carbonate, Na_2CO_3, does not promote hot corrosion. Likewise Hardt, Gambino, and Bergman (12) showed pure nickel coated with Na_2SO_4-$NaNO_2$ mixtures had slower oxidation rates compared to Na_2SO_4 coated nickel. Bornstein and DeCrescente (13) reported that coatings of Na_2CO_3 actually slowed the corrosion rate of pure nickel.

On the other hand, burner rig experiments using different sulphur levels in the fuels by Bergman (14) indicated that for two superalloys the attack at 1600°F was more severe at the 2 ppm sulphur level than the 88 ppm sulphur level. Bergman's work also showed that the four superalloys tested were corroded more at the 2 ppm sulphur level than the 88 ppm sulphur level at 1800°F. This is in direct contradiction to the expected result if the sulphidation hot corrosion mechanism was controlling the hot corrosion attack. With more sulphur available the attack should have been more widespread and severe. Bergman's work does point out that at least some sulphur may be needed as nearly sulphur free fuels showed little or no attack.

Work by Schirmer and Quigg (15) also indicated that the sulphur content of the fuel had little bearing on the hot corrosion of the specimens in burner rig tests. By varying the sulphur content in the

fuel from 0.0002% to 0.40% and the sodium chloride of the air from 0 to 10 ppm, the amount of sulphur and sodium sulphate were varied in a preselected manner. Five alloys; U-500, IN-713C, IN-100, SM-200, and MDC-1 coated IN-713; were tested. The results indicate no consistent change with the variation in sulphur and sodium chloride. This is in contrast to the expected consistent increase in the corrosion with the increase in sodium sulphate and sulphur predicted by the sulphidation theory.

Other work for the coal gasification systems indicates that in the conditions experienced in the coal gasification fluidized bed reactor, sodium carbonate, Na_2CO_3, can promote hot corrosion. The effect is, however, not as severe as the hot corrosion of the same materials under similar conditions with sodium sulphate present.

One other possibility for the role of sulphur in the sulphidation model must be considered. The various sulphur compounds either have low melting points or form low melting point eutectics with either oxides or the metal itself. If the sulphur is removed and another element is substituted, i.e. carbon, the melting points of the corresponding systems are higher. Thus a liquid phase that allows ready transport of reactants and products is removed from the system. The role of the sulphur may thus be providing a rapid transfer medium for the system.

2.1.2 FLUXING MODELS

The designation of basic and acidic fluxing comes from considering the sodium sulphate to be composed of a basic and an acidic component, namely Na_2O and SO_3. The sodium sulphate can disassociate according to the chemical equation

(2) $$Na_2SO_4 = Na_2O + SO_3$$
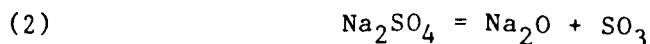
The salt can then become enriched in the acidic portion, SO_3, by a reaction that consumes the basic portion, Na_2O or actually the O^{2-} ion, and promote acidic fluxing, or the salt can become enriched in the basic portion by the consumption of the acidic portion, SO_3, and cause basic fluxing. The fluxing process involves the dissolution of the protective oxide layer at the salt/oxide interface and the reprecipitation of the oxide as a porous layer near the salt/atmosphere interface. Both models assume that there is an oxygen and sulphur gradient established in the salt as explained in the sulphidation model section. The assumption is also made that the oxide ion concentration has a gradient similar to the sulphur gradient, namely a high activity at the salt/oxide interface and a low activity at the salt/atmosphere interface. This assumption comes from the chemical equilibria associated with the chemical equations

$$(3) \qquad\qquad SO_4^{2-} = O^{2-} + SO_3$$

$$(4) \qquad\qquad SO_3 = SO_2 + 1/2\ O_2$$

which show that high oxygen activities decrease the oxide ion activity in the salt.

As the oxide ion concentration in the sulphate melt changes, the solubility of the oxides and the method by which the oxides are dissolved into the sulphate melt changes. This is shown in Figure 8. The solubility curves also point out another important consideration. Conditions that cause strong acidic fluxing for one oxide can be innocuous or cause strong basic fluxing for another oxide. This explains to some extent the observed differences in the response of alloys forming different oxide layers to similar environments. For fluxing to be a major cause of corrosion, the solubility of the oxide formed must be high under the conditions of

the test.

With this in mind, the major questions are how is the sodium sulphate layer changed by the oxidation/corrosion process and how do these changes affect the oxide layer.

2.1.2.1 BASIC FLUXING

Most of the ideas dealing with basic fluxing come from the work done by Goebel and Pettit (16). Figure 9 shows schematically the basic fluxing model they proposed for nickel. The sodium sulphate is present on the metal surface as a liquid layer. The sodium sulphate reacts with the metal so the oxygen activity is decreased and the oxide ion concentration increased at the metal/salt interface. The oxide ions react with the oxide layer to form a complex ion soluble in the liquid sodium sulphate layer, e.g. NiO_2^{2-} for NiO. The ions diffuse outward along the concentration gradient until the oxide ion activity falls below the equilibrium value needed for the complex ions to be stable. The complex ions decompose to form an oxide ion and an oxide precipitate. The oxide precipitates combine to form a porous oxide layer. The reactions continue until the protective oxide layer is breached.

When the oxide layer is compromised, the sulphur which has an increased activity near the metal/salt interface due to the oxidation reaction, reacts with the metal to form sulphides. This reaction sustains the high oxide concentration by consuming sulphur from the sulphate ions. This forces equation 3 to the right. Eventually all the sulphate is used up by the reaction, and the sulphidation reaction can no longer supply oxide ions. The oxide ion concentration at the salt/oxide interface decreases, and the fluxing reaction can no longer be sustained. The fluxing reaction ceases. Oxygen diffuses through the porous oxide layer and reacts with the

metal and sulphides to form a dense oxide layer beneath the porous oxide layer. The kinetics of the corrosion process are thus returned to those for simple oxidation.

The basic fluxing model has been demonstrated for several metals by the use of potentiostatic electrochemical measurements in sulphate melts (17,18). The depth of attack increased with decreasing potential for IN 738 and IN 939 exposed for 100 hours. This indicates an increased attack rate as the material is forced to a more basic chemistry by the applied voltage. It should be noted that basic fluxing was not initiated until an applied voltage of over -1000 mV relative to a standard silver electrode was applied. Less corrosion resistant alloys also showed a tendency for very large negative potentials for the onset of basic fluxing. IN 100 required a potential of approximately -1250 mV for a fifty hour exposure. The other easily corroded alloy cited, IN 713 exposed for 100 hours, showed two regions in the negative potential portion of the tests where accelerated attack occurred with increasing negative potential. The first occurred at approximately -600 mV and the second at approximately -1300 mV. It should be noted that corresponding voltages for acidic fluxing were normally between 0 and +100 mV. No data could be found for pure nickel specimens.

These measurements indicate that the oxide ion concentration for basic fluxing to occur must be rather high. It is therefore reasonable to assume that basic fluxing occurs under only local conditions due to a sudden increase in oxide ion activity or as a transient condition for the system, most likely during the initial formation of the oxide layer when the oxygen activity is being most rapidly reduced and more oxygen has not had time to diffuse to the salt/metal interface.

From the available data, the basic fluxing model does appear to

be reasonable. The potentiostatic electrochemical measurements do indicate that acidic fluxing which occurs at no or low applied potentials is a more likely occurrence.

2.1.2.2 ACIDIC FLUXING

Acidic Fluxing occurs when the acidic portion of the sodium sulphate melt increases for one of several reasons. The resulting acidic salt attacks the protective oxide layer by converting the oxides to soluble metal ions and oxide ions. The acidic fluxing mechanism is further subdivided into gas and alloy induced acidic fluxing depending on the source of the acidifying constituent. In both cases the basics of the mechanisms are the same.

2.1.2.2.1 GAS INDUCED ACIDIC FLUXING

As the name implies, the cause of the acidification of the sodium sulphate layer is taken from the atmosphere in which the material is operating. A schematic representation of this form of hot corrosion attack appears in Figure 10. The cause for the acidification is the diffusion of SO_3 from the atmosphere through the salt layer to the sulphate/oxide interface. There the oxide ion concentration is lowered by reaction of the SO_3 with the oxide ion as given in equation 3. The oxide is fluxed when the oxide ion concentration is lowered to the point where the reactions

$$(5) \qquad NiO = Ni^{2+} + O^{2-}$$
$$(6) \qquad Al_2O_3 = 2\ Al^{3+} + 3\ O^{2-}$$
$$(7) \qquad Cr_2O_3 = 2\ Cr^{3+} + 3\ O^{2-}$$
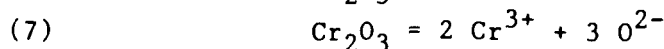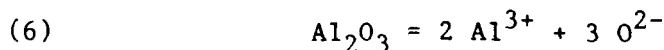
can proceed. The metal ions produced diffuse outward along the concentration gradient toward the sulphate/atmosphere interface. The oxide ion concentration increases as the ion diffuses outward until

the metal ion recombines with oxide ion(s) to precipitate a porous, non-protective oxide layer.

The primary problem with the gas induced acidic fluxing model is the requirement for the presence of SO_3 in the atmosphere. Experiments done by Kohl, Stearns, and Fryburg (19) showed that the mole fraction of SO_3 in a typical $CH_4-O_2-H_2O-NaCl-SO_2$ flame which is similar to the conditions in a gas turbine engine was 5×10^{-5}. With a typical gas engine operating at Mach 1, the residence time for this small amount of SO_3 would be approximately 5 milliseconds. Under these conditions the movement of large amount of SO_3 from the atmosphere to the oxide is unlikely in a gas turbine. Gas induced fluxing can be important in other systems where the gas is moving at a lower speed so that the gas is in contact with the sulphate for a longer time and/or the gas has a significantly higher mole fraction of SO_3. These conditions tend to be uncommon, and as a result gas induced acidic fluxing is not often encountered. The more common cause is alloy induced acidic fluxing.

2.1.2.2.2 ALLOY INDUCED ACIDIC FLUXING

Alloy induced acidic fluxing is caused by elements in the alloy reacting with the sodium sulphate to lower the oxide ion concentration near the oxide. A schematic representation of this form of attack appears in Figure 11. The lowered oxide ion concentration again causes the production of metal ions which diffuse outward as in the gas induced acidic fluxing model. The alloying elements that cause acidic fluxing are those whose oxides form basic complex ions. In most cases these are elements that have high partial pressures for their oxides, such as tungsten, molybdenum, and vanadium. Chromium can be volatilized at the typical operating temperatures for gas turbine engines, but there is no direct evidence for acidic fluxing by chromium and considerable

evidence that chromium stops hot corrosion. The need for oxygen to form the complex ion may play a role in the reduced hot corrosion of chromia former alloys.

The alloy induced fluxing mechanism occurs when the acidifying element is oxidized to form a portion of the oxide layer. The oxide reacts with the oxide ions in the sulphate layer by the chemical reactions

$$(8) \qquad MoO_3 + O^{2-} = MoO_4^{2-}$$
$$(9) \qquad WO_3 + O^{2-} = WO_4^{2-}$$
$$(10) \qquad V_2O_5 + O^{2-} = 2VO_3^{-}$$
$$(11) \qquad Cr_2O_3 + 2\ O^{2-} + 3/2\ O_2 = 2\ CrO_4^{2-}$$
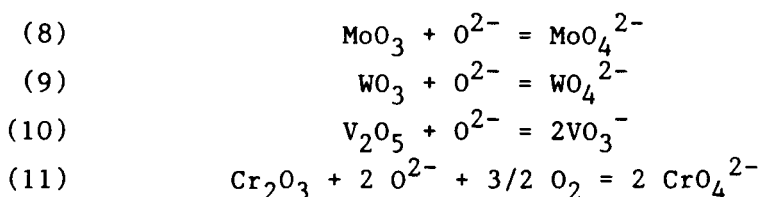
The complex ions diffuse outward due to the concentration gradient for the ions. The oxide is fluxed at the same time by the breakdown of the oxide into metal and oxide ions. The sulphate ion concentration is also increased at the same time by the lowered oxide ion concentration and diffuses along with the metal ions and the complex ion toward the sulphate/atmosphere interface. As the three ions approach the interface, the metal ions react with the oxide ions available at the interface to form a porous, non-protective oxide layer. The complex ions and the sulphate ions are reduced at the same time. The volatile metal oxide and SO_3 are lost from the sulphate layer to the atmosphere.

It should be pointed out that the alloy induced acidic fluxing is self-sustaining as long as there is a source of sodium sulphate. As the metal is attacked, more of the acidifying element is released into the sulphate layer. The sulphate layer is not saturated because of the time required for the transport of the complex ions through the sulphate layer and the continuous loss of the acidifying element as a volatile oxide.

Goebel, Pettit, and Goward (20) investigated the effect of the acidifying element by examining the fluxing of alumina by sodium sulphate with the oxides as an addition. Alumina crucibles were fluxed by the sodium sulphate/oxide mixture. Work done by Misra (21) also shows that alloys with these acidifying elements show acidic fluxing behavior.

2.1.3 OTHER HOT CORROSION MECHANISMS

In addition to the sulphidation and fluxing models, Kawakami et al (3) also pointed out in their paper three other proposed mechanisms. While they are not as widely accepted as the mechanisms already discussed, they may have some applications.

2.1.3.1 PSEUDO-SCALE MODEL

The pseudo-scale model was proposed by Reising (22,23,24). A schematic representation of the model proposed by Reising is shown in Figure 12. Reising opposed the fluxing model proposed by Goebel and Pettit and other investigators. Instead Reising considered the sulphate layer to be a scale through which oxygen molecules and cations can migrate. According to Reising, the high temperature oxidation of metals and alloys, i.e. nickel, is dominated by the one-way diffusion of cations toward the metal/oxide interface causes a dense, adherent oxide scale to form. When the salt is present, the reaction

$$(12) \qquad Ni + 1/2 \ O_2 = Ni^{2+} + O^{2-}$$
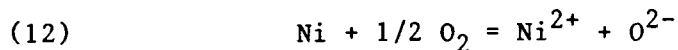
can occur at the metal/salt interface. The nickel ions diffuse outward and the oxide ions diffuse inward. This results in a two-way diffusion situation. The nickel ions are oxidized as they approach

the atmosphere/salt interface to form a porous, non-protective oxide layer. When sufficient nickel oxide is formed and the sulphate layer used up, the nickel forms a dense oxide layer beneath the porous oxide layer by the diffusion of oxygen from the atmosphere through the porous oxide to the metal/porous oxide interface. The dense oxide layer continues to grow by the same mechanism as simple oxidation.

Reising examined the effects of the addition of chromium to nickel. His conclusion was that the formation of a chromium sesquioxide layer when the chromium level was greater than 20 w/o accounted for the improved hot corrosion resistance of chromium containing alloys.

Another pseudo-oxide layer model was proposed by Cutler and Grant (25). They incorporated a consideration for the cathodic reduction of SO_3 to SO_2 and O^{2-} at the oxide/salt interface. Cutler and Grant proposed that a sulphide layer formed beneath an oxide layer that is not completely protective. The sulphide gradually increased until the corrosion process reached a steady state which is controlled by the transfer of sulphur and oxygen through the sulphate layer as SO_3. Cutler and Grant supported their model by comparing the relative amounts of sulphide and oxide formed experimentally to that which was calculated from diffusion flux equations.

2.1.3.2 FORMATION OF VOLATILE PRODUCTS

The chemical process that produces the sodium sulphate layer is derived in part from the presence of sodium chloride, NaCl. When excess sodium chloride is present, the sulphate layer can become a sodium sulphate-sodium chloride mixture. The result is often an increase in the hot corrosion rate and the formation of blisters and

cracks in the oxide layer as shown in Figure 13. Davin, Coutsourradis, and Habraken (26) attributed the blistering of the scale to the formation of metallic chlorides under locally reducing conditions that are volatile at the test temperature. The chlorides are oxidized when the conditions change to oxidizing. The chlorine gas generated blisters the oxide layer being formed. Jones (27) gave a similar explanation.

Hurst, Johnson, Davies, and Hancock (28) disagreed. They argued that the gaseous sodium chloride would diffuse through the oxide layer to the metal/oxide interface. There it would react to form volatile chromium oxychlorides, e.g. $Cr_2O_2Cl_2$ (g). The resulting pressure would lift the oxide layer off the metal, resulting in cracking and blistering. The sodium sulphate would then have direct contact with the metal.

Stearns, Kohl, and Fryburg (29) investigated the effect of NaCl(g) on a chromium containing alloy in a simulated engine environment. Their results indicate that three gaseous chromium compounds of the type $(NaCl)_xCrO_3$ where x = 1, 2, or 3 depending on NaCl(g) and O partial pressures. This result indicates that the reactions between NaCl and Cr can form a volatile species as proposed. This in turn supports the volatile products hypothesis.

One other possibility should be mentioned when considering the role of sodium chloride on the hot corrosion process. Smeggil and Bornstein (30) showed a distinct change in the oxide morphology to a less protective form and an increase in the oxidation rate for NaCl(g)-O_2 mixtures. The role of sodium chloride in hot corrosion may be the changing of the oxide layer from a protective to non-protective layer.

2.1.2.3 LOCAL CELL MODEL

Rapp and Goto (31) examined the possibility that the hot corrosion reaction can be divided into two sets of half cell reactions as shown in Figure 14, namely

$$(13) \qquad M = M^{2+} + 2 \ e^-$$

at the metal/salt interface and

$$(14) \qquad 1/2 \ O_2 + 2 \ e^- = O^{2-}$$
$$(15) \qquad SO_3 + 2 \ e^- = O^{2-} + SO_2$$

at the salt/atmosphere interface. If an oxide layer has already been established with a transition metal impurity, Me, in the salt, the reaction

$$(16) \qquad Me^{2+}_{oxide} + Me^{3+}_{salt} = 2 \ Me^{2+}_{salt} + h_{oxide}$$
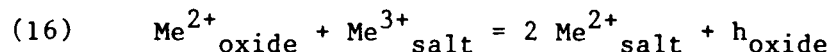
could occur. The cations would diffuse to the gas/salt interface through the salt. If the level of Me in the salt was sufficiently great, the alternate possibility of electronic hopping in the salt may occur. The electrochemical reaction is transferred in either manner to the gas/salt interface where the reactions

$$(17) \qquad 2 \ Me^{2+} + 1/2 \ O_2 = 2 \ Me^{3+} + O^{2-}$$
$$(18) \qquad 2 \ Me^{2+} + SO_3 = 2 \ Me^{3+} + O^{2-} + SO_2$$
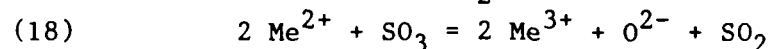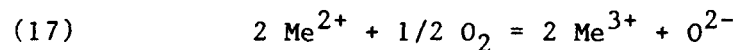
occur. The Me^{3+} cations would diffuse back to the oxide layer and react with the oxide. The cathodic reaction is assumed to generate locally high basicity which helps to establish the solubility gradient of the metal oxide. The hot corrosion reaction continues until there is no longer a solubility gradient that supports the

outward movement of metal cations to the salt/gas interface. The metal cations combine with the oxide ions or oxygen to form a porous oxide layer.

The advantage of the local cell model is that it combines the electrochemical and oxide/salt chemistry into an integrated format rather than the disjointed arguments of some of the other models. Some experimental research does support the local cell model as at least a contributing cause for hot corrosion. Simons, Browning, and Liebhafskey (32) examined the effect of applied potential on hot corrosion and found that the hot corrosion rate was dependent on the applied potential. More work on the experimental verification of the model and the salt/oxide chemistry must be done.

2.2 HOT CORROSION TESTING METHODS

There are three major methods for testing the hot corrosion resistance of a metal. Each has its own advantages and disadvantages.

2.2.1 CRUCIBLE TEST

As the name implies, the crucible test is performed in a crucible as shown in Figure 15. A sample is buried in a salt mixture partially or totally, and the entire crucible exposed in a furnace. The atmosphere can be controlled for simulating various environments. In more advanced tests, electrical potentials can be applied and the salt chemistry altered by bubbling gases through the salt to determine the effects of applied voltage, the potential of the corrosion reactions, and the solubility curves for the oxide in the salt.

Advantages to the crucible tests are that it is cheap, easy to perform, relatively fast, and can accommodate a wide variety of salts and metals. These advantages combine to make the crucible test a good screening test.

The primary disadvantage to the crucible test is that it does not accurately reflect the typical operating environment in which hot corrosion occurs. The thick salt layer is actually a better representation of a salt bath heat treatment furnace. The thick salt layer also may cause the accumulation of products at the metal/salt interface that would be lost in the typical hot corrosion environment and retards the transport of reactants from the salt/gas interface. These could combine to inaccurately reflect the hot corrosion resistance of the metal. Crucible/salt and crucible/metal or metal oxide reactions can also play a major role as the same

reactions that can affect oxide scales will be acting on ceramic crucibles.

2.2.2 TGA EXPERIMENTS

Thermogravimetric apparatus (TGA) testing of samples involves corroding a sample in a furnace and continuously monitoring the samples weight in situ. A typical test rig arrangement is shown in Figure 16. The sample is typically hung in a vertical furnace with a platinum wire connecting the sample to a microbalance. The hot corrosion is caused by introducing sodium sulphate or another salt as a coating or by introducing a gaseous mixture that promotes hot corrosion.

Advantages to the TGA method include continuous monitoring of the samples weight change, the easy control of the gaseous environment, and the elimination of other reactions, i.e. the salt/crucible reactions. The TGA method has the additional advantage of allowing for much easier analysis of the hot corrosion process to determine mechanisms. Disadvantages include the lack of renewal of the sodium sulphate layer and the relatively low gas flow rates and pressures compared to the typical gas turbine engine.

2.2.3 BURNER RIG TESTING

The burner rig testing method most accurately reflects the conditions in a gas turbine engine. A schematic representation of a typical burner rig test is shown in Figure 17. The sample geometry can be modified by the proper holders to reflect the typical gas turbine blade with its hot and cold spots and varying gas flow rates. Mach one plus burner rigs allow for analysis of the effects of varying gas flow rates on the hot corrosion process. High pressure rigs can also reproduce the high pressures experienced in

today's newer jet engines. Variations in fuel and atmospheric conditions on the hot corrosion process can be evaluated. The primary disadvantage of the burner rig test is the high cost of the burner rig.

2.3 HOT CORROSION OF NICKEL AND SUPERALLOYS

Extensive work has been done on analyzing the hot corrosion of metals under a wide variety of conditions using many different methods. The corrosion of pure nickel and nickel-, cobalt-, and iron-base alloys will be reviewed in this section. Particular attention will be paid to the hot corrosion of nickel since it is the original material used in developing the basic fluxing model. The role of the individual elements in the superalloys will be examined rather than alloys to try to appreciate how each element can affect the various hot corrosion processes. Where appropriate examples will be cited.

2.3.1 HOT CORROSION OF NICKEL

The hot corrosion of nickel has been studied extensively to determine the hot corrosion mechanism in a simplified case. The work on this subject done by Goebel and Pettit (16) has been considered the best explanation for the system and is the basis for the basic fluxing model shown in Figure 9. Work by other researchers has raised questions concerning their hypotheses.

Goebel and Pettit examined the effect of a sodium sulphate layer on the weight gain of pure nickel at 1000°C compared to simple oxidation. The weight gain in air was significantly larger at even short times with only light coatings of sodium sulphate. At fifteen hours, the nickel coated with 0.5 mg/cm^2 Na$_2$SO$_4$ had a weight gain of 34 mg/cm^2 versus 1 mg/cm^2 for nickel oxidized in air. The nature of the oxide layer formed was noted to change from a dense NiO layer to a porous NiO with a nickel sulphide sublayer.

Goebel and Pettit first examined the stability of the various components of the system to determine under what conditions each constituent would exist and how the changes in the system with time

due to chemical reactions occurring affect the stability of each constituent. The result was a set of diagrams analogous to the Porbaix diagram. These are shown in Figures 2 and 3. Goebel and Pettit chose the co-ordinates to be in terms of p_{O_2} and p_{SO_3} to reflect the changes in the acidic and basic components of the sodium sulphate melt. In the Na_2SO_4 portion of the Na-S-O stability diagram the nickel base phases stable are Ni (s), NiO (s), $NiSO_4$ (s), and NiS_x, a series of liquid sulphides. As can be seen, under most conditions the $NiSO_4$ phase can be ignored since p_{SO_3} must be 1 atmosphere or greater. The phases of interest are thus simplified even more to Ni, NiO, and NiS_x.

Goebel and Pettit explained the need for the sodium sulphate layer to have hot corrosion by assuming that the layer was needed to establish a compositional gradient across the sodium sulphate to permit non-equilibrium conditions at the sodium sulphate/metal interface, the equilibrium in this case being the equilibrium established at the sodium sulphate/atmosphere interface. This was proposed because the nickel does not hot corrode in an atmosphere with p_{O_2} and p_{SO_3} equal to the equilibrium conditions. The gradient was proposed to be established by the inability of the sodium sulphate to transport reactants and products as quickly as they are consumed or formed. In this particular case, the oxygen formed a gradient in the sodium sulphate when the oxygen was consumed by the formation of a nickel oxide layer on the nickel.

With time, the partial pressure of oxygen is decreased by the formation of the oxide layer. If the reaction proceeds sufficiently, the reaction between the nickel and the sodium sulphate begins to produce nickel sulphide instead of nickel oxide. This assumes that the sulphur in the sodium sulphate is not lost by some means such as the loss of SO_3 gas from the melt. This requires a large decrease in the oxygen partial pressure and would result in the formation of

nickel sulphide on top of the nickel oxide layer. This does not coincide with the experimental observations. An alternative explanation was therefore proposed.

Goebel and Pettit also pointed out that the sulphur could diffuse through the NiO layer as SO_2 and react with the nickel at significantly lower oxygen partial pressures. They supported this by showing that nickel would form a liquid sulphide layer beneath the oxide if the nickel was exposed to pure SO_2. The low diffusivity of elemental sulphur tends to rule out sulphur as the transported species.

With the removal of the sulphur from the sodium sulphate, the oxide ion concentration in the sodium sulphate increases as given by the chemical reaction

$$(19) \qquad SO_4^{2-} = O^{2-} + 1/2 \; S_2 + 3/2 \; O_2$$
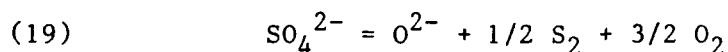
With the increased oxide ion concentration Goebel and Pettit proposed that the oxide ions react with the protective oxide layer to produce the soluble nickelate ion, NiO_2^{2-}. The nickelate ion diffuses outward toward the sodium sulphate/atmosphere interface because of the concentration gradient in the sodium sulphate melt. Since the oxide ion concentration decreases as the nickelate ion approaches the sulphate/atmosphere interface, the nickelate ion is reduced back to NiO. The NiO precipitates out as a porous, non-protective layer.

With time the sulphur is used up, and the production of the oxide ion ceases. The nickel saturated sodium sulphate layer precipitates out the NiO as a dense, protective oxide layer at the sulphide/sulphate interface. The dense layer stops the accelerated oxidation.

The model proposed by Goebel and Pettit explains the observed morphology and kinetics for the hot corrosion of the nickel. The presence of the sulphide layer under the oxide layer is explained by the sulphidation of nickel when the porous oxide layer layer is being formed during the basic fluxing of the nickel oxide layer. The incubation time seen in the tests is explained by the need for the reactions to proceed to some extent to establish the gradients in the sodium sulphate layer. These reactions take some time to progress sufficiently to create the concentration gradient and the oxide concentration at the oxide/sodium sulphate interface necessary to form the complex oxide ions. The degradation and reformation of the oxide layer with time is explained by the fluxing of the oxide layer to form the outer, porous nickel oxide layer and the subsequent inward growth of the nickel oxide layer to form the compact oxide layer. It also explains why hot corrosion can occur in systems with no sulphur. Since the corrodant responsible for the degradation of the oxide layer is the oxide ion, any salt that will release oxide ions and can support an oxide ion concentration gradient will cause hot corrosion. Sodium sulphate is liquid at most of the temperatures of interest and is a ready source of oxide ions. As such it is particularly good at promoting hot corrosion and is the cause of most observed hot corrosion. The model suffers primarily from the unproven assumptions of a gradient through the sulphate layer and the reaction between the oxide layer and the oxide ions.

Further work on the hot corrosion of nickel at 900°C was done by Arbab and Shatynski (33) using mixtures of Na_2SO_4 and $CaSO_4$. Their work also investigated additions of PbO and V_2O_5 to the sulphate mixture. The results were correlated to existing hot corrosion mechanisms.

The samples coated with pure sodium sulphate showed results similar to Goebel and Pettit's work. The greater extent of hot corrosion attack was attributed to the greater amount of sulphate present (2 mg/cm^2 versus 0.5 mg/cm^2). Calcium sulphate melts at 1450°C and is thus solid at the test temperature. The various fluxing models require a liquid layer on the metal, so they should not be operative at this test temperature. If there is no other hot corrosion mechanism active, i.e. sulphidation hot corrosion, the weight gain in the samples should not be increased. The samples exposed with a pure calcium sulphate layer showed no acceleration in the weight gain compared to simple oxidation. This indicates that no fluxing of the protective oxide layer is occurring.

Mixtures of Na_2SO_4-$CaSO_4$ with varying relative amounts of each sulphate were applied to nickel samples, and the samples exposed as before. The mixtures are all solid at the test temperature according to the two component phase diagram. The samples showed a relatively uniform decrease in weight gain with increasing calcium sulphate content with the exception of the Na_2SO_4-40% $CaSO_4$ mixture. This mixture showed an unusually high weight gain compared to the two tests with slightly higher and lower ratios. A rather unconvincing argument was made by the researchers that the high weight gain was caused by the presence of a low melting point eutectic mixture of Na_2SO_4-$CaSO_4$-NiO. The problem is not central to the hot corrosion problem and may only be a variation in experimental results caused by outside influences. The important result is the decrease in hot corrosion with increasing calcium sulphate.

Arbab and Shatynski examined the cross-sections of their hot corroded samples to determine the corrosion morphology. As in Goebel and Pettit's work, the morphology was a porous nickel oxide layer on top of a dense nickel oxide layer. A sulphide layer identified as essentially NiS by EDS analysis existed below the compact oxide

layer. The effect of the increasing $CaSO_4$ content in the sulphate mixture is to decrease the sulphide layer and increase the relative amount of the dense oxide layer compared to the porous oxide layer. Above 80% $CaSO_4$ there is no sulphide layer.

These observations give strong support to Goebel and Pettit's fluxing mechanism. The higher stability of the $CaSO_4$ combined with the lack of a liquid layer does not allow the formation of the conditions needed for the breakdown of the sulphate into oxide ions to flux the oxide layer of the sample. As a result the amount of attack decreases. Likewise the amount of sulphide present decreases because there is less sulphur being released by the sulphate layer. It should also be noted that very localized hot corrosion attacks did occur with the pure calcium sulphate coatings. These were attributed to the solid state breakdown of the calcium sulphate. All these observations are consistent with the fluxing model proposed by Goebel and Pettit.

From these papers and others it is relative certain that the hot corrosion of nickel follows the model presented by Goebel and Pettit, namely basic fluxing. The addition of other elements can radically affect this model though as can be seen in the case of the superalloys.

2.3.2 HOT CORROSION OF SUPERALLOYS

Superalloys are a class of alloys designed for high temperature applications, i.e. gas turbines. They are often complex systems with ten or more major additions. As a result the response of the superalloys to hot corrosion differ widely from totally unaffected for long periods of time to totally destroyed in a few hours.

With this wide divergence in response, it is almost impossible

to review the individual superalloys. Rather, the effect of the various elements contained in the superalloys will be examined as presented in the available literature. It should be noted that the interactions between elements and relatively modest changes in chemistry can dramatically affect the response of two or more materials being compared and lead to inaccurate conclusions regarding the role of the element in hot corrosion.

The following sections are devoted to the various elements commonly used in superalloys. Each section will present the proposed role for each element and some literature to support and, if available, contradict the proposed roles.

2.3.2.1 NICKEL, COBALT, AND IRON

Nickel, cobalt, and iron are the most common base metals for the superalloys. They are also the bases for the new intermetallic compounds currently under development for gas turbine and other applications. Iron-based superalloys are generally used for low temperature applications up to 1200°F. The nickel- and cobalt-based superalloys are the mainstay of the hot sections of the gas turbine engines in use today.

The role of these elements in hot corrosion is far from well understood. The primary controversy surrounding nickel and cobalt, and indirectly iron, is whether the cobalt-based alloys are intrinsically better for hot corrosion applications than nickel-based alloys. This stems from the generally better performance of the cobalt-based alloys and the higher melting points of the cobalt sulphides and the $Co-Co_3S_4$ eutectic. Both sulphides and the eutectic are solid at the normal operating temperatures tested. On the other hand nickel sulphides and the nickel-nickel sulphide eutectic are liquid over much of the temperature range of interest. It is felt by

many that the lack of a liquid phase imparts a degree of superiority
to hot corrosion to the cobalt-based superalloys by removing a rapid
diffusion path. If this is the case, iron-based alloys should have a
better response than the cobalt-based alloys as iron sulphide and
the iron-iron sulphide eutectic melt at an even higher temperature.

Another possible explanation for the difference in the hot
corrosion resistance of nickel- and cobalt-based alloys exists.
Nickel-based superalloys derive their strength primary from a fine
precipitate of gamma prime, $Ni_3(Al,Ti)$. Solid solution strengthening
and dispersion strengthening of the newer P/M materials are also
common strengthening methods. As a result they have relatively high
aluminum contents, low carbon contents, and low to intermediate
chromium contents. In contrast the cobalt-based superalloys derive
their strength from dispersion strengthening by carbides and solid
solution strengthening. They have little or no aluminum and high
carbon, molybdenum, tungsten, and chromium contents. While the
precise reason why is not clear, it is accepted that 20 w/o chromium
imparts essentially complete hot corrosion resistance. The cobalt-
based superalloys all have this much chromium or more while nickel-
based superalloys generally have considerably less to avoid
embrittlement problems.

Wheatfall (34) investigated the relative hot corrosion
resistance of nickel- and cobalt-based alloys by reviewing the
literature to determine if any definitive trend could be found.
Drawing heavily on burner rig tests conducted at General Electric
(35) Wheatfall showed that under identical conditions over a wide
temperature range, unalloyed cobalt suffered the same degree of
attack as unalloyed nickel. If the cobalt and nickel were alloyed
with 25 w/o chromium, both suffered negligible hot corrosion attack
over the range of temperatures studied. Nickel with lower levels of
chromium, 10 and 15 w/o, showed little attack at the lowest

temperature. The 10 w/o alloy showed significant attack at the
intermediate temperature, and both alloys showed severe attack at
the high temperature. From this it is more reasonable to conclude
that the relative chromium levels of the cobalt-based alloys give
them superior hot corrosion resistance.

Additional research has been done by several researchers to
determine if the liquid sulphides and eutectics can accelerate
corrosion. Nickel, cobalt, and iron along with chromium were exposed
in high sulphur activity gaseous environments to promote the
formation of sulphides. The oxygen liberated from this reaction then
oxidized the metal and/or sulphides. If the liquid sulphides were
promoting rapid corrosion, the metals would be expected to show a
marked increase in corrosion at the eutectic and sulphide melting
temperatures. If the sulphides are accelerating the attack, the
substitution of nitrogen and carbon for sulphur should decrease the
rate of attack as these elements form solid compounds at the
temperatures of interest.

Several researchers have conducted experiments of this type. In
1967 Seybolt and Beltran (36) conducted a comparison of nickel,
cobalt, and some superalloys using both sodium sulphate in an
evacuated crucible and an atmosphere with H_2S or SO_2. The morphology
in all three cases was the same. The materials formed a sulphide or
eutectic that extended into the material, usually along grain
boundaries. This sulphide was preferentially oxidized when the
samples were exposed to an oxygen bearing environment. While there
is a legitimate question as to whether the evacuated crucible and no
oxygen environments lead to a reasonably representative
microstructure and the same reactions as in hot corrosion, the tests
do point out that the sulphides and eutectics will be preferentially
oxidized. No kinetic data was presented to show if an overall
increase in the oxidation rate was achieved, though. Seybolt and

Beltran did determine that to obtain equivalent degrees of attack, the cobalt samples had to be raised 100°C above the temperature for the nickel samples. This lent some credence to the assumption that the cobalt-based materials are inherently better.

More recent work on the subject has been done by Giggins and Pettit (37) testing nickel, cobalt, and iron in gaseous atmospheres of sulphur-oxygen, hydrogen-sulphur-oxygen, carbon-oxygen, and nitrogen-oxygen. Emphasis was placed on the sulphur-oxygen and hydrogen-sulphur-oxygen systems.

Nickel tested in the various sulphur-oxygen gases showed a sulphide layer beneath an oxide layer for (SO_2/O_2) ratios of 0.2 and 2 at 900°C and a (SO_2/O_2) ratio of 0.2 at 600°C. Pure SO_2 at 600°C and 900°C and a (SO_2/O_2) ratio of 2 at 600°C on the other hand developed an intermixed sulphide-oxide layer with the sulphide appearing primarily as stringers in the oxide. Growth rates for the intermixed sulphide-oxide layer were substantially higher than that for the samples with separate layers. Quartz markers indicate that the corrosion occurs by the transport of nickel and sulphur through the sulphide channels.

Cobalt and iron samples were exposed to identical conditions. The cobalt samples showed massive, intermixed scales of sulphides and oxides for a (SO_2/O_2) of 2 and pure SO_2 when the gas was not passed over a platinum catalyst. These large areas appeared only in cobalt samples exposed to a (SO_2/O_2) ratio of 2 if a platinum catalyst was used. Other cobalt samples exposed at 900°C showed only localized intermixed oxide-sulphide regions with the dominant morphology being discrete sulphide and oxide layers. At 600°C no sulphides were formed. Iron exhibited a layered sulphide-oxide structure under all the test conditions.

Pure nickel, cobalt, and iron samples and alloys showed no substantially different corrosion rates when exposed in carbon-oxygen and nitrogen-oxygen environments in most cases. In both gases a complete oxide scale was formed under the conditions tested. Some carburization and nitriding was observed, but was not of major importance. The carbon-oxygen system did have cases where the carbon diffused through the oxide and reacted to form CO_2 gas which exerted sufficient pressure to destroy the oxide layer. No analogous intermixed layers were found for either system.

These tests indicate that the increased corrosion rate in both nickel and cobalt are caused by the presence of sulphide channels in the oxide layer allowing the ready transport of oxygen and metal through the oxide layer. The sulphide or eutectic does not have to be liquid as shown by the increase in corrosion rate for nickel at 600°C, a temperature below the melting point of both. The cobalt does not have a tendency to form the intermixed sulphide-oxide regions, so the corrosion rate would be less. At 600°C the corrosion rate would be substantially lessened by the total absence of sulphides. This may be the reason for the observed better hot corrosion resistance of cobalt-based alloys, especially at lower temperatures. Iron would enjoy a distinct advantage at these temperatures because it does not form intermixed regions at all.

The results of Giggins and Pettit are somewhat contradictory to the results obtained in the burner rig tests performed at General Electric. No ready answer is available for the discrepancies. The most likely answer is that the burner rig tests which develop a sodium sulphate layer on the sample compromises a more complex environment where the transport of material in the sulphate layer and other chemical species, i.e. NaCl, play a major role. The experiments by Giggins and Pettit do show that the possibility exists for cobalt- and iron-based alloys to have an intrinsically

better hot corrosion resistance.

Gesmundo and De Asmundis (38) performed the same type of experiment with cobalt exposed to a pure SO_2 atmosphere. Their work indicated that the cobalt formed a duplex layer at temperatures between 600°C and 1000°C. At temperatures at and below 900°C the sulphides are intermixed with the oxides. At 1000°C the sulphide layer is confined beneath the oxide layer. This is in direct contradiction to the work of Giggins and Pettit who did not observe any sulphides below 900°C. Gesmundo and De Asmundis also observed a protective type of corrosion with the corrosion rate decreasing in an essentially parabolic manner with time. The exceptions were at 900°C when a liquid Co-S phase ruptured the oxide layer and allowed breakaway corrosion. The results also showed a strong decrease in the corrosion rate between 900°C and 1000°C. At 1000°C the material always formed a continuous protective outer oxide layer. This reduced the corrosion rate by stopping the oxidation of the sulphides. The oxide was presumably ruptured at times, but the high temperature allowed for the extremely rapid oxidation of the exposed sulphide to reform the oxide layer. No explanation was given by the authors, though.

The divergence in test results in identical test situations shows how difficult it is to definitively state that a give base material is superior to another. The basic arguments of the relative melting points of the sulphides and eutectics do indicate that cobalt and iron have possible superiorities. The experimental results further indicate that iron and to a lesser degree cobalt tend to be sulphidized/oxidized in such a manner as to form corrosion layer(s) that retard further corrosion. From this viewpoint, iron is superior to cobalt which is superior to nickel. Alloying additions play such a key role in modifying the behaviors of the base metals that it is difficult to determine if the

differences cited really have any bearing on the corrosion of the various alloys used today. More work to isolate the effects of nickel, cobalt and iron in a hot corrosion environment needs to be done before any conclusions can be drawn.

2.3.2.2 CHROMIUM

Chromium is universally recognized as being beneficial to the hot corrosion resistance of metals as shown by numerous tests. No definitive mechanism has been presented to explain chromium's dominant role in hot corrosion. All that can be presented is a series of observations about what chromium could do and what it has been shown to do.

Chromium is added to alloys primarily for oxidation and corrosion resistance. The alloys with chromium additions tend to form a chromia layer on the exposed surfaces which is more resistant than the base metal oxides. The chromium levels determine whether the oxide of the base metal dominates, the chromia is present as an internal oxide with a spinel layer between the chromia and base metal oxide, or the chromia completely overgrows the surface of the metal as a protective oxide layer. Chromium also forms a carbide, $Cr_{23}C_6$, and can strengthen materials through dispersion strengthening. Cobalt-based alloys in particular take advantage of this mechanism. Chromium does have a drawback in nickel-based alloys. Nickel-based alloys are strengthened by the precipitation of gamma prime. This depletes the matrix of nickel and aluminum and enriches the matrix in chromium. In the temperature range of 1500°F to 1700°F the chromium enriched regions can form the brittle Laves phase. This significantly reduces the ductility and strength of the material. The protective layer formed by chromium is also subject to loss by the volatilization of the chromia. This becomes a concern above 1000°C.

While the reason for the improved hot corrosion resistance of chromium containing alloys is not definitively known, the observations do point toward several possible mechanisms that could retard the hot corrosion mechanism operative under the test conditions. It must be remembered though that the hot corrosion mechanism(s) is itself not understood, and, as a result, the role of chromium must be viewed in terms of the imperfect models that have been proposed.

The slowing of the hot corrosion fluxing reaction(s) by chromium in the alloy is often ascribed to the reduction of the oxide ion concentration in the sodium sulphate layer. Quets and Dresher (39) proposed the reaction

$$(20) \qquad Na_2SO_4 + 9/2 \ Ni + 1/2 \ Cr_2O_3 + 3/4 \ O_2 =$$
$$Na_2CrO_4 + 3 \ NiO + 1/2 \ Ni_3S_2$$
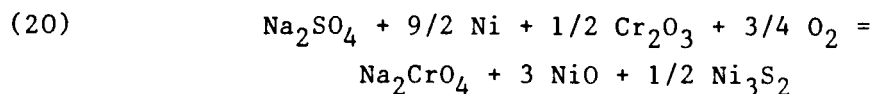
to explain the fluxing of the chromia layer to lower the oxide ion concentration. With the removal of sodium sulphate from the system it is assumed that the reaction that produces sodium oxide from the sodium sulphate is reversed so that the sodium oxide is consumed, not created.

The major problem with this reaction is that the product Ni_3S_2 is not favored in most systems containing chromium. Of the major alloying additions, aluminum sulphide is the only element to be more thermodynamically favored than chromium sulphide. It has been shown that nickel sulphide will be formed only when the chromium is almost totally depleted (40,41,42). The presence of sodium chromate in measurable quantities has been experimentally confirmed though (43).

A more reasonable reaction that lowers the oxide ion

concentration was proposed by Seybolt (44). Seybolt acknowledged
that the reaction

(21) $3 Na_2SO_4 + 7 Cr_{alloy} + 3/2 O_2 = 3 Na_2CrO_4 + Cr_2S_3 + Cr_2O_3$
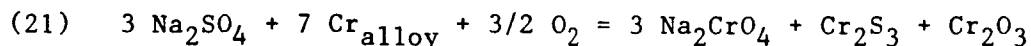
could not be correct since the products cannot exist in equilibrium
with one another. Rather Seybolt proposed that the reaction was the
sum of a series of reactions. Support is given to this idea by the
presence of the products where the sulphur and oxygen activities
would favor their formation. Namely the sulphide is found near the
metal and the oxide is found near the atmosphere.

If the chromia layer is fluxed, the probable reaction is either

(22) $2 Na_2SO_4 + Cr_2O_3 + 1/2 O_2 = 2 Na_2CrO_4 + 2 SO_2$
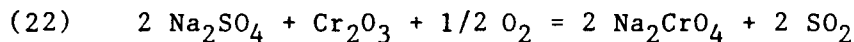
as proposed by Seybolt or

(23) $Cr_2O_3 + O^{2-} = Cr_2O_4^{2-}$
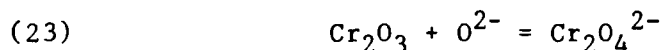
as proposed by several investigators. In both cases the oxide ion
concentration is decreased. In the first case the sulphate layer is
acidified by the introduction of SO_2 which may also diffuse through
the oxide layer to sulphidize the metal.

The presence of chromate ions in the sulphate layer has been
observed by Goebel and Pettit (16). Samples of Ni-5 Cr were exposed
in a hot stage microscope after coating with a thin sodium sulphate
layer. The sodium sulphate layer turned yellow, indicating the
presence of chromate ions. It should be noted that no chemical
analysis was reported to confirm this observation. The chromate ions
were most likely present though.

If chromia is added directly to the sodium sulphate layer, the hot corrosion rate is lowered (44). This would be consistent with the idea that the chromium lowers the oxide ion concentration. It is not consistent with the sulphidation hot corrosion models, though.

If one assumes that the primary cause of hot corrosion is the sulphidation model, chromium plays an important role in tying up the sulphur in an innocuous form, namely chromium sulphide. As stated earlier, the formation of chromium sulphide is thermodynamically favored over the formation of nickel, cobalt, and iron sulphides. As a result the sulphidation reaction must deplete the chromium in the material. Daneck (45) offered three possible mechanisms for the sulphidation hot corrosion attack of alloys containing chromium.

The first mechanism is that sulphur reacts with the chromium to form globules of Cr_2S_3. The underlying matrix is depleted in chromium. The matrix oxidizes rapidly and flakes off, carrying the sulphide globules with it. The depletion of the matrix near the chromium sulphides is fairly well documented. Flaking of the oxidized matrix could also explain the morphology of many hot corrosion samples. No definitive proof is available.

The second mechanism is based on the higher stability of oxides compared to sulphides. In the presence of oxygen, the sulphides of all the major elements in superalloys will be oxidized, releasing sulphur. The mechanism is proposed to be that the chromium forms Cr_2S_3. The lowering of the sulphur activity results in an increase in the oxygen activity. The sulphide is oxidized, and the sulphur released diffuses inward. Oxygen later diffuses through the chromia and oxidizes the sulphides and the depleted matrix formed beneath the chromia. The reaction continues as long as oxygen can reach the sulphide. This type of mechanism would produce the type of morphology seen in hot corrosion samples, but as with the first

mechanism no proof exists for this mechanism.

The third and least likely mechanism proposes that the sulphides at elevated temperature are in fact nickel sulphides. The nickel sulphides undergo a replacement reaction on cool down to form chromium sulphides. The nickel sulphides are assumed to be liquid at temperature. The liquid sulphides are rapidly oxidized to give the high rates of corrosion. This type of reaction has been proposed by several researchers, but no experimental results support it. The thermodynamics, as pointed out before, do not favor the formation of nickel sulphide.

If a chromium sulphide layer is formed by some mechanism, work by Tedmon and Seybolt (46) indicates that the sulphide is very resistant to oxidation and further sulphidation of the metal if the form of chromium sulphide present is Cr_7S_8. Work done shows that the chromium sulphide is oxidized at the surface. The sulphur diffuses inward and reacts with the chromium sulphide to shift the stoichiometry towards Cr_2S_3. The reaction between the sulphur and the sulphide does not involve the metal and therefore does not promote increased weight gains. The oxidized sulphide also forms a protective oxide layer which further slows the corrosion process. The overall reaction rates would be similar to that for oxidation.

De Asmundis, Gesmundo, and Bottino (47) studied the sulphidation/oxidation of pure chromium in SO_2 at various temperatures for up to eight hours. At 700°C the material was corroded to some extent as shown by the presence of a greenish layer on the surface. No reliable weight gain could be detected. At 800°C the chromium was corroded at a parabolic rate for the first five hours, but after five hours the weight was constant. The test at 900°C showed the same type of behavior. The 1000°C test showed a decreasing rate of reaction over the entire test, but the rate was

still significant after the eight hours of the test.

Microscopic examination of the scales from the 1000°C tests indicate the scale is chromium oxide with a small amount of sulphur intermixed with the oxide. X-ray analysis does not indicate the presence of any chromium sulphide. This is in contrast to the expected result of a mixed oxide/sulphide corrosion layer as indicated by the chemical equation

$$(24) \qquad 7\ Cr + 3\ SO_2 = 2\ Cr_2O_3 + 3\ CrS$$
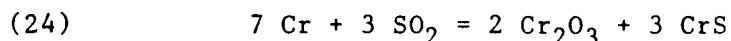
De Asmundis et al proposed that the high oxygen potential formed at the gas/metal interface by the disassociation of the SO_2 causes the metal to establish a Cr_2O_3 layer at the metal/gas interface. The high oxygen activity precludes the formation of any sulphides at this point. For the formation of sulphides, the sulphur must travel through the chromia layer to the metal/oxide interface where there is a much lower oxygen activity. Sulphur can diffuse either by dissolving in the chromia and diffusing inward or diffusing through the chromia along microcracks as SO_2. Tests have shown that the diffusivity of sulphur in chromia is relatively high at 1000°C (48). The solubility of sulphur is also significant, being about 0.5 a/o. Under these conditions, any sulphur should have ready access to the metal/oxide interface. The lack of any sulphides at the metal/oxide interface indicates that the activity of the conditions, any sulphur should have ready access to the metal/oxide interface. The lack of any sulphides at the metal/oxide interface indicates that the activity of the sulphur is low in the gas and therefore it cannot release enough sulphur to cause sulphidation. The alternative sulphidation route, diffusion of the SO_2 to the metal, is assumed to be stopped by the highly compact nature of the oxide layer.

If the hot corrosion conditions are similar, these results indicate that the chromium would form a compact, protective oxide layer that cannot be bypassed to cause sulphidation at the metal/oxide interface. This stops the sulphidation hot corrosion mechanism.

2.3.2.3 ALUMINUM

Aluminum is added to the nickel-based alloys to form gamma prime to strengthen the alloy. Aluminum is also added for high temperature oxidation resistance above the useful operating temperature of chromia formers. Alumina is probably the most protective oxide layer available. Cobalt-based alloys do not have high aluminum contents because cobalt-based alloys have a different strengthening mechanism. Iron-based alloys can have varying aluminum content depending on the strengthening mechanism and corrosion resistance desired. As a result the cobalt- and iron-based alloys are less likely to be alumina formers. The new aluminides have extremely high aluminum contents and form an oxide layer that is almost pure alumina.

The role of aluminum in hot corrosion is somewhat controversial, and, as with chromium, not truly understood. Many observations have been presented in technical papers, often conflicting with each other. Some researchers have reported that aluminum is beneficial while others have shown that aluminum accelerates the hot corrosion of alloys.

Doering (49) examined the role of aluminum in hot corrosion by examining the changes aluminum produces in the electrochemistry of the system. Doering inferred from his results that the aluminum was detrimental as the high titanium to aluminum ratio gamma prime was more resistant to corrosion than the low titanium to aluminum ratio

gamma prime. Wall and Michael (50) examined the role of aluminum at a rather low temperature range, 1250°F to 1450°F. Their results inferred that the higher aluminum contents were harmful over this temperature range, but no well defined relationship could be demonstrated.

Bergman, Sims, and Beltran (51) showed that for simple alloys aluminum contents were increasingly detrimental with increasing aluminum content over the temperature range of 1675°F to 1900°F. With a more complex alloy, PDRL 163, the high aluminum content was judged to be beneficial.

Other researchers have stated that the increased aluminum contents are beneficial to the hot corrosion resistance of alloys. Among those researchers finding a generally improved resistance were Darken and Gurry (52); Llewellyn (53); and St. John, Rentz, and Freeman (54). While the trend was not well defined, high aluminum alloys were generally more resistant that low aluminum alloys of similar compositions. Kaufman (55) examined the role of aluminum by varying the aluminum content of simple alloys similar to nickel-based superalloys and in the beta nickel aluminide range. In burner rig tests conducted at 1675°F and 1800°F, the higher aluminum alloys showed superior hot corrosion resistance to low aluminum alloys.

Lewis and Smith (56) also made another important correlation concerning the hot corrosion resistance of aluminum alloy. They determined that the hot corrosion resistance of a wide range of alloys at 1675°F in Na_2SO_4-NaCl mixtures depended on their chromium and aluminum + titanium contents. Using the percent chromium as the Y axis and percent aluminum + 1.5 times the percent titanium as the X axis, Lewis and Smith showed an excellent correlation of the severity of the attacks in the mixtures to the amount of alloying additions. From this comes the concept of a chromium equivalent

based on the amount of aluminum and titanium present. With a higher chromium equivalent content the alloys showed less hot corrosion. While not perfect, this correlation does strongly indicate that aluminum is beneficial even at low concentrations, especially in conjunction with chromium and titanium. It should be pointed out that the possibility of a synergetic type of mechanism between the aluminum and chromium and/or titanium that improves the hot corrosion resistance of the alloys cannot be ruled out from data presented. This is a possibility since the titanium and chromium form a protective oxide layer rapidly that is later overgrown by the slower growing, more protective alumina layer if the aluminum content is sufficiently high. The chromium and titanium may thus provide a protective layer that stops hot corrosion from starting and repairs any cracks in the alumina layer formed later on.

2.3.2.4 REFRACTORY METALS

Molybdenum and tungsten are added to nickel-, cobalt-, and iron-based alloys for solid solution strengthening. They also form stable carbides that act as dispersion strengtheners. Other refractory metals are also added for dispersion and solid solution strengthening. Some are also added for corrosion resistance and to modify the microstructure. Refractory metals form highly volatile oxides at elevated temperatures. The high volatility of the oxide layer is in fact the reason these metals cannot be used for high temperature applications despite their extremely high melting points.

Several studies have been done to determine how refractory metals affect the hot corrosion resistance of alloys. As pointed out in section 2.1.3.2, molybdenum and tungsten promote alloy induced acidic fluxing by reacting with the oxide ions in the melt to form complex ions that are soluble in the sulphate. The consumption of

the oxide ions shifts the equilibrium for the breakdown of the oxide into the metal ion and oxide ion toward the side of the ions. The complex molybdenum and tungsten ions diffuse outward toward the sulphate/gas interface where they decompose into oxide ions and metal oxide gas. The loss of the molybdenum or tungsten oxide from the oxide layer also leaves a hole in the oxide layer which allows direct access to the metal. The other refractory metals seem to have a similar role.

One of the better studies of the hot corrosion induced by molybdenum and tungsten was done by Huang and Meier (57). The sources for the molybdenum and tungsten were the carbides in the nickel-based alloy IN-738 and a series of alloys that simulated the major alloying additions to IN-738. Their findings indicated that the carbides were the sites for the initiation of the penetration of the oxide layer. Huang and Meier offered two possible explanations for this. Either the carbides incorporated into the oxide layer afford a physical discontinuity in the oxide layer or the carbides form a strongly acidic local region that fluxes away the oxide layer. Huang and Meier supported the latter based on the strong influence of the carbides composition on the attack. In carbon free samples of the selected compositions previously tested with carbon levels comparable to IN-738, Huang and Meier found that the refractory metals molybdenum, tungsten, and columbium slowed the hot corrosion attack. This beneficial effect was attributed to the acidification of the sulphate to the point that basic fluxing could not occur but not to the point that acidic fluxing of the oxide happened.

Huang and Meier found that columbium caused the molybdenum content of the carbides to increase. The columbium itself also strongly acidified the sulphate by reacting to form Cb_2O_5. Their results were in agreement with those of Johnson, Whittle, and

Stringer (58). The strongly acidified sulphate melt rapidly attacked the chromia layer and hot corrosion was extensive in the columbium containing alloys. Those alloys not containing columbium were not attacked as extensively even if they contained other refractory metals.

The difference in the attack of the carbon versus the no carbon alloys suggests that the other studies done may be strongly influenced by how the refractory metals are present in the alloy being tested and the chemistry of the carbides when present. This calls into question the results obtained by various researchers and may explain differences between experiments.

Other researchers have tested materials to determine if the refractory metals influence hot corrosion. Among them Walters (41) indicated that the refractory metals that formed grain boundary carbides were harmful because the carbides were sulphidized into complex sulphides of chromium and the refractory metals. Bergman, Sims, and Beltran (51) indicated that for nickel-based alloys molybdenum was increasingly detrimental with increasing temperature, tungsten had no effect at 1750°F but did increase the hot corrosion at 1900°F, and tantalum decreased the hot corrosion of the alloys. Cobalt-based alloys were severely attacked when molybdenum was added to the alloy. The cobalt-based alloy WI-52 which has a typical composition except for a 2 percent columbium addition was particularly poor in burner rig tests. Tungsten was somewhat detrimental in a single ternary alloy. The other refractory metals seemed to have no effect on the hot corrosion resistance of the alloys studied.

Conde, Erdos, and Rahmel (59) reported that in addition to their roles in acidic fluxing, molybdenum and tungsten decreases the melting point of the sulphate deposits by reactions between the

sulphates and the molybdenum and tungsten oxide. This was more important at lower temperatures where the sulphate is not normally liquid. Conde et al also indicated that molybdenum was more important than tungsten in inducing corrosion, but both elements have an ill defined threshold level below which the hot corrosion was not significantly influenced by the tungsten and molybdenum. This is in agreement with Huang and Meier's (57) observations about the increased hot corrosion resistance of alloys containing smaller amounts of refractory metals.

Kaufman (55) indicated that tungsten and tantalum had no effect on nickel-based alloys and little effect on cobalt-based alloys. A combination of 2% chromium and 5% titanium or molybdenum was helpful in stopping the hot corrosion of nickel aluminides.

While no definitive conclusions can be drawn from the literature, it is likely that the additions of refractory metals affects hot corrosion. Whether it increases or decreases the alloys hot corrosion resistance appears to be highly dependent on how the refractory metals are incorporated into the alloy.

2.3.2.5 RARE EARTH ADDITIONS

Rare earth elements such as lanthanum, yttrium, and zirconium are added to alloys in small quantities to improve the oxidation resistance of the alloys. How the rare earth additions improve the oxidation resistance of alloys is not understood. Original observations of transverse sections of oxidized samples indicated that the rare earth additions oxidized and mechanically keyed the oxide layer to the metal. Later work has shown that mechanical keying is an uncommon mechanism. More recent proposals have centered on the concept that the rare earth elements improve the adhesion of the oxide to the metal. The concept is that the rare earth elements

getter tramp elements, particularly sulphur, that tend to form thin layers at grain boundaries and interfaces. By removing these weak layers from the system the oxide is held to the metal better. Typical applications of these newer alloys are in parts normally subject to oxide spalling.

The role of rare earth elements in hot corrosion is even less well understood. Some testing has been done, but no significant theory based on the testing has been advanced to explain the role of the rare earths and other reactive elements in hot corrosion.

Viswanathan (60) tested U-700 with additions of lanthanum and yttrium in a controlled atmosphere combustion furnace. A salt consisting of equal parts sodium sulphate and magnesium sulphate were applied to the samples. Testing was conducted at 1500°F with the exposure lasting 200 hours. The hot corrosion of the alloys was evaluate by determining the weight loss per unit area of the metal after removal of the scale. The results indicated that the addition of 0.1% yttrium halved the weight loss and 0.1% lanthanum decreased the weight loss by two thirds. The addition of 0.2% of these elements was slightly more effective, but the addition of 0.3% lanthanum increased the weight loss to slightly above the weight loss for 0.1% lanthanum. Samples with the rare earth additions retained extremely good surface quality as shown by the macrophotographs of the exposed samples.

Viswanathan suggested that the rare earth elements either "plugged" the grain boundaries by stopping diffusion or the rare earth additions decreased the participation of the nickel in the oxide so that the oxide was nearly pure chromia. Viswanathan discounted the theories that the rare earths formed oxides at grain boundaries that improved adhesion and the rare earths formed complex spinels with the chromium that decreased the cation diffusion rate.

The theory that the formation of mechanical keys at grain boundaries enriched in rare earths decreased the shear stress of the oxide layer could not be discounted since enriched grain boundaries were observed. No definitive proof could be sighted for any of the above theories.

More recent work has been done by Huber and Gessinger (61) looking at the affect of yttria, Y_2O_3, on the hot corrosion resistance of IN-738, a commonly used nickel-based superalloy. The yttria was added by mechanically alloying the material. A comparison was done to cast, coarse grained material without yttria additions. A burner rig was used to test the hot corrosion resistance of the alloys. Fifteen ppm sodium and five ppm vanadium were added to the fuel as naphthenates to accelerate the corrosion. It should be pointed out that the addition of the vanadium makes this a particularly severe test condition. The addition of the yttria lowered the corrosion rate at 850°C and 950°C. Huber and Gessinger attributed the reduction in corrosion to the formation of complex yttrium oxysulphides which suppresses the formation of other sulphides. The reaction proposed was

$$(25) \qquad Y_2O_3 + S_{alloy} + 2/3 \, Cr = Y_2O_2S + 1/3 \, Cr_2O_3$$
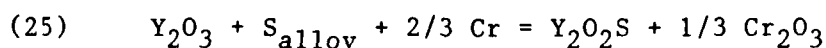
Other strong oxide formers such as aluminum or titanium could substitute for the chromium. The gettering of sulphur stopped the formation of the chromium and nickel sulphides that were the principle form of attack in the cast alloy not containing yttria. At 950°C the role of yttria is reduced because the attack changes from a predominantly sulphidation/hot corrosion attack to internal oxidation. Yttria is still beneficial though.

Additional work in sulphur bearing environments was done by Strafford and Hunt (62). They examined the influence of zirconium on

the corrosion of a Ni-15 Cr alloy at 850°C in an oxygen/sulphur dioxide atmosphere. Zirconium contents ranged from 0.5 w/o to 10 w/o. The results of testing the alloys indicated that the best resistance was achieved with a 1 w/o addition of zirconium. The measured rate constant decreased by a factor of 20 at this zirconium level. High zirconium content alloys showed more extensive weight gains than the control Ni-15 Cr alloy. This probably reflects the high reactivity of the zirconium which apparently lead to the selective attack of the zirconium. The controlling factor in the attack seemed to be the formation of an essentially pure chromia layer formed on the low zirconium alloys as compared to the duplex scale formed on the control alloy. Internal attack was also observed in all cases. The internal attack was principally oxides at 5 and 10 w/o zirconium with large volume fractions at the surface region, 5.4% and 8.2% by point count methods. At 1 w/o zirconium, the internal attack had changed to zirconium oxide stringers with sulphide particles containing zirconium and chromium. The volume fraction had decreased to only 1.0%. In contrast, the control Ni-15 Cr alloy showed rounded 'CrS' particles in the substrate material occupying 4.5% by volume. From these observations the conclusions were drawn that the zirconium slows the inward diffusion of sulphur and suppresses the formation of a transient nickel oxide layer during the initial stages of corrosion. This would be helpful in hot corrosion, and it is likely that a hot corrosion study of these materials would show that zirconium is beneficial to hot corrosion.

2.3.2.6 CHLORINE

Chlorine is an important element in hot corrosion not because it plays a direct role in the hot corrosion process but rather because it can modify the oxide layer in such a way as to make it less protective. The exception is when a large amount of chlorine is present and it reacts with the oxide layer to form volatile

chlorides such as $CrCl_2$. It is also important indirectly because so many tests have been conducted with sodium chloride added to the salt that the increased corrosion rate with the sodium chloride additions must be explained.

Sodium chloride is present in the gas turbine engine primarily as a gas though some large salt particles ingested with the air may remain as a solid for significant lengths of time.

Conde, Erdos, and Rahmel (59) examined the literature on the influence of chlorides on the hot corrosion process. All available literature indicates that the presence of chlorides such as NaCl and HCl do not influence the hot corrosion mechanism. Rather, the initiation stage is influenced. The chlorides disrupt the normal formation of the oxide layer to produce spalling and cracking at even low chloride levels. In the presence of stress, there are some indications that intergranular chloride attack can occur.

2.4 HOT CORROSION OF COATINGS

Coatings are applied to metal substrates to protect the metal substrate from oxidation, corrosion, or thermal shock. Coatings typically consist of a metal or a ceramic applied by one of a variety of processes. An intermediate layer between the coating and the substrate to reduce thermal stresses or lower the interdiffusion between the coating and base metal is also common. For the purposes of simplification and because they are the most common types of coatings used for hot corrosion resistance, the discussion will be limited to aluminide, MCrAl, and MCrAlY coatings applied to superalloys. The platinum group metal (PGM) coatings which utilize small additions of the noble elements for increased hot corrosion resistance will also be discussed.

Hwang, Meier, Pettit, Johnston, Provenzano, and Smidt (63) studied the initiation of the hot corrosion of CoCrAlY and CoCrAl coating materials at 700°C in a gas mixture of oxygen and SO_3. The samples were preoxidized at 700°C in air for 1 hour to extend the initiation stage. The results of the optical and SEM examinations revealed the formation of holes in the oxide layer at the time the coating began to fail. The holes were associated with the yttria in the oxide layer when yttrium was added to the coating, but there was no corresponding phase present in the CoCrAl coating to explain the holes. The yttria in the alumina was found to react with the sodium sulphate coating to form a soluble yttrium sulphate in the CoCrAlY metal. Since the materials were not being tested as a coating but rather as a metal, no diffusion between coating and metal substrate could have occurred to introduce another element that could explain the holes in the oxide layer.

Steinmetz, Roques, Dupre, Duret, and Morbiolt (64) examined the hot corrosion process for coatings under oxidizing and reducing

conditions with an oxygen partial pressure of approximately 10^{-15} atmospheres. The superalloys IN-100, IN-738, and IN-939 were pack aluminized using the HI15 process and the equivalent vapor deposition process which resulted in the formation of a beta NiAl layer on the surface of the superalloys. Both static and cyclic exposures were performed at 850°C. The samples that were pack aluminized showed the presence of pack inclusions that were preferentially attacked and limited the life of the coating.

Steinmetz et al proposed that under oxidizing conditions alumina forms initially. The oxide ion activity is too low at this point to flux the alumina. The presence of some chromia in the oxide layer causes a further lowering of the oxide ion concentration by the fluxing of the chromia. Under these conditions the alumina layer would remain protective indefinitely. The alumina layer is compromised though by cracks in the oxide layer caused by growth stresses, thermal shock, and other similar processes. This allows the beta NiAl to come into direct contact with the sulphate melt. The aluminum and chromium react with the oxygen in the melt to reverse the oxide activity from low to high. The alumina adjacent to the crack is fluxed under the locally basic conditions, and a non-protective, porous alumina scale is formed in the melt above the crack. As the reaction progresses and the oxygen potential is reduced even further, the possibility exists that the sulphate adjacent to the metal is reduced. The reduction of the sulphate can be further divided into two substages to take into account differences in the prevailing conditions. In the first stage sulphur is reduced from S^{4+} to S^0 simultaneously with the formation of alumina. The reactions increase the oxide ion activity and promote the self-sustained basic fluxing of the alumina. The S^0 is further reduced at the salt/metal interface in the second stage. The products depend on the local composition of the metal. If no chromium or titanium is present in the metal, the aluminum cannot

form the sulphide Al_2S_3 which would form a barrier between the metal and sulphate because the sulphide would react with the highly basic sulphate melt to form the aluminate ion. Under these conditions the metal would be continuously exposed to the sulphate melt and extensive corrosion would occur. If chromium or titanium is present in the coating either by the aluminizing process or by diffusion from the base metal, the chromium or titanium can form a stable sulphide at the metal/sulphate interface that protects the metal. Acceleration of the attack on the coating could then occur only if oxygen reached the sulphides to react with them and release sulphur.

From this consideration, the distribution of chromium in the coatings becomes important. As time progresses, chromium in the base metal diffuses outward into the coating. This can change the reaction mechanism as shown in the preceding paragraph. The importance of this phenomena was shown in the poor hot corrosion resistance of the coated IN-100 which has little chromium compared to the coated IN-738 which has a high chromium content. The diffusion of the chromium outward also affects the metal underneath the coating by depleting it of chromium. The depletion of the chromium in the metal can cause major problems when the coating is breached.

Lau and Bratton (65) studied the effect of a sodium sulphate layer on the degradation of porous plasma-sprayed ceramic thermal coatings. They found that the coatings were destroyed not by hot corrosion but by a combination of thermo-mechanical effects of the condensed salt and the disruptive chemical reactions between the salt and ceramic coating. Some reactions similar to the hot corrosion of metals was observed, but in general the destruction of the ceramic coating in the tests were not related to hot corrosion. The hot corrosion of ceramics can therefore be ignored.

Recently the addition of platinum and other PGM metals to
coatings has shown success when normal coatings were ineffective at
stopping hot corrosion. Coupland, Corti, and Selman (66) examined
the role of platinum in a structural alloy with a composition
similar to a PGM coating. Coupland et al found that the platinum
acted as a mechanical key to hold the oxide layer to the metal in
simple oxidation. In hot corrosion the platinum was assumed to
decrease the diffusion rates in the alloy. The increase in the
depleted zone at the surface was sited as evidence of this enhanced
diffusion rate. It is assumed that the platinum has similar effects
in coatings.

2.5 HOT CORROSION OF B2 NICKEL ALUMINIDES

The B2 nickel aluminides are ordered body centered cubic (BCC) alloys with exceptionally high melting points and strengths. The stoichiometric NiAl melts congruently at 1650°C. The ordered structure tolerates a wide range of compositions from a minimum of 16 w/o Al at 1375°C to a maximum of 38 w/o at 1150°C as shown in Figure 1. The use of the B2 nickel aluminides is severely limited by the extremely low ductility of the material at room temperature. The high temperature properties of the materials and the excellent oxidation resistance derived from the high aluminum content combined with the low density of the alloys make them prime candidates for gas turbine engine applications once some room temperature ductility can be achieved.

To understand the hot corrosion of the nickel aluminides it is imperative to first understand the oxidation of the beta nickel aluminides. The formation of the alumina scale with the several transient forms of alumina and slow kinetics may be of great importance in determining the hot corrosion resistance of the nickel aluminides. A review of the oxidation of the nickel aluminides will be presented first before the less well documented hot corrosion of nickel aluminides.

2.5.1 OXIDATION OF B2 NICKEL ALUMINIDES

Pettit (67) examined the oxidation of nickel-aluminum alloys with aluminum contents between 3 and 25 weight per cent in the temperature range of 900°C to 1300°C in pure oxygen. The aluminum content range covers the gamma, gamma prime, and beta phase regions. From Pettit's theoretical work three separate mechanisms for the formation of the oxide layer were discovered, Two of the mechanisms do not permit the formation of a continuous alumina scale and in

fact result in a higher oxidation rate than that for pure nickel. A summary of the mechanisms proposed by Pettit as a function of temperature and aluminum content are presented in Figure 18. Experimental data using TGA experiments and microscopy indicate that the theoretical mechanisms represent the oxidation of the alloys studied.

The first mechanism is operative at low aluminum contents. The aluminum content of the alloy for this mechanism to operate is determined by the amount of aluminum needed to change the oxidation of the aluminum from internal oxidation to external oxidation at a given temperature. The reaction product(s) is determined by the oxygen activity in the gaseous atmosphere compared to the alloy-Al_2O_3-$NiAl_2O_4$ and alloy-$NiAl_2O_4$-NiO equilibrium oxygen activities.

If the oxygen activity of the atmosphere is less than the alloy-Al_2O_3-$NiAl_2O_4$ equilibrium oxygen activity but greater than the oxygen activity for the formation of Al_2O_3 on the alloy, i.e. greater than the bulk alloy-Al_2O_3 equilibrium value, the only stable oxide is Al_2O_3. The oxygen activity is not sufficient to cause an external oxidation of the aluminum, so the Al_2O_3 forms internally.

If the oxygen activity of the gas is greater than the alloy-Al_2O_3-$NiAl_2O_4$ equilibrium as in the last case but less than the alloy-$NiAl_2O_4$-NiO equilibrium value, the internal Al_2O_3 particles can be converted to the spinel $NiAl_2O_4$.

Finally, if the oxygen activity is greater than the alloy-$NiAl_2O_4$-NiO equilibrium, NiO forms at the surface with a subscale of $NiAl_2O_4$.

If sufficient aluminum is present in the alloy to form an external alumina layer, the flux of aluminum to the alloy surface

determines the oxidation mechanism. As the aluminum is converted to alumina at the surface, a concentration gradient is established in the alloy. The outward flux of the aluminum is increased in the alloy and decreased in the alumina layer. The aluminum fluxes will reach a steady-state value since the aluminum must be supplied from the interior for the scale to grow. The composition of the alloy immediately beneath the alumina layer becomes critical since the composition will determine if oxides other than Al_2O_3 will be stable. The equilibrium for the chemical reaction

$$(26) \quad 3\ NiAl_2O_4 + 2\ Al_alloy = 4\ Al_2O_3 + 3\ Ni_alloy$$
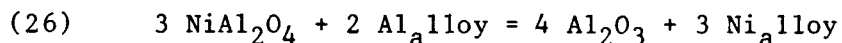
determines if the spinel will be stable. The stability of the spinel is determined by the (a^3_{Ni}/a^2_{Al}) ratio in the intermediate time before the steady state condition is reached. If the aluminum flux from the interior of the alloy exceeded the aluminum flux through the oxide layer, the Al_2O_3 will be stable at all times regardless of the oxygen partial pressure in the atmosphere. If the aluminum flux through the alloy is less than the aluminum flux through the oxide layer, the oxides that will form are determined by the oxygen activity in the atmosphere. $NiAl_2O_4$ will form if the oxygen activity is less than the alloy-$NiAl_2O_4$-NiO equilibrium value, and NiO will form if the oxygen activity is greater than the equilibrium value.

Experimental work in conjunction with the theoretical work presented above showed good agreement in the oxidation products and the location of the products. The kinetics of the oxidation showed that the alloys that did not form a continuous alumina scale exclusively had a higher oxidation rate than pure nickel. The high aluminum alloys that formed a continuous alumina layer had a rate constant three orders of magnitude lower than that for nickel.

Work by various other workers (68) in more recent years has

cast doubt on the breakdown of the alumina layer after it has formed as Pettit proposed for his Mechanism II. Samples of gamma prime exposed in the temperature range that Mechanism II would be operative show excellent oxidation resistance for extended periods of time. How this would affect the hot corrosion of the alloys is not readily apparent, but the stability of the alumina layer should be beneficial.

Nickel aluminides have sufficient aluminum content to form a continuous alumina scale on the surface. The other conditions that promote the formation of other oxides are operative only if the depleted metal beneath the alumina scale is exposed. The degradation of the alumina scale is therefore important in determining the oxidation resistance of the metal.

Smialek (69) examined the degradation of the oxide layer of Ni-42 a/o Al at 1100°C under both static and cyclic test conditions. The primary cause for oxide loss was found to be oxide spalling. The spalling occurred primarily at the metal/oxide interface. Kirkendall voids formed at the metal/oxide interface and weaken the metal-oxide bond. One hour cyclic oxidation tests did show some improvement over the static tests. The improvement was attributed to the self-healing by the repeated cycling of the samples.

Since chromium is an important alloying addition to superalloys to increase the hot corrosion resistance of the alloys, chromium is a logical addition to nickel aluminides for environments that promote hot corrosion. The effect of chromium on the oxidation of the alloys is therefore important in understanding the hot corrosion of chromium containing nickel aluminide alloys.

2.5.2 OXIDATION OF Ni-Cr-Al ALLOYS

The addition of chromium to the nickel-aluminum alloys dramatically improves the oxidation resistance of the alloys by lowering the aluminum level necessary to form a protective, continuous external alumina layer.

Giggins and Pettit (70) studied the oxidation of alloys with aluminum contents between 0 and 8.9 w/o and chromium contents between 0 and 30.0 w/o. These compositions correspond to gamma or gamma plus gamma prime phase regions with some of the high chromium alloys containing elemental chromium in the form of alpha chromium precipitates. If chromium was not present these alloys would oxidize to form non-protective nickel oxide layers, possibly with some spinel or alumina. Giggins and Pettit's work showed that the chromium additions change the composition ranges over which these products form in a manner favorable to the oxidation resistance of the materials. A graphical summary of their work is shown in Figure 19.

The oxidation study was conducted at temperatures of 1000°C, 1100°C, and 1200°C using a 0.1 atmosphere oxygen environment. Three mechanisms for the oxidation of the nickel-chromium-aluminum alloys were observed.

For all three mechanisms the initial oxidation is identical. The outermost atomic layers are oxidized to form a mixed oxide layer consisting of nickel oxide and $Ni(Cr,Al)_2O_4$ spinel. The rapidity of the oxidation prevents the transport of oxygen via diffusion into the metal. As the oxidation progresses, oxygen diffuses through the outer oxide layer into the metal where it reacts to form internal alumina and chromia particles. The progression of the oxidation from this point determines the ultimate oxide layer after the steady

state condition is reached.

The first mechanism applies to the low chromium and aluminum alloys, and is denoted Mechanism I in Figure 19. With low aluminum and low chromium compositions the internally oxidized aluminum and chromium cannot form a continuous subscale. Under these conditions the relatively fast growing external nickel oxide layer overgrows the spinel formed initially to become the predominant oxide. As noted in previous sections, the nickel oxide is not as protective as the alumina layer, and, as a result, the alloys have a comparatively high oxidation rate. Compared to the simple binary alloys, the range of compositions over which nickel oxide is the predominant oxide layer is reduced from 0 to 15 w/o aluminum with no chromium to 0 to 7 w/o with 1 w/o chromium additions. A minimum aluminum content that still forms a complete alumina layer is reached at 10 w/o chromium. At this chromium level, the addition of as little as 2 w/o aluminum can still form the alumina layer. At higher chromium levels the second mechanism dominates the oxidation of the alloys.

At high chromium contents but low aluminum levels, the second mechanism denoted as Mechanism II in Figure 19 results in the formation of a continuous chromium rich duplex oxide layer beneath the initial oxide layer. After the initial oxide layer is established, the alloy is oxidized internally forming a continuous duplex oxide layer consisting of alumina and chromia. The duplex scale is enriched in chromium by the diffusion of chromium into the duplex scale where it is oxidized, but the aluminum is still being oxidized internally beneath the duplex oxide layer by the diffusion of oxygen through the duplex oxide layer. The result is an internal oxide scale closely associated with the nickel-chromium binary alloys. The scale is reasonably protective, but is still inferior to the alumina scale.

The third and final oxidation mechanism denoted Mechanism III in Figure 19 occurs in the higher aluminum alloys and results in the formation of a continuous alumina layer that protects the metal. As with the high chromium alloys, the alloy is oxidized internally to form a continuous duplex oxide layer consisting of alumina and chromia. The aluminum content of the alloy is sufficiently high to form a continuous alumina scale beneath the duplex scale. The alumina scale blocks the diffusion of chromium to the duplex scale and the inward diffusion of oxygen. As a result the oxidation rate is decreased. The continuous alumina layer is the most protective.

Overall, the most important effect of the addition of chromium to the nickel-aluminum binary alloys is the reduction of the amount of aluminum needed to form the continuous protective alumina layer.

2.5.3 HOT CORROSION OF B2 NICKEL ALUMINIDES

Only a limited amount of hot corrosion testing has been conducted for the beta nickel aluminides. The primary reason for this is probably the lack of any applications for these alloys until the room temperature ductility of the alloys can be increased. Much of the testing conducted has been to either understand the role of aluminum in hot corrosion or to examine the hot corrosion resistance of coatings without any interdiffusion with the metal substrate.

Kaufman (55) did a detailed analysis of the hot corrosion reactions in the nickel aluminide alloys. In addition to stoichiometric NiAl, additions of chromium, titanium, molybdenum, and cobalt were evaluated. Nickel- and cobalt-based alloys were also evaluated at the same time. A list of the alloys tested by Kaufman appears in Table 1a.

Investment cast samples were exposed in a burner rig at 1675°F

and 1800°F. Sulphur content of the JP-5 fuel was reported to be 0.34%. Sodium chloride was added to the fuel at concentrations of 0 and 200 ppm. The samples were exposed from 0.25 hours to 100 hours to determine the kinetics of the attack. The degree of attack was measured by the effective metal diameter left and maximum depth of attack in the sample below the effective metal diameter.

Kaufman analyzed the phases present on the surface in the samples after 100 hours using X-ray diffraction. The results are presented in Table 1b. Kaufman does not indicate the dominate oxide present for the tests, but from his descriptions alumina dominates the surface corrosion products. Nickel oxide is present in moderate amounts. Oxides of the additions were not detected except in two cases where they were listed as possibilities. Spinels were listed as occurring but were not identified.

The more important finding of Kaufman came from the analysis of transverse sections of the corroded samples. The sections showed that the samples had an orange colored layer preceding the reaction front into the metal. The orange layer was determined to be gamma prime, Ni_3Al, by electron microprobe analysis. The presence of the orange layer in front of the reaction front and extending back to the surface indicated that the aluminum in the alloys was being moved from the samples to the surface to form alumina at a rate greater than the diffusion of aluminum to the surface from the interior of the sample. The lowered aluminum content of the alloys forced a phase change. The phase change is accompanied by a volume change in the alloy and the formation of voids. The samples swell as a result. The swelling ruptures the protective oxide layer and allows rapid corrosion to take place. The alloys are further depleted as the alumina layer attempts to reform. As Pettit (67) pointed out, the loss of aluminum changes the oxidation mechanism to a less protective one as NiO and $NiAl_2O_4$ are formed. These oxides

promote more rapid hot corrosion.

From these observations Kaufman proposed that three things can improve the hot corrosion resistance of the nickel aluminides. The first was the forming of a surface oxide other than alumina to avoid the depletion of aluminum in the alloy and the subsequent formation of Ni_3Al. This does not seem to be an important mechanism for stopping hot corrosion as all the alloys tested formed an alumina layer and wide variations in hot corrosion resistance existed.

The second way proposed to increase the hot corrosion resistance is to interfere with the diffusion of aluminum to the surface so that the alloy remains rich in aluminum longer. This method may extend the time for the initiation of the hot corrosion attack, but it must be weighed against the lowering of the diffusion of aluminum in the alloy to retain a uniform high level. Also, if aluminum cannot move freely in the alloy, even more severe aluminum depletion could occur at the surface. The resulting aluminum depletion could result in the formation of a gamma region underneath the scale. When the scale is breached at some point, catastrophic corrosion of this highly depleted region could result in a more severe corrosion problem than in alloys with more mobile aluminum.

The final method for improving the hot corrosion resistance of the nickel aluminides is to add elements that stabilize the corrosion resistant beta structure. Low Ni:Al ratio alloys which retain their beta structure the longest were shown to be the best. With no formation of the gamma prime phase and the resulting swelling of the samples, the oxide layer can both increase in thickness and not be cracked for longer lengths of time. Another benefit from the stabilization can be traced to the relatively good performance of the beta phase in sulphidation types of corrosion compared to the gamma prime phase.

From the X-ray diffraction results and the observations about the relative hot corrosion resistance of the beta and gamma phases, Kaufman developed a complex sulphidation/oxidation mechanism to explain the hot corrosion of the beta nickel aluminides. Kaufman proposed a four step mechanism for the hot corrosion process. The chemical equations for the proposed mechanism are

$$(27) \qquad 12 \ NiAl + 6 \ O_2 = 4 \ Al_2O_3 + 4 \ Ni_3Al$$

$$(28) \qquad 4 \ Ni_3Al + 2 \ Na_2SO_4 + 9/2 \ O_2 = $$
$$2 \ Al_2O_3 + 9 \ NiO + Ni_3S_2 + Na_2O$$

$$(29) \qquad Ni_3S_2 + 9/2 \ O_2 = 3 \ NiO + SO_3$$

$$(30) \qquad Na_2O + SO_3 = Na_2SO_4$$
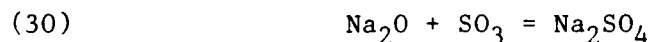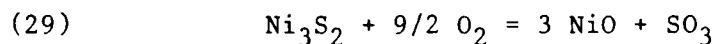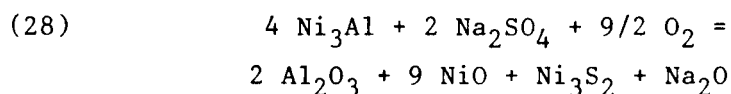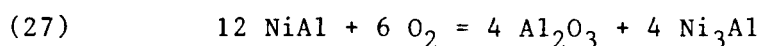
Initially the beta is oxidized to form gamma prime and alumina. The gamma prime phase reacts with the sodium sulphate to form alumina, nickel oxide, sodium oxide, and a nickel sulphide. The sulphide is unstable in the presence of oxygen, so it is oxidized to form nickel oxide and sulphur trioxide. The sulphur trioxide is trapped at the interface and in the sodium sulphate and can react with the sodium oxide formed in the second step to reform sulphur sulphate. The reaction can thus continue for extended periods of time since the sodium sulphate is not consumed rapidly.

Kaufman did not give any substantiating thermodynamic or other data to support the proposed mechanism. It must be noted though that the sulphide and oxide of nickel in this mechanism can not co-exist. Therefore the second reaction as stated must be incorrect. The splitting up of the second step into the formation of the sulphide followed by the oxidation of the sulphide, step 3, may be more

appropriate.

Kaufman's work was carried further by McCarron, Lindblad, and Chatterji (71). McCarron et al studied the hot corrosion of pure and alloyed nickel-aluminum alloys in both the gamma prime and beta phase regions. Additions of chromium, yttrium, titanium, tantallum, and tungsten were evaluated. Burner rig tests were performed at 871°C (1600°F) using a 1% sulphur fuel with 125 ppm sodium added as an emulsified sea salt. The extent of the corrosion was measured by metallographic examinations of the sample's cross section. Total penetration was determined by subtracting the total thickness of the sound material from the original thickness of the specimens and dividing by two.

McCarron et al found that the stoichiometric beta nickel aluminide was inferior to the beta phase-based alloys. This may not be completely accurate as the sample with an atomic Ni:Al ratio of 65:35 was only tested for 50 hours and had a penetration comparable to the penetration for the stoichiometric alloy. Longer time exposure may have shown the 65:35 alloy to be the worst alloy. The sample containing 10 w/o chromium was the best alloy tested. The sample with 2.5 w/o chromium + 1.0 w/o yttrium also shows good hot corrosion resistance. The alloys with 2.5 w/o chromium and 2.5 w/o chromium + 0.1 w/o yttrium had an intermediate hot corrosion resistance. The hot corrosion morphology was shown to be a porous, non-protective oxide at the surface with oxide penetrating into the base alloys. Sulphides preceded the oxides into the alloy. With time the morphology became more extended with the phases being more pronounced.

Hot corrosion tests of the gamma prime alloys, both pure and alloyed, showed that the alloys catastrophically corroded within 120 hours. This is in contrast to the stoichiometric beta alloy which

was catastrophically corroded only after longer exposures of between 200 and 300 hours. The best alloy, NiAl + 10 w/o chromium, had only minimal corrosion after 800 hours. The significantly lower hot corrosion resistance of these alloys underscores the desirability of maintaining a beta structure in the alloy.

A comparison of the test results indicates that the pure gamma prime alloy undergoes an incubation period of 100 hours and then corrodes catastrophically. The pure beta alloys continue to corrode at a predictable rate for extended lengths of times past 100 hours. The incubation period was attributed to the formation of an oxide scale on the alloys from the uptake of oxygen from the sodium sulphate layer. The increased sulphur activity results in the sulphidation of the alloys to form solid Al_2S_3. As the aluminum is depleted by the formation of aluminum oxide and aluminum sulphide, nickel oxide begins to form. The depletion of aluminum to the point that the alloy immediately in front of the corrosion interface is nearly aluminum free leads to the formation of a liquid Ni-S eutectic. The liquid eutectic promotes the sudden failure of the oxide layer by splitting open the oxide layer and allowing rapid transport of reactants to the metal.

The yttrium additions were found to be mildly beneficial for the beta alloys. McCarron et al explained this by assuming that the yttrium scavenges the sulphur diffusing through the alloy from the sodium sulphate layer. The preferential formation of yttrium sulphides stops the depletion of the alloy by the formation of aluminum sulphide. Chromium appears to have different roles.

McCarron et al found that chromium may do four different things to improve the hot corrosion resistance of the beta nickel aluminides. Perhaps the most important mechanism is that chromium stabilizes the beta phase. This can be seen by examining the

tertiary Ni-Al-Cr phase diagram for the nickel rich corner shown in
Figure 20. If the simplifying assumption is made that only aluminum
is removed from the alloy by the corrosion process, the composition
of the alloy can be traced by a straight line almost parallel to the
Ni-Al side of the phase diagram. The line move toward a higher
nickel and chromium composition as the aluminum is depleted. This
increase in the relative amount of nickel and chromium would also
help to stabilize the beta phase even further. From this it can be
seen that alloys containing chromium retain the beta phase longer
before gamma prime begins to form. Since the beta phase is more
resistant to hot corrosion, the alloy has a better hot corrosion
resistance. The same argument can be used to explain the better hot
corrosion resistance of the high aluminum beta alloys. In addition
to the increased stability of the beta phase, the alloys with
chromium would form less gamma prime than the unalloyed samples
according to the phase rule. The lower gamma prime content would
improve the performance of the alloys even when they are undergoing
a more extensive type of attack.

Oxidation studies of Ni-Al-Cr alloys (70,72) show that the
critical aluminum content for the formation of a pure alumina layer
during oxidation is reduced from approximately 40 a/o for the binary
to approximately 15 a/o aluminum by the addition of only 5 a/o
chromium. The improved oxidation resistance of the alloys with
chromium is attributed to the formation of a chromia layer on the
surface that restricts oxygen diffusion into the alloy. Aluminum
transport to the gas/oxide interface is enhanced. As a result, no
internal oxides form in the aluminum depleted regions of the alloy,
and the alumina layer grows at the external interface more easily. A
similar role for chromium in the hot corrosion process could explain
the increased hot corrosion resistance.

Nickel rich beta nickel aluminides can undergo a martensitic

transformation. Chatterji and Ritzer (73) showed that even minor
additions of chromium suppress this reaction. If the martensite is
less corrosion resistant than the beta phase, the corrosion
resistance of the alloy would suffer from the formation of the
martensite. The role of chromium would thus be the suppression of
the less corrosion resistant phase. No supportive evidence of the
relative hot corrosion resistance of the martensitic NiAl was
available for this hypothesis, though. Since the martensitic phase
is no longer present at the temperatures that gas turbines normally
operate, this mechanism would only be important for low temperature
applications.

Finally, the depletion of the alloy of chromium is
thermodynamically less favored than the formation of the aluminate
ion, $Al_2O_4^{2-}$. The alloy is therefore not as easily depleted of the
chromium as it is of the aluminum. The chromium may continue to
suppress the hot corrosion reaction by the various mechanisms listed
previously or simply continue to stabilize the beta phase for longer
periods of time.

3 EXPERIMENTAL PROCEDURE

A basic experimental procedure was developed for the testing of
beta nickel aluminides based on an exposure in a TGA furnace
followed by X-ray diffraction analysis of the surface phases and
optical, SEM, and electron microprobe analysis of transverse
sections. Two small changes in the basic procedure were made. A
series of samples was exposed for specific times to study the hot
corrosion mechanism, and a sample was exposed in argon to
differentiate between two possible hot corrosion mechanisms.

3.1 ALLOYS

A series of alloys were selected to test the effects of
stoichiometry, rare earth additions, and chromium on the hot
corrosion of B2 beta phase nickel aluminides. The effects of
processing were examined by comparing two alloys of the same
composition processed by both casting and powder metallurgy (P/M). A
list of the sample compositions is given in Table 2. The sample
identification numbers, nominal compositions, and exposures are
listed in Table 3.

The two basic compositions tested were beta nickel aluminides
with 45 a/o and 50 a/o aluminum content. Samples were prepared with
and without zirconium to examine the effects of the addition of a
rare earth element. To examine the role of chromium, samples with 2,
5, and 15 w/o chromium additions were cast. Aluminum contents for
the alloys were determined by assuming the chromium replaced the
aluminum in the metal lattice in a one-to-one manner. From an
examination of the tertiary Ni-Cr-Al phase diagram it can be seen
that the 2 and 5 w/o alloys are a single phase at equilibrium while
the 15 w/o alloy is a multiphase alloy containing alpha chromium.
From this it appears that the assumption that the chromium is

substituting for the aluminum is a reasonable assumption for low
chromium content alloys.

Since casting could lead to the segregation of the aluminum
and/or chromium in the samples and result in two or more phases
according to the phase diagram and conventional solidification
theory, a Ni-45 a/o Al-0.2 w/o Zr alloy was prepared from pre-
alloyed powder by P/M to examine the effects of segregation and
processing.

3.2 MATERIAL PREPARATION

Two types of samples were used, cast and P/M. The majority of
the samples used were made by casting.

Cast material was drop cast in a vacuum furnace. Titanium scrap
was cast prior to the samples to remove any oxygen remaining in the
furnace after the vacuum was established. Approximately 75 grams of
reagent grade elemental metal was used for each casting. The melt
was cast into a two inch deep chilled copper mold with a 1/2-inch
square cross section. The extra material in the melt collected on
top of the sample as a button. The button was used for the chemical
analysis of the material to determine the sample's composition. The
assumption was made that the button's composition, particularly the
gases in the button, were the same as that for the whole casting.

The P/M samples were made from pre-alloyed powder. The powder
was placed in a mild steel can, the can evacuated, and the can
welded shut. The cans were extruded in a vertical press at 1800°F to
the final diameter of 1 inch. The reduction in area was
approximately 96%. A fully dense material was assumed, and no voids
were observed in the material to indicate otherwise. The samples
were centerlessly ground to a final diameter of 1/2-inch. All the

can was removed during the machining.

Samples were machined from the stock material by Electron Discharge Machining (EDM) due to their extreme brittleness. The stock material was sectioned into two to four millimeter thick samples. A small hanger hole, typically 2-mm, was EDMed into the upper portion of samples.

All surfaces except the hanger hole were polished through 600 grit silicon carbide (SiC) paper. After polishing the samples were ultrasonically cleaned in acetone to remove any SiC particles and degrease the surfaces.

3.3 HOT CORROSION EXPOSURES

After polishing the samples were immediately weighed on a Sartorius balance with a digital readout to four or five places past the decimal point depending on the particular balance used. The samples were measured using Ultra-Cal Digital Calipers to determine the surface areas of the samples. Selected samples were pre-oxidized at 900°C in oxygen and 1200°C in air to examine the possibility that a pre-existing alumina layer would stop or slow hot corrosion of the alloys. The 900°C samples were exposed in a Thermo-Gravimetric Apparatus (TGA) vertical furnace. Oxygen was passed through the furnace tube at a rate of 400 cc/min. The samples were attached to a Cahn microbalance via a platinum chain and wire. The weight was converted into a voltage by the microbalance. A weight suppression unit allowed the initial weight of the sample and platinum chain to be removed from the signal, so only the change in weight was monitored. The weight was continuously monitored using a strip chart recorder. A Hewlett-Packard HP-85 microcomputer recorded the weight change every 30 seconds for the first 12 minutes and then every six minutes thereafter. The computer was also used to generate the

weight gain plots.

The 1200°C air oxidation samples were exposed in a box furnace with no air flow supplied. The weight of the sample was measured only at the beginning and end of the oxidation run.

The remainder of the samples were exposed in the bare metal state.

The samples were coated by spraying a saturated aqueous solution of sodium sulphate onto samples preheated on a hot plate. When the water evaporated a thin, uniform sodium sulphate layer was left on the surface of the samples. The coated samples were weighed using the Sartorius balance again to determine the weight of the sodium sulphate coating. The weight of the coating was normalized in all cases to the area of the sample's surface.

The samples were hot corroded at 900°C in oxygen using the same TGA furnace used for the 900°C pre-oxidation. Oxygen was again passed through the furnace at a rate of 400 cc/min. The weight gain was again monitored by the same methods as before. The samples were exposed until either a long time had elapsed or the weight gain exceeded the measuring capacity of the equipment. The samples were again weighed using the Sartorius balance to confirm the weight gains measured by the Cahn microbalance.

A series of Ni-45 a/o Al-0.2 w/o Zr samples from the P/M stock material were exposed for intermediate times to examine the changes in the system when dramatic changes in the weight gain rates were occurring and to determine the intermediate corrosion products in the samples. From the great uniformity of the weight gain curve shapes, it was assumed that the samples would be representative of all the nickel-aluminum and nickel-aluminum-zirconium compositions tested. For the intermediate time exposures of 5 and 30 minutes the

SO_2 content of the exit gas was measured. Problems with the
equipment did not allow accurate quantitative measurements of the
SO_2 content to be made, but qualitative observations were possible.

A single Ni-45 a/o Al-0.2 w/o Zr sample taken from the P/M
stock was exposed in argon to differentiate between the two
different hot corrosion mechanisms proposed for these materials that
are discussed in Section 5.1. Bottled argon was used for the source.
It was assumed that the argon was sufficiently dry that the oxygen
partial pressure of the argon atmosphere was essentially zero. The
furnace was flushed with argon overnight using a bottom feed for the
argon to remove any oxygen in the furnace. The sample was exposed
for 2 hours. Previous work indicated that the hot corrosion
initiated within 1.5 hour.

3.4 SAMPLE EXAMINATIONS

Samples were initially examined using an Olympus stereo
microscope with a ring light. Continuously variable magnifications
between 7.5X and 64X were available. Macrophotographs of the exposed
surfaces were taken using a Polaroid-type camera attachment.
Polaroid type 52, 56, and 57 films were used as the situation
dictated.

After the initial examination, selected samples were submitted
for X-ray diffraction analysis. Whole surfaces of the pre-oxidized
samples were used to determine the oxide phases present without
disrupting the oxide layer. Corrosion product was scraped from some
samples considered to be representative for X-ray powder diffraction
analysis. Problems were encountered when it was discovered that the
corrosion product was extremely adherent with the exception of a
thin outer layer probably corresponding to any oxide layer formed
early in the hot corrosion process. No corrosion product could be

gathered from within the blisters that formed on the sample surfaces. To obtain information about the composition of the blisters, the whole surface of some of the corroded samples were irradiated like the oxidation samples.

After all whole sample examinations had been made, the samples were cold mounted in Epoxide Resin. The cold mounting was used to preserve the corrosion product and allow easy handling of the samples. The mounted samples were cut to expose a transverse section of the sample with a corrosion site using a low speed diamond wafering blade on a Leco VP-10 diamond saw. The exposed sample surfaces were wet polished through 600 grit silicon carbide paper. Diamond paste abrasives through either 1 micron or 1/4 micron were used for the fine polishing. No alumina or chromic oxide abrasives were used to avoid contamination of the samples with outside sources of the corrosion products. Most samples were examined in the as polished condition. Some were etched using a solution of 33% acetic acid-33% nitric acid-33% water-1% hydroflouric acid as the etchant when an examination of the corrosion product's relationship with the microstructure was desired.

Optical photomicrographs of the samples were taken using a Nikon metallograph. A variety of magnifications were used as the sample dictated. Dark field microscopy did dramatically highlight the blue-green spinel phase present in the corrosion product. Some color pictures were taken of the samples to show the yellow/yellow-orange phase present in front of the corrosion interface that did not photograph well with black-and-white films.

After optical examination the samples were examined using a Amray 2000B Scanning Electron Microscope (SEM) with an EDAX X-ray spectrum analyzer for chemical analyses. The surface of the samples were coated with palladium to stop charging in the corroded areas.

Palladium was selected because of its ready availability and because the palladium X-ray peaks do not overlap the sulphur X-ray peaks like gold. Secondary electron imaging was used in almost all cases for photographing the microstructural features. Back Scattered Electron (BSE) imaging was attempted, but the microscope used did not produce good images in this mode. An accelerating voltage of either 15 kV or 30 kV was used for both the imaging and X-ray analysis of the samples. X-ray mapping of the areas photographed was used to show differences in the nickel, aluminum, and chromium concentrations. Sulphur and sodium were not readily observed using this process. Likewise the low concentration of zirconium did not allow the analysis of the distribution of this element. The X-ray spectrum analyzer was not sensitive to the oxygen X-ray wavelengths, so the distribution of oxygen could not be examined.

Finally, selected samples were analyzed using an electron microprobe (EMP) to determine the distribution of elements through the depth of a sample. The microprobe was also used to examine the changes in the chemical composition of the samples and the position of the sodium and sulphur as the hot corrosion progresses by analyzing the samples stopped at various points in the hot corrosion process. X-ray maps were also produced using the EMP since the X-ray detector was sensitive to the oxygen X-ray wavelength and the overall quality of the results were better than that available with the Amray SEM.

4 RESULTS

The results of the study are subdivided into sections dealing
with the weight gain curves, optical microscopy, scannning electron
microscopy, X-ray diffraction, electron microprobe, the sulphur
dioxide analysis of the exit gas, and the argon atmosphere exposure.

4.1 WEIGHT GAIN CURVES

The weight gain curves are presented in Figures 21 through 27.
All the weight gain curves were normalized to the sample's initial
surface area. A typical weight gain curve with the stages of hot
corrosion marked on the figure is presented in Figure 28. The weight
gain curves for the chromium containing alloys are not presented
with the exception of a Ni-15 w/o Cr-13 w/o Al-0.2 w/o Zr sample hot
corroded in the bare metal condition because the weight gain rate
was essentially constant and small. The exception did show a sudden
change in weight after a long incubation time, so the weight gain
curve is included. Additional weight gain curves are presented in
Appendix A. Weight gain curves for the samples using axes
appropriate for parabolic weight gain behavior are also presented in
Appendix A to show that the weight gain did not conform to parabolic
behavior except during the incubation stage.

It should be noted that the weight gain curves implicitly
assume that the samples are corroding uniformly. From even the most
casual examination of the samples it is obvious that this is not the
case. The samples have an attack morphology more reminiscent of
pitting. Isolated local areas are heavily attacked while adjacent
areas show little or no attack. The weight gain rates reported are
thus too low.

The weight gain curves have almost identical shapes that can be

72

described as five stages. A composite typical weight gain curve is presented in Figure 28. The stages described below are marked on the figure for easy reference. Some samples have an incubation period designated Stage I where the weight gain is identical to that for oxidation. After this incubation period the sample undergoes extremely rapid corrosion at the fastest rate of the entire process. The high corrosion rate last for only a short period of time, typicallys one half hour, and is designated Stage II. After the rapid weight gain stage, the weight gain slows to a rate approximately ten times the rate for simple oxidation for the period designated Stage III. The samples corrode at this slower rate for an extended period of time until a change in the corrosion process occurs that once again increases the hot corrosion rate significantly for the period designated Stage IV. The sample then corrodes rapidly for an extended period of time during which the majority of the damage to the sample is done. Finally, some samples show a slowing of the corrosion rate designated Stage V. Not all samples show this, but it was assumed that if the samples were exposed for extended period of time all the samples would have shown the decreased rate. The equipment constraints mentioned in the Experimental Procedure section 3.3 did not allow for the extended times in most cases.

The overall weight gains for all the samples are listed in Table 4. The rates for the weight gains are listed in Table 5. Section 5.1 contains the proposed mechanism to explain the various observed stages.

4.2 OPTICAL MICROSCOPY

Typical micrographs of the as received samples are presented in Figure 29. They show a uniform microstructure except for the chromium alloys. The unexpected homogeneity of the cast beta nickel

aluminide samples was attributed to the following mechanism. The samples solidify at approximately 1650°C with only about a 10°C difference between the liquidus and solidus temperatures for the 45 a/o aluminum alloys and a congruent melting point for the 50 a/o aluminum alloys. The samples probably solidify by dendritic growth. At least two phases, beta and gamma prime, would be present. The high temperatures allow for the rapid diffusion of the aluminum and nickel to homogenize the material. The high temperature would also aid the growth of any equiaxed grains in the material. The grains grow and replace the dendritic portion of the castings. The end result is an equiaxed beta microstructure. Some evidence exist to support this mechanism. Analysis of the alloys indicates that the grain boundaries are bowed for the zirconium containing alloys. Assuming the zirconium combines with the nickel to form small amounts of Ni_5Zr precipitates or oxygen to form ZrO_2, these precipitates would pin the grain boundaries as they grow. The resulting microstructure would be identical to the observed microstructures. The proposed mechanism was not investigated further since it is not a prime consideration of this study.

The chromium containing alloys also solidified in a dendritic manner. In the case of these alloys, though, the diffusion and homogenization process could not occur rapidly enough. It is thought that the low to moderate solubility of chromium in the beta phase and the assumed low diffusivity of chromium through the beta phase combined with the short time at elevated temperature during cool down lead to the nonhomogeneous microstructure even for the lower chromium content alloys.

Typical macrophotographs of the samples after exposure appear in Figure 30. Additional macrophotographs of the samples appear in Appendix B. The low magnification photographs indicate that the samples corroded non-uniformly. Isolated portions of the samples

corroded extensively while adjoining areas showed little visible corrosion. Near the corrosion sites the oxide layer could be seen lifting up off the sample. This would tend to expose more metal directly to the corrosive environment. Failures in the oxide layer were also closely associated with the corrosion sites as can be seen in the comparison photographs for the preoxidized samples presented in Appendix B. Where the pre-oxidized samples had a flaw in the oxide layer extensive corrosion occurred. In the areas with a good oxide layer the samples were generally not affected.

This repeated observation shows that the failure of the oxide layer is associated with the extensive hot corrosion. If the oxide layer can be improved by reducing the flaws and improving the adherence, hot corrosion could be stopped. The later observation is shown by the extremely good condition of the samples in areas with good oxide layers initially even after extended exposures.

Optical photomicrographs of the transverse sections showed some very interesting results. Typical transverse photomicrographs are shown in Figure 31. Additional optical photomicrographs appear in Appendix C. The samples have a large amount of metal left in the corrosion product. This metal appeared to be yellow/yellow-orange in color as opposed to the silver of the unaffected metal. The yellow layer extended beyond the corrosion product for some distance in advance of the corrosion interface. In the corrosion product itself, the samples showed long oxide stringers surrounding large amounts of uncorroded metal. The incorporated metal exhibited two layers corresponding to the gamma and gamma prime phases according to the electron microprobe analysis of the corrosion product. The oxides in the corrosion product also showed a layered type of microstructure. In general the outer layer of the corrosion product showed a very strong blue/blue-green color in dark field microscopy. From CRC Handbook of Physics and Chemistry (74), it was found that nickel

aluminate, $NiAl_2O_4$, had this color. It was therefore thought that the outer layers have this spinel as the corrosion product. X-ray analysis of the corroded surfaces, Section 4.4, gives results that indicate that there was a spinel similar to the nickel aluminate, but with a slightly different lattice parameter. The X-ray analysis section will deal with this phenomena in more detail. The inner region shows some minor amounts of the spinel, but the dominant corrosion product has a gray color. From optical analysis no determination could be made about the corrosion product. Microprobe analysis of the transverse sections in conjunction with X-ray mapping and X-ray diffraction analysis were used to determine all of the corrosion products at a later stage in the examination of the samples.

Macrophotographs samples that were exposed for predetermined times to trace the hot corrosion mechanism appear in Figure 32, and the corresponding transverse micrographs appear in Figure 33. As can be seen, the hot corrosion process begins in highly localized regions with minimal penetration into the material. As time progressed, the penetration into the material increased, and the oxidation shifted from external to internal. At the later stages of the hot corrosion process, the material exhibited cracking. The significance of these observations will be discussed in Section 5.1.

4.3 SCANNING ELECTRON MICROSCOPY

Typical scanning electron micrographs appear in Figure 34. Additional micrographs appear in Appendix D. Many of the micrograph have a corresponding X-ray maps for the major elements included in the figure. The secondary electron images do not show any differences from the comparable optical micrographs except that the SEM micrographs and X-ray maps show no indications of the yellow-orange layer observed in the optical micrographs.. This is most

likely attributable to the layer having a compositional difference
that could not be detected by the SEM. The back scattered electron
image does show the corrosion product more distinctly, but it too
misses the yellow-orange layer. The reason for this is not well
understood as the imaging method is designed to detect compositional
differences. The most likely explanation available is that the
problems associated with the poor imaging quality for this method
did not allow the discrimination of the small compositional
difference in the material.

X-ray mapping was useful since it showed a good anti-
correlation between nickel and aluminum in the corrosion product.
Comparisons between the micrographs indicate that the corrosion
product is nickel rich. From this nickel oxide was expected as the
corrosion product in the inner regions of the sample. This is in
contrast to Pettit's work (67) which indicated that the corrosion
product in low partial pressures of oxygen such as would occur in
the interior of the sample would be alumina, Al_2O_3.

4.4 X-RAY DIFFRACTION

The results for the X-ray diffraction analysis of the samples
is listed in Table 6. The samples marked as powder for the analysis
method were analyzed by either scraping a small amount of corrosion
product from the surface or using some of the scale which dropped
off the sample during handling. It should again be noted that the
corrosion product proved to be extremely adherent and, other than a
thin outer scale, could not be removed even when scraped with a
stainless steel spatula. The samples marked diffractometer for the
analysis method were analyzed by irradiating large portions of the
surface of the sample in a diffractometer. The position of the
phases analyzed would be dependent on the corrosion products. Thin
oxide scales would allow for penetration into the underlying metal.

Thick corrosion scales would stop the X-rays in the scale and not allow any X-rays to reach the deeper portion of the scale or the underlying metal. From the observed Ni-Al phases in the diffractometer results, it appears that in most cases the corrosion product did allow penetration to at least the depth of the incorporated metal and possibly all the way to the aluminum depleted but not corroded metal. The precise position of the phases was not considered critical for this method of analysis since the position of the phases would be determined by electron microprobe analysis of transverse sections after sectioning.

The most significant result of the X-ray diffraction data is the change from the formation of alumina in the oxidized samples to the formation of nickel oxide in the hot corroded samples. The alumina in the hot corrosion samples is nonexistent or minimal during the early stages of hot corrosion. From this it must be concluded that the aluminum activity in the metal is reduced, possibly by the depletion of the aluminum by the formation of the oxides detected by the X-ray diffraction analysis. Also of note is the presence of delta alumina in the samples that were only oxidized. The delta form of alumina will eventually transform to the alpha phase. The transformation can generate stresses that will rupture the oxide scale and cause the premature failure of the oxide scale. This could in part explain the sudden failure of the oxide scale and the ensuing rapid hot corrosion.

The X-ray diffraction data indicates that the sodium sulphate remains on the samples even after extended periods of time. The form present is listed as Form V in the X-ray powder diffraction file. The sodium sulphate sample taken from the chromium bearing sample showed no chromate present despite the strong yellow coloration. It is hypothesized that the volatile chromate reached a steady-state concentration in the sodium sulphate that was too low for the X-ray

diffraction method to detect it. The presence of an unidentified second phase lends some credence to this idea.

It should also be noted that the chromium containing alloy oxidized at 900°C contained only alpha alumina in the scale as predicted by Giggins and Pettit (70).

One of the more interesting results of the X-ray diffraction analysis was the identification of a spinel with a lattice parameter of approximately 8.10 angstroms. From the optical microscopy portion of the investigation, the nickel aluminate spinel was expected. The lattice parameter of the nickel aluminate is 8.034 angstroms (74). This is close to the observed lattice parameter, but sufficiently different that experimental error can not explain the discrepancy. Also, the spinel tends to form a range of spinels with lattice parameters of at least 8.10 angstroms. No positive proof exists as to why the spinels have such a large lattice parameter, but all the analysis done on the samples indicates that the spinels are rich in nickel and aluminum. This indicates that the spinal should be based on the nickel aluminate spinel. The two most likely explanation are that something is substituting for the nickel, aluminum, or oxygen that expands the lattice parameter or additional atoms are present in the spinel as interstitials and increase the lattice parameter. No detailed study of the spinel was conducted, so the true reason for the increased lattice parameter cannot be ascertained at this time.

4.5 ELECTRON MICROPROBE

Electron microprobe analysis was performed for samples exposed for extended periods of time with 45 a/o and 50 a/o aluminum and the 15 w/o chromium sample. In addition the samples exposed for intermediate times were also analyzed. An analysis was done for

nickel, aluminum, chromium, zirconium, sodium, sulphur, and oxygen as was appropriate. The results are shown in Figure 35. Additionally secondary electron and back scattered electron images and X-ray maps of the areas probed are presented in Figure 36.

The results for the electron microprobe were not what was anticipated from prior literature and the other results of this study. Analysis of the exposures of 5 and 30 minutes indicates that the 45 a/o aluminum sample has no detectable depletion of aluminum at the corrosion interface. This is in contradiction with the optical work that suggests a depleted zone. The intermediate time exposures for the 45 a/o aluminum samples do show a definite aluminum depleted zone near the interface. This depletion is sufficient to form significant amounts of gamma prime.

Analysis of the 50 a/o aluminum alloy exposed for an extended length of time is not consistent with the 45 a/o aluminum results. There is a depleted zone, but only to about 43 a/o aluminum. This aluminum level is significant because at 900°C, the phase boundary between beta and beta plus gamma prime is 43 a/o aluminum. The depleted region was expected to have a minimum aluminum content of approximately 25 a/o aluminum, the aluminum content of gamma prime. Also, the shape of the aluminum and nickel concentration profiles are unusual. The curvature of the curves can be described as concave while the expected curvature for a diffusion controlled transfer of matter to the interface would be S-shaped. Four separate profiles were done on the sample and all four profiles were consistent with one another in terms of the shape of the curve and the observed levels of nickel and aluminum. The data is also self consistent within each profile with the nickel and aluminum curves mirroring each other. Based on this, the results must be considered accurate. Unfortunately this strange curvature can not be explained on diffusion alone. An additional process must have been acting on the

sample that was not directly observed in this experiment. No
reasonable explanation to identify this process could be formulated.

The 15 w/o chromium alloy exposed for an extended time showed a
wide scatter in the data consistent with alpha chromium precipitates
being present in the metal as predicted from the phase diagram. The
samples also showed a depleted zone of both aluminum and chromium at
the corrosion interface. The depletion of chromium and aluminum at
the interface indicates that these elements are being preferentially
oxidized as expected. The remaining material is becoming enriched in
nickel. As a result gamma prime forms in the depleted zone.

The presence of sulphur and in some cases sodium was monitored
to determine if sodium sulphate penetrated the scale and if
sulphides formed at the interface. The X-ray maps and electron
microprobe results strongly indicate that the materials form
discrete sulphides at the interface. The presence of sodium in some
regions of the scale indicates that at least some sodium sulphate is
incorporated into the material. Whether it becomes mixed with the
scale as a result of a fluxing action or if it enters the scale
through cracks in the scale could not be determined from these
results.

While zirconium was monitored in several cases, in most
instances no detectable concentrations of zirconium above the amount
expected from a complete solid solution of the zirconium in the
material could be detected. In one instance there was a zirconium
peak corresponding to a sulphur peak. This indicates that some
zirconium-sulphur compound may for during the hot corrosion process.
Since only this one peak was observed, the zirconium data was
removed from the plots for easier analysis of the data. Typically
the level of zirconium was near 0.2 w/o.

C-2

The analysis of oxygen in the material indicates that, as
expected, the scale is primarily oxides with some incorporated metal
and sulphides, and little oxygen penetrated into the material to
form internal oxides. In the few cases where the oxygen level was
somewhat high in the material it is believed that the microprobe was
hitting both metal and oxide. The small but consistent oxygen level
in the material in the uncorroded material is easily attributed to
the oxidation of the cut surface and not an actual oxygen pickup
during corrosion.

4.6 SULPHUR DIOXIDE CONTENT OF THE EXIT GAS

The exit gas of the 5 and 30 minute hot corrosion tests was
analyzed using a pulsed florescent analyzer. It was discovered after
the fact that the values obtained were not accurate. The qualitative
trends observed were determined to be accurate by alternative
observations of the response of the values to the introduction of
SO_2. The observed trend was the evolution of SO_2 at the highest rate
when the sample was corroding at the greatest rate, specifically
early in Stage II. It was also observed that a large amount of SO_2
was evolved on cool down. It was felt that this corresponded to the
release of the SO_2 dissolved in the liquid sodium sulphate when it
solidified. The temperature of the sample when the SO_2 was evolved
was not noted at the time.

4.7 ARGON ATMOSPHERE EXPOSURE

The sample exposed in argon exhibited no hot corrosion. No
weight change was observed and no phase other than beta nickel
aluminide and sodium sulphate was detected using X-ray diffraction.
Optical examination also did not reveal any hot corrosion. The
sodium sulphate was still visible on the surface after the exposure.

5 DISCUSSION

From the results obtained in this study, a mechanism was developed to explain the hot corrosion process for the beta nickel aluminides. The observed effects of additions of zirconium and chromium are examined in light of the proposed mechanism. The role of aluminum is examined separately as an effect of stoichiometry and aluminum depletion at the surface. Finally, the results obtained and the proposed mechanism are compared to previous work done on the beta nickel aluminides.

5.1 MECHANISM OF HOT CORROSION OF B2 NICKEL ALUMINIDES

The mechanism for the hot corrosion of the B2 nickel aluminides is not a simple one. Rather it is a complex interaction between several competing and cooperative processes. The following mechanism is proposed to explain the total process and indicate which processes are important. The proposed mechanism also allows for easy modification to allow for the presence of other phases and processes not observed in this study.

Stage I of the hot corrosion of the beta nickel aluminides is the oxidation of the surface of the sample. The oxygen dissolved in the sodium sulphate layer and the oxygen that diffuses through the sodium sulphate reacts with the sample to form a continuous, protective alumina layer. The weight gain of the sample is thus governed by the parabolic growth law. In the samples that do not show a Stage I, it is assumed that the activity of the aluminum in the alloy is too low to form the alumina layer under the test conditions. These samples immediately undergo Stage II hot corrosion.

The samples that do exhibit a Stage I remain in Stage I until the protective alumina layer is compromised. Possible reasons for the failure of the protective alumina layer are numerous. Growth stresses in the alumina layer could lead to cracks in the alumina layer. The cracks would in turn allow the sodium sulphate direct access to the underlying

83

failure of the protective alumina layer are numerous. Growth stresses in the alumina layer could lead to cracks in the alumina layer. The cracks would in turn allow the sodium sulphate direct access to the underlying metal. The correspondence between the cracked areas in the pre-oxidized samples and subsequent hot corrosion sites strongly indicates that this mechanism is operative.

Another possible contributing process is the transformation of the delta alumina to alpha alumina in the presence of sodium sulphate may lead to a nonprotective oxide layer. Fluxing of the alumina layer may occur if the sodium sulphate reacts with the alumina layer. Spalling of the oxide may also occur. The formation of vacancies in the underlying metal by the beta to gamma prime transition may cause decohesion of the oxide layer if the vacancies move to the oxide/metal interface and form voids. The swelling of the metal because of either the formation of internal oxides or the beta to gamma prime transition may also crack the oxide layer. The compromise of the oxide layer after extended periods of time is particularly damaging as the metal can become depleted in aluminum because of the oxidation of the metal.

For the pre-oxidized samples, it is assumed that they are subject to the same mechanisms for the failure of the oxide layer as the alloys that exhibit a Stage I. The pre-existing alumina layer acts as a barrier between the sodium sulphate and the metal. When the alumina layer is compromised, the sodium sulphate gains access to the metal and hot corrosion proceeds in much the same manner as it would if no alumina layer was present initially. It should be pointed out that the presence of these crevices in the oxide layer where the corrosion is actually occurring can lead to a crevice effects and major changes in the salt chemistry in the crevice. The most likely change is an increased sulphur activity and decreased oxygen activity. The decreased oxygen activity may affect the oxidation process, but the extremely low oxygen partial pressure necessary for the formation of

alumina would indicate that alumina has a good chance of forming. The high sulphur activity combined with the lowered oxygen activity could, however, lead to the formation of stable sulphides. Since this study did not seek to examine the crevice chemistry and local conditions, this question can not be answered at this time. It is a point to be considered in future experiments of this type.

Stage II begins when the protective alumina layer is compromised. For samples that do not exhibit a Stage I, Stage II begins directly because a continuous oxide layer cannot form and the aluminum activity is low. These two conditions combine to create an imperfect oxide layer that is immediately compromised. What alumina does form is spotty in nature and is immediately undercut by the corrosion of the underlying metal.

Since the hot corrosion occurs only in the areas where the oxide fails, the hot corrosion is confined to local sites. Since Stage II lasts only 30 to 45 minutes, diffusion in the bulk metal is too slow to contribute to the local conditions during the hot corrosion process by transporting new material, particularly aluminum, from within the metal to the surface. Diffusion along grain boundaries which would be faster than that of the matrix may have some effect, but the relatively small fraction of grain boundaries in the material makes the contribution by diffusion negligible.

X-ray diffraction of the entire sample surface indicates the presence of the nickel sulphide Ni_7S_6 in the surface scale during the beginning and end of Stage II. The thickness of the corrosion scale as observed from the transverse sections indicates that the X-rays should have penetrated most if not all of the corrosion scale. It is therefore assumed that the dominant sulphide in the corrosion product is Ni_7S_6. The other nickel sulphides and aluminum sulphides were also considered. The lack of any supporting evidence for their existence in

the corrosion product tends to indicate that they are minor phases if present. A problem exist with this assumption. Ni_7S_6 decomposes at 833 K, 340°C below the test temperature. This means that the sulphide must be formed on cool down. Since it is unlikely sulphur was absorbed into the scale from the sodium sulphate, particularly after the sodium sulphate solidified, the sulphide present at temperature must have a higher sulphur content, or a mixture of sulphides with the same net sulphur content is present in the scale. Ni_3S_2 and NiS are both possible candidates. The Ni_3S_2 is a particular concern since this sulphide is liquid at the test temperature. Since no definitive data exists to show which sulphide is present at temperature, Ni_7S_6 will be used in the development of the mechanism to represent the overall reaction.

X-ray diffraction of the surface also indicates the presence of two oxides, an orientated alumina that is associated with the normal growth of the alumina layer on the beta nickel aluminide and large amounts of nickel oxide. The presence of nickel oxide in the corrosion product was confirmed by the electron microprobe of the corrosion product. From the work done by Pettit (67), the nickel oxide would form only in very high oxygen partial pressures or low aluminum activities. Since all portions of the sample were exposed to approximately the same partial pressure of oxygen and only local portions of the samples showed the presence of nickel oxide, the conclusion must be made that the aluminum activity in the local regions affected must be lowered in some manner. Examination of the X-ray diffraction pattern does indicate the presence of gamma prime as well as beta nickel aluminide. Electron microprobe also indicates no depletion of aluminum at the corrosion interface though. If discrete gamma prime regions are formed locally that are either not in equilibrium with the beta, likely because of the inability to diffuse aluminum rapidly enough, or depleted in aluminum sufficiently to move away from the two phase region and into the single phase gamma prime

region, the activity of the aluminum can be lowered several orders of magnitude (67). The lowering of the aluminum activity may have major effects on the oxidation mechanism of the sample as pointed out in Section 5.2. The change to an internal oxidation mechanism may in fact help initiate Stage II. Since few if any internal oxides were observed, the internal oxidation of the metal can probably be ignored. A large aluminum gradient in the region immediately adjacent to the surface would also tend to limit the depth of internal oxidation as the aluminum activity would rapidly rise to a value greater than the maximum for internal oxidation.

Unfortunately, the electron microprobe data for the cross section of the samples undergoing Stage II corrosion do not support this hypothesis. Some depletion of the aluminum at the corrosion interface is observed, but not nearly as much as would be expected for the formation of gamma prime. No truly good explanation exists for this. The electron microprobe used standards that have in the past consistently produced aluminum contents in good agreement with the values obtained by other means such as wet chemistry. A small difference of a few weight per cent would be reasonable, but the difference between beta and gamma prime is approximately 15 w/o. Experimental error can be ruled out. The aluminum level recorded by the electron microprobe is significant in that it corresponds to the phase boundary between beta and beta plus gamma prime at 900°C. It is felt that this is not a chance occurrence, but the meaning of this could not be divined. The best hypothesis is that any gamma prime that forms is immediately attacked. Since it is attacked so rapidly, the amount of gamma prime present at any given time is miniscule and could not be detected by the methods used. Some credence for this idea is given by the kinetics of Stage II which are extremely rapid, especially when normalized to the actual area undergoing attack.

The analysis of the sulphur dioxide content of the exit gas

during Stage II showed that the greatest amount of sulphur dioxide was generated during the fastest rate of weight gain. This indicates that the corrosion process is using sodium sulphate, the only source of sulphur. The sudden release of large quantities of sulphur on cool down indicates that SO_2 is trapped in the sodium sulphate and released on solidification due to the decreased solubility of the solid phase.

From the X-ray diffraction data, the micrographs of the transverse sections of the samples, the reported diffusivities for the aluminum, the changes in the sulphur dioxide content of the exit gas, and the electron microprobe analysis of the samples, two possible mechanisms for Stage II of the hot corrosion of beta nickel aluminides under the test conditions were proposed. The first mechanism is based on the assumption that the aluminum activity of the local region must be lowered to form the nickel sulphide and nickel oxide. This is accomplished by the removal of the aluminum as an oxide which in turn results in the formation of discrete gamma prime regions with significantly lower aluminum activities. It was also assumed as most other researchers in the past have assumed and/or shown that the sulphide will form first in a low oxygen potential region and than be subsequently oxidized as oxygen diffuses inward to the sulphide and reacts to form an oxide and sulphur. The presence of the sulphur dioxide in the exit gas was explained by the oxidation of the sulphur generated in the reaction. Sulphur dioxide is assumed to diffuse both inward and outward, but the low diffusivity of elements in the beta phase leads to the assumption little inward movement of sulphur would be possible. Rather the outward diffusion of the gas through the liquid sodium sulphate layer dominates. Even so, the sulphur dioxide does have a definite if short residence time at the metal/oxide/sodium sulphate interface which probably increases as oxides begin to form and move into the sodium sulphate. An increasing probability exists that the sulphur dioxide will react with the metal and produce a sulphidation/oxidation type of attack. It is assumed for the same

reasons stated earlier that the aluminum activity must be lowered for the metal to be sulphidized, so the sulphur dioxide is assumed to react with the gamma prime instead of the beta. The five steps envisioned in this mechanism are:

Step 1 $3 \text{ NiAl} + 3/2 \text{ O}_2 = \text{Ni}_3\text{Al} + \text{Al}_2\text{O}_3$

Step 2 $14 \text{ Ni}_3\text{Al} + 36 \text{ Na}_2\text{SO}_4 = 6 \text{ Ni}_7\text{S}_6 + 7 \text{ Al}_2\text{O}_3 + 36 \text{ Na}_2\text{O} + 87/2 \text{ O}_2$

Step 3 $\text{Ni}_7\text{S}_6 + 19/2 \text{ O}_2 = 7 \text{ NiO} + 6 \text{ SO}_2$

Step 4 $14 \text{ Ni}_3\text{Al} + 36 \text{ SO}_2 = 6 \text{ Ni}_7\text{S}_6 + 7 \text{ Al}_2\text{O}_3 + 51/2 \text{ O}_2$

Step 5 $\text{Ni}_7\text{S}_6 + 19/2 \text{ O}_2 = 7 \text{ NiO} + 6 \text{ SO}_2$
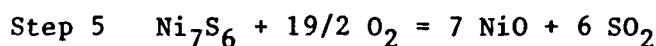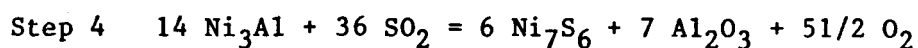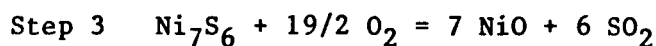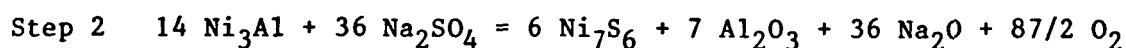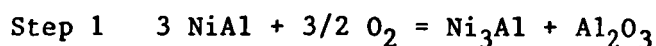
The last two steps have a balanced use/generation of SO_2, so as long as Ni_3Al is present and oxygen can reach the metal/sodium sulphate interface, the reaction will repeatedly cycle through steps 4 and 5. Since the assumption has been made in the mechanism that the aluminum activity is low enough that the oxidation of any of the beta phase will produce gamma prime and oxygen is readily available initially from either dissolved oxygen or the oxygen diffusing through the sodium sulphate, gamma prime will be produced in relatively large amounts. A lack of gamma prime for step 4 is thus not considered likely in the early portion of Stage II. At the end of Stage II the oxygen partial pressure has dropped sufficiently from the consumption of the oxygen in the melt and the lack of enough oxygen diffusing through the sodium sulphate layer to sustain the necessary oxygen partial pressure for oxidation to stop the oxidation reactions.

The high weight gain for the system can be explained by examining the weight gain per molecule of NiAl consumed for the reaction steps. If one assumes that the total reaction goes from step 1 to step 5 with

all the steps going to completion, the net reaction would be

$$42 \text{ NiAl} + 87/2 \text{ O}_2 + 18 \text{ Na}_2\text{SO}_4 = 21 \text{ Al}_2\text{O}_3 + 42 \text{ NiO} + 18 \text{ Na}_2\text{O} + 18 \text{ SO}_2$$
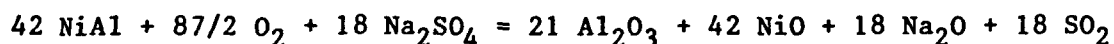
which gives a modest increase of approximately 5.7 amu per molecule of
NiAl reacted. This increase can not explain the extremely high weight
gain rate observed. If one assumes as stated before that the extent of
step 1 is sufficient to supply an unlimited amount of gamma prime to
step 4, the net reaction for each cycle, step 1 to step 4 to step 5
with the SO$_2$ recycled back to step 4, is

$$42 \text{ NiAl} + 105/2 \text{ O}_2 = 21 \text{ Al}_2\text{O}_3 + 42 \text{ NiO}$$
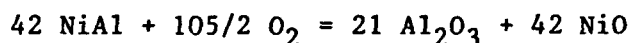
which gives an increase of 40 amu per molecule of NiAl reacted. This
is an increase of a factor of 7 in the weight gain per molecule of
NiAl reacted compared to the last reaction. The cyclic reaction is
thus the cause of the high weight gain rate.

The reaction continues until the SO$_2$ is lost to the atmosphere by
diffusion before the SO$_2$ can react or the oxygen is exhausted.

The most important observations about the reactions for this
mechanism is that they require oxygen to be initiated, and they turn
the remaining sodium sulphate basic as the sodium oxide remains in the
sodium sulphate layer and the sulphur dioxide diffuses outward into
the atmosphere. The requirement for oxygen from the atmosphere to
start the hot corrosion mechanism is in direct contrast to the second
mechanism.

The premise for the second mechanism is that the activity of the
aluminum in the alloys was sufficiently low that the beta nickel
aluminide could react directly with the sodium sulphate, and no
reaction to form gamma prime was required. From this variation the

second mechanism was generated. The four steps for this mechanism are:

Step 1 $7 \text{ NiAl} + 6 \text{ Na}_2\text{SO}_4 = \text{Ni}_7\text{S}_6 + 6 \text{ Na}_2\text{O} + 7/2 \text{ Al}_2\text{O}_3 + 15/2 \text{ O}_2$

Step 2 $\text{Ni}_7\text{S}_6 + 19/2 \text{ O}_2 = 7 \text{ NiO} + 6 \text{ SO}_2$

Step 3 $7 \text{ NiAl} + 6 \text{ SO}_2 = \text{Ni}_7\text{S}_6 + 7/2 \text{ Al}_2\text{O}_3 + 3/2 \text{ O}_2$

Step 4 $\text{Ni}_7\text{S}_6 + 19/2 \text{ O}_2 = 7 \text{ NiO} + 6 \text{ SO}_2$
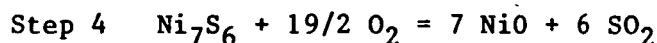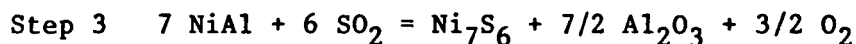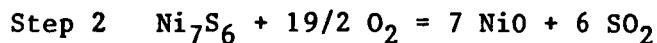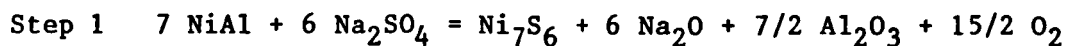
As with the first mechanism, the last two steps, step 3 and step 4, are cyclic in nature and have a balanced use/generation of SO_2. If one assumes again that all the reactions go to completion as before the first time through the mechanism the net reaction is

$$14 \text{ NiAl} + 6 \text{ Na}_2\text{SO}_4 + 12 \text{ O}_2 = 7 \text{ Al}_2\text{O}_3 + 14 \text{ NiO} + 6 \text{ Na}_2\text{O} + 6 \text{ SO}_2$$
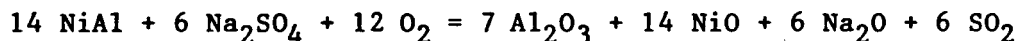
which gives no increase in the weight of the system. The cyclic reactions would have a net reaction of

$$7 \text{ NiAl} + 8 \text{ O}_2 = 7/2 \text{ Al}_2\text{O}_3 + 7 \text{ NiO}$$
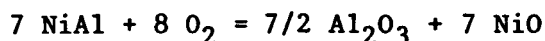
and would increase the weight of the system by 37.6 amu per molecule of NiAl reacted. Again, the large weight increase comes from the cyclic reactions rather than from the initial reaction of the metal with the sodium sulphate.

Since both mechanism give a substantial weight gain, another method had to be selected to differentiate between the two mechanisms. The second mechanism does not require any oxygen to initiate the hot corrosion while the oxidation of the beta phase is critical to the first mechanism. Because of this difference in the two mechanisms, it was decided to expose a sample in 1 atmosphere argon to see if the

removal of oxygen changed the hot corrosion kinetics and the corrosion products. If the beta phase reacts directly with the sodium sulphate as postulated in the second mechanism, nickel sulphides would be formed and a small weight loss via loss of O_2 from step 2 and SO_2 from step 3 would be expected. If the sodium sulphate cannot react directly with the beta phase as postulated in the first mechanism, no weight change and no nickel sulphide would be detected. The results of the argon atmosphere exposure were that there was no weight change and no nickel sulphides could be detected at the surface using X-ray diffraction analysis. It must be noted though that the X-ray diffraction method does not detect extremely small quantities of phases, so if the reactions did not proceed very far due to the lack of oxygen some nickel sulphide could be present and undetected. The lack of any weight change as measured with a microbalance capable of detecting changes in weight of less than 0.1 mg/cm^2 gives strong supportive evidence though that no nickel sulphide was present. These results strongly indicate that the first mechanism alone is operative and that a non-equilibrium condition with a decreased aluminum activity at the surface or the establishment of an aluminum depleted zone at the surface must be obtained for the beta nickel aluminides to undergo hot corrosion.

It must be noted that while the reactions are written as the metal reacting directly with the sodium sulphate, many researchers prefer to represent the reaction between the metal and sodium sulphate as the dissociation of the sodium sulphate into Na_2O and SO_3. The SO_3 then reacts with the metal in the sulphidizing reaction in step 2 for the first mechanism and step 1 for the second mechanism. As the SO_3 is removed from the sodium sulphate, the equilibrium shifts to create more SO_3 and Na_2O. The sodium sulphate becomes enriched in Na_2O as before, and sulphur is readily supplied. Rewriting the proposed mechanism for Stage II in this format gives the steps

Step 1 $3\ NiAl + 3/2\ O_2 = Ni_3Al + Al_2O_3$

Step 1a $Na_2SO_4 = Na_2O + SO_3$

Step 2 $14\ Ni_3Al + 36\ SO_3 = 6\ Ni_7S_6 + 7\ Al_2O_3 + 87/2\ O_2$

Step 3 $Ni_7S_6 + 19/2\ O_2 = 7\ NiO + 6\ SO_2$

Step 4 $14\ Ni_3Al + 36\ SO_2 = 6\ Ni_7S_6 + 7\ Al_2O_3 + 51/2\ O_2$

Step 5 $Ni_7S_6 + 19/2\ O_2 = 7\ NiO + 6\ SO_2$
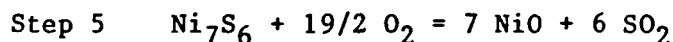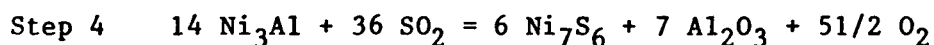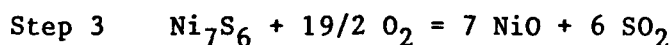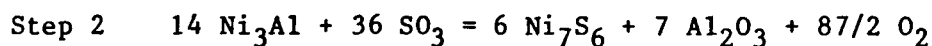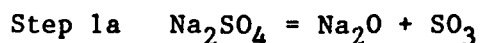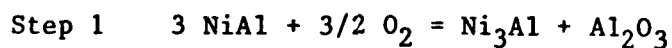
As a result of the Stage II hot corrosion mechanism, the sodium sulphate layer is turned basic and basic fluxing could occur. The layered texture of the oxides are assumed to support this idea though the alternative explanation that the oxides were undercut, broke off, and floated into the sodium sulphate melt could also explain this morphology. The basic fluxing compounds the problem of hot corrosion by making the oxides that form in the corroded areas unprotective.

Stage III may be the most important part of the hot corrosion process. Several processes are believed to be operative during this stage, all of them detrimental. From the optical transverse sections it is observed that an orange layer or layers forms beneath the oxide layer and the corrosion layer. From X-ray diffraction this layer was identified as gamma prime nearest the unaffected metal and gamma nearest the surface assuming the greatest depletion of aluminum nearest the corrosion interface. The gamma layer was not always observed using X-ray diffraction, but was usually present in the longer term exposures. This is also in agreement with the results obtained by Kaufman (55). The gamma and gamma prime can only form if the flux of aluminum outward at the surface to form the oxide scale is greater than the flux of aluminum diffusing to the surface from the

interior of the sample. A more detailed discussion of this is given in Section 5.2. With the formation of the depleted region, the oxidation mechanism turns from a protective external oxide to a nonprotective internal oxide. The internal oxides extend over a hundred micrometers into the interior of the sample. The internal oxides and the gamma and/or gamma prime formed underneath the oxide layer have a greater specific volume than the beta that they replace. As a result the oxide layer is further disrupted by the cracking and lifting of the oxide layer. Basic fluxing of the oxides at the surface further disrupt the oxide layer and promotes rapid corrosion.

During the Stage III to Stage IV transition localized areas of corrosion extending considerable distances into the unaffected beta metal are acting much as a wedge used for splitting logs. The larger volume of gamma prime and spinel/oxides that replace the beta in the sample results in considerable tensile and shear stresses underneath the corrosion sites in the unaffected metal. The problem is compounded by the presence of internal oxides that concentrate the stresses and lower the load carrying area of the metal and the rough oxide/metal interface that acts as a series of notches. This tends to split the metal much as the wedge splits the log. The problem is aggravated by the moderately low ductility of the metal even at 900°C, allowing easy crack growth once the crack initiates. The material may also be notch sensitive and have a low value for K_{IC} though no data on the system at temperature was available. During the transition in mechanisms considerable amounts of new surface area is exposed.

During testing the observation was made that the sodium sulphate wet the surface extremely well and tended to flow into cracks. The sodium sulphate may cause embrittlement of the material near the crack tip by the sulphidation mechanism given in the Stage II mechanism. With the embrittlement of the crack tip, the crack would tend to advance great distances into the sample easily. Even more crack

surface would be exposed than in the simple oxidation of a crack in beta nickel aluminide samples. The presence of sulphides at the interface even at long times as shown by the electron microprobe and X-ray maps supports this idea.

In Stage IV the major operative processes are the oxidation of the metal exposed by cracking, the propagation of the cracks, and the oxidation of the metal incorporated into the corrosion layer. Lose of the protective oxide layer by decohesion or swelling in the areas near the hot corrosion sites is also a contributing factor, but the area involved in comparison to the other processes makes it a secondary process. As stated previously, the area exposed by the cracking of the metal is oxidized readily. The oxidized metal forms an oxide that has a greater volume than the metal being oxidized. As a result the crack is forced open and stresses in the metal are generated. This is similar to the process in the Stage III to Stage IV transition, but there is an important difference. Now the stresses are acting on a pre-existing crack. The stresses generated act to propagate the crack deeper into the material, exposing more new surface to be oxidized in turn. The controlling processes for Stage IV are the transport of oxygen to the crack surfaces and the propagation of the cracks. As can be readily seen, the process will continue so long as oxygen can reach the metal and oxidize it or, in the extreme case, a sample remains.

In addition to the oxidation of the crack surfaces, the metal incorporated in the corrosion layer is being oxidized by oxygen diffusing through the corrosion product. The oxidation contributes to the weight gain for the sample and also helps to continue applying stress to the metal. The stresses generated may also be responsible for the observed ruptures in the corrosion product that allows oxygen direct access to the underlying metal.

Internal oxidation of the metal beneath the corrosion product and

adjacent to the cracks is also observed in this stage. It is assumed that the aluminum activity in these regions is sufficiently low that internal oxidation can occur. The oxygen is assumed to be supplied via diffusion through the cracks and the corrosion product. The connecting of the internal oxides and the oxides in the cracks is assumed to generate the observed transverse morphologies.

Stage V is characterized by a slowing of the corrosion rate. This stage was not observed in all cases. The equipment limitations previously mentioned in Section 3.3 were primarily responsible for not observing Stage V in most samples. It is is assumed that the samples would have all exhibited a Stage V if sufficient time was allowed providing the samples were large enough to remain intact all through Stage IV. The decrease in the weight gain rate for all the samples at long times is strong supportive evidence for this hypothesis. The slowing of the weight gain rate is assumed to be caused by the consumption of any remaining sodium sulphate and the lengthening of the diffusion path for oxygen. Blunting of the crack tip due to oxidation at the tip prior to the advancement of the crack may also help slow the kinetics of the corrosion. The presence of more metal in the corrosion product also tends to exhaust the oxygen in the corrosion product as it is used up to oxidize the incorporated metal rather than oxidize the metal at the corrosion product/metal interface. With the reduction of the oxygen reaching the interior of the sample and the formation of a thick corrosion layer, the weight gain rate decreases. Eventually the material would theoretically reach the weight gain rate for the protective alumina as the oxygen partial pressure at the interface is lowered to the point where only the alumina can form, and all the incorporated metal is oxidized completely.

5.2 ALUMINUM DEPLETION

During Stage III and Stage IV of the hot corrosion process, aluminum is depleted at the surface of the samples and in the metal incorporated in the corrosion product as shown by the optical micrographs and the electron microprobe analysses of the cross sections. The preferential oxidation of the aluminum because of its high affinity for oxygen leads to this loss of aluminum. The depletion of the aluminum leads to three effects; a change in the phase(s) present, an increase in the diffusion rate for elements in the aluminum depleted region, and a change in the oxidation process.

In simple oxidation the alloys show a uniform aluminum content through the thickness of the sample (72). The very slow oxidation kinetics allow for the diffusion of aluminum through the sample to remove any aluminum gradient at the surface. As a result, the alloys undergo a uniform aluminum loss during the oxidation process with no significant aluminum gradients being established in the sample. In hot corrosion a distinct aluminum gradient is observed because the removal of the aluminum at the surface is faster than the diffusion of aluminum from the interior of the sample to the surface. The aluminum level at the surface will decrease to such a point that the beta phase will no longer be stable, and the surface region will transform to gamma prime. The interior regions of the sample will still have a high aluminum content and will remain beta. Further oxidation of the surface will lead to the transformation of the gamma prime to the gamma phase. These transformations are important because the gamma prime and the gamma phase have higher oxidation rates (67).

The high rate of aluminum consumption at the surface is caused by the manner in which the samples are hot corroded. During Stage II sodium oxide, Na_2O is generated by the reaction of the gamma prime

97

with the sodium sulphate. The sodium oxide is actually present as Na^+ and O^{2-} ions dissolved in the liquid sodium sulphate melt. The oxide ions react with the alumina to basically flux the alumina (Section 2.1.2.1). The fluxing of the alumina prevents the formation of a protective oxide layer. The lack of a protective oxide layer means that the weight gain rate will remain high. With the high rate of aluminum consumption at the surface and slow diffusion of aluminum through the beta phase, the aluminum concentration of the surface region falls rapidly, and phase changes ensue. The transformation of the beta phase to gamma prime and gamma was confirmed by X-ray diffraction and electron microprobe of the late Stage III and Early Stage IV samples.

As the beta phase transform to gamma prime, vacancies are created (55). These vacancies can disrupt the oxide layer adhesion by migrating to the metal/oxide interface and coalescing as voids. The coalescence of vacancies as voids at the metal/oxide interface was not directly observed in this study as transmission electron microscopy of the oxide at the metal/oxide interface was not done. SEM observations did indicate the presence of voids in the corrosion product and material. Based on this, the decohesion of the alumina layer at the metal/oxide interface cannot be discounted. The vacancies have a more important role in the corrosion process, though.

With the transformation of the beta phase to gamma prime and the generation of vacancies in the process, the specific volume of the material changes. The gamma prime and voids formed have a greater volume than the beta that they replaces (55). As a result the material swells. The swelling induces stresses in the oxide layer that leads to the oxide layer cracking. Figure 37 shows this phenomena particularly well. The cracked oxide is no longer protective since the sodium sulphate comes into contact with the

gamma prime phase. Rapid corrosion ensues. While this mechanism may
be operative in these samples, the formation of internal oxides is
actually more likely to cause the observed swelling as will be
explained later.

As the gamma prime and gamma phases form in the surface region
of the sample, the diffusion of aluminum through the depleted region
is believed to increase. The diffusivities of aluminum through the
gamma, gamma prime, and beta phases are not directly measurable
since the longest lived radioactive isotope of aluminum has a half-
life of only 11 minutes (76). Some data has been generated by
Janssen (77) for the temperature range of 1000°C to 1300°C with
experiments to determine the ratios of the intrinsic diffusion
coefficients of nickel and aluminum at 1000°C. These results indicate
that the diffusivity of aluminum increases with decreasing aluminum
content. This is probably related to the increase in disorder of the
crystal structure with decreasing aluminum content.

Since the aluminum is rapidly consumed at the surface and the
depleted regions have higher aluminum diffusivities that allow rapid
transport of the aluminum to the surface, the depleted regions move
inwards rapidly. It is inferred that the diffusivities of oxygen and
sulphur also increase as the material becomes more disordered. The
increased diffusivities of these reactants allow more rapid movement
of the reactants into the sample.

Finally and most importantly, as the material undergoes
aluminum depletion and phase changes, the oxidation mechanism shifts
from an external alumina oxide to nickel-aluminum spinel and/or
nickel oxide as shown by Pettit (67). The spinel and nickel oxide
can occur as either an external layer or internal oxide particles.
These oxides are less protective than the alumina layer and have an
oxidation rate greater than that for pure nickel (67). The internal

oxides are particularly damaging since the volumes of the oxides is greater than the corresponding metal that they replace. The material will swell as a result. This type of swelling is probably the primary reason for the observed increase in the volume of the samples. With the destruction of the external oxide layer by cracking from the swelling and the increased oxidation rate of the spinel and nickel oxide, the weight gain rate increases. This most likely accounts for the higher weight gain rate observed in Stage III compared to Stage I or simple oxidation.

In summary, the depletion of aluminum at the surface results in the swelling of the material and a shift in the oxidation mechanism from a protective external oxide to less protective oxides that occur both externally and internally. The internal oxides also aid in the swelling of the material which cracks the protective oxide layer. The aluminum depletion is increased by the increased diffusion of aluminum through the aluminum depleted phases.

5.3 HOT CORROSION KINETICS OF THE BETA NICKEL ALUMINIDES

The kinetics of the hot corrosion of the nickel aluminides are not determined by a single mechanism or event. Rather the kinetics reflect the sum of the processes occurring in a sample at a given time. The observed kinetics are also strongly affected by the actual surface area undergoing attack.

The kinetics of the hot corrosion attack were measured by determining the slope of the weight gain curve for each of the five stages. In all cases the initial surface area for the sample was used to normalize the weight gains.

During the early stages of hot corrosion, the hot corrosion is confined to a relatively small portion of the sample surface. The rate of weight gain for the unaffected areas undergoing oxidation is extremely slow compared to the overall weight gain rate observed. The conclusion is that the hot corrosion causes a much higher weight gain rate in the areas it is affecting than is observed in the weight gain curves. An estimate was made that in Stage II, the fastest weight gain rate stage, only four percent of the total surface area was actually affected. The weight gain rate in these regions is thus in excess of 100 mg/cm^2 hr.

In Stage III, the material is not only corroding on the surface, but it is also undergoing internal oxidation. While most researchers still report the data in terms of the area of the sample's surface, the internal oxidation increases the weight gain by involving a larger volume of material and increases the surface area of the sample by forming new surfaces internally. The weight gain rate does not reflect this gain in surface area, but it should be considered when comparing the kinetics of the reaction to the kinetics of the reaction for simple external oxidation.

The kinetics of Stage III also reflect the growth of three distinct oxides; alumina, the nickel-aluminum rich spinel, and nickel oxide. The observed kinetics are the sum of the growth of all three. The simple growth of alumina on the surface would have a reasonably negligible effect on the kinetics since the growth of an established alumina layer is extremely slow. The growth of the alumina layer in the regions where alumina is being fluxed cannot be ignored though since no protective alumina layer is formed. The lack of the protective oxide shifts the kinetics from a slow parabolic growth to a more rapid growth. If one assumes that the alumina forms only a very thin oxide layer at best, the rate of weight gain would remain near the instantaneous weight gain rate exhibited for samples undergoing oxidation with the same thickness of oxide, and the kinetics would change from parabolic growth to linear growth. An examination of the weight gain curves for these alloys in simple oxidation shows that the instantaneous weight gain rates during the early stages of oxidation are considerable. Based on this the kinetics for the formation of the porous alumina layer cannot be ignored.

The kinetics of the formation of the porous alumina layer are not the only kinetics to be considered in Stage III. During Stage III at least two other oxides are also formed, the nickel-aluminum spinel and nickel oxide. The oxidation mechanism also changes from external to external and internal. For the internal oxides, transport of oxygen via diffusion through the metal may be the limiting step rather than the actual oxidation mechanism. As pointed out in Section 5.2, the rate of diffusion for aluminum is thought to be dependent on the metallic phase present with the lower aluminum phases found near the surface having a higher diffusivity. Where the internal oxides form with respect to the surrounding metallic phases will thus have a major effect on the kinetics. For the external oxides, the oxide formed will determine the kinetics of the

oxidation process. Pettit (67) showed that the kinetics for the formation of the nickel-aluminum spinel and nickel oxide on the nickel-aluminum alloys was greater than the kinetics for the simple oxidation of nickel and hence is considerably greater than the kinetics of the formation of alumina. Based on this, an increase in the weight gain rate would be expected from the change in corrosion products.

Taking into account all the factors affecting the kinetics of Stage III, qualitatively an increase in the weight gain rate is expected. How each of the various processes occurring in the sample quantitatively affects the weight gain rate is not known since no experiments were conducted to try to isolate each process. The various processes that occur in Stage III also occur in Stage IV with one more important process added.

In Stage IV, the weight gain rate is dramatically increased not by an increase in the rate of the reaction(s), but rather by the increase in the surface area. Extensive cracking of the sample exposes large areas of metal to the environment. Because of the extensive cracking of the material, the surface area is greatly increased. This would account for the observed increase in the weight gain rate reported.

From these considerations it is obvious that the weight gain rates reported for the samples must be considered in light of the surface areas actually undergoing each of the various processes operative at a given time. Modifications would need to be made to the Stage II weight gain rate to increase the rate, while the weight gain rate for Stage IV should be decreased. Since the study did not attempt to quantitatively measure these surfaces areas, only semi-quantitative and qualitative modifications to the weight gain rates can be presented.

5.4 EFFECT OF SPECIFIC ELEMENTS ON THE HOT CORROSION
OF BETA NICKEL ALUMINIDES

The effects of the specific elements examined in this study are presented in terms of the proposed mechanism and previous work.

5.4.1 EFFECT OF ALUMINUM

Higher aluminum contents are beneficial to the hot corrosion resistance of the beta nickel aluminides. This is graphically demonstrated by the comparative resistance of the 45 a/o and 50 a/o aluminum alloys tested. The 50 a/o aluminum alloy has a Stage I lasting for approximately 10 hours. The 45 a/o aluminum alloy undergoes hot corrosion as soon as it is exposed at temperature or within a few hours after the exposure begins.

The better hot corrosion resistance of the high aluminum alloys is primarily the result of an extended Stage III. The 45 a/o alloys have a Stage III lasting approximately 30 to 50 hours. In contrast the 50 a/o aluminum alloys have a Stage III that can extend to over 100 hours.

The improved hot corrosion corrosion resistance is attributable to the activity of the aluminum. The activity of the aluminum is greater in the high aluminum alloy as demonstrated by simple thermodynamics. This higher activity has the beneficial effect of confining the oxidation of the alloy to the external surface as shown by Pettit (67). This creates a protective oxide layer.

The higher aluminum alloys also have more aluminum available at the surface for oxidation. Since the depletion of the aluminum at the surface and the subsequent phase transformation from beta to gamma prime is one of the primary problems associated with the hot

corrosion of the beta nickel aluminides, the high aluminum levels allow more aluminum to be converted into alumina while still maintaining the beta structure. The extra aluminum is also beneficial since the aluminum depletion in simple oxidation was shown by Smialek (72) to result in a flat composition profile through the sample as oxidation progressed with the overall aluminum content of the sample being lowered. With more aluminum in the alloy initially it will again take longer to deplete the alloy.

It is assumed that even higher aluminum contents would be beneficial to the hot corrosion resistance of the beta nickel aluminides. A sample was to be cast with 55 a/o aluminum, but the melter added 0.3 w/o chromium instead of 0.3 w/o zirconium to the melt. As a result, the material had to be discarded. The replacement material was not available by the end of this study due to equipment problems. If the higher aluminum activity and greater amount of aluminum are actually controlling the hot corrosion process, then logic indicates that the 55 a/o aluminum alloy will be more resistant than either the 45 a/o or the 50 a/o aluminum alloys. Complications could arise from the formation of new phases not considered in this study. Of particular concern is the formation of high aluminum compounds with even less ductility than beta at temperature. Cracking due to the formation of internal stresses that leads to Stage IV may become easier and result in a decrease in the hot corrosion resistance.

5.4.2 EFFECT OF ZIRCONIUM

No difference could be discerned in the hot corrosion of beta with and without zirconium additions. Referring to Strafford and Hunt (62), the level of zirconium that was necessary to achieve significantly improved resistance in a sulphur bearing gaseous environment was 1 w/o. The largest zirconium level tested in this

study was only 0.3 w/o. It is therefore quite likely that the amount of zirconium in the materials was too little to affect the hot corrosion. If more zirconium or other rare earth addition was added to the material, the additions could stop or slow Stage II of the hot corrosion process. Since all the rare earths are highly reactive, the rare earths should react with the oxygen and sulphur in the sodium sulphate melt. This would lower both the oxygen and sulphur activities near the metal/oxide/sodium sulphate interface. The lower oxygen activity would result in less beta nickel aluminide being converted to gamma prime by oxidation and less oxidation of any sulphides formed. The lowered sulphur activity would result in less sulphidation of any gamma prime that did form. Under these conditions the extent of the hot corrosion reactions would be significantly decreased. The weight gain rate would reflect this by being lowered.

Zirconium would also be useful in Stage III if sufficient levels of zirconium were present to stop the inward diffusion of oxygen by reacting with the oxygen at the surface. The lower levels of oxygen internally would mean little or no internal oxidation. This would stop the swelling of the material by the internal oxides and preserve the integrity of the oxide layer. Stresses that lead to the cracking of the metal at the end of Stage III and during Stage IV would also be minimized by the change in oxidation to a more external mechanism. The length of time that the sample is in Stage III could therefore be increased, and the overall hot corrosion resistance increased.

Alternatively, the rare earth additions could improve the external oxides formed by increasing adhesion, improving homogeneity, or increasing the compactness of the oxide layer. These effects are observed in oxidation and could result in a more protective oxide layer. With the more protective external oxide

layer, the sample would undergo less oxidation both externally and internally. The length of Stage I and III would be extended, and the overall corrosion resistance of the alloys increased.

While these effects would be beneficial, the level of zirconium inferred from limited tests reported in the literature needed for hot corrosion resistance may be sufficiently large to degrade the mechanical properties by forming Ni-Zr intermetallic precipitates. These intermetallic precipitates may even be more brittle than the beta nickel aluminide and therefore compound an already major property problem of the material. The weight gain rate from oxidation of the material can also be increased significantly since the rare earths tend to react very readily with oxygen even in low oxygen partial pressure atmospheres. It must also be remembered though that researchers such as Viswanathan (60) saw marked improvement in superalloys with even the low amounts of rare earth additions used in this study. It may be that zirconium is either not as effective as the lanthanum and yttrium used by Viswanathan or the beneficial effects of the zirconium are masked by the large weight gains. In either case, a more reasonable approach is to add chromium.

5.4.3 EFFECT OF CHROMIUM

Chromium improves the hot corrosion resistance of the beta nickel aluminides by lowering the basicity of the sodium sulphate layer, stabilizing the beta phase, gettering sulphur, and repairing the protective oxide layer when it fails.

Chromium can act to lower the basicity of the sodium sulphate by reacting with the sodium oxide generated in Stage II to form sodium chromate, Na_2CrO_4. This removes sodium oxide and hence oxide ions from the melt and stops any fluxing that could occur otherwise.

It is felt that the effect of the chromium in stopping the fluxing allows the formation of a protective oxide layer from the oxidation of the aluminum that could not occur without the chromium.

Since chromium has the BCC crystal structure, the addition of chromium tends to stabilize the B2 structure of the nickel aluminide. As a result, the beta phase persists over a much larger range of aluminum contents. Of particular interest is the lowering of the minimum aluminum content for the beta phase to exist alone or with alpha chromium by as much as 5 a/o per cent for a 15 w/o alloy. As indicated by the different responses of the 45 a/o and 50 a/o aluminum alloys, the increase of even 5 a/o aluminum significantly increases the hot corrosion resistance of the alloys.

Since the hot corrosion mechanism is dependent on the sulphidation of the alloy, the addition of chromium can stop or reduce the hot corrosion of the alloy by forming stabler chromium sulphides at the surface that do not allow the sulphur to react with the nickel to form nickel sulphides. The chromium sulphides remove the sulphur from the system by forming a solid compound as opposed to the liquid nickel sulphide. The chromium sulphides would react with oxygen to form an oxide and a sulphur compound such as SO_2, but since it is a solid state reaction the kinetics are limited by the much slower solid state diffusion. The result is the lowering of the overall kinetics and stopping the second step of the Stage II mechanism.

Perhaps most importantly, chromium will rapidly oxidize in the presence of oxygen to form a protective oxide layer. This results in the repair of the oxide layer when it is breached by a crack or other means. Alumina cannot do this since the kinetics for alumina formation are too slow to allow for the easy repair of ruptures. A new alumina layer can form under the chromia that occupies the crack

surface and a continuous alumina layer re-established. As a result the Stage I portion of the hot corrosion mechanism can be extended.

5.5 COMPARISON OF RESULTS TO OTHER STUDIES

No direct comparisons between this study and others using beta nickel aluminides is possible since the other studies sighted in the literature review used a burner rig test apparatus. These studies also used the depth of attack as the criterion for measuring the extent of hot corrosion. Few attempts were made to examine the kinetics of the hot corrosion process. Differences in temperatures for the tests also affects the hot corrosion results of these tests. Nonetheless several similarities between the results of this study and the results of the other researchers do indicate that the mechanism in all cases was the same or at least very similar.

Kaufman (55) reported surface phases for alloys with compositions similar to the samples used in this study that were similar to this study. The major exception was the presence of sodium sulphate on the samples tested in the burner rig. This is easily attributable to the continuous renewal of the sodium sulphate from the burner. No such renewal was possible in the TGA tests. The phases reported by McCarron, Lindblad, and Chatterji (71) also correspond to the observations made in this study.

The morphology of the hot corrosion products is also strongly indicative of a similar mechanism. The outer aluminum depleted region of the sample was first reported by Kaufman. The extensive, localized nature of the attack is readily apparent in the transverse micrographs for both Kaufman and McCarron et al. Long oxide stringers extending from the surface to the interior of the sample could be caused by either the linking of internal oxides or the cracking and subsequent oxidation of the crack surface. No cracks were reported in the text or seen in the micrographs, but they may have been present and not noted.

The beneficial effects of chromium were reported by both Kaufman and McCarron et al. The concept of the chromium stabilizing the beta phase comes directly from McCarron et al. Once again the results of these researchers is in agreement with the observations of this study.

Some mechanisms for the hot corrosion of beta nickel aluminides and gamma prime nickel aluminides were advanced in the literature. While the mechanisms may have been applicable to the test conditions of those researchers, the results obtained in this test indicate that under the test conditions used, none of these mechanisms was applicable. The mechanism proposed by Kaufman (55) does have many similarities to the proposed mechanism. The concept that the gamma prime is undergoing sulphidation originally comes from Kaufman. The two theories diverge from there as the one proposed by this study presumes that the material is sulphidized and subsequently oxidized as is consistent with the thermodynamics of the system whereas Kaufman proposes sulphidation and oxidation at the same time in the same process. Kaufman proposed that the SO_3 generated by the oxidation of the sulphides recombines with the Na_2O released during the sulphidation/oxidation step recombines to reform sodium sulphate. This would account for the general observation that the amount of sodium sulphate in hot corrosion is decreased only slightly during the hot corrosion process. In the proposed mechanism an alternative route for the oxidation of the sulphides was taken. In this case the oxides were assumed to form SO_2. While the amount of sodium sulphate on the sample after exposure was not determined, the continual reuse of a small amount of SO_2 for the hot corrosion process would also account for a low usage of sodium sulphate in the hot corrosion process. Both ideas must be considered.

It must be stressed though that all indications are that even minor variations in composition, test atmosphere, temperature, and

test method can have profound effects on the hot corrosion mechanism. For this reason, none of the mechanisms examined in this thesis can be ruled out. However, it is felt that the mechanism proposed in this study has greater applicability for the nickel aluminides as it better explains the observed phases and the morphology of the hot corrosion scale. The mechanism can also be easily modified to take into account any other corrosion products or phases observed in the hot corrosion process. For this reason the proposed mechanism is felt to be superior to the previously proposed mechanisms.

6 CONCLUSIONS

A study was made to gather basic information on the hot corrosion process of beta nickel aluminides. From the information gathered, the following conclusions were made.

1. Prior processing and homogeneity had no distinguishable effect on the hot corrosion resistance of the alloys. The simple nickel aluminides and nickel aluminides with zirconium that were cast did not have the segregation expected due to the diffusion in the material at extremely high temperatures and grain growth allowing complete homogenization of the samples. Even when segregation was present in the chromium alloys no preferential attack of one phase was observed.

2. The beta nickel aluminides are not hot corrosion resistant despite the high aluminum contents and excellent oxidation resistances of the alloys. Catastrophic weight gain rates were observed with weight gains in excess of 20 mg/cm^2 after 50 hours being typical for the 45 a/o aluminum alloys.

3. The hot corrosion mechanism is a complex combination of several processes. Among the processes occurring are the sulphidation enhanced oxidation of the metal, the depletion of aluminum at the surface, basic fluxing of the protective oxide layer, internal oxidation, phase changes, and crack propagation. Other processes may also be occurring in the system that were not observed.

4. The kinetics reported in this study do not really reflect the true kinetics of the system since only the overall kinetics are presented and no correction was made for the actual surface area undergoing attack. A more proper treatment of the kinetics

would involve the careful measurement of the actual areas undergoing each of the several corrosion attacks, i.e. simple external oxidation, hot corrosion, and internal oxidation. Unfortunately the problems inherent in measuring the surface area of the sample precluded this. The qualitative effects at least should be considered when using the kinetic data presented.

5. The addition of zirconium and presumably other rare earths in the small amounts tested has no effect on the hot corrosion of the beta nickel aluminides. Larger additions of the rare earth elements may be beneficial.

6. Higher aluminum contents are beneficial because the activity of the aluminum is increased and more aluminum is available at the surface. The higher aluminum activity prevents the Stage II mechanism from being operative so that the oxidation of the metal proceeds as if no sodium sulphate was present until the total aluminum content of the sample was lowered sufficiently. More aluminum in the alloy also allows for a greater amount being removed prior to a phase change from beta to gamma prime at the surface.

7. Additions of chromium are beneficial because the chromium stabilizes the beta phase, repairs the oxide layer when it is breached, reacts with sulphur to remove it from the system or at least reduce its activity, and reduces the basicity of the sodium sulphate by reacting with the sodium oxide to form sodium chromate.

7 FURTHER WORK

Since the study completes the requirements for the Masters thesis, no further work is planned. Some unanswered questions do indicate the need for additional tests anyway.

1. The beneficial effect of higher aluminum contents should be tested. A 55 a/o alloy should be exposed as planned for this study.

2. A more detailed thermodynamic analysis of the Stage II mechanism with emphasis on possible alternative products, particularly aluminum sulphides, should be done. The analysis of the water soluble components of the corrosion layer would also be useful in establishing the basicity of the sodium sulphate layer and for determining if any complex ions such as NiO^{2-} or $Al_2O_4^{2-}$ are present.

3. Testing of the next generation of nickel aluminides that exhibit good ductility and impact strength should be done both to check the hot corrosion resistance of the alloys and to determine if the cracking associated with Stage IV can be stopped.

4. Additional testing with alloys containing large amounts of rare earth additions would be useful in establishing whether rare earth additions can be beneficial.

REFERENCES

(1) W.T. Reid, R.C. Corey, and B.J. Cross, Trans ASME, 67, p. 279, (1945)

(2) J Stringer, Hot Corrosion in Gas Turbines, MCIC Report 72-08, Metal and Ceramic Information Center, Columbus, (June 1972)

(3) M. Kawakami, K.S. Goto, and R.A. Rapp, Trans ISIJ, 20, p. 646, (1980)

(4) C.T. Sims, ASME Preprints, 70-GT-24, (May 1970)

(5) A.U.Seybolt, High Temperature Metallic Corrosion by Sulphur and its Compounds, Electrochemical Society, New York, p. 160, (1970)

(6) A.U. Seybolt, Trans. Met. Soc. AIME, 242, p. 752, (1968)

(7) L.D. Graham, J.D. Gadd, and R.J. Quigg, Hot Corrosion Problems Associated with Gas Turbines, ASTM STP 421, ASTM, 1967, p. 105, (1970)

(8) G.J. Santaro, Oxid. of Metals, 13, p. 405, (1979)

(9) J. Stringer and D.P.Whittle, High Temperature Corrosion of Superalloys, p. 283

(10) P.A. Bergman, High Temperature Metallic Corrosion by Sulphur and its Compounds, Electrochemical Society, New York, p. 224, (1970)

(11) A.U. Seybolt, GE Research Center Report 70-C-189, (June 1970)

(12) R.W. Hardt, J.R. Gambino, and P.A. Bergman, Hot Corrosion

Problems Associated with Gas Turbines, ASTM STP 421, p. 64, (1967)

(13) N.S. Bornstein and M.A. DeCrescente, Final Report 3051 to US Naval Ship R and D Lab on Contract N00600-68-C-0639, (April 1969)

(14) P.A. Bergman, Corrosion, 23, p. 72, (March 1967)

(15) R.M. Shirmer and H.T. Quigg, Hot Corrosion Problems Associated with Gas Turbines, ASTM STP 421, ASTM, p. 270, (1967)

(16) J.A. Goebel and F.S. Pettit, Met Trans, 1, p. 1943, (July 1970)

(17) A. Rahmel and W.T. Wu, Oxid of Metals, to be published

(18) M. Scmidt, Dissertation, Technische Hochschule Darmstadt, (1981)

(19) F. J. Kohl, C.A. Stearns, and G.C. Fryburg, NASA-TM-79225, (June 1979)

(20) J.A. Goebel, F.S. Pettit, and G.W. Goward, Electrochemica Acta, 20, p. 479, (1978)

(21) A.K. Misra, Oxid. of Metals, 25, p. 129, (April 1986)

(22) R.F. Reising, Corrosion, 33, p. 84, (1977)

(23) R.F. Reising, Proceedings "Metal-Slag-Gas Reactions and Processes", Symp., Z.A. Foroulis and W.W. Smeltzer eds., The Electrochemical Society, p. 747, (1975)

(24) R.F. Reising, Corrosion, 13, p. 153, (1975)

(25) A.J.B. Cutler and C.J. Grant, Proceedings "Metal-Slag-Gas Reactions and Processes", Symp., Z.A. Foroulis and W.W. Smeltzer eds., The Electrochemical Society, p. 591, (1975)

(26) A. Davin, D. Coutsouradis, and L. Habraken, Proceedings "Metal-Slag-Gas Reactions and Processes", Symp., Z.A. Foroulis and W.W. Smeltzer eds., The Electrochemical Society, p. 678, (1975)

(27) R.L. Jones, Proceedings "Metal-Slag-Gas Reactions and Processes", Symp., Z.A. Foroulis and W.W. Smeltzer eds., The

Electrochemical Society, p. 762, (1975)

(28) R.C. Hurst, J.B. Johnson, M. Davies, and P. Hancock, Deposition and Corrosion in Gas Turbines, A.B. Hardt and A.J.B. Cutler eds., John Wiley & Sons Inc., p. 143, (1973)

(29) C.A. Stearns, F.J. Kohl, and G.C. Fryburg, Properties of High Temperature Alloys with Emphasis on Environmental Effects, p. 655, 1976

(30) J.G. Smeggil and N.S. Bornstein, NASA CR-159747, (Jan 1980)

(31) R.A. Rapp and K.S. Goto, Proc. "2nd International Symposium on Molten Salts", J. Braunstein ed., The Electrochemical Soceity, (1979)

(32) E.L. Simons, G.V. Browning, and H.A. Liebhafskey, Corrosion, 11, p. 505, (1955)

(33) M. Arbab and S.R. Shatynski, J. Electrochemical Soc., 132, p. 2264, (Sept. 1985)

(34) W.L. Wheatfall, AGARD Conf. Proc. 120 on High Temp. Corr. of Aerospace Alloys, J. Stringer, R.I. Jaffee, and T.F. Kearns eds., NATO/AGARD, p. 235, (1972)

(35) Hot Corr. Mechanism Studies, General Electric Co., MEL-sponsored Report 132/66, Final Report under Contract N600(61533)63219, AD 629-598. (Feb. 1966)

(36) A.U. Seybolt and A. Beltran, Hot Corrosion Problems Associated with Gas Turbines, ASTM STP 421, p. 21, (1967)

(37) C.S. Giggins and F.S. Pettit, Oxid. of Metals, 14, p. 363, (1980)

(38) F. Gesmundo and C. De Asmundis, Behavior of High Temperature Alloys in Aggressive Environments, I. Kirman ed., The Metals Soceity, London, p. 435, (Oct. 1979)

(39) J.M. Quets and W.H. Dresher, J. Mater. 4, p. 583, (1969)

(40) P.A. Bergman, C.L. Sims, and A.W. Beltran, Hot Corrosion Problems Associated with Gas Turbines, ASTM Special Publication No. 421, Philadelphia, p. 38, (June 1966)

(41) J.J. Walters, Technical Report AFML-TR-67-297, AVCO/Lycoming Division, Contract No. AF33(615)-5212, (Sept. 1967)

(42) A.U. Seybolt and A.N. Beltran, Hot Corrosion Problems Associated with Gas Turbines, ASTM Special Publication No. 421, Philadelphia, p. 21, (June 1966)

(43) P.A. Bergman, Corrosion, 23, p. 72, (1967)

(44) A.U. Seybolt, GE Research Center Report 70-C-189, (June 1970)

(45) G.J. Danek, Jr., Naval Engineers Journal, 77, p. 859, (1965)

(46) C. Tedmon and A.U. Seybolt, Corr. Sci., 8, p. 125, (1968)

(47) C. DeAsmundis, F. Gesmundo, and C. Bottino, Oxid. of Metals, 14, p. 351, (1980)

(48) A.U. Seybolt, Trans. Met. Soc. AIME, 242, p. 752, (1968)

(49) H.V. Doering, J. Mater, 4, p. 457, (1969)

(50) F.J. Wall and S.T. Michael, Hot Corrosion Problems Associated with Gas Turbines, ASTM STP 421, ASTM, p. 223, (1967)

(51) P.A. Bergman, C.L. Sims, and A.N. Beltran, Hot Corrosion Problems Associated with Gas Turbines, ASTM STP 421, ASTM, p. 33, (1967)

(52) L.S. Darken and R.W. Gurry, Phys. Chem. of Metals, McGraw Hill, New York, p. 361, (1953)

(53) G. Llewellyn, Hot Corrosion Problems Associated with Gas Turbines, ASTM Special Publication No. 421, Philadelphia, p. 3, (June 1966)

(54) F.J. St. John, W.A. Rentz, W.R. Freeman, Jr., Sixth Annual National Conference on Aircraft and Propulsion Systems, (Sept 1966)

(55) M. Kaufman, Trans. Quarterly ASM, 62, p. 590, (1969)

(56) H. Lewis and R.A. Smith, First International Congress on

Metallic Corrosion, London, p. 202, (April 1961)

(57) T.T. Huang and G.H. Meier, Second Semi-Annual Report on Grant No. NSG-3214, NASA CR-159718, (Aug. 1979)

(58) D.M. Johnson, D.P. Whipple, and J. Stringer, Corr. Sci., 15, p. 721, (1975)

(59) J.F.G. Conde, E. Erdos, and A.Rahmel, High Temperature Alloys for Gas Turbines 1982, Liege, Belgium, D. Reidel ed., Kluwer, Boston, (Oct. 1982)

(60) R. Viswanathan, Corrosion, 24, p. 359, (Nov. 1968)

(61) P. Huber and G.H. Gessinger, Materials and Coatings to Resist High Temperature Corrosion, Applied Science Publishers, London, p. 71, (May 1977)

(62) K.N. Strafford and P.J. Hunt, Materials and Coatings to Resist High Temperature Corrosion, Applied Science Publishers, London, p. 39, (May 1977)

(63) S.Y. Hwang, G.H. Meier, F.S. Pettit, G.R. Johnston, V.Provenzano, and F.A. Smidt, High Temperature Protective Coatings, S.C. Singhal ed., TMS/AIME, Warrendale, p. 121, (March 1983)

(64) P. Steinmetz, B. Roques, B. Dupre, C. Duret, and R. Morbiolt, High Temperature Protective Coatings, S.C. Singhal ed., TMS/AIME, Warrendale, p. 135, (March 1983)

(65) S.K. Lau and R.J. Braton, High Temperature Protective Coatings, S.C. Singhal ed., TMS/AIME, Warrendale, p. 305, (March 1983)

(66) D.R. Coupland, C.W. Corti, and G.L. Selman, <u>Behaviour of Nigh Temperature Alloys in Aggressive Environments</u>, I. Kirman ed., The Metals Soceity, London, p. 525, (Oct. 1979)

(67) F.S. Pettit, Trans. of the TMS/AIME, <u>239</u>, p. 1296, (Sept 1967)

(68) Discussions of papers presented at ASM Annual Meeting, Intermetallics Session, October 7-8, 1986, Orlando, Florida

(69) J.L. Smialek, Met. Trans. A, <u>9A</u>, p. 309, (March 1978)

(70) C.S. Giggins and F.S. Pettit, J. Electrochemical Soc., <u>118</u>, (Nov. 1971)

(71) R.L. McCarron, N.R. Linblad, and D. Chatterji, Corrosion, <u>2</u>, p. 476, (Dec. 1976)

(72) J. Smialek, personal communications

(73) D. Chatterji and A. Ritzer, to be published

(74) <u>CRC Handbook of Chemistry and Physics, 65th Edition</u>, Editor-in-Chief R.C. Weast, CRC Press, Boca Raton, p. B-118, (1984)

(76) W. Walker, D.G. Miller, and F. Feiner, Chart of the Nuclides, Revised 1983

(77) M.M.P. Jansen, Met. Trans., <u>4</u>, p. 1623, (June 1973)

Table 1a

Compositions Used by Kaufman

Alloy	Ni	Al	Cr	Ti	Mo	Co
CENIAL-1	67.73	32.27				
CENIAL-2	66.50	31.55	1.95			
CENIAL-3	65.03	30.35	4.62			
CENIAL-4	60.95	29.51	9.54			
CENIAL-5	66.30	31.65		2.05		
CENIAL-6	60.18	29.40		10.42		
CENIAL-7	62.72	30.67	4.56	2.05		
CENIAL-8	63.34	28.94	4.84		2.88	
CENIAL-9	60.64	29.60	4.79			4.97
CENIAL-10	57.88	27.51	4.74			9.87
CENIAL-11	65.40	29.78				4.82
CENIAL-12	61.05	29.07				9.88
CENIAL-13	54.39	26.07				19.54

All values are taken from Reference 55, Table 2, Composition of NiAl-base Alloys

Table 1b

External Corrosion Products With and Without Sodium

Fuel Additions for 1675°F Hot Corrosion Burner Rig Tests

External Corrosion Products, 200 ppm Salt Tests

Phase	Alloys	Comments
Na_2SO_4	All	Form III always present, strongest at 100 hours. Meta-thenardite present at short times, virtually disappearing by 100 hours. Thenardite in very small quantities found, mostly at 16 hours.
Ni_3S_2	CENIAL-1,11,12 CENIAL-3,4,5,11 CENIAL-7 CENIAL-6,9	Very small amounts at 1/2 hour Very small amounts at 2 hours Very small amount at 16 hours Very small amounts at 100 hours
NiO*	CENIAL-1,5,11, 12,13 All others	Moderate amounts at all times Increases with time to moderate amounts after 16 - 100 hours
Spinel+	All	Low parametr type present in small amounts at all times, except CENIAL-2 which has a moderate amount of high parameter type at 100 hours. Most have traces of the high parameter type at 1/2 hour
Al_2O_3	CENIAL-1,5,11, 12,13	Moderate amounts at 1/2 hour and 2 hours. Decreasing thereafter.
Others	CENIAL-12,13	Possibly CoO present at 16 hours

Table 1b (Cont.)

External Corrosion Products With and Without Sodium

Fuel Additions for 1675°F Hot Corrosion Burner Rig Tests

External Corrosion Products, No Salt Tests

Phase	Alloys	Comments
NiO*	CENIAL-1,2,9, 11,12	None
	CENIAL-5	Moderate amounts at 100 hours
	CENIAL-6,7	Very slight amounts at 100 hours
	CENIAL-13	Small amounts at 1 - 100 hours. Slightly higher lattice parameter.
Spinel+	CENIAL-1,2,11,13	None
	CENIAL-5	Moderate amounts at 100 hours, low parameter.
	CENIAL-7	Possible trace at 1 and 100 hours, high parameter at 1 hour, low parameter at 100 hours.
Al_2O_3	All	Increases to small or moderate amounts by 100 hours, rare at 1 hour.
Others	CENIAL-6	TiO_2 increasing to moderate amount at 100 hours.
	CENIAL-10,13	Trace of SiO_2 at short times.

* NiO with slightly higher parameter formed frequently in CENIAL-4,7,8,10,12,13. Occasionally both normal and high parameter types were found together in CENIAL-5,6,9,10,12,13. High parameter indicates that other element dissolved in NiO, but no identification was made.

+ High parameter (a_o=8.27 - 8.33 angstroms) indicate Ni-Cr or Co-Cr spinels. Low parameter (a_o=8.06 - 8.08 angstroms) are usually Ni-Al spinels.

All values and comments taken from reference 55, Table 7, NiAl Alloys External Products of Corrosion, 200 ppm Salt Tests, and Table 8, NiAl Alloys External Products of Corrosion, No-Salt Tests.

Table 2

Alloy Compositions

Beta NiAl-based Alloys

Ni-27 w/o Al-0.2 w/o Zr, P/M stock material

	Ni	Al	Zr
w/o	73.4	26.4	0.2
a/o	56.0	43.9	0.1

Ni-27 w/o Al-0.2 w/o Zr

	Ni	Al	Zr	S	C
w/o	72.4	27.4	0.2	<5	25
a/o	54.8	45.1	0.1		

Ni-31.5 w/o Al

	Ni	Al	S	C
w/o	67.8	32.2	<5	25
a/o	49.2	50.8		

Ni-31.5 w/o Al-0.3 w/o Zr

	Ni	Al	Zr	S	C
w/o	67.5	32.2	0.3	<5	29
a/o	49.0	50.8	0.1		

Chromium Containing Alloys

Ni-30 w/o Al-2 w/o Cr

	Ni	Al	Cr	S	O	N	C
w/o	69.0	28.6	2.4	<5	32	144	23
a/o	51.5	46.5	2.0				

Ni-29 w/o Al-5 w/o Cr

	Ni	Al	Cr	S	O	N	C
w/o	66.6	27.8	5.4	<5	38	123	21
a/o	50.0	45.4	4.6				

Ni-13 w/o Al-15 w/o Cr-0.2 w/o Zr

	Ni	Al	Cr	Zr	S	O	N	C
w/o	74.1	11.9	13.8	0.2	<5	63	5	55
a/o	64.1	22.3	13.5	0.1				

Sulfur, oxygen, nitrogen, and carbon are in ppm. All other elements are as indicated. The trace elements are the average of two or more analysses.

Table 3

Sample Designations, Nominal Compositions,

and Test Conditions

Sample	Nominal Composition	Test Conditions
1	Ni-45 Al-0.2 Zr (P/M)	Hot Corrosion
2	Ni-45 Al-0.2 Zr (P/M)	Hot Corrosion
3	Ni-45 Al-0.2 Zr (P/M)	900°C Preox. + H.C.
4	Ni-45 Al-0.2 Zr (P/M)	900°C Preox. + H.C.
5	Ni-45 Al-0.2 Zr (P/M)	1200°C Preox. + H.C.
6	Ni-45 Al-0.2 Zr (P/M)	900°C Oxidation
7	Ni-45 Al-0.2 Zr (P/M)	1200°C Oxidation
8	Ni-45 Al-0.2 Zr (P/M)	1200°C Cyclic Oxidation
9*	Ni-45 Al-0.2 Zr	900°C Oxidation
10	Ni-45 Al-0.2 Zr	Hot Corrosion
11	Ni-45 Al-0.2 Zr	1200°C Preox. + H.C.
12*	Ni-45 Al-0.2 Zr	900°C Oxidation
13	Ni-22 Al-15 Cr-0.2 Zr	900°C Preox. + H.C.
14	Ni-22 Al-15 Cr-0.2 Zr	Hot Corrosion
15	Ni-22 Al-15 Cr-0.2 Zr	1200°C Oxidation
16	Ni-50 Al-0.3 Zr	Hot Corrosion
17	Ni-50 Al-0.3 Zr	1200°C Preox. + H.C.
18	Ni-50 Al	1200°C Oxidation
19	Ni-50 Al-0.3 Zr	1200°C Cyclic Oxidation
20	Ni-50 Al	1200°C Cyclic Oxidation
21	Ni-45 Al-0.2 Zr	1200°C Cyclic Oxidation
22	Ni-50 Al	Hot Corrosion
23	Ni-50 Al	900°C Preox. + H.C.
24	Ni-50 Al-0.3 Zr	900°C Preox. + H.C.
25	Ni-22 Al-15 Cr-0.3 Zr	Hot Corrosion
26	Ni-50 Al	1200°C Preox. + H.C.
27	Fe-40 Al-0.2 Zr	Hot Corrosion
28	Ni-22 Al-15 Cr-0.3 Zr	900°C Preox. + H.C.
29	Ni-45 Al-5 Cr	Hot Corrosion
30	Ni-45 Al-0.2 Zr (P/M)	Hot Corrosion (Stop Test)
31	Ni-45 Al-0.2 Zr (P/M)	Hot Corrosion (Stop Test)
32	Ni-45 Al-0.2 Zr (P/M)	Hot Corrosion (Stop Test)
34	Ni-45 Al-0.2 Zr (P/M)	Hot Corrosion (Stop Test)
36	Ni-45 Al-0.2 Zr (P/M)	Argon Atmosphere Exposure
37	Ni-46 Al-2 Cr	Hot Corrosion

* - Sample 9 spalled. Redone as Sample 12.

Nominal compositions are given in atomic percent for aluminum, weight percent for all other elements.

Table 4

Weight Gains and Exposure Times

Sample	Time	Temp	Weight Gain	Thick	Time	Coating	Weight Gain
1					68.2	1.38	26.29
2					65.3	1.08	21.52
3	121.0	900	0.24	1.28	94.2	2.42	30.01
4	164.7	900	0.89	4.75	44.0	3.29	17.73
5	90.0	1200	0.75	4.00	121.9	3.08	31.43
6	96.9	900	0.51	2.72			
7	96.5	1200	0.54	2.88			
9	168.3	900	0.61	S			
10					50.1	0.48	17.93
11	145.0	1200	2.40	12.81	96.2	1.60	29.95
13	165.0	900	0.27	1.44	838.5	8.25	6.05*
14					314.3	3.40	13.81
15	192.2	1200	2.10	S			
16					141.8	2.04	16.86
17	191.2	1200	1.96	10.46	166.0	3.25	19.49
18	165.0	1200	0.90	S			
22					117.2	2.30	23.44
23	19.4	900	0.02	0.11	97.6	2.06	19.99
24	169.2	900	-0.12	N/A	140.0	2.14	38.83
25					837.1	2.48	13.59*
26	0.5	1200	0.09	0.48	71.2	6.03	23.24
28	145.7	900	-0.91	N/A			
29					400.0	3.04	3.11
30				.	0.1	1.08	1.34
31					0.5	0.99	1.30
32					19.5	1.02	4.68
34					30.0	0.92	1.09
36					2.0	1.02	0.00
37					555.2	9.31	13.03

S - Oxide layer spalled
* - Formed volatile Na_2CrO_4

All times are in hours.

Temp - Temperature of oxidation exposure (°C)

Thick - Thickness of alumina layer assuming a weight gain of 1 mg/cm^2 is equivalent to a 5.339 um thick layer of alumina.

Weight Gain = (Final Weight - Initial Weight) / Initial Surface Area

Coating and weight gains are in units of mg/cm^2

Table 5

Rate Constants for Hot Corrosion

Ni - 45 a/o Al - 0.2 w/o Zr (P/M)

	I	II	III	IV	V
Bare Metal H.C.		3.48	0.14	0.55	
900°C Preox. + H.C.	0.03	1.90	0.10	0.65	
1200°C Preox. + H.C.	0.07	4.79	0.28	0.40	0.18

Ni - 45 a/o Al - 0.2 w/o Zr

	I	II	III	IV	V
Bare Metal H.C.		1.45	0.15	0.46	0.33

Ni - 50 a/o Al

	I	II	III	IV	V
Bare Metal H.C.	0.01	2.50	0.07	0.32	
900°C Preox. + H.C.	0.07	2.02	0.05	0.43	
1200°C Preox. + H.C.	0.07	2.02	0.05	0.43	

Ni - 50 a/o Al - 0.3 w/o Zr

	I	II	III	IV	V
900°C Preox. + H.C.	0.05	0.96	0.05	0.55	0.28
1200°C Preox. + H.C.	0.01	1.35	0.02	0.27	

Ni - 22 a/o Al - 15 w/o Cr - 0.2 w/o Zr

	I	II	III	IV	V
Bare Metal H.C.	0.01	8.64	0.04	0.06	

Stage I Rates for Chromium Containing Alloys Exhibitting Only Stage I

Ni - 46 a/o Al - 2 w/o Cr
Bare Metal H.C. 0.02

Ni - 45 a/o Al - 5 w/o Cr
Bare Metal H.C. 0.01

Ni - 22 a/o Al - 15 w/o Cr - 0.3 w/o Zr
900°C Preoxidation + H.C. 0.01

All rates are in mg/cm^2 hr.

Table 6

Results of Selected X-ray Diffraction Analysses

Sample 3: Ni-45 a/o Al-0.2 w/o Zr

Oxidized 121 hours in 1 atm O_2 at 900°C:

Alpha alumina, delta alumina, beta NiAl
Unknown low intendity peaks at d=4.00 and d=3.51 angstrom.
Phases determined by diffractometer.

After subsequent hot corrosion for 94 hours:
NiO (s), Na_2SO_4 (Form V) (m), Al_2O_3 (w), lambda Na_2O*chi Al_2O_3
(vw)
Powder analyzed using Guinier de Wolfe film technique.

Sample 13: Ni-15 w/o Cr-13 w/o Al-0.2 w/o Zr

Oxidized 165 hours in 1 atm O_2 at 900°C:

Alpha alumina, gamma prime or gamma prime + gamma, beta NiAl
Unknown low intensity peak at d=2.74 angstrom.
Determined by diffractometer.

Sample 14: Ni-15 w/o Cr-13 w/o Al-0.2 w/o Zr

Bare metal hot corrosion test:
NiO (m), spinel (s)
Spinel phase is a range of spinels with lattice parameters of
8.10 to 8.15 angstrom.
Powder analyzed using Guinier de Wolfe film technique.

Sample 15: Ni-15 w/o Cr-13 w/o Al-0.2 w/o Zr

Oxidized 192 hours in air at 1200°C:
Alpha alumina (s), gamma prime or gamma prime + gamma (s),
spinel (vw), ZrO_2 (vw)

Spinel phase has a lattice parameter of 8.10 angstrom.
Sample exhibitted major spallation on cooling and could not be
used for hot corrosion.
Phases determined by diffractometer.

Sample 23: Ni-50 a/o Al

Oxidized 19.5 hours in 1 atm O_2 at 900°C and hot corroded for 97
hours:
NiO (s), Al_2O_3 (w), spinel (w), Na_2SO_4 (vw)

Spinel has a lattice parameter of 8.10 angstroms.
Powder analyzed using Guinier de Wolfe film technique.

Table 6 (Cont.)

Results of Selected X-ray Diffraction Analysses

Sample 24: Ni-50 a/o Al-0.3 w/o Zr

Oxidized 169 hours in 1 atm O_2 at 900°C and hot corroded for 140 hours:

    NiO (s), Al_2O_3 (w), spinel (w), Na_2SO_4 (vw)
    Unknown peaks at d=3.03, 2.71, and 2.57 angstroms.
    Spinel has a lattice parameter of 8.10 angstroms.
    Powder analyzed using Guinier de Wolfe film technique.

Sample 25: Ni-15 w/o Cr-13 w/o Al-0.3 w/o Zr

Bare metal hot corrosion for 837 hours:
    NiO (s), spinel 1 (s), spinel 2 (m)
    Spinel 1 has a lattice parameter of 8.15 angstroms.
    Spinel 2 has a lattice parameter of 8.30 angstroms.
    Darkening of film between sharp peaks indicates there is
    actually a range of spinels present in the sample.
    Powder analyzed using Guinier de Wolfe film technique.

Sample 26: Ni-50 a/o Al

Oxidized 0.5 hours in air at 1200°C and hot corroded for 71.2 hours:
    NiO (s), Al_2O_3 (m) spinel (vw), Na_2SO_4 (vw)
    Spinel has a lattice parameter of 8.10 angstroms.
    Powder analyzed using Guinier de Wolfe film technique.

Sample 29: Ni-29 w/o Al-5 w/o Cr

Bare metal hot corrosion for 404 hours:
    Na_2SO_4 (Form V) (s)
    Sample is part of the sodium sulfate layer left after the
    exposure. The layer had a distinctive yellow color.
    Na_2CrO_4 was expected but not detected.
    Powder analyzed using Guinier de Wolfe film technique.

Sample 30: Ni-45 a/o Al-0.2 w/o Zr (P/M)

Sample exposed for 5 minutes:
    NiO (m), orientated Al_2O_3 (s), beta NiAl (vs), Ni_7S_6 (w)
    Al_2O_3 is orientated on (012). Orientation comes from normal
    growth of oxide layer on majority of sample.
    Phases identified by diffractometer.

Sample 31: Ni-45 a/o Al-0.2 w/o Zr (P/M)

Sample exposed for 30 minutes:
    NiO (m), orientated Al_2O_3 (s), randomly orientated Al_2O_3 (w),
    beta NiAl (vs), Ni_7S_6 (w)
    Al_2O_3 is orientated as in Sample 30.
    Phases identified by diffractometer.

Table 6 (Cont.)

Results of Selected X-ray Diffraction Analysses

Sample 32: Ni-45 a/o Al-0.2 w/o Zr (P/M)

Sample exposed 20 hours:
NiO (m), Al_2O_3 (s), beta NiAl (vs), possible $NiAl_2O_4$ (w),
possible gamma or gamma prime (w)
Al_2O_3 is randomly orientated.
Phases determined by diffractometer.

Sample 34: Ni-45 a/o Al-0.2 w/o Zr (P/M)

Sample exposed 30 hours:
Al_2O_3 (m), NiO (m), ZrO_2 (monoclinic and cubic) (w), beta
NiAl (s), gamma or gamma prime (w), possible $NiAl_2O_4$ (w)
NiO/Al_2O_3 peak height ratio increased compared to Sample 32
indicating NiO is becoming predominant phase.
Phases determined by diffractometer.

Figure 1

Nickel - Aluminum Phase Diagram

Figure 1

Nickel - Aluminum Phase Diagram
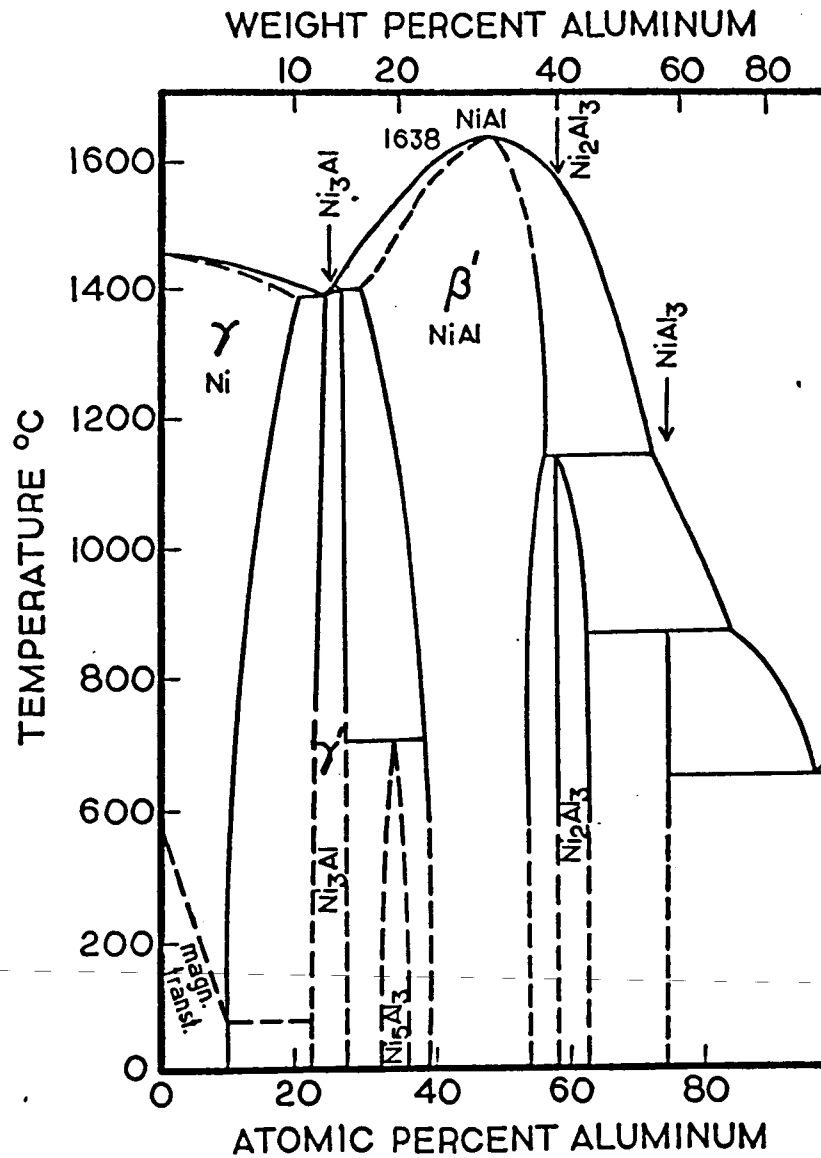
Figure 2

Sodium - Sulphur - Oxygen Phase Stability Diagram at
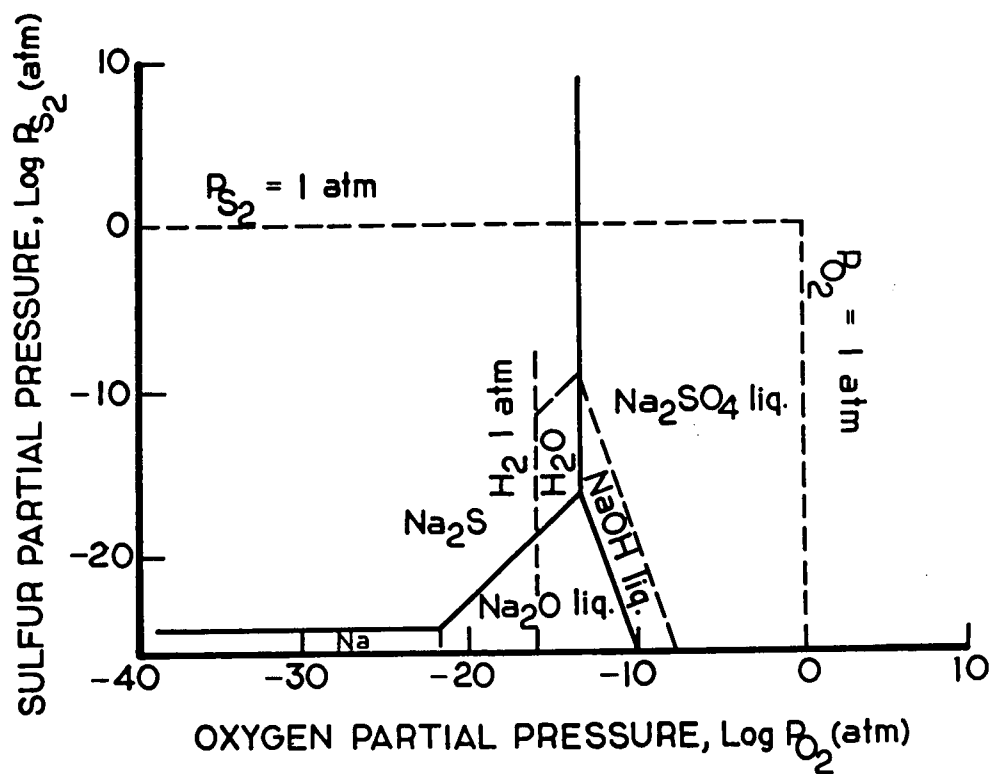
1200 K

From Quets, J.M. and Dresher, W.H. (39)

Figure 3

Nickel - Sulphur - Oxygen Phase Stability Diagram

(a) Three Dimensional Phase Stability Diagram.
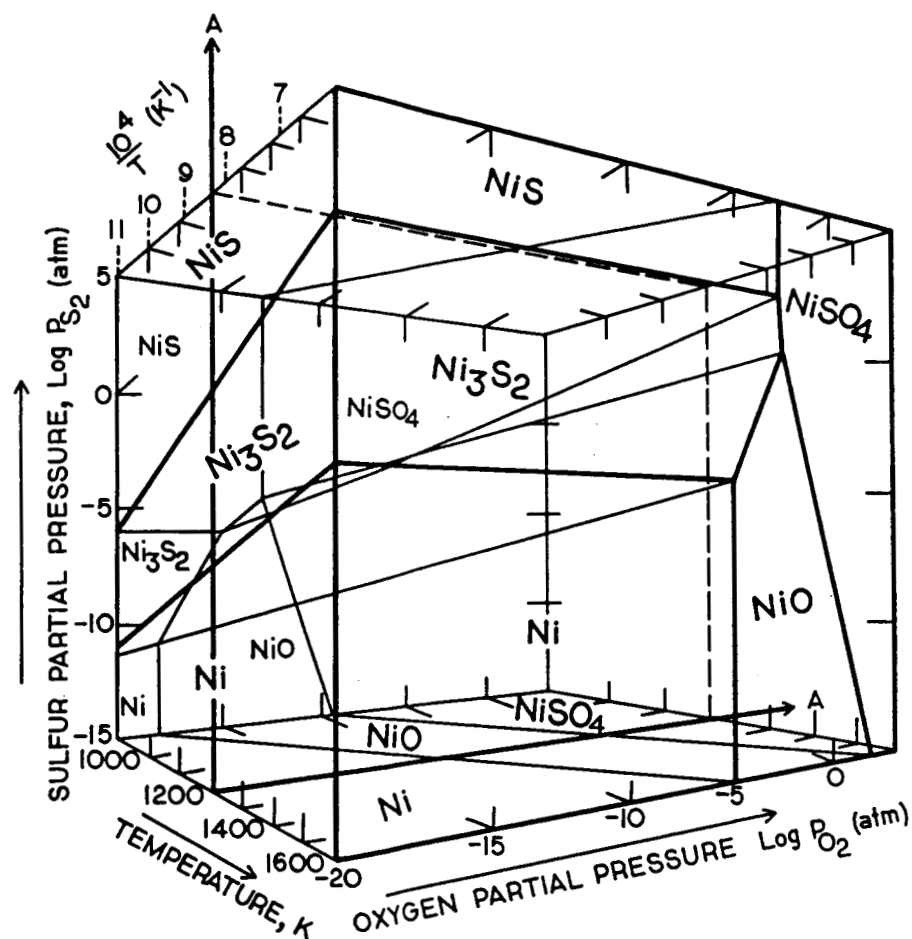
From Quets, J.M. and Dresher, W.H. (39)

(b) Phase Stability Diagram at 1200 K

From Quets, J.M. and Dresher, W.H. (39)

Figure 4

Cobalt - Sulphur - Oxygen Phase Stability Diagram

(a) Three Dimensional Phase Stability Diagram

From Ingraham, T.R., Canad. Met. Quarterly, 3, p 221 (1964)

<u>(b) Phase Stability Diagram at 1000°C</u>
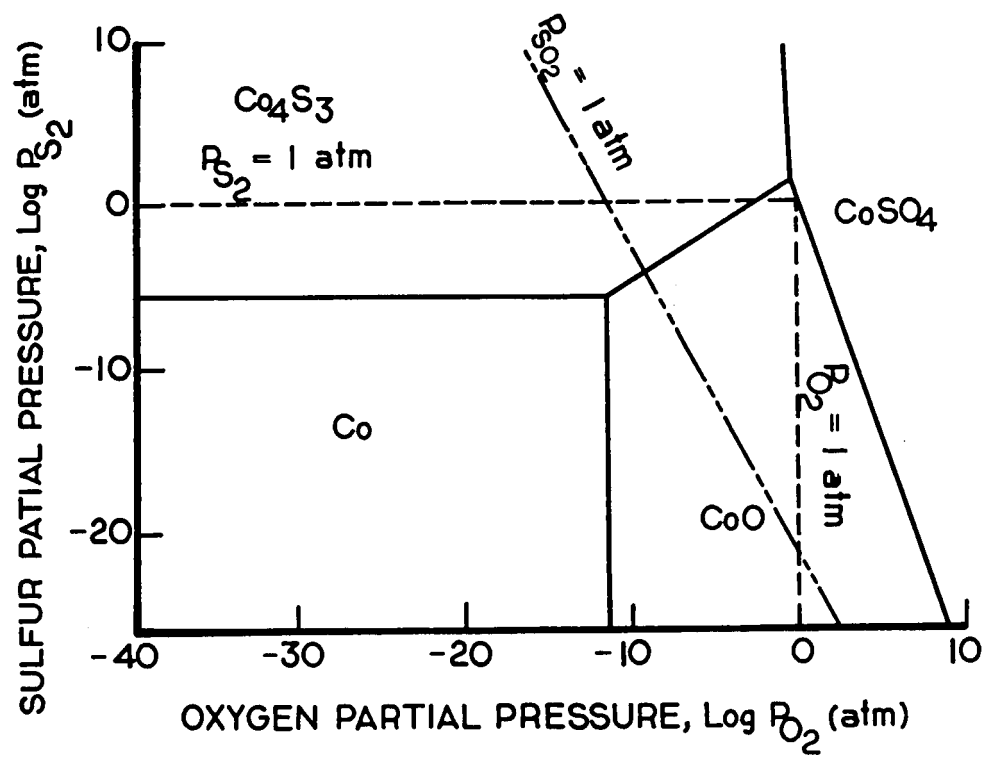
From Ingraham, T.R., Canad. Met. Quarterly, <u>3</u>, p 221 (1964)

Figure 5

Chromium-Sulphur-Oxygen and Sodium-Chromium-Sulphur-Oxygen Phase Stability Diagrams

(a) Chromium-Sulphur-Oxygen Phase Stability Diagram at 1200 K
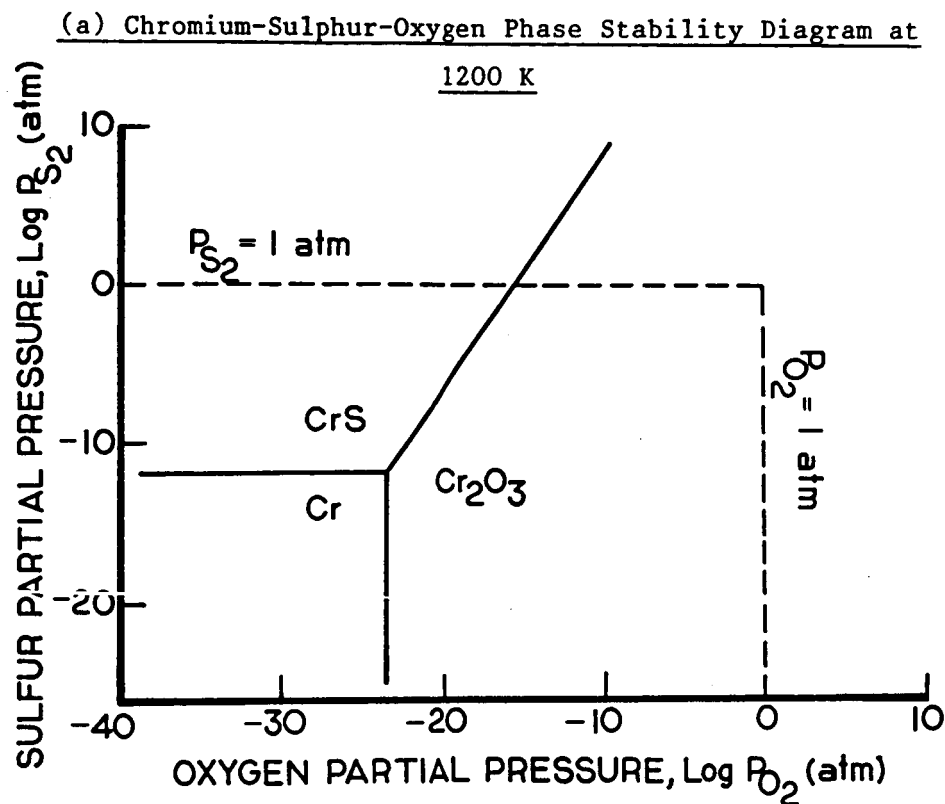
From Quets, J.M. and Dresher, W.H. (39)

(b) Sodium - Chromium - Sulphur - Oxygen

Phase Stability Diagram at 927°C
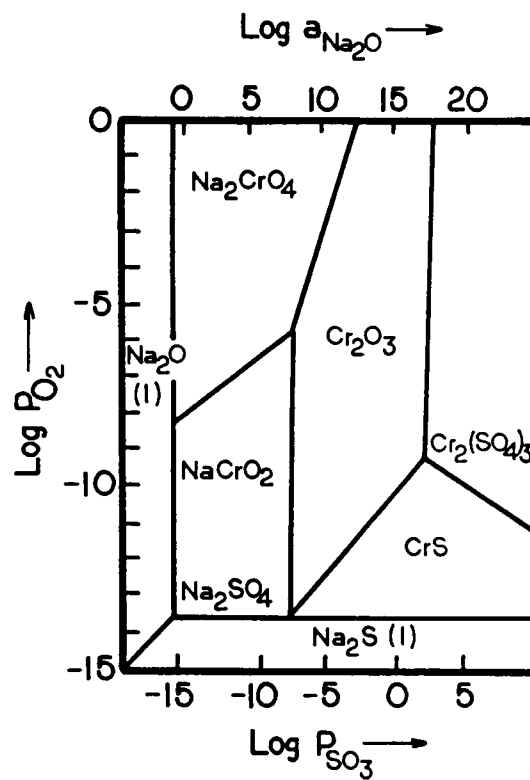
From M. Kawakami, K.S. Goto, and R.A. Rapp (3)

Figure 6

Sodium - Aluminum - Sulphur - Oxygen
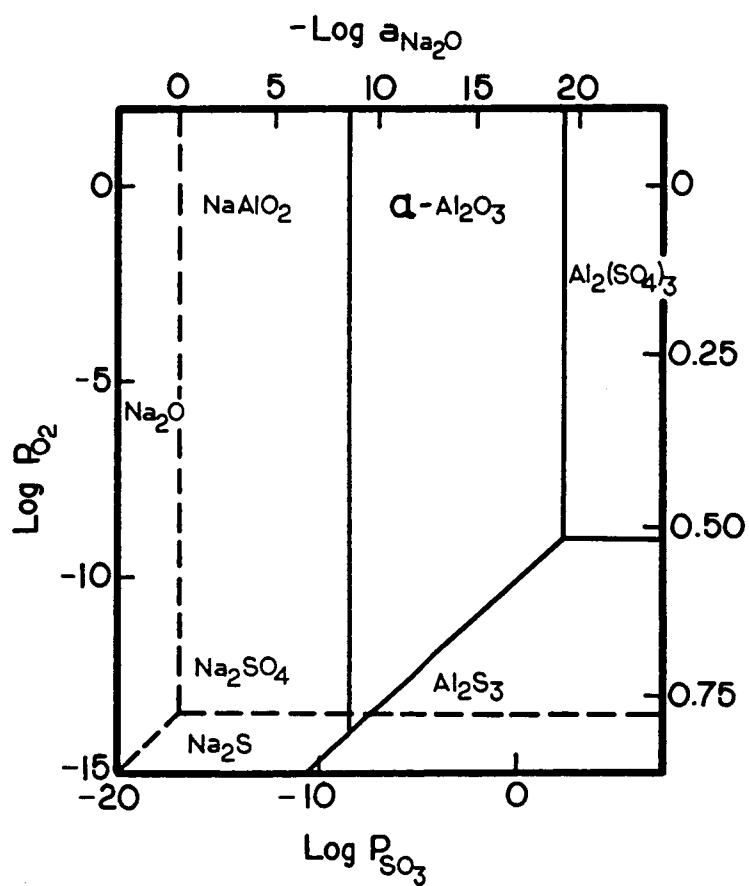
Phase Stability Diagram at 927°C

From W.P. Stroud and R.A. Rapp: Proc. "High Temperature Metal Halide Reactions" Symp., D.L. Hildenbrand and D.D. Cubicciotti eds., The Electrochemical Society, Princeton, p 574 (1978)

Figure 7

Sulphidation Model Schematic Diagram

Step 1 Oxidation

Na_2SO_4

Cr_2O_3 ///////////

Ni-Cr Alloy

$Na_2SO_4 \rightarrow 2Na^+ + SO_4^{2-}$

$SO_4^{2-} \rightarrow S^{2-} + 2O_2$

$2Cr + \frac{3}{2}O_2 \rightarrow Cr_2O_3$

Na_2SO_4 supplies oxygen for the growth of the Cr_2O_3 layer. The activity of sulphur at the Na_2SO_4/Cr_2O_3 interface is increased.

Step 2 Sulphidation

Na_2SO_4

Cr_2O_3 ////////// S

Ni-Cr Alloy   Cr-depleted zone CrS_x

$Cr + xS \rightarrow CrS_x$
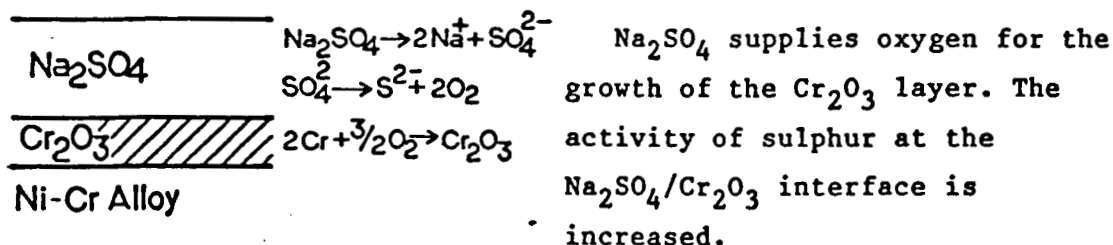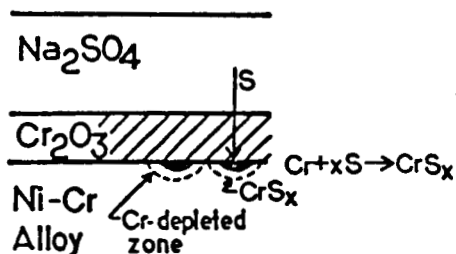
Sulphur diffusing through the Cr_2O_3 layer reacts with the Cr in the alloy to form CrS_x. The surrounding alloy becomes depleted in Cr because of the reaction.

Step 3 Formation of Eutectic and Oxidation of Sulphides

Na_2SO_4

O_2

Oxide Layer ///////

MS

Cr-depleted region

Ni-Cr Alloy

$2MS + O_2 \rightarrow 2MO + S_2$

$2M + S_2 \rightarrow 2MS$
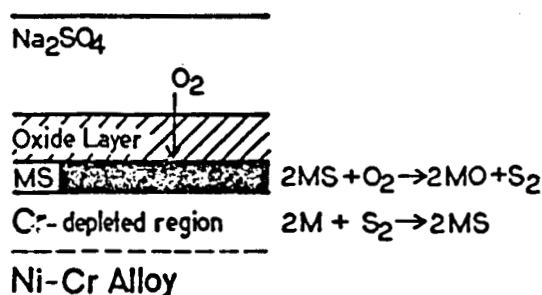
Sulphidation leads to the formation of Cr depleted region and a complete sulphide layer. This layer can be a liquid Ni-Ni_2S_3 or NiO-NiS eutectic. The oxide layer can also change from Cr_2O_3 to a mixture of Ni-Cr oxides. Oxygen diffusing through the oxide layer oxidizes the sulphides. The sulphur diffuses inward to once again react and form more sulphides.

Figure 8

Solubilities of Aluminum and Chromium Ions in Sodium Sulphate as a Function of Oxide Ion Concentration

From W.P. Stroud and R.A. Rapp: Proc. "High Temperature Metal Halide Reactions" Symp., D.L. Hildenbrand and D.D. Cubicciotti eds., The Electrochemical Society, Princeton, p 574 (1978)

143

Figure 9

Basic Fluxing Model Schematic Diagram

Step 1 - Oxidation

O_2

Na$_2$SO$_4$

MO

M

$M + \frac{1}{2}O_2 \rightarrow MO$

Oxidation of the metal M to form MO establishes an oxygen activity gradient across the Na$_2$SO$_4$ layer as in the sulphidation model.

Step 2 - Fluxing and Sulphidation

O_2

MO→

Na$_2$SO$_4$

MO

M   MS

MO$_2^{2-}$

$MO_2^{2-} \rightarrow MO + O^{2-}$

$MO + O^{2-} \rightarrow MO_2^{2-}$

$M + \frac{1}{2}S_2 \rightarrow MS$
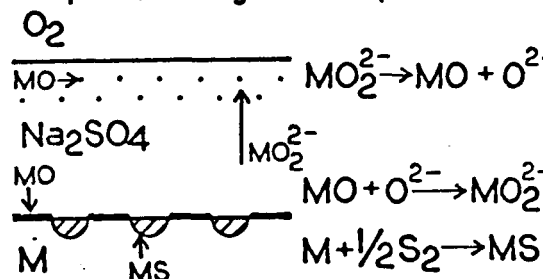
Sulphur reacts with the metal to form MS. Oxide ions react with MO to form soluble MO$_2^{2-}$ ions that diffuse outward due to the oxygen activity gradient. Near the Na$_2$SO$_4$/O$_2$ interface the MO$_2^{2-}$ ions decompose to form a porous MO layer and O^{2-} ions.

Step 3 - Saturation and Return To Normal Oxidation

O_2

MO (porous)

MO (dense)

MS

M
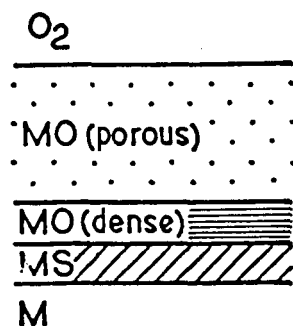
Na$_2$SO$_4$ layer becomes saturated with M. MO forms on the metal surface as a continuous protective oxide layer with MS layer underneath the MO layer.

144

Figure 10

Gas Induced Acidic Fluxing Model Schematic Diagram

Step I – Acidification of Na_2SO_4

O_2/SO_3 SO_3

Na_2SO_4

$SO_3 + O^{2-} \rightarrow SO_4^{2-}$

MO

M

SO_3 enters Na_2SO_4 from the environment. Reaction between the SO_3 and O^{2-} ions lowers the O^{2-} ion concentration at the MO/Na_2SO_4 interface.

Step 2 – Fluxing of Oxide

O_2/SO_3 SO_3

$M^{2+} + O^{2+} \rightarrow MO$

Na_2SO_4 MO

MO M^{2+}

$MO \rightarrow M^{2+} + O^{2-}$

M
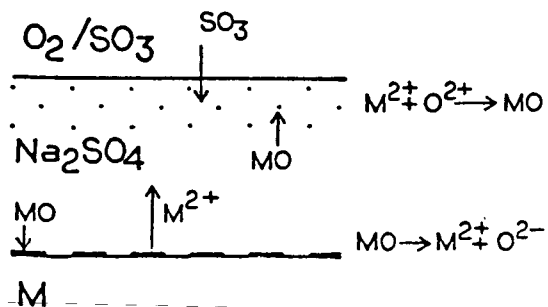
Low O^{2-} ion concentration leads to the disolution of the MO into M^{2+} and O^{2-} ions. M^{2+} ions diffuse outward until the O^{2-} ion concentration is sufficient to reform the MO. Reaction continues as long as SO_3 is available and the Na_2SO_4 layer does not become saturated.

145

Figure 11

<u>Alloy Induced Acidic Fluxing Model Schematic Diagram</u>

Step 1- Acidification of Na_2SO_4

O_2

Na_2SO_4

MO MeO_3 $\uparrow MeO_4^{2-}$

$MeO_3 + O^{2-} \rightarrow MeO_4^{2-}$
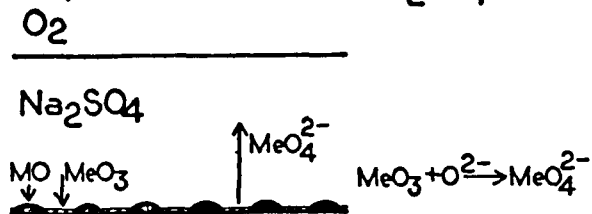
Acidifying alloy addition Me reacts to form MeO_4^{2-} ions and lowers O^{2-} ion concentration at the MO/Na_2SO_4 interface.

Step 2 - Fluxing

O_2

Na_2SO_4 MeO_3 MO

$\dot{M}O \quad \uparrow M^{2+} \quad \uparrow MeO_4^{2-}$

M/Me

$MeO_4^{2-} \rightarrow MeO_3 + O^{2-}$
$M^{2+} + O^{2-} \rightarrow MO$
$MeO_3 + O^{2-} \rightarrow MeO_4^{2-}$
$MO \rightarrow M^{2+} + O^{2-}$
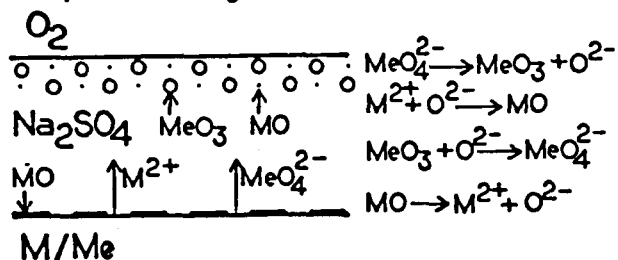
Lowered O^{2-} concentration leads to the disolution of MO into M^{2+} and O^{2-} ions. The M^{2+} diffuses outward until the O^{2-} concentration is sufficient to form MO. MeO_3 continues to acidify the Na_2SO_4 layer.

Step 3 - Volatilization

O_2 $\uparrow MeO_x (g)$

Na_2SO_4 $\uparrow MO$ $\uparrow MeO_3$

MO

M/Me

$MeO_3 \rightarrow MeO_x(g) + \frac{3-x}{2}O_2$
$MeO_4^{2-} \rightarrow MeO_3 + O^{2-}$
$M^{2+} + O^{2-} \rightarrow MO$
$MeO_3 + O^{2-} \rightarrow MeO_4^{2-}$
$MO \rightarrow M^{2+} + O^{2-}$
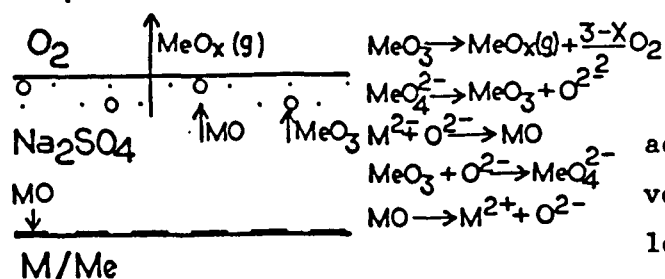
At temperature, the acidifying element oxides are volatile. As a result Me is lost to the atmosphere and the Na_2SO_4 can not become saturated with Me.

Figure 12

Pseudo-Scale Model Schematic Diagram

Step 1-Initial Conditions / Initiation of Hot Corrosion

$$O_2$$

$$\overline{Na_2SO_4 (\ell)} \quad \uparrow M^{2+} \quad M^{2+} + O^{2-} \longrightarrow MO$$
$$O^{2-} \quad$$
$$O_2 \downarrow \quad M + \tfrac{1}{2}O_2 \xrightarrow{Na_2SO_4} M^{2+} + O^{2-}$$

M

Metal is oxidized at the M/Na_2SO_4 interface to form M^{2+} and O^{2-} ions that migrate through the Na_2SO_4 layer.
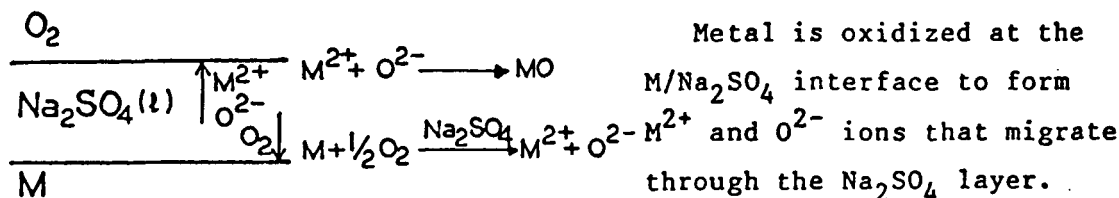
Step 2-Growth of Porous MO Layer

$$O_2$$

$$\overline{MO \,(porous)} \cdots \downarrow O_2 \quad M^{2+} + O^{2-} \longrightarrow MO$$

$$\overline{Na_2SO_4 (\ell)} \quad \uparrow M^{2+} \quad$$
$$O^{2-} \downarrow O_2 \quad M + \tfrac{1}{2}O_2 \xrightarrow{Na_2SO_4} M^{2+} + O^{2-}$$

M

M^{2+} and O^{2-} ions reach the Na_2SO_4/O_2 interface and form a porous MO layer that allows O_2 to diffuse through it. The reaction continues at the Na_2SO_4/M interface.
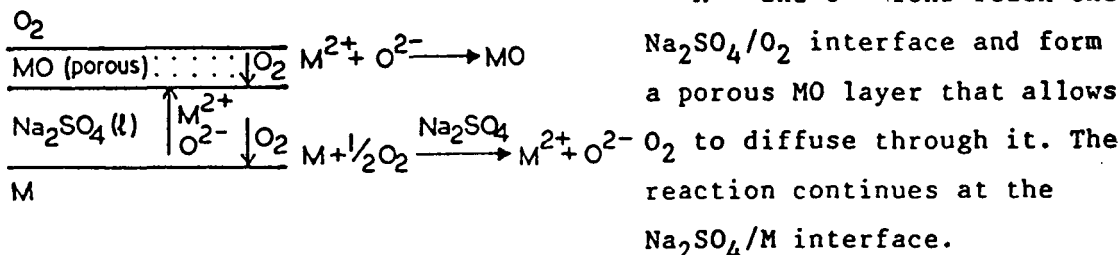
Step 3-End of the Growth of the Porous MO Layer

$$O_2$$

MO (porous) $\downarrow O_2$

M

Inward growth of the porous MO layer continues until all the Na_2SO_4 layer is incorporated into the MO layer. O_2 can still diffuse through the porous MO layer and reach the MO/M interface.
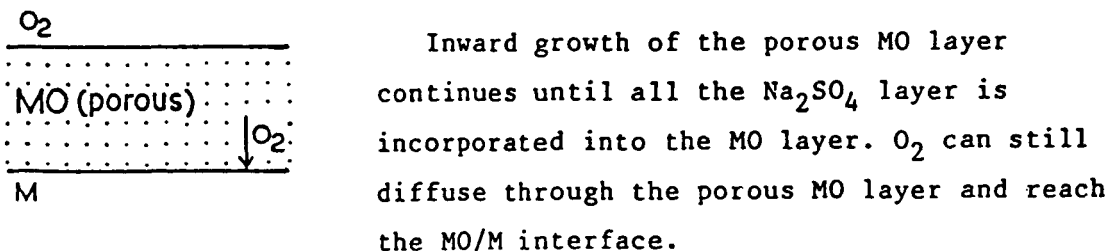
Step 4-Formation of dense MO Layer

$$O_2$$

MO (porous) $\downarrow O_2$

MO (dense) $\quad M + \tfrac{1}{2}O_2 \longrightarrow MO$

M

Metal undergoes normal oxidation under the porous MO layer
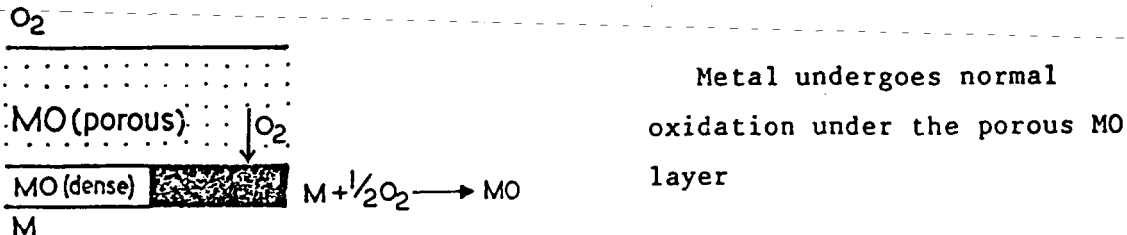
Figure 13

Volatile Product Hot Corrosion Mechanism

As Proposed by Davin et al

$$MCl_2 + \tfrac{1}{2}O_2 \rightarrow MO + Cl_2$$

$$MO + 2\,NaCl \rightarrow MCl_2 + Na_2O$$
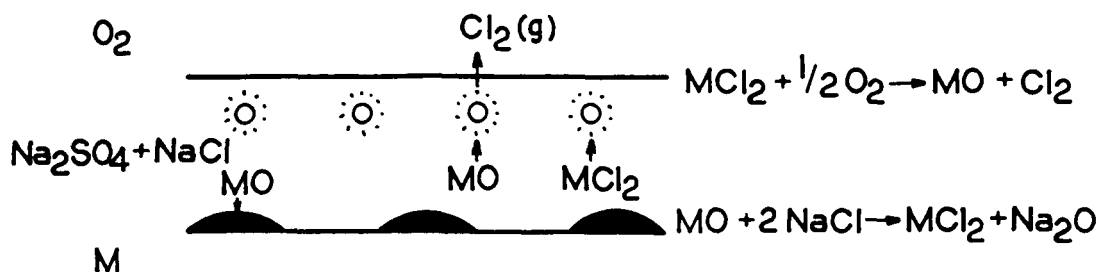
The MO at the Na_2SO_4+NaCl/M interface reacts with the NaCl to form MCl_2 particles. The MCl_2 particles move into the Na_2SO_4+NaCl layer. Near the Na_2SO_4+NaCl/O_2 interface, the MCl_2 particles are oxidized to form Cl_2 (g) and MO precipitates.

As Proposed by Hurst et al
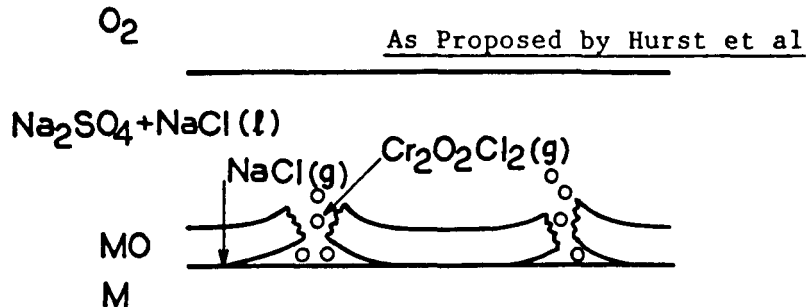
Gaseous NaCl reaches the M/MO interface where it reacts to form $Cr_2O_2Cl_2$ (g) bubbles. The high pressures generated ruptures the MO layer. Fresh salt with a high O_2 potential and NaCl concentration can make direct contact with the metal surface.

From Kawakami, Goto, and Rapp (3)

148

Figure 14

Local Cell Model Proposed by Rapp and Goto

For High Permeability of O_2 in Thin Salt Layer

O_2

Na_2SO_4 $SO_3 + 2\bar{e} \longrightarrow SO_2 + O^{2-}$ Or

$\frac{1}{2}O_2 + 2\bar{e} \longrightarrow O^{2-}$

MO $\uparrow M^{2+} \uparrow 2\bar{e}$ Low C_{O_2} High

M $M \longrightarrow M^{2+} + 2\bar{e}$
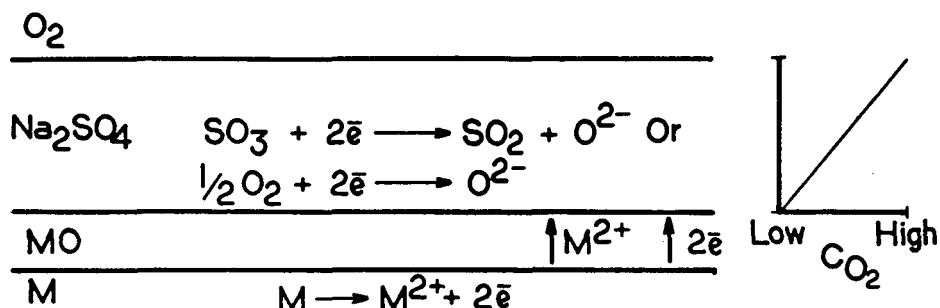
An anodic half-reaction occurs at the M/MO interface and results in M^{2+} ions and electrons. A variety of cathodic half-reactions can occur at the MO/Na_2SO_4 interface that reduce O_2 or SO_2 to form O^{2-} ions. The O^{2-} ions generate locally basic conditions. Acidic or basic fluxing of the MO layer can occur depending on the O^{2-} concentration at the MO/Na_2SO_4 interface.

O_2 For A Transition Element Impurity Me^{3+}

$2Me^{2+} + \left\{ \begin{array}{l} \frac{1}{2}O_2 \\ SO_3 \end{array} \right\} \longrightarrow 2Me^{3+} + \left\{ \begin{array}{l} O^{2-} \\ O^{2-} + SO_2 \end{array} \right\}$

Na_2SO_4 Low C_x High Me^{2+}

MeO $Me^{2+}_{oxide} + Me^{3+}_{Na_2SO_4} \longrightarrow 2M^{2+}_{Na_2SO_4} + {}^{h}oxide$ $\uparrow M^{2+} \uparrow 2\bar{e}$

M/Me $Me \longrightarrow Me^{2+} + 2\bar{e}$
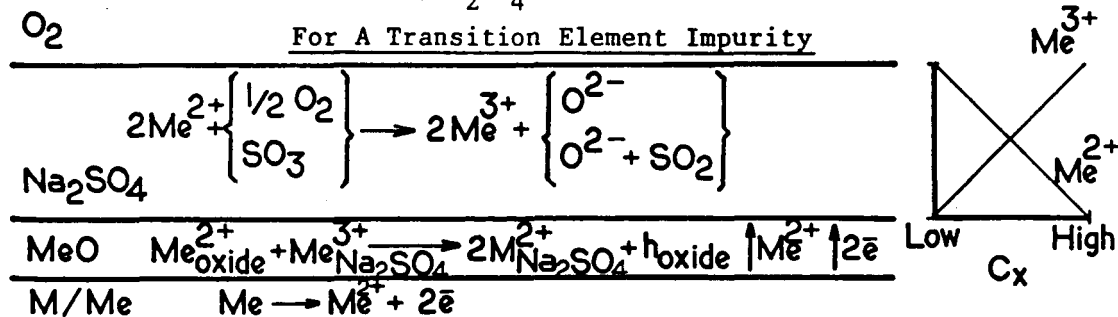
The transition element Me is reduced from Me^{3+} to Me^{2+} at the MeO/Na_2SO_4 interface. The Me^{2+} ions migrate to the O_2/Na_2SO_4 interface where they are oxidized to form Me^{3+} and O^{2-} ions. Acidic or basic fluxing of MeO can occur. Thinning of the protective MeO layer leads to accelerated metal recession and consumption of the protective Me.

149

Figure 15
Crucible Hot Corrosion Test Method
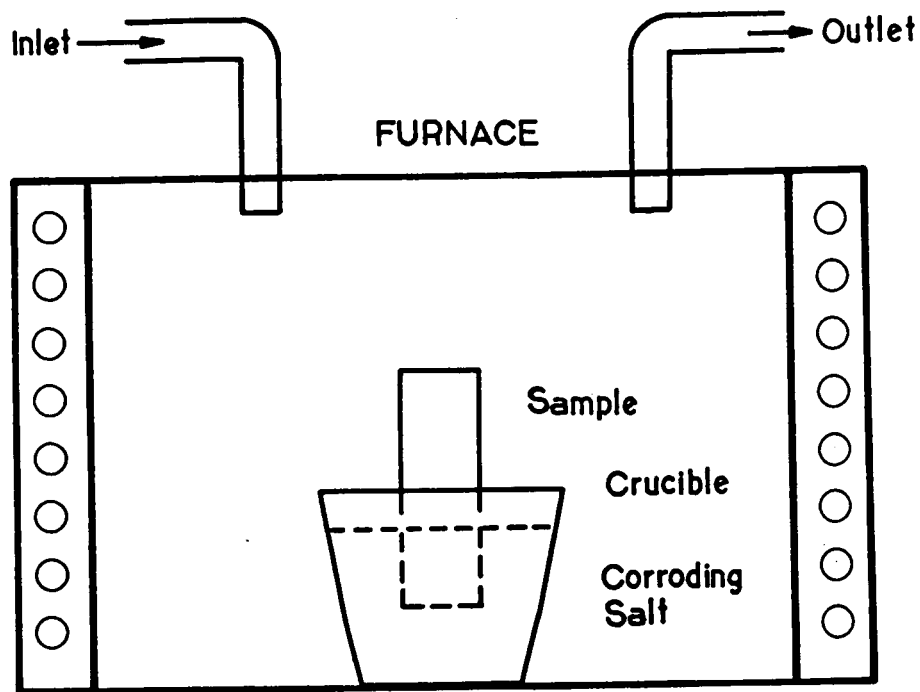
In addition to the atmosphere control indicated in the figure, gases can be bubbled through the salt and an electrical potential applied between the salt and sample.

Figure 16
Typical TGA Furnace Rig
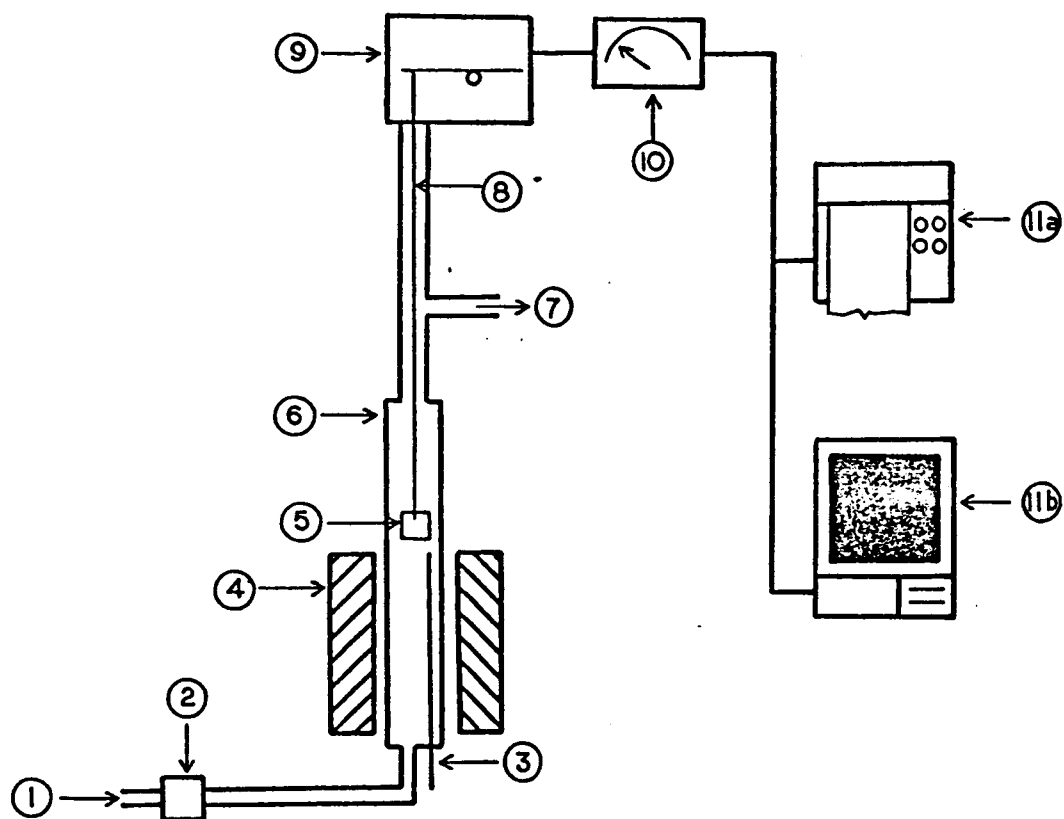
① Input Gas   ⑦ Exit Gas
② Flow Controller   ⑧ Platinum Wire
③ Thermocouple   ⑨ Microbalance
④ Raisable Verticle Furnace   ⑩ Weight Suppression Unit
⑤ Sample   ⑪a Strip Chart Recorder
⑥ Sealed Furnace Tube ⑪b Computer

Figure 17

General Electric Burner Rig Schematic
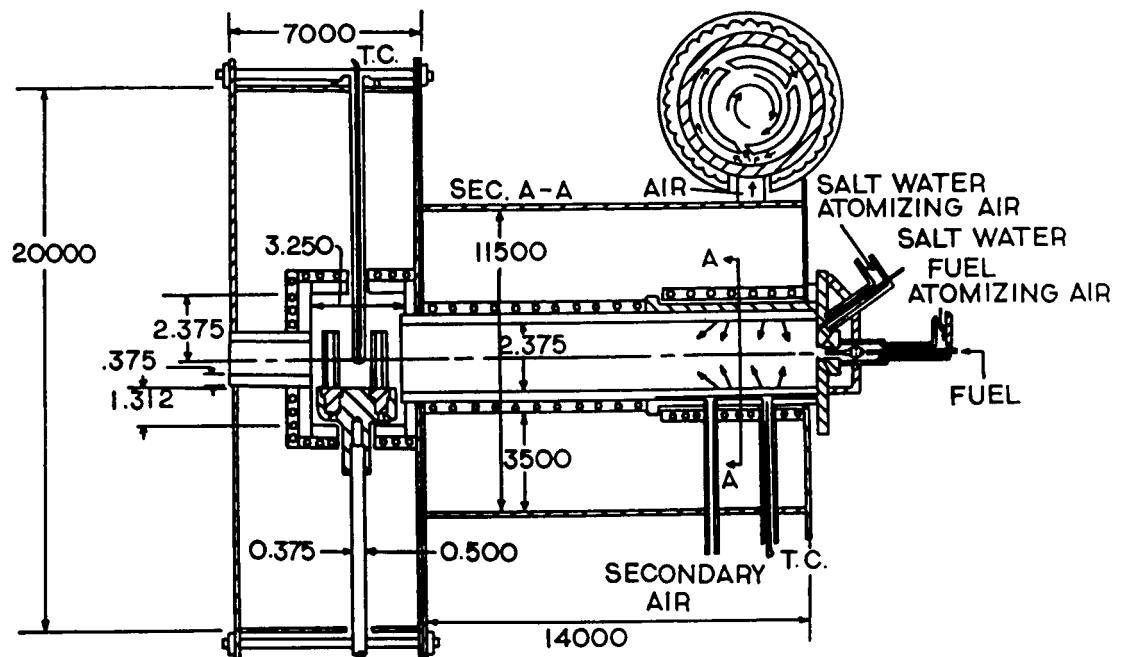
From Bergman, P.A., Sims, C.L., and Beltran, A.N. (40)

Figure 18

Oxidation Map for Nickel - Aluminum Alloys
Between 900°C and 1300°C
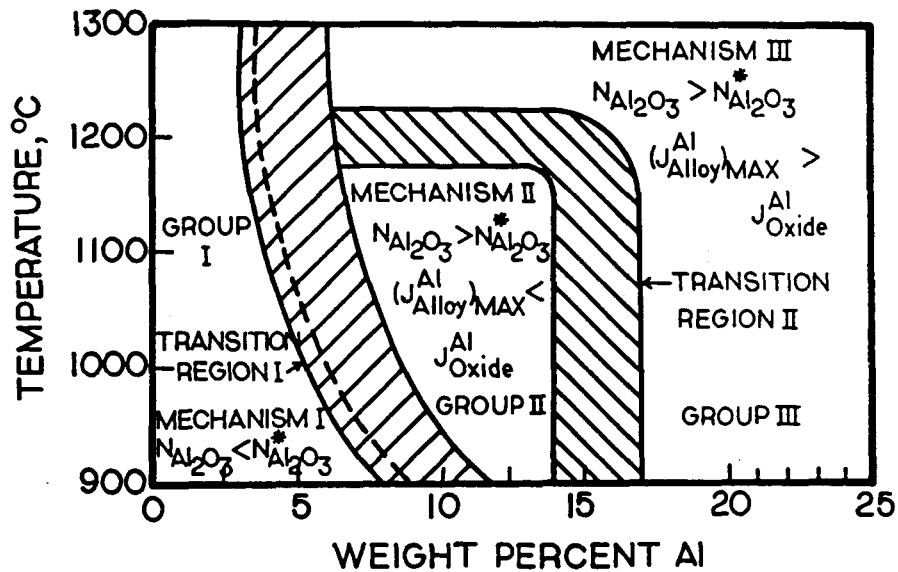
Mechanism I - Nickel oxide scale

Mechanism II - Nickel - aluminum mixed oxide scale

Mechanism III - Alumina scale

From Petit, F.S. (67)

Figure 19

Nickel – Chromium – Aluminum Oxidation Map for Nickel-Rich

Alloys Between 1000°C and 1200°C

(a) Oxidation Maps
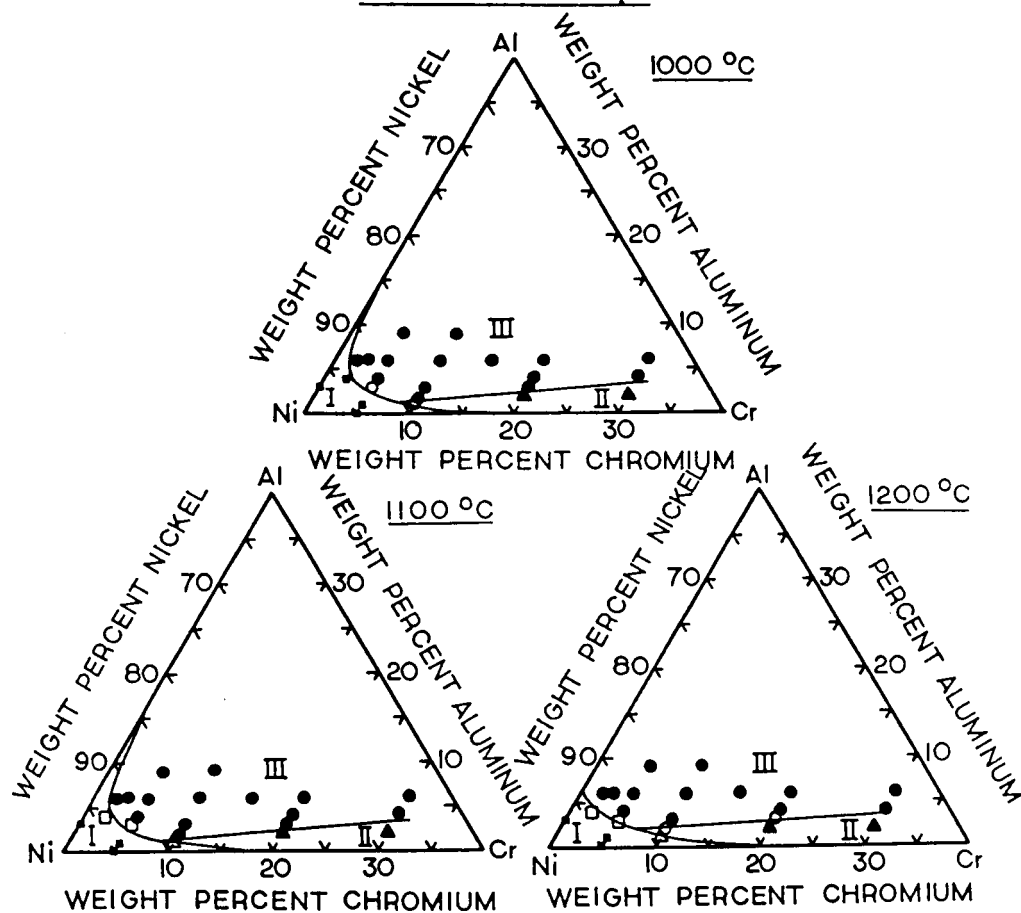
From Giggins, C.S., and Pettit, F.S. (70)

(b) Oxidation Mechanisms

S : Ni(Cr,Al)$_2$O$_4$

● : Cr$_2$O$_3$

○ : Al$_2$O$_3$
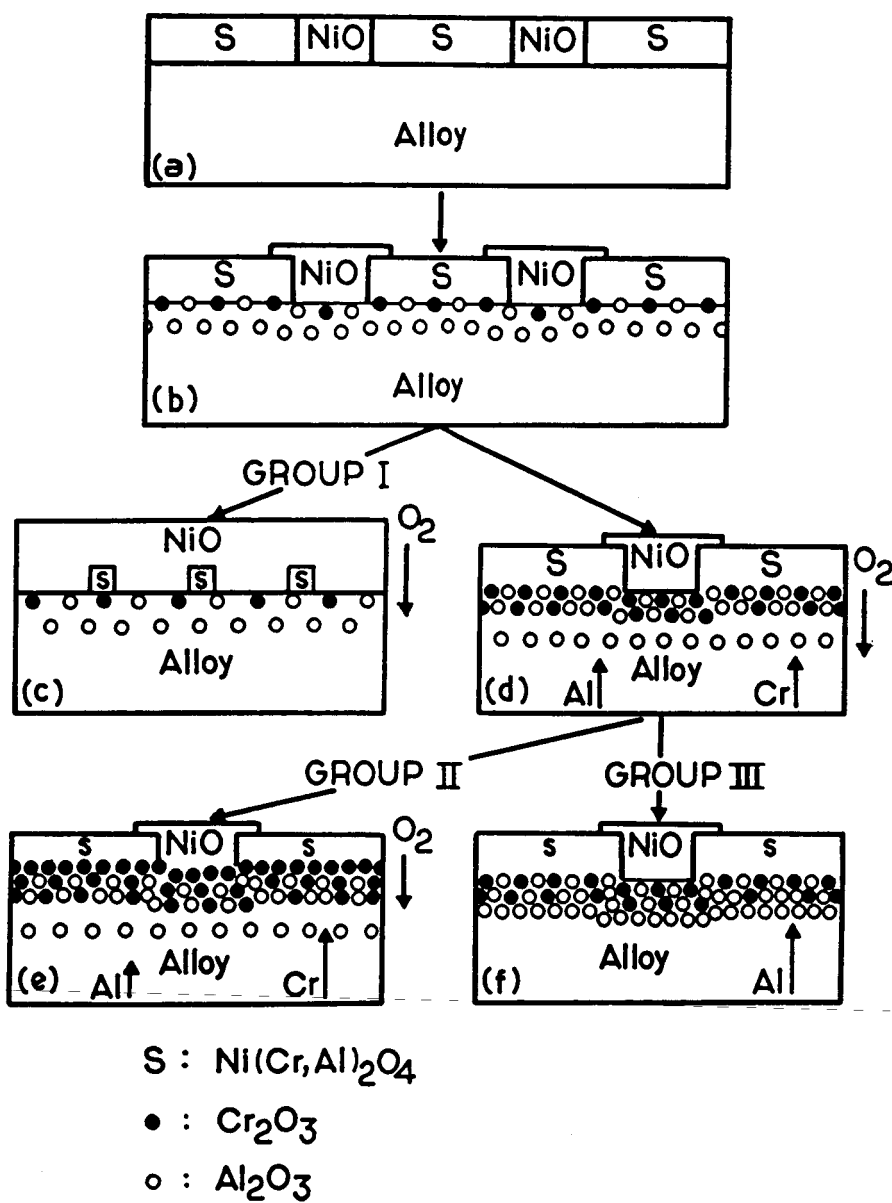
From Giggins, C.S., and Pettit, F.S. (70)

Figure 20

Nickel – Chromium – Aluminum Phase Diagram
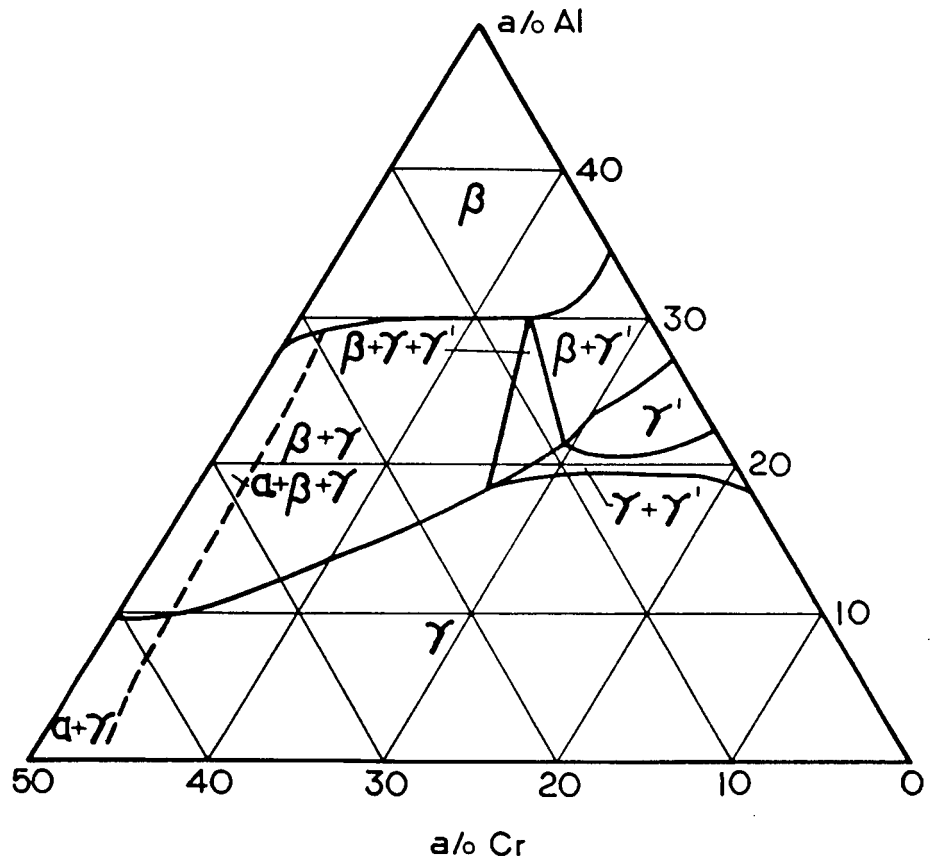
From McCarron, R.L., Lindblad, N.R., and Chatterji, D. (71)
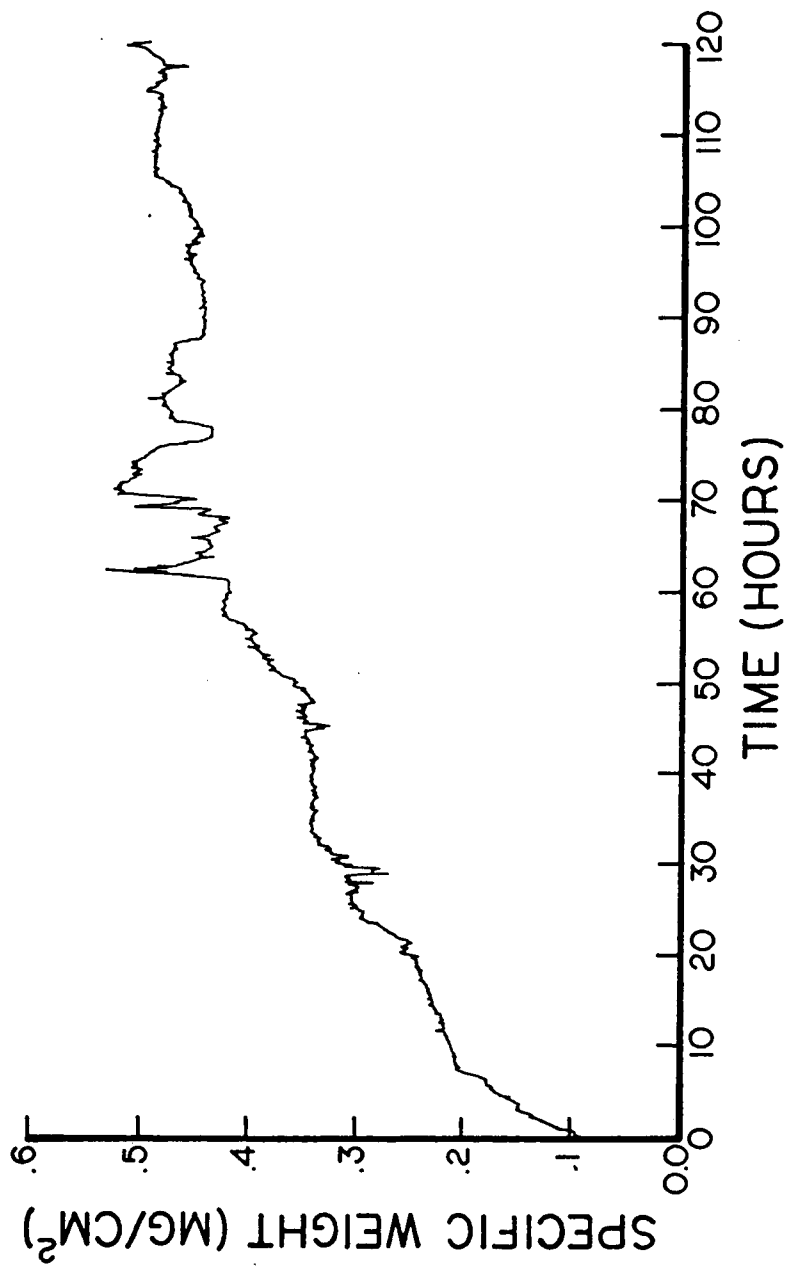
Figure 21

Ni – 45 a/o Al – 0.2 w/o Zr (P/M) 900°C Oxidation Weight Gain Curve
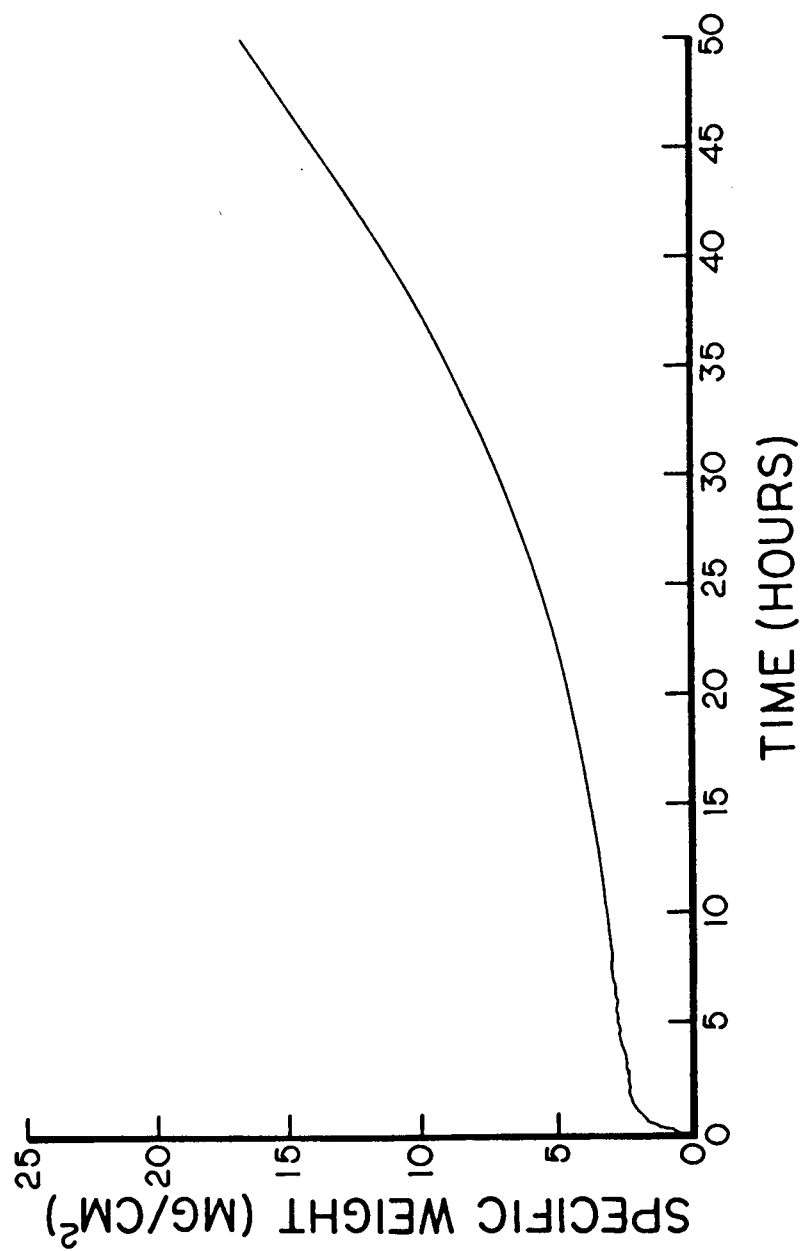
Figure 22

Ni - 45 a/o Al - 0.2 w/o Zr (P/M) Hot Corrosion Weight Gain Curve
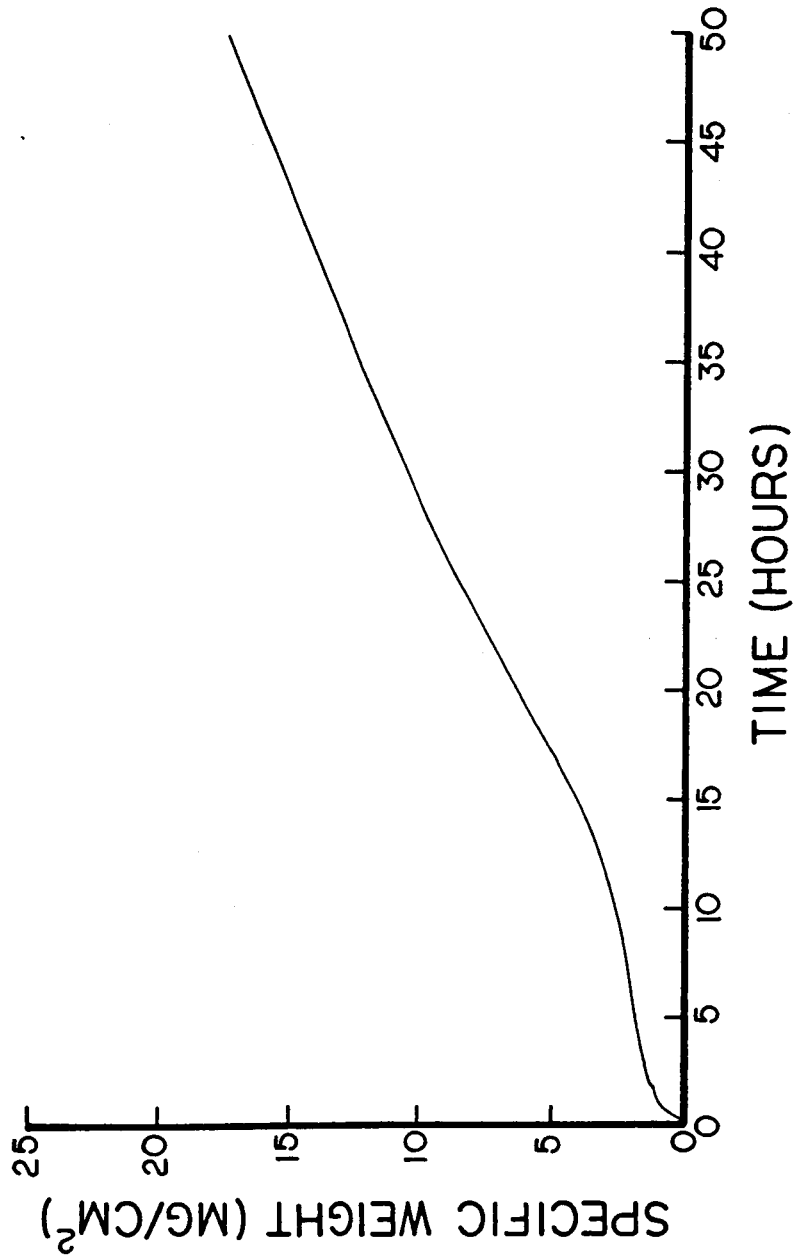
Ni – 45 a/o Al – 0.2 w/o Zr Hot Corrosion Weight Gain Curve
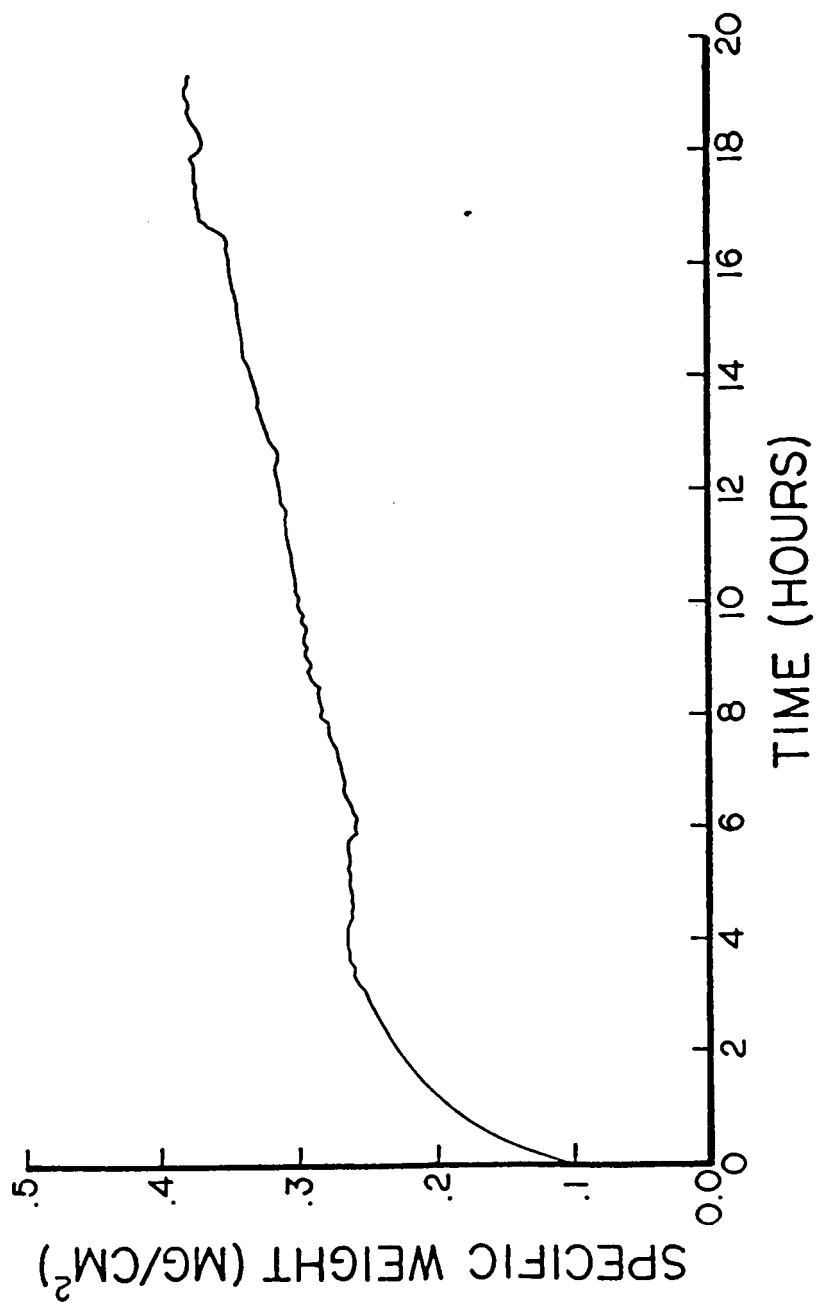
Figure 23

Figure 24

Ni – 50 a/o Al 900°C Oxidation Weight Gain Curve
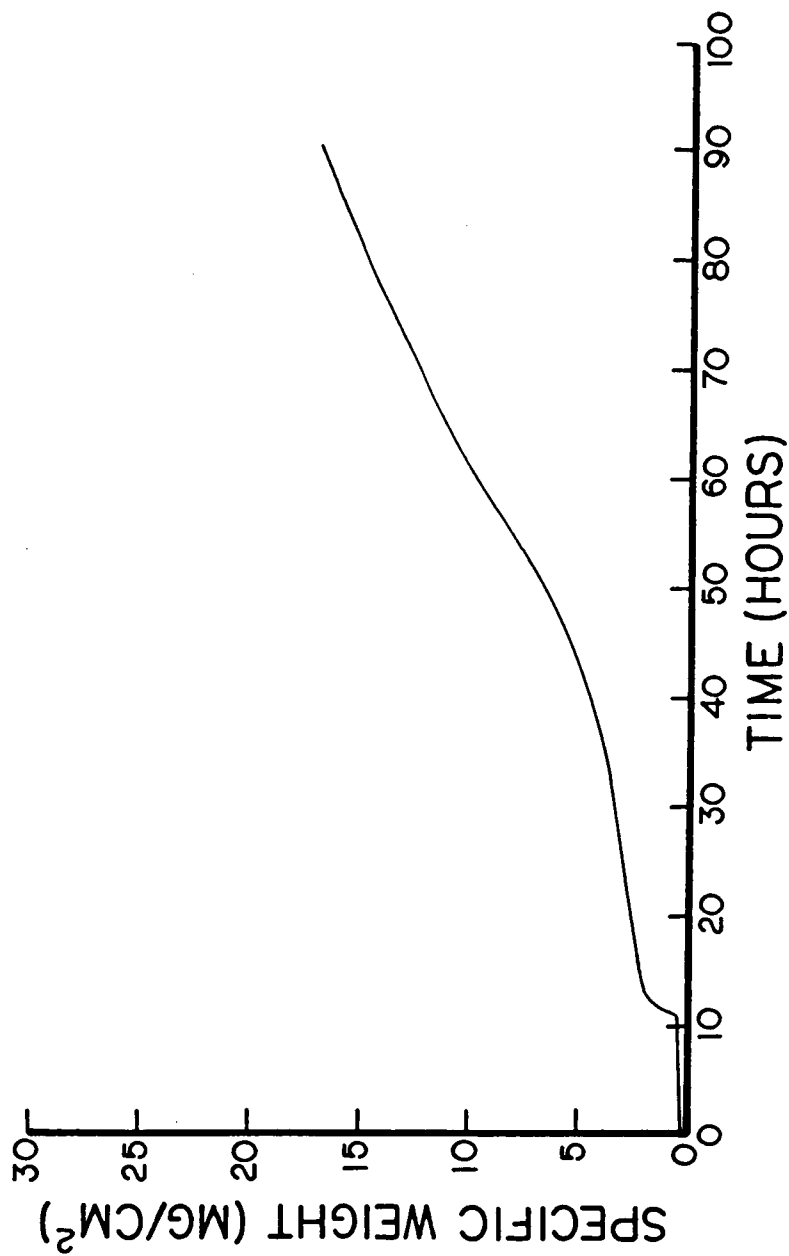
Figure 25

Ni - 50 a/o Al Hot Corrosion Weight Gain Curve
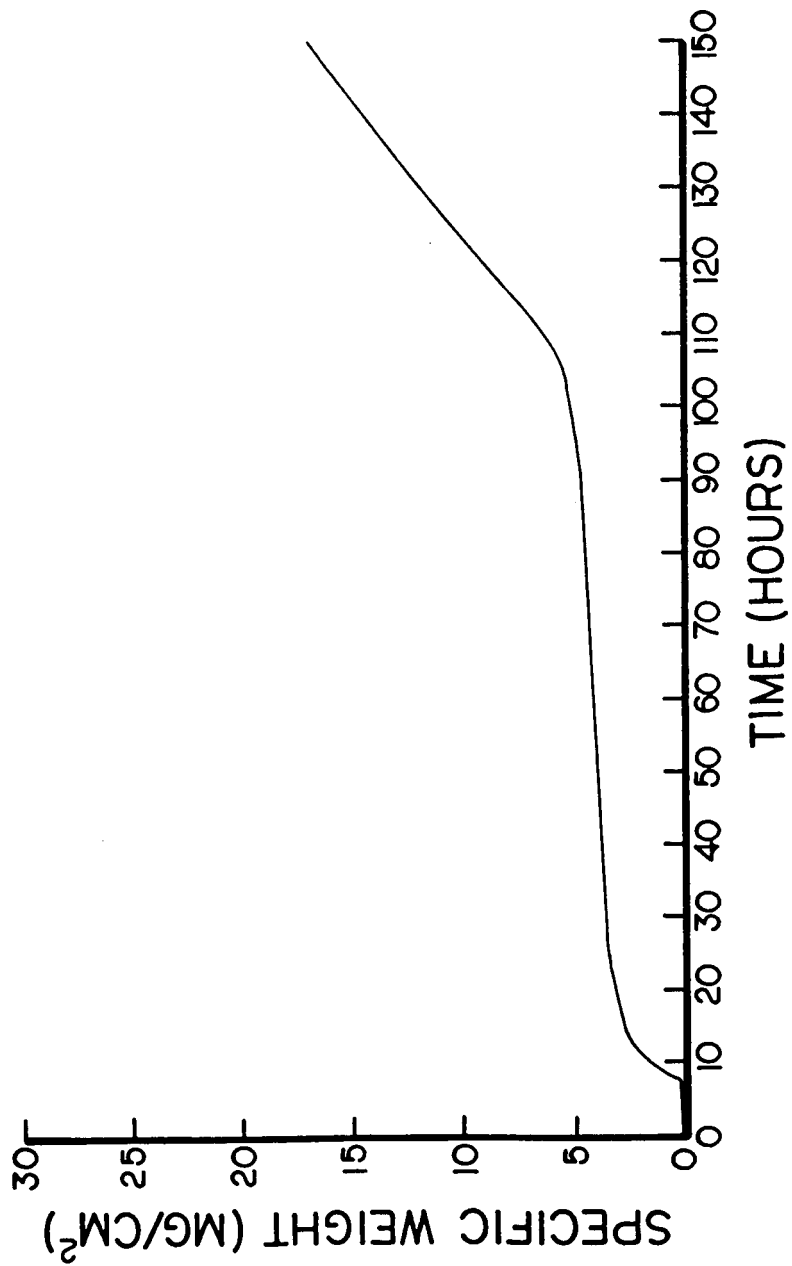
Figure 26

Ni – 50 a/o Al – 0.3 w/o Zr Hot Corrosion Weight Gain Curve
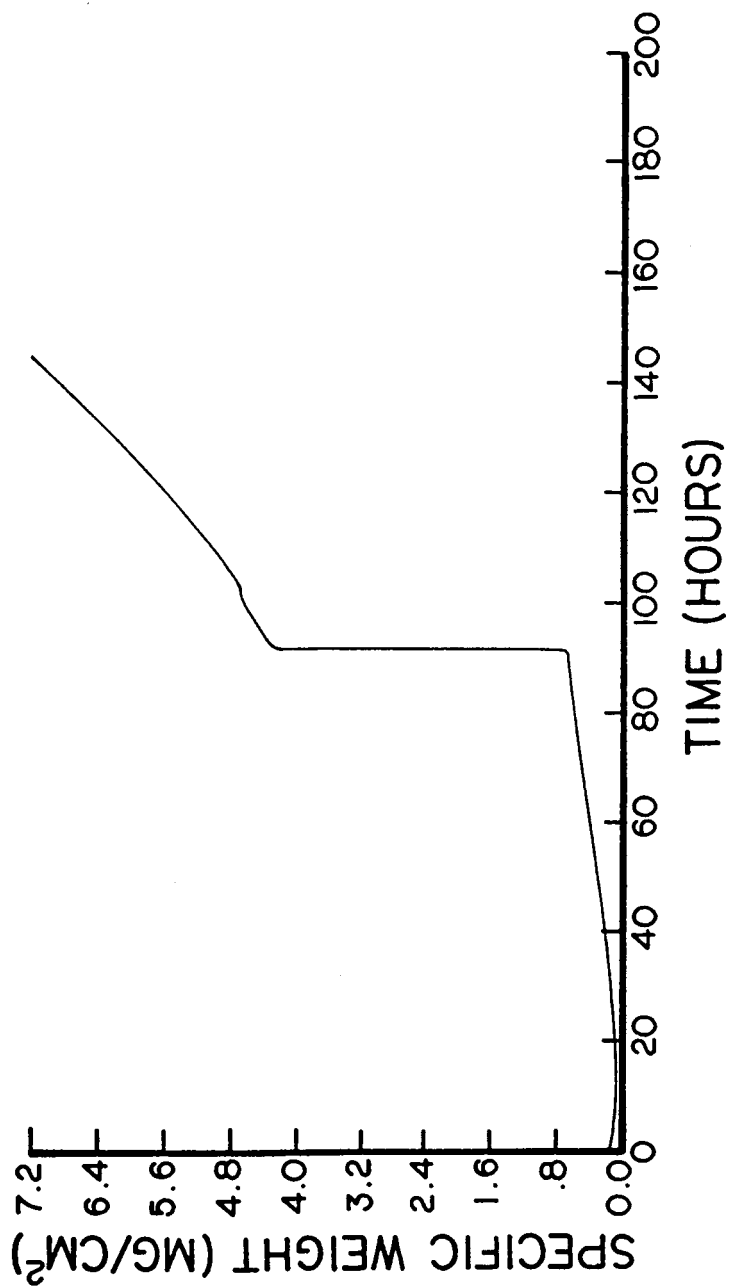
Figure 27

Ni – 24 a/o Al – 15 w/o Cr – 0.3 w/o Zr Hot Corrosion Weight Gain Curve
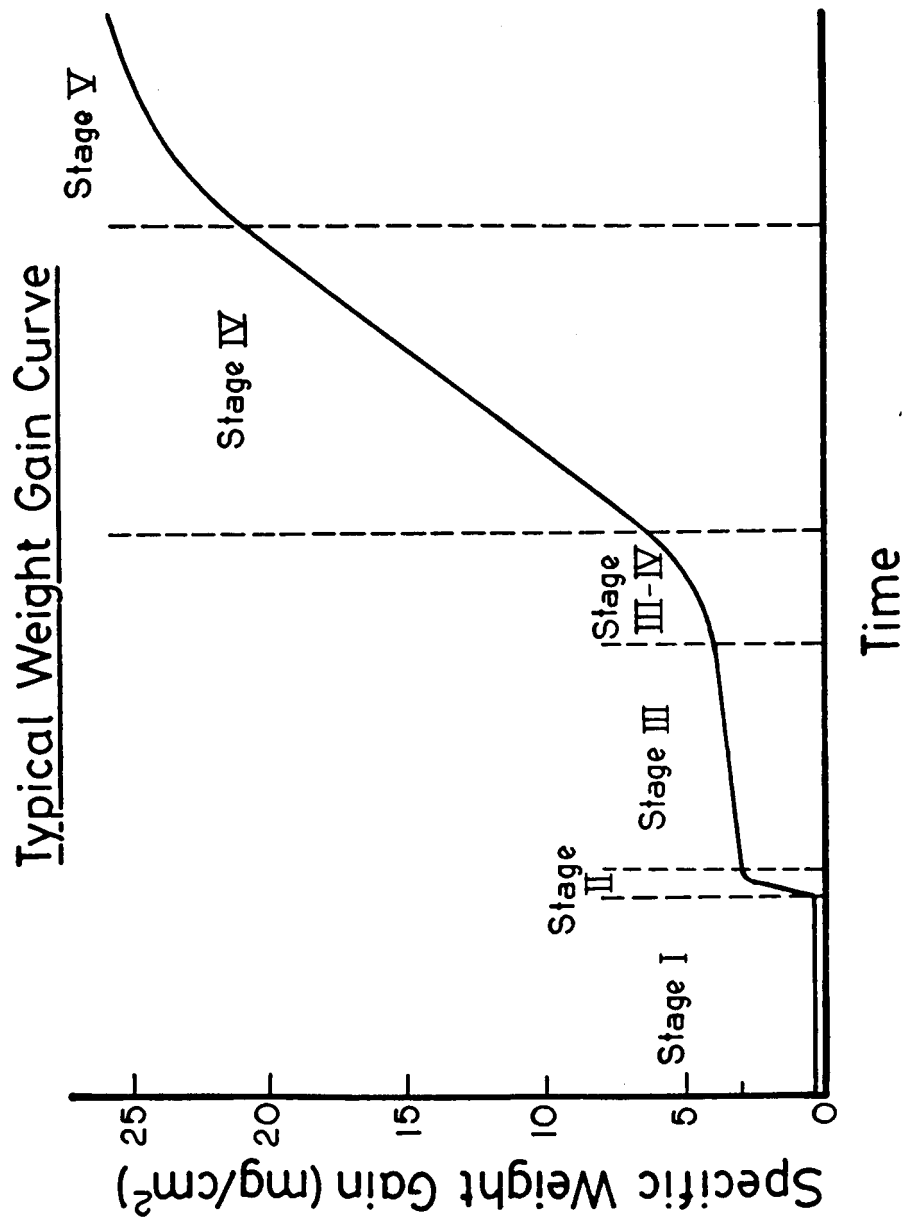
Figure 28

Figure 29

Typical As Received Optical Micrographs
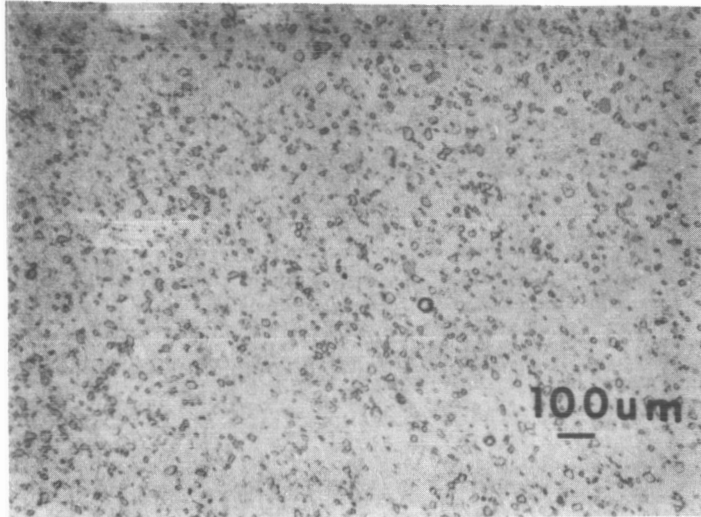
(a) P/M Ni - 45 a/o Al - 0.2 w/o Zr
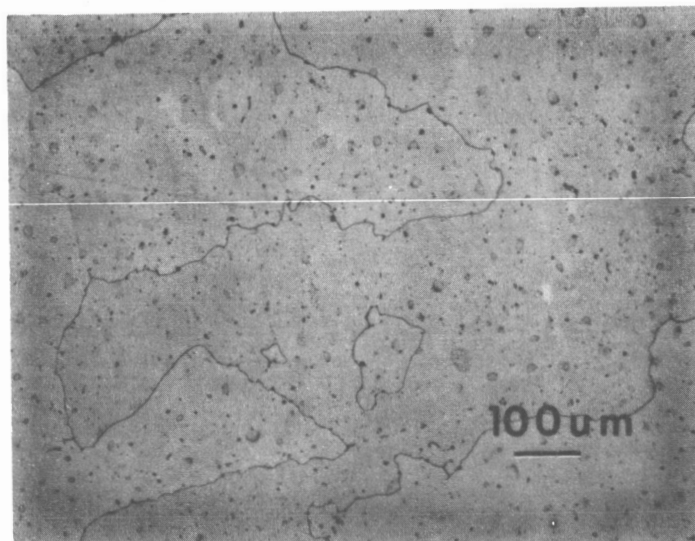
(b) Cast Ni - 45 a/o Al - 0.2 w/o Zr
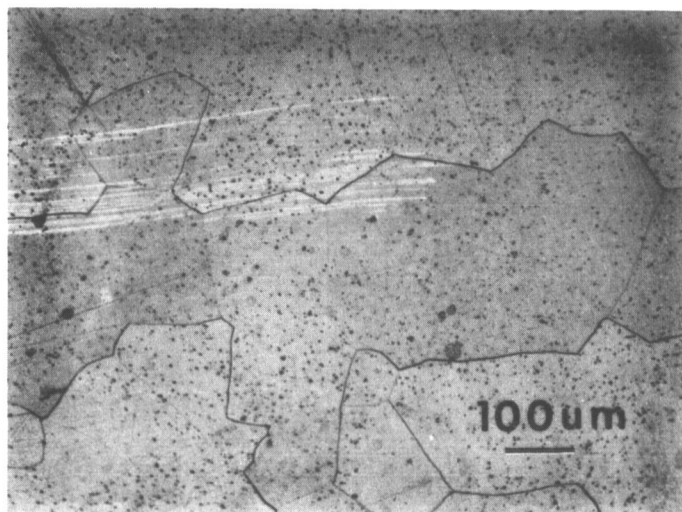
(c) Cast Ni - 50 a/o Al
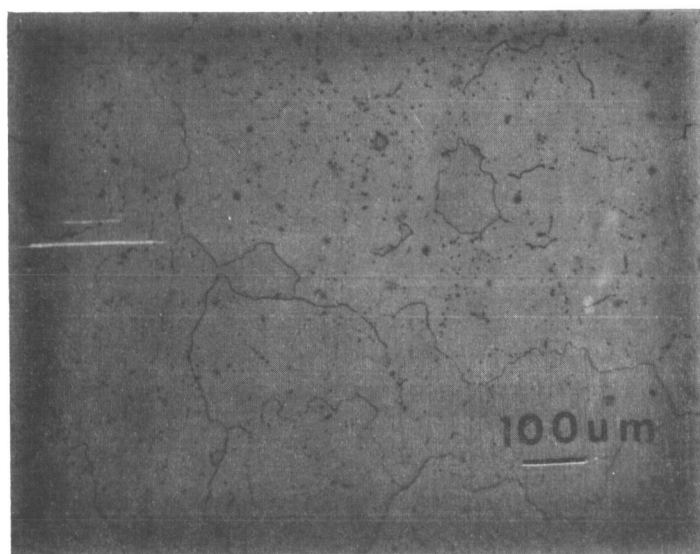
(d) Cast Ni - 50 a/o Al - 0.3 w/o Zr
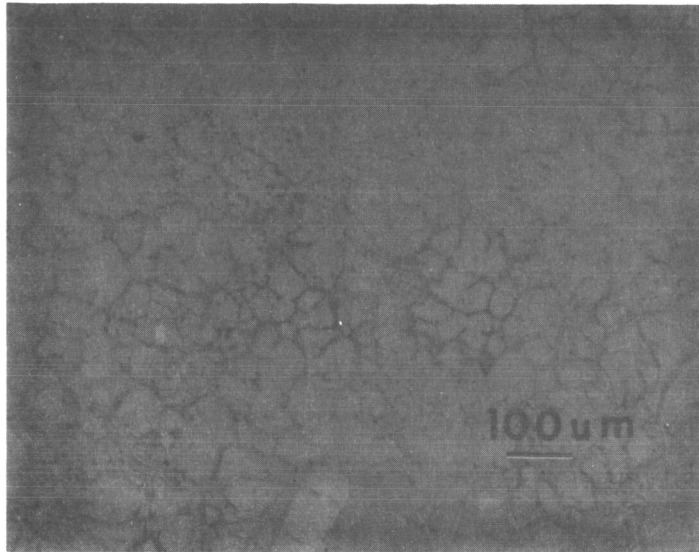
(e) Cast Ni - 48 a/o Al - 2 w/o Cr
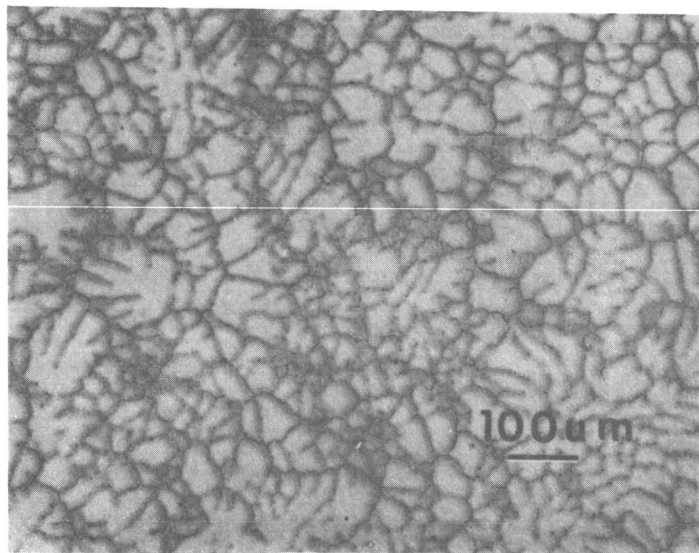
(f) Cast Ni - 47 a/o Al - 5 w/o Cr
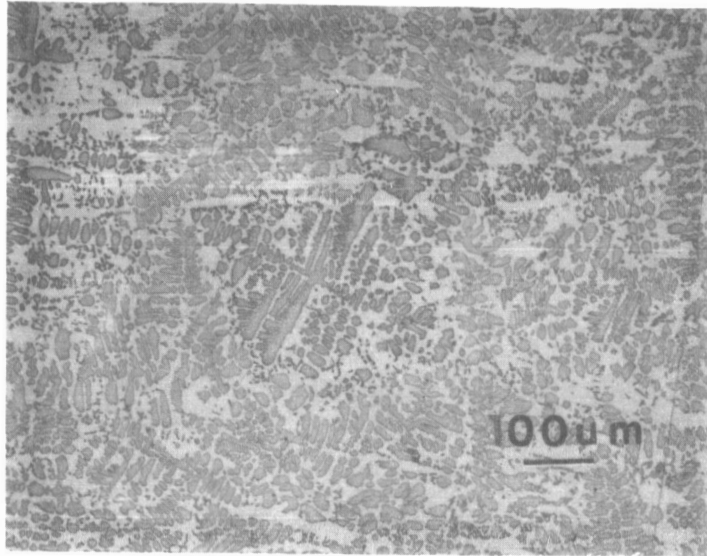
(g) Cast Ni - 24 a/o Al - 15 w/o Cr - 0.2 w/o Zr

Figure 30

Typical Optical Macrographs of Hot Corroded Specimens
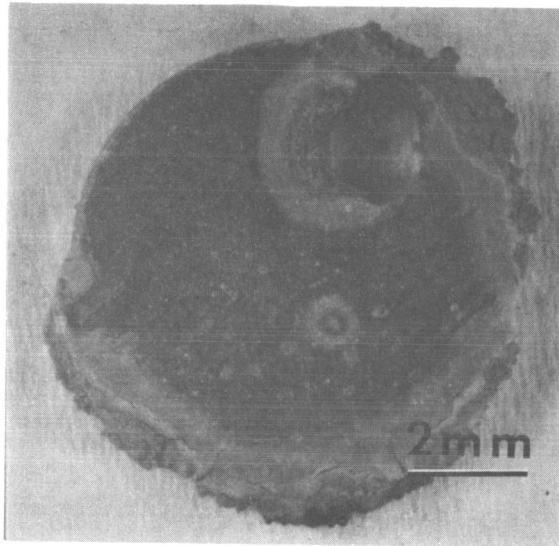
(a) P/M Ni - 45 a/o Al - 0.2 w/o Zr

(b) Cast Ni - 50 a/o Al

169
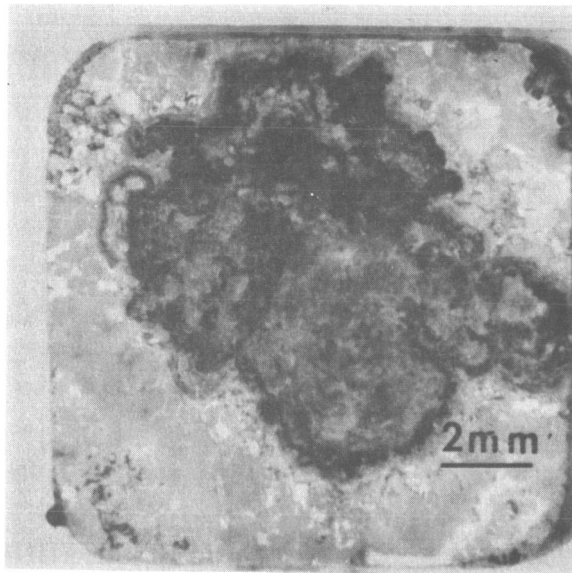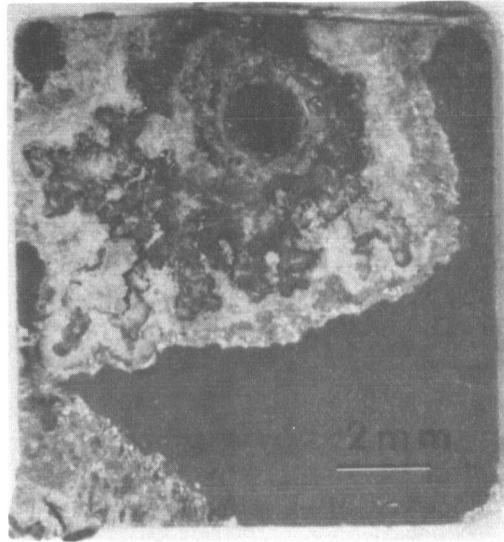
(c) Cast Ni - 50 a/o Al - 0.3 w/o Zr
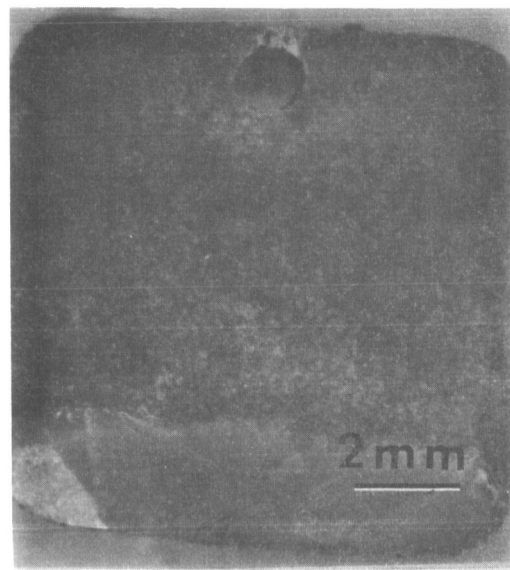
(d) Cast Ni - 47 a/o Al - 5 w/o Cr
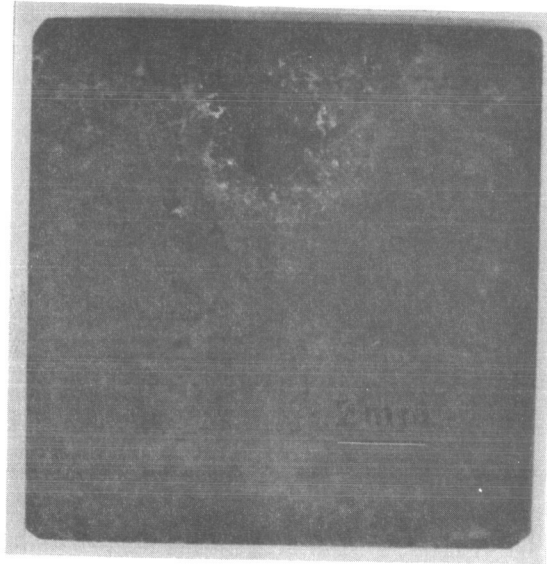
(e) Cast Ni - 24 a/o Al - 15 w/o Cr - 0.2 w/o Zr

Figure 31
Typical Transverse Optical Micrographs of
Hot Corroded Specimens

(a) P/M Ni – 45 a/o Al – 0.2 w/o Zr

(b) Cast Ni – 45 a/o Al – 0.2 w/o Zr

172
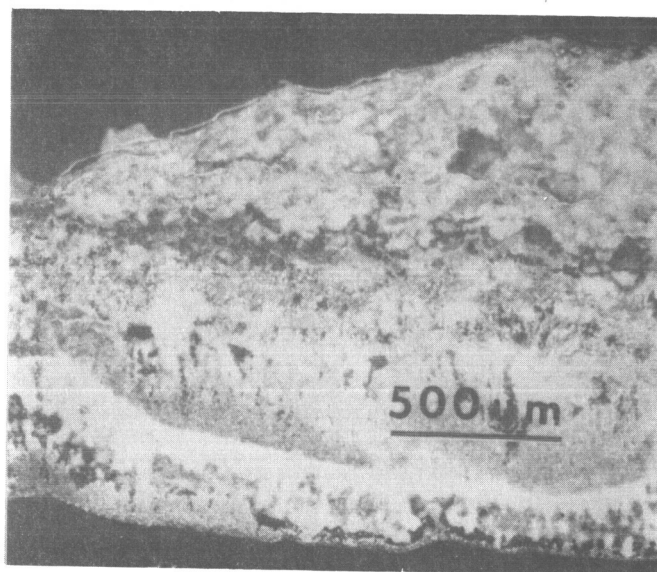
(c) Cast Ni - 50 a/o Al

(d) Cast Ni - 50 a/o Al - 0.3 w/o Zr

(e) Cast Ni – 24 a/o Al – 15 w/o Cr – 0.2 w/o Zr

(a) Exposed 5 minutes

(b) Exposed 30 minutes

175

(c) Exposed 20 hours

(d) Exposed 30 hours

Figure 33

Transverse Optical Micrographs of Ni-45 a/o Al-0.2 w/o Zr Samples

Exposed for Intermediate Times
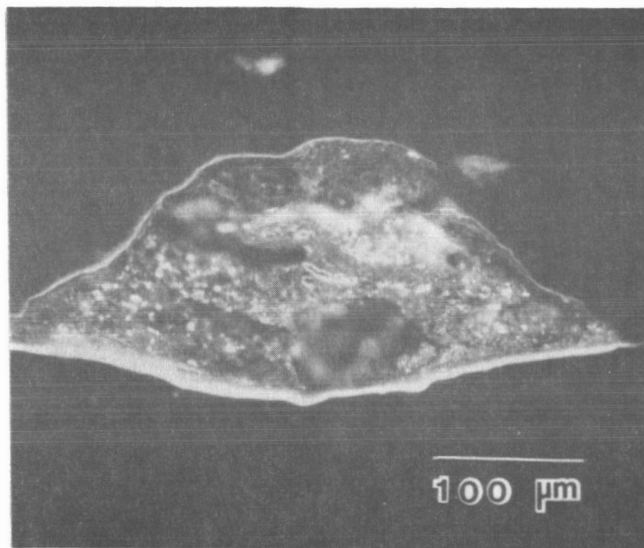
(a) Exposed 5 minutes
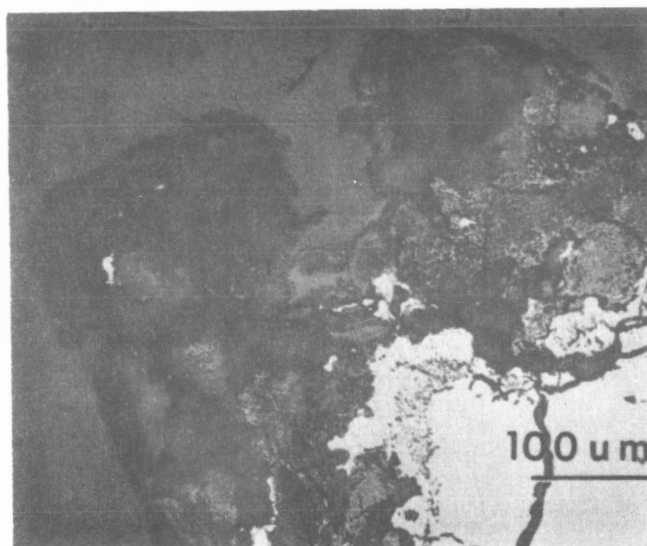
(b) Exposed 30 minutes
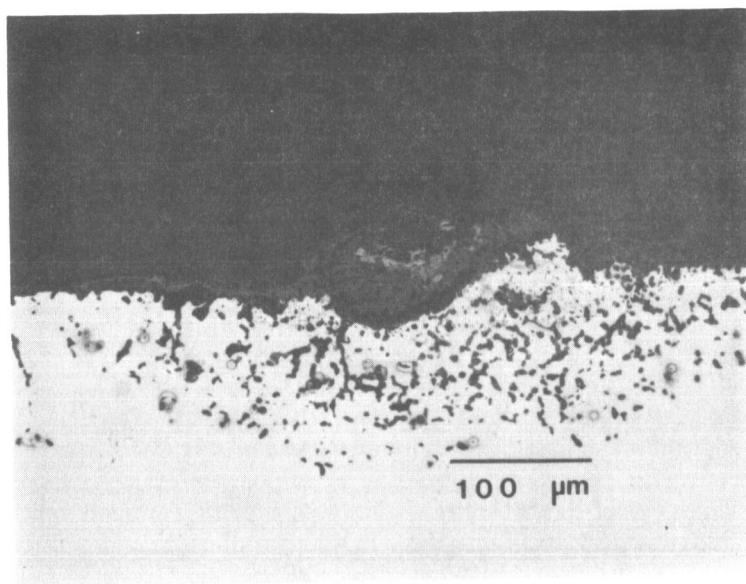
(c) Exposed 20 hours
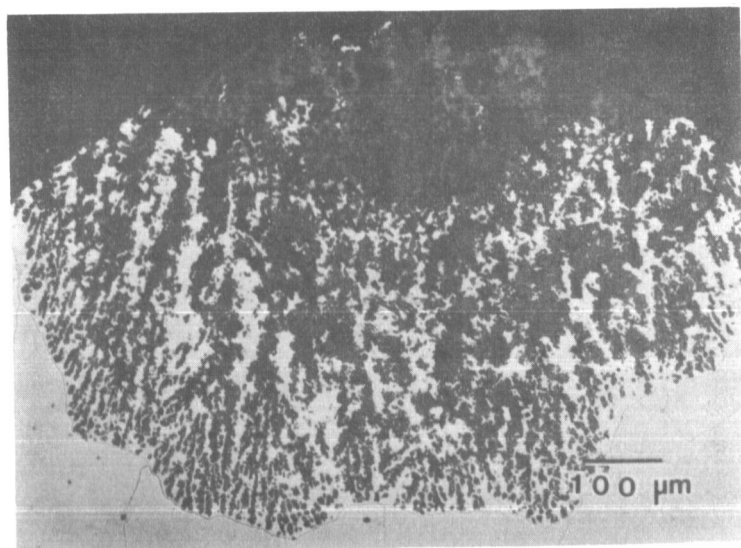
(d) Exposed 30 hours

C-3

Figure 34
Typical Scanning Electron Micrographs with
X-ray Maps of Important Elements
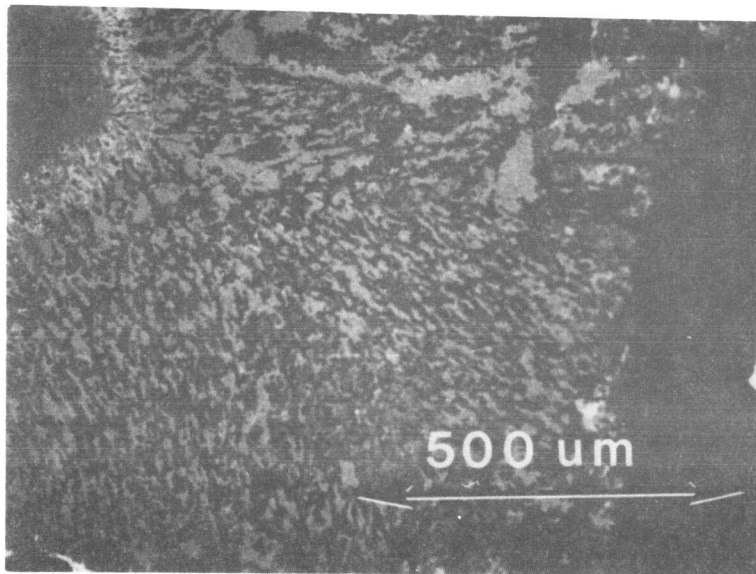
(a) Ni - 45 a/o Al - 0.2 w/o Zr (P/M)

(b) Ni X-ray Map of (a)

179
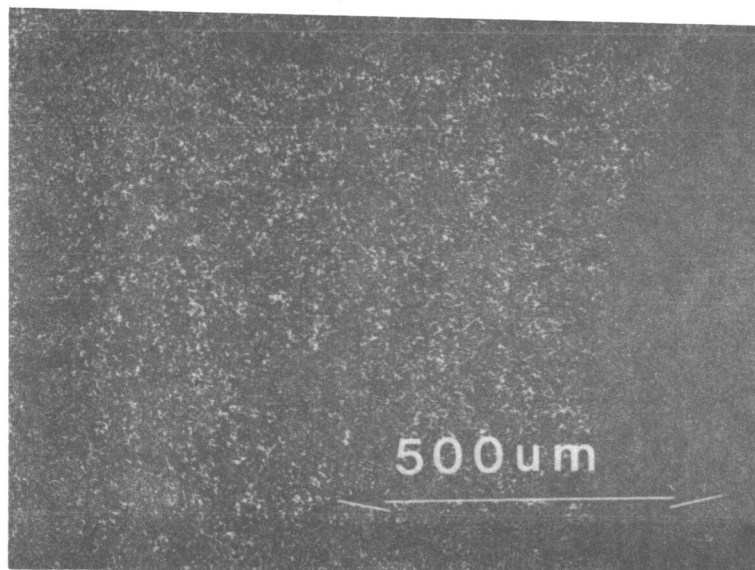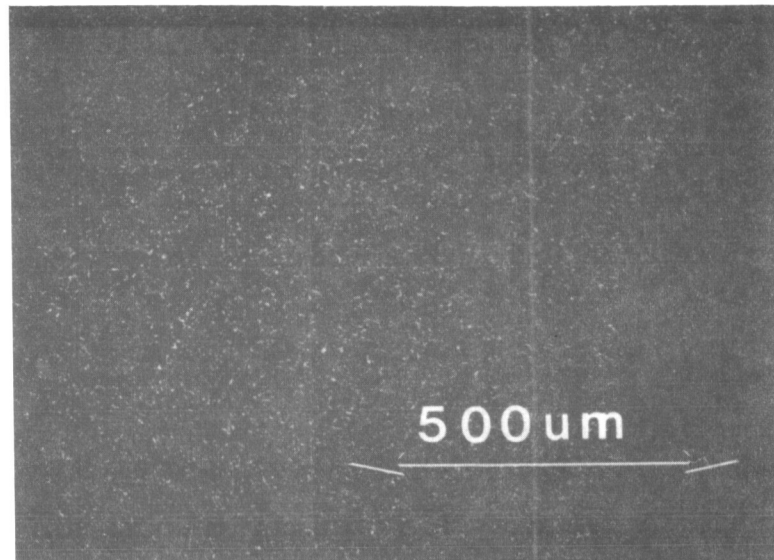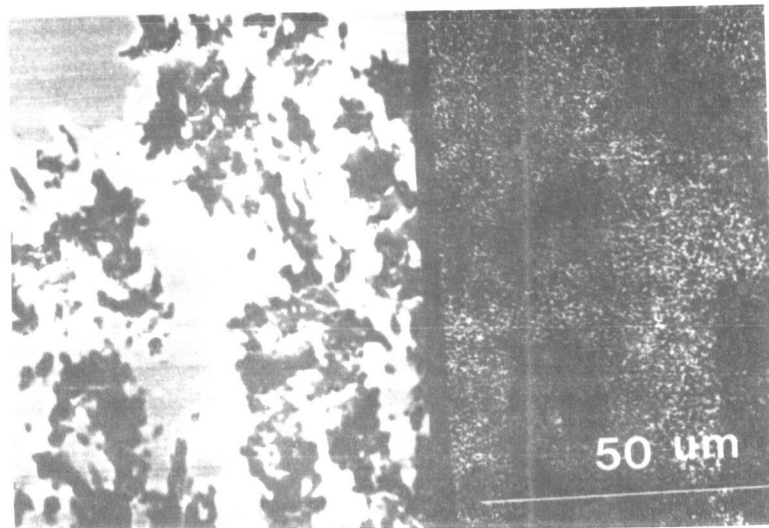
(c) Al X-ray Map of (a)

(d) Ni - 45 a/o Al - 0.2 w/o Zr sample with Ni X-ray Map
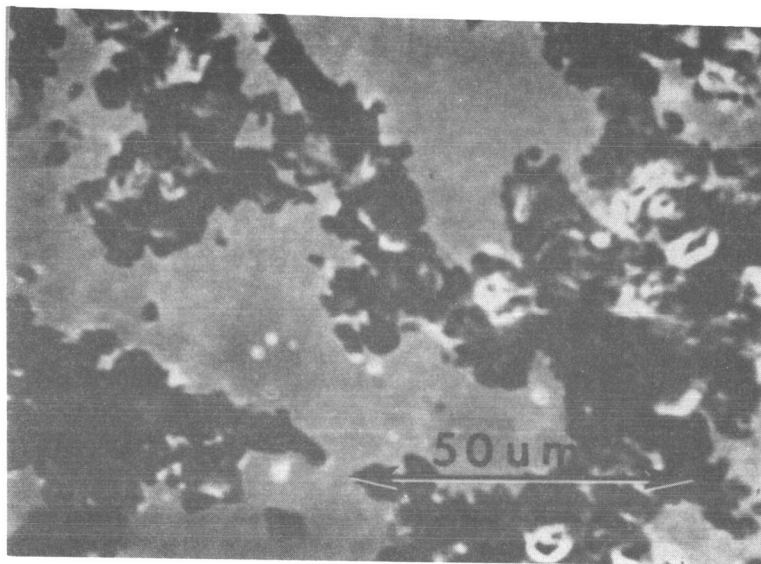
(e) Ni - 50 a/o Al - 0.3 w/o Zr
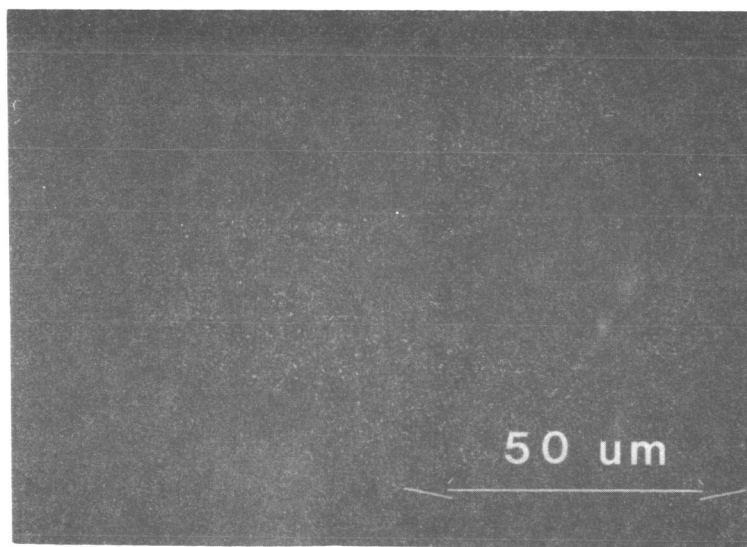
(f) Ni X-ray Map of (e)
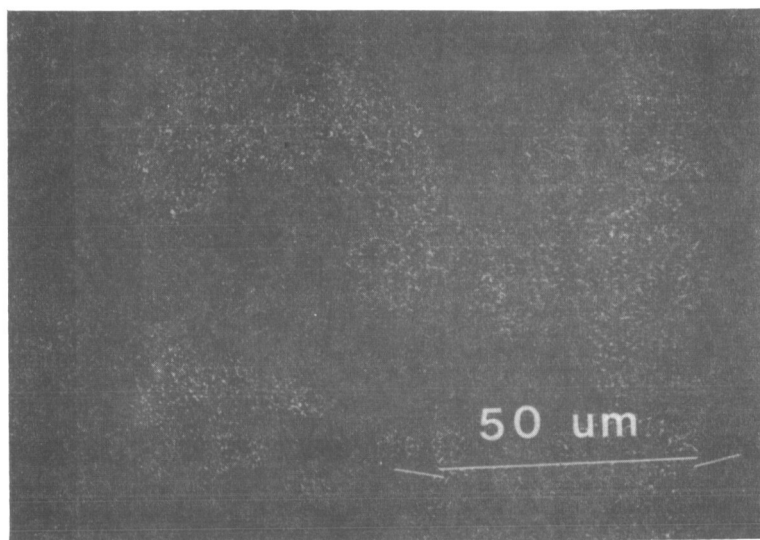
(g) Al X-ray Map of (e)
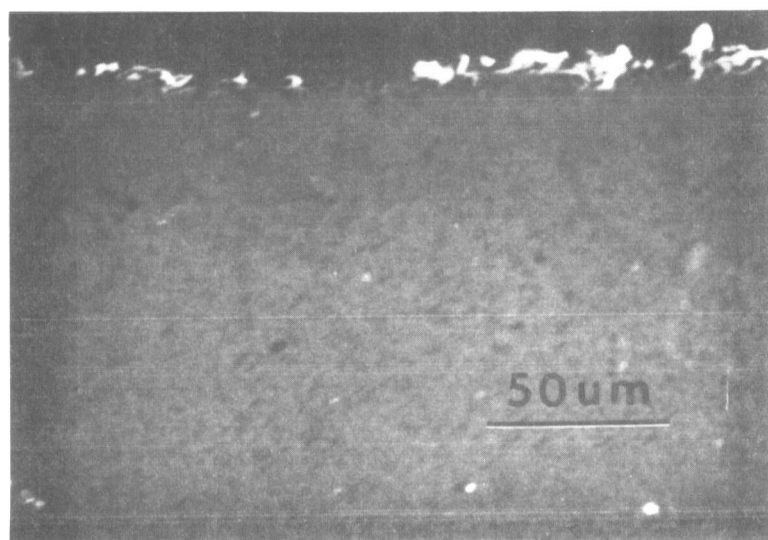
(h) Ni - 24 a/o Al - 15 w/o Cr - 0.3 w/o Zr

183
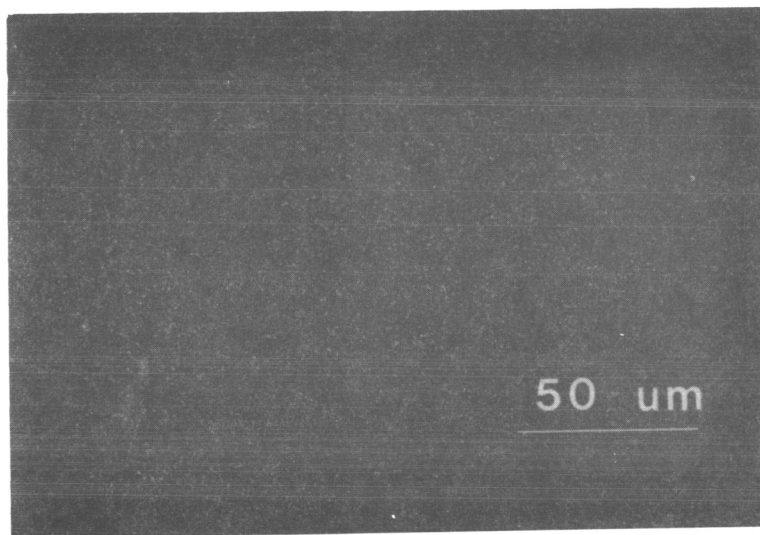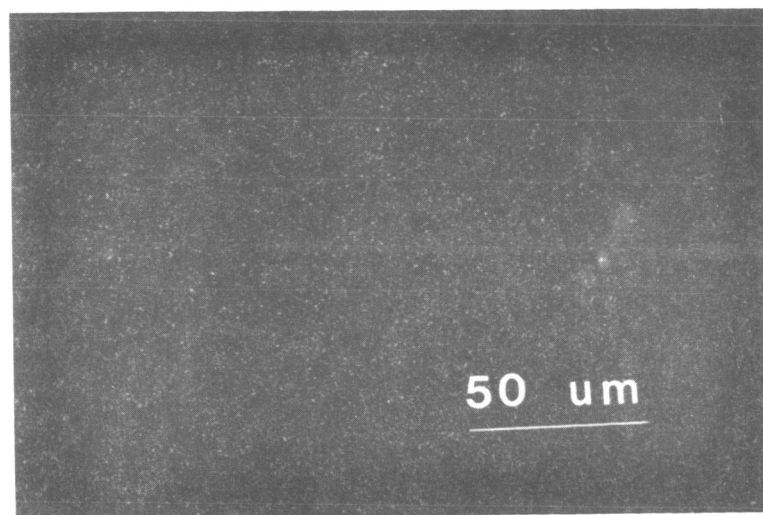
(i) Ni X-ray Map of (h)

(j) Al X-ray Map of (h)
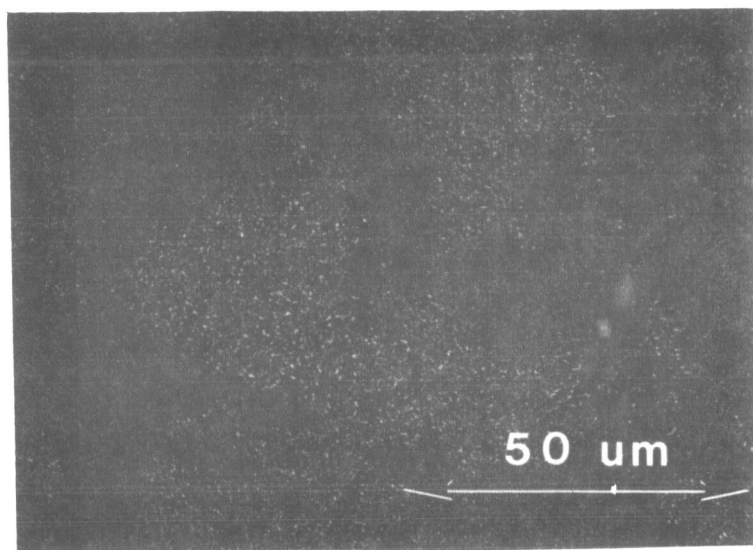
(k) Cr X-ray Map of (h)

Figure 35

(a) Composition Profile Through the Thickness of the Ni - 45 a/o Al - 0.2 w/o Zr Sample Exposed 5 Minutes

185
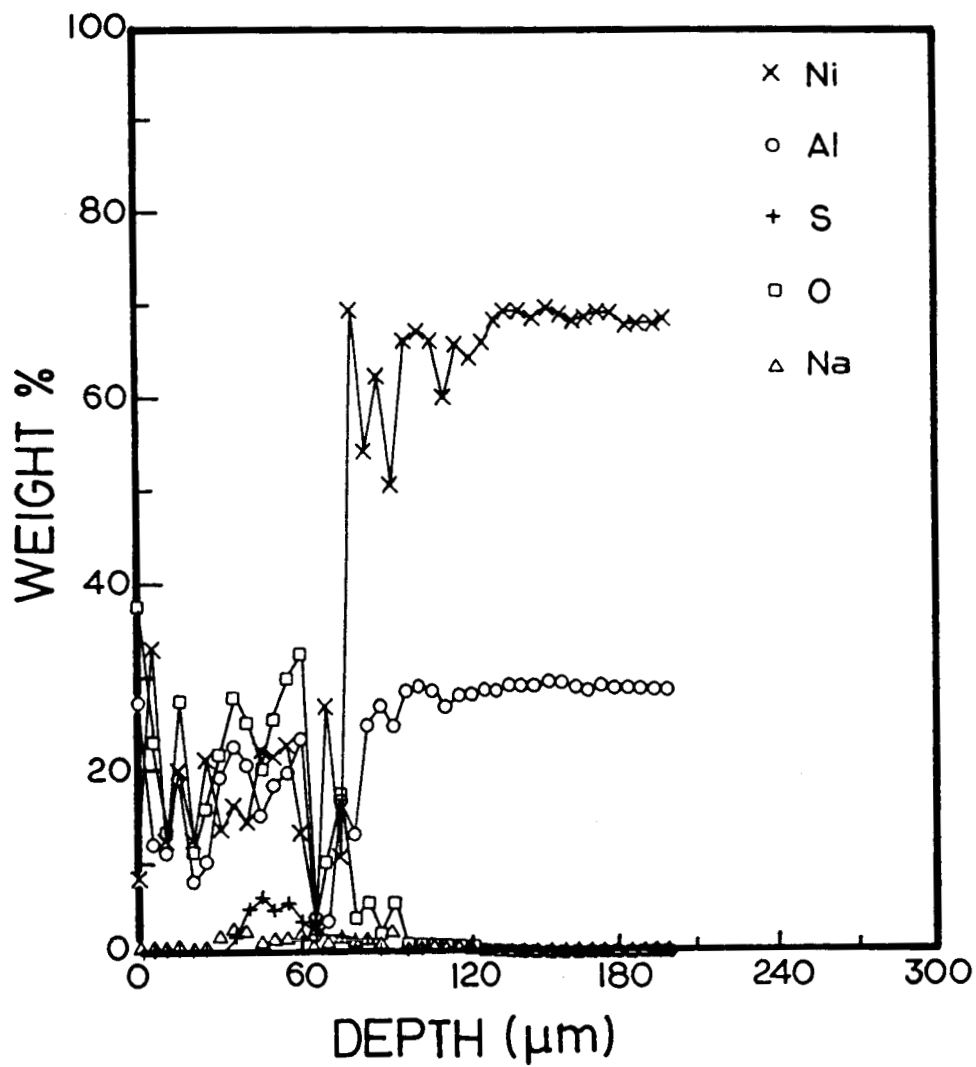
Figure 35

(b) Composition Profile Through the Thickness of the
Ni - 45 a/o Al - 0.2 w/o Zr Sample Exposed 30 Minutes
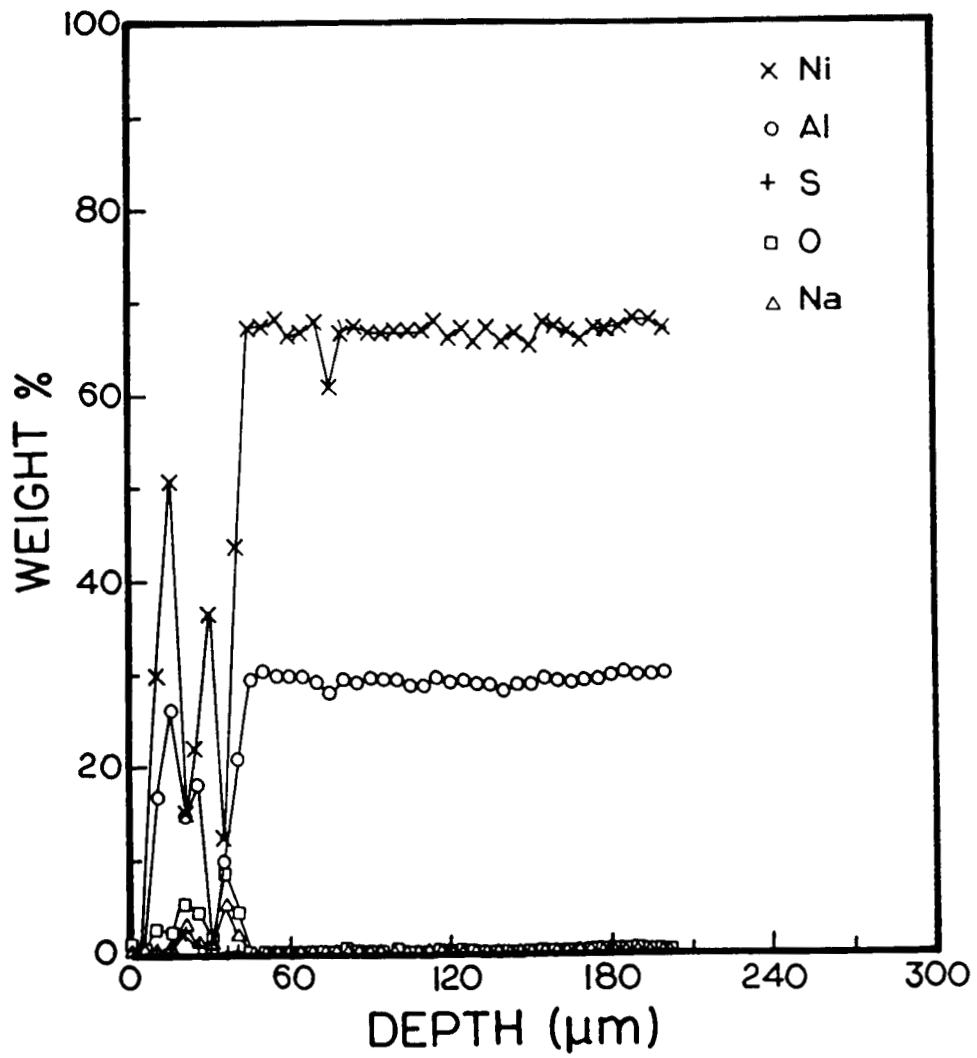
Figure 35

(c) Composition Profile Through the Thickness of the
Ni – 45 a/o Al – 0.2 w/o Zr Sample Exposed 20 Hours
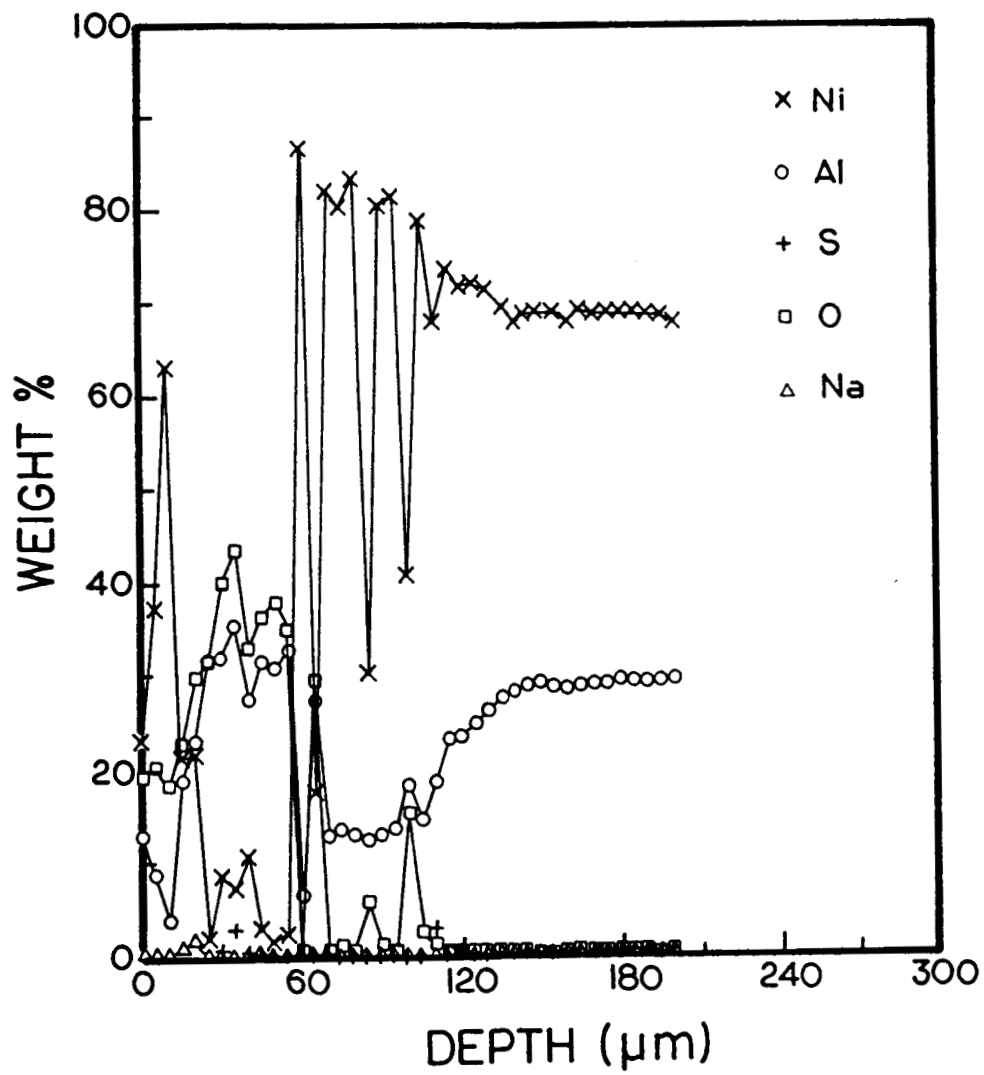
Figure 35

(d) Composition Profile Through the Thickness of the
Ni – 45 a/o Al – 0.2 w/o Zr Sample Exposed 30 Hours
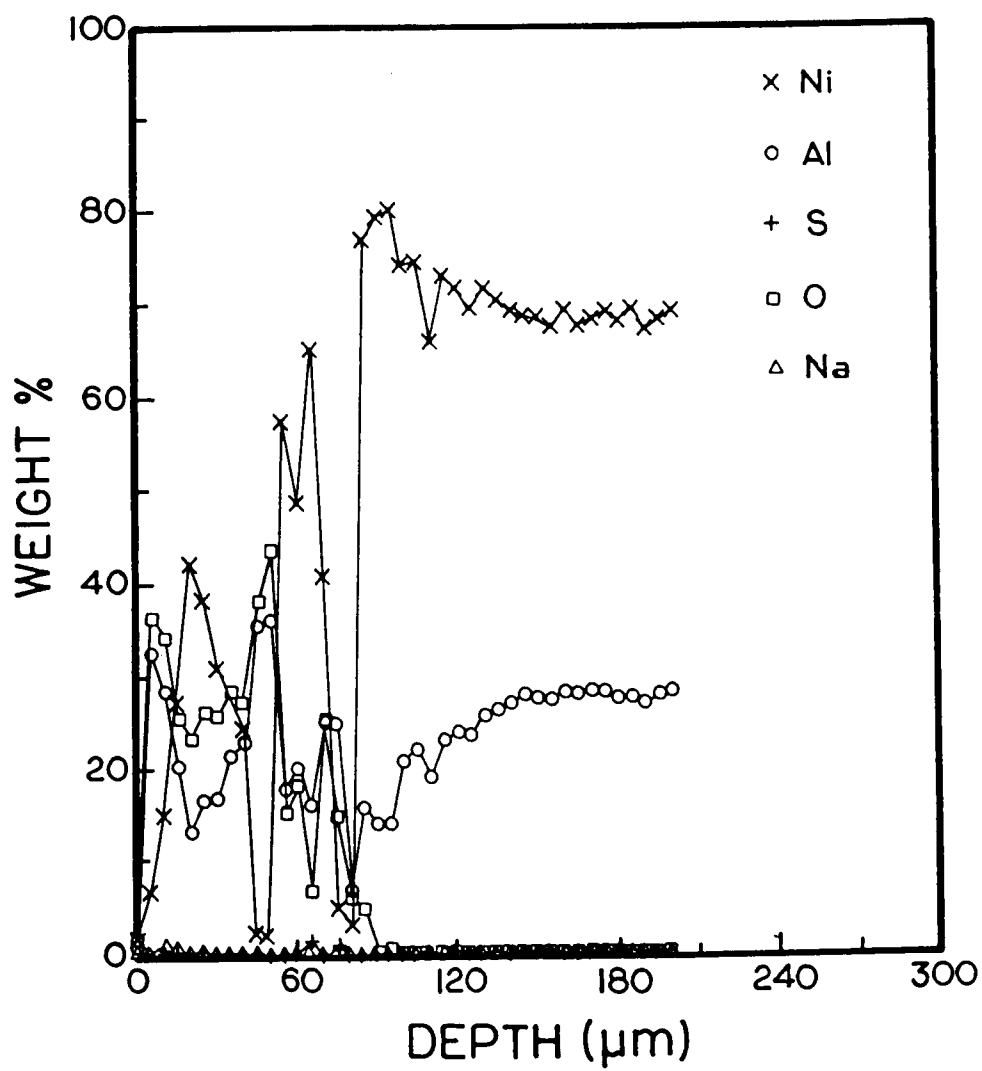
Figure 35

(e) Ni and Al Profiles Through the Thickness of a

Ni - 50 a/o Al - 0.3 w/o Zr Sample in a Badly Corroded Region
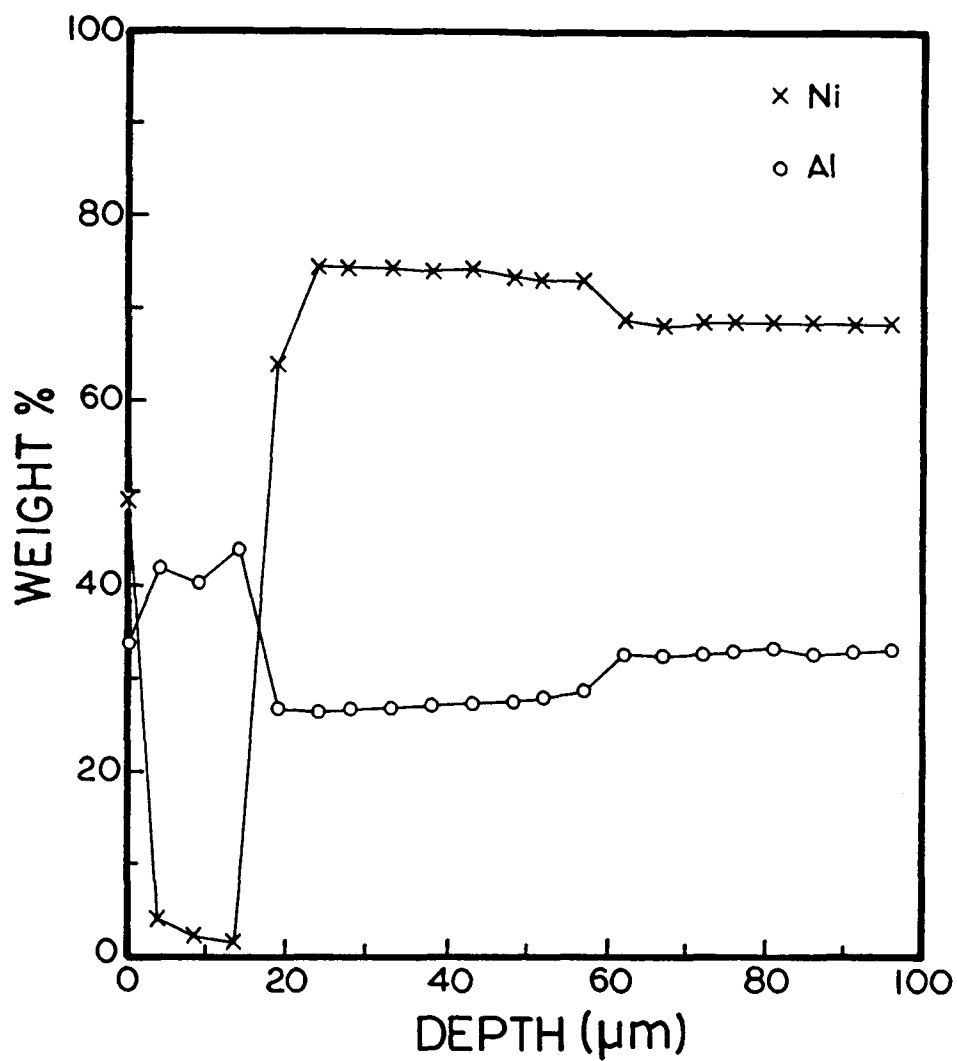
Figure 35

(f) Ni and Al Profiles Through the Thickness of a
Ni - 50 a/o Al - 0.3 w/o Zr Sample in a Uncorroded Region
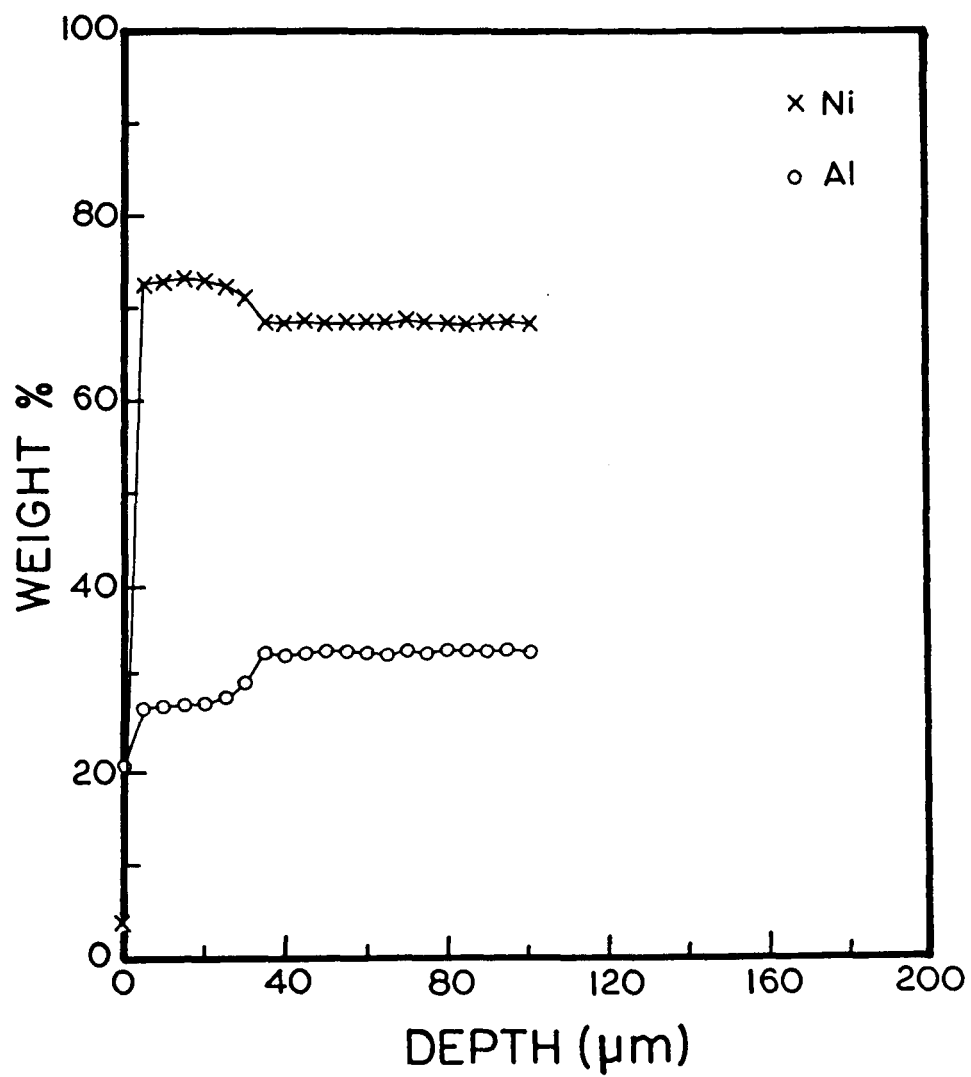
Figure 35

(g) Composition Profile Through the Thickness of the
Ni - 24 a/o Al - 15 w/o Cr - 0.2 w/o Zr Sample
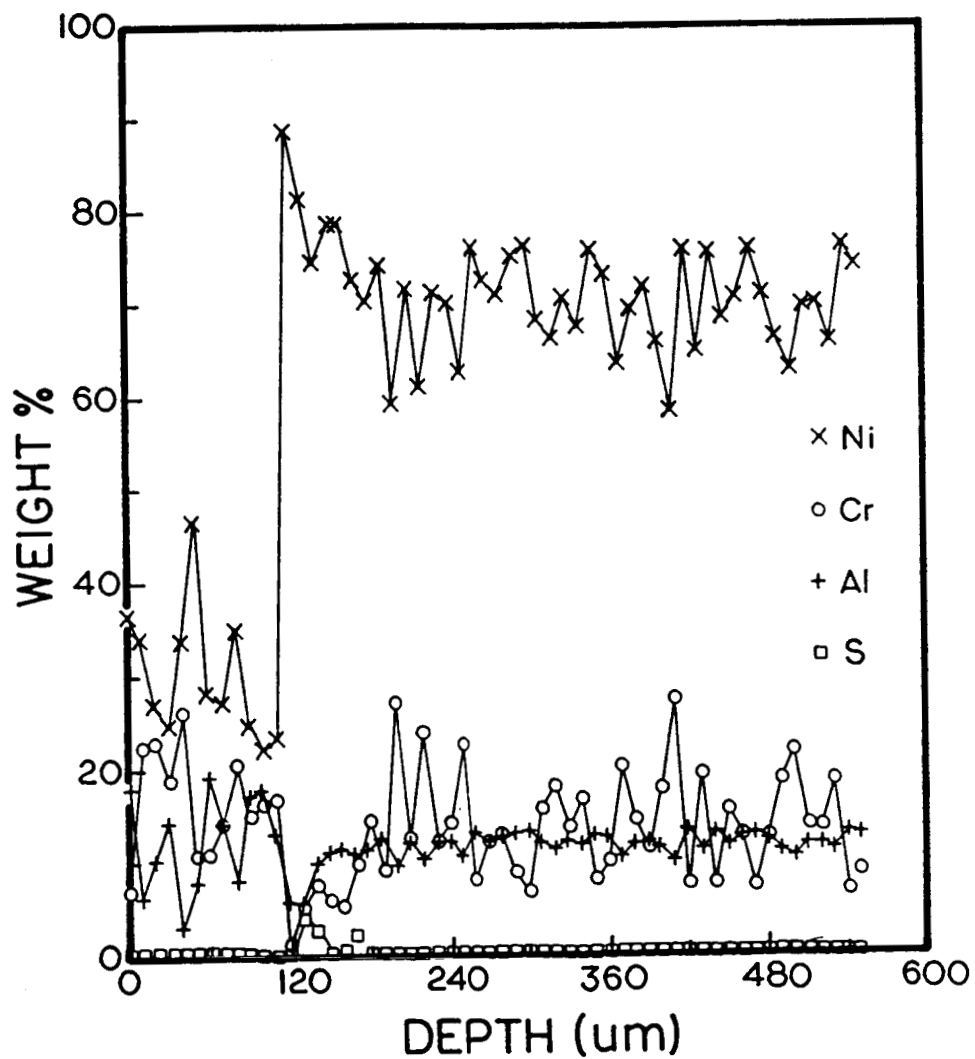
Figure 36

Electron Microprobe SE and BSE Images with

Corresponding X-ray Maps
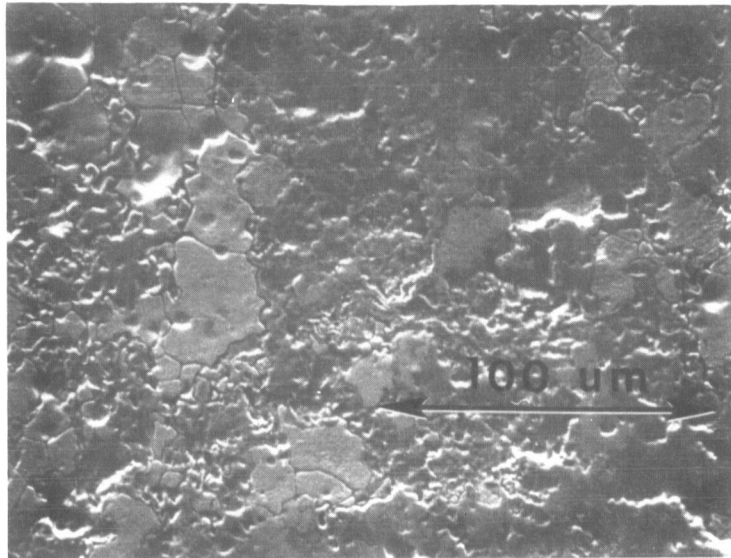
(A1) SE Image of P/M Ni-45 a/o Al-0.2 w/o Zr Sample
Near Surface After Long Term Exposure
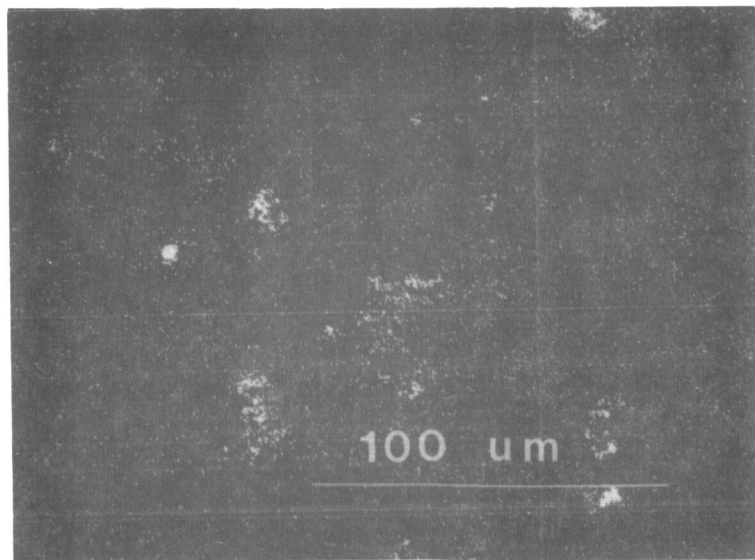
(A2) S X-ray Map of (A1) Showing Sulphides
Incorporated in Oxide
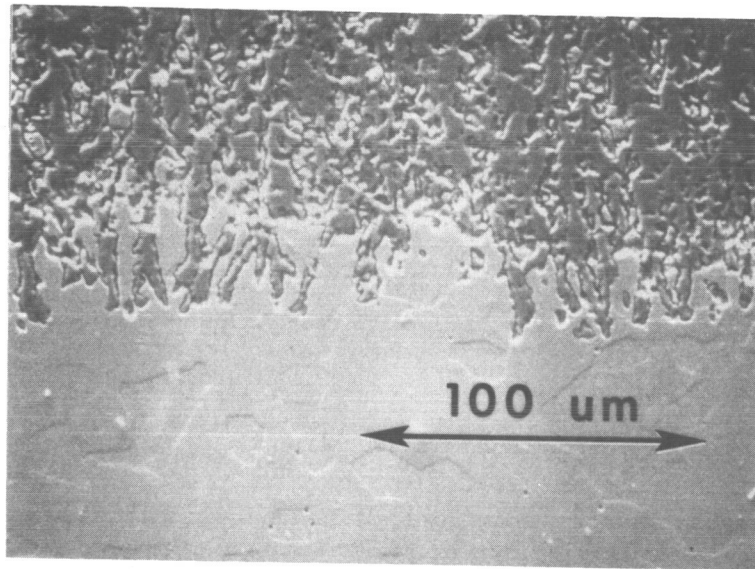
(B1) SE Image of Ni-45 a/o Al-0.2 w/o Zr Sample
At Corrosion Interface After Long Term Exposure

(B2) BSE Image of (B1)

194
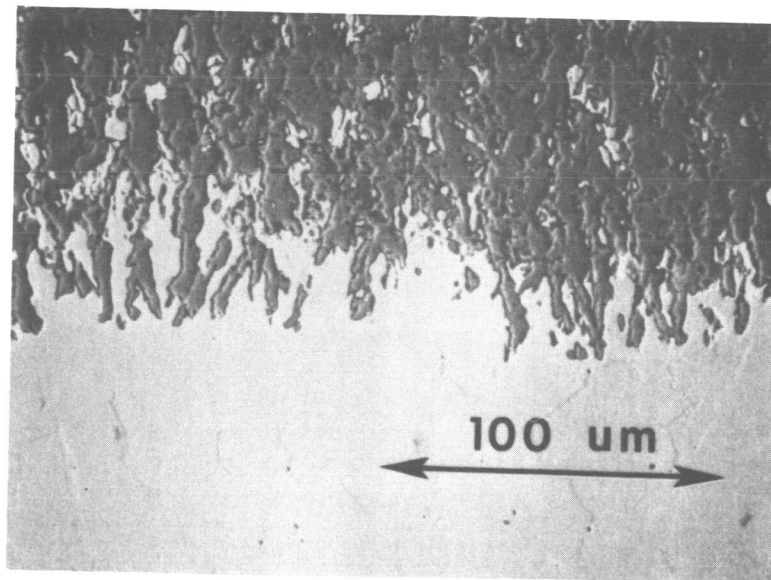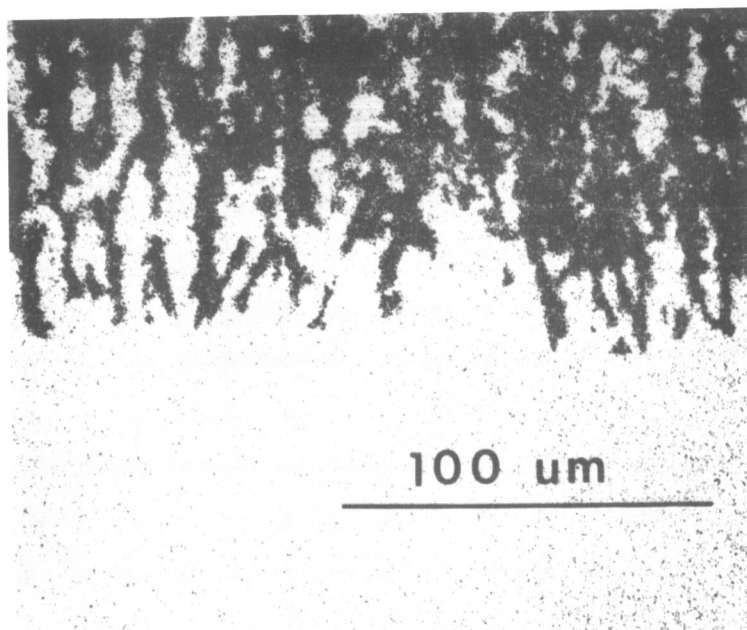
(B3) Ni X-ray Map of (B1)

(B4) Al X-ray Map of (B1)

195
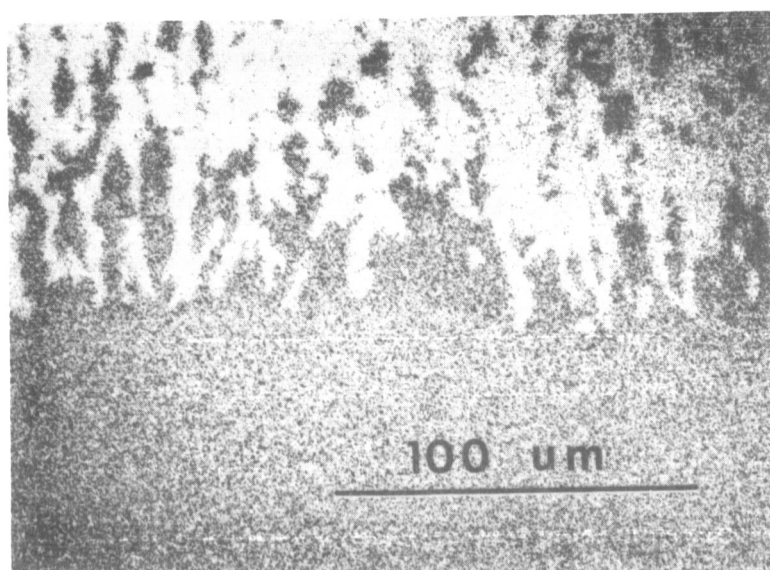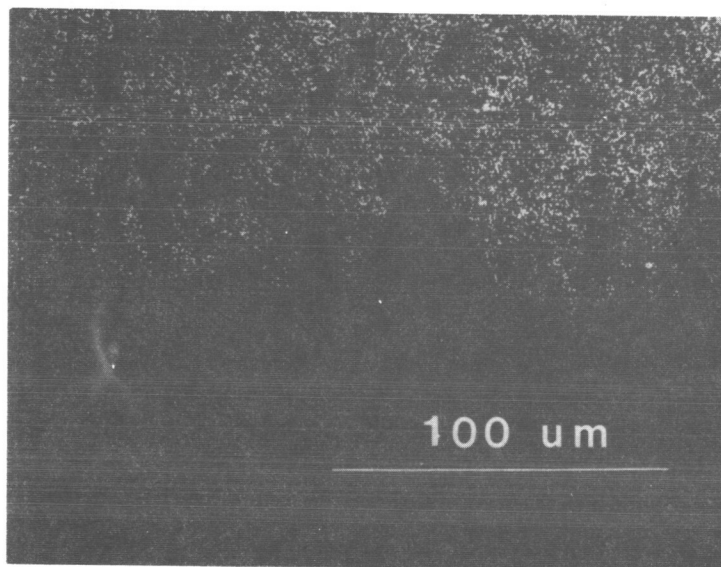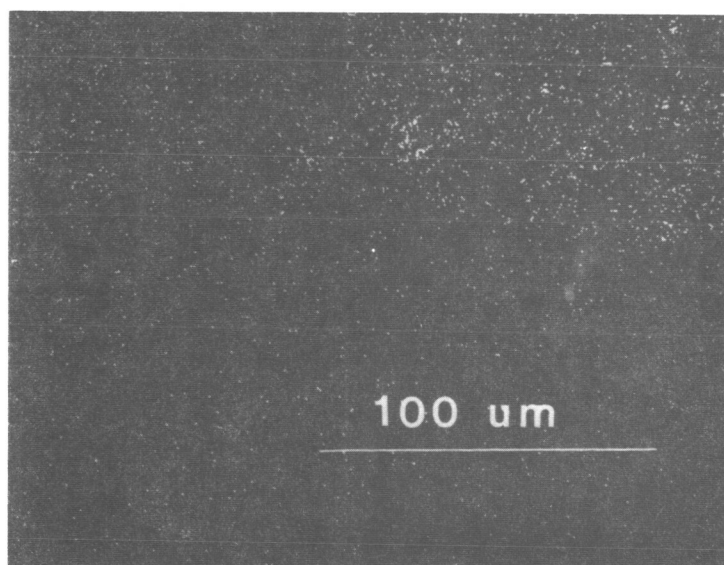
(B5) O X-ray Map of (B1)

(B6) S X-ray Map of (B1)
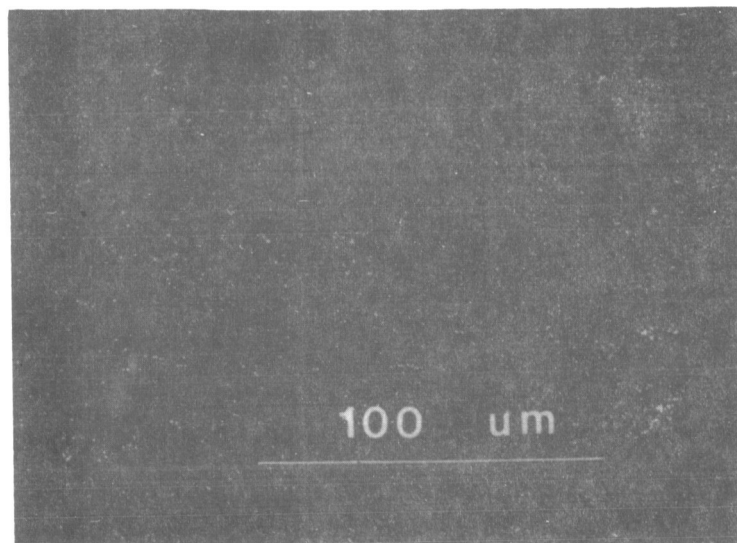
(B7) Zr X-Ray Map of (B1)
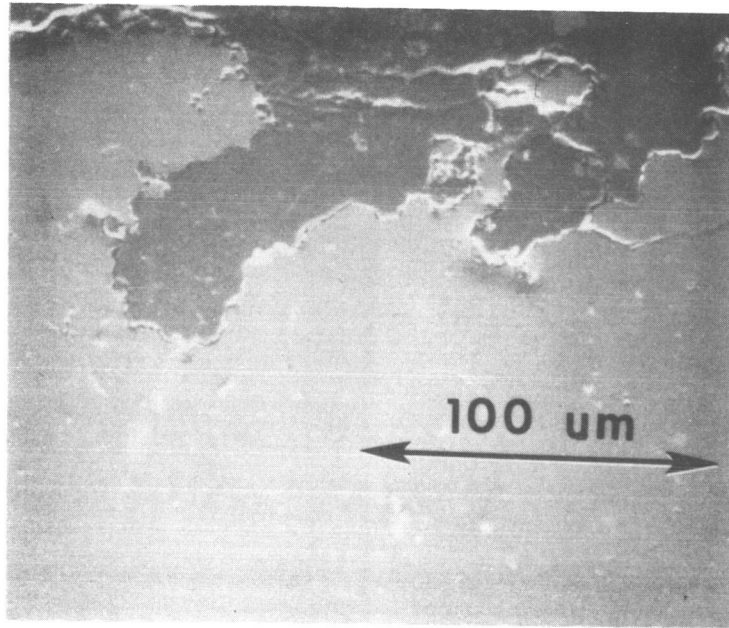
(C1) SE Image of Cast Ni-50 a/o Al-0.3 W/o Zr Sample
At Corrosion Interface After Long Exposure
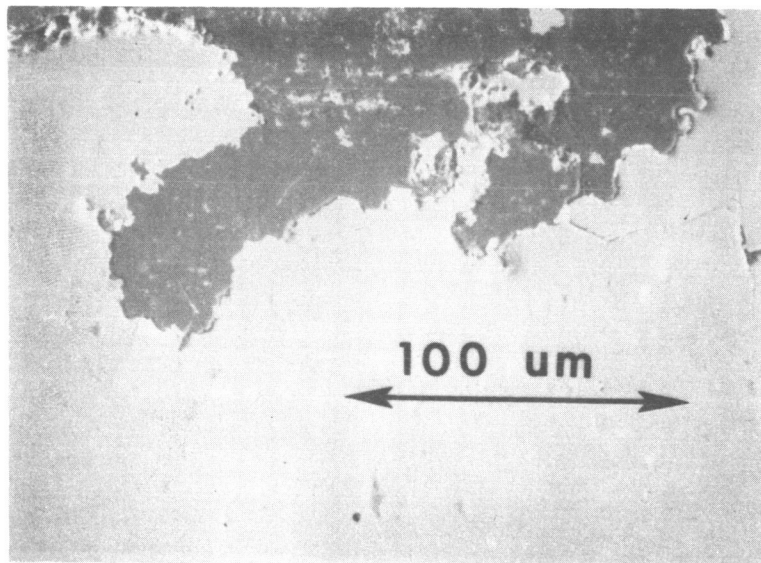
(C2) BSE Image of (C1)
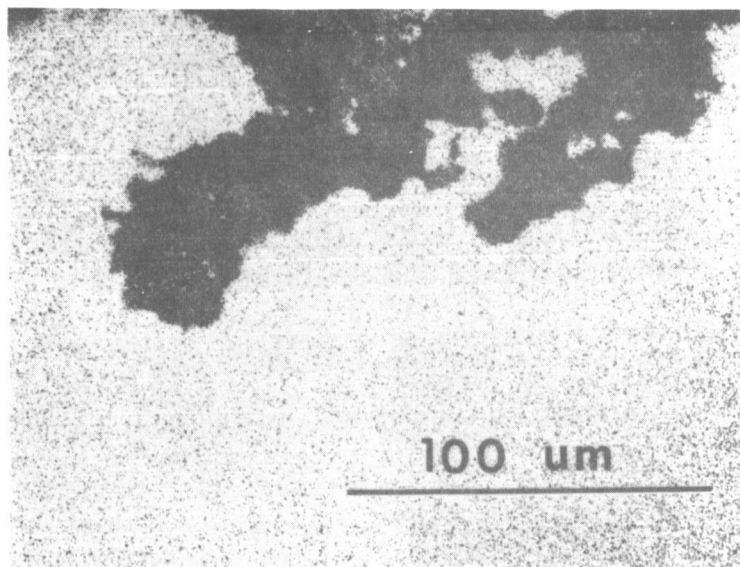
(C3) Ni X-ray Map of (C1)
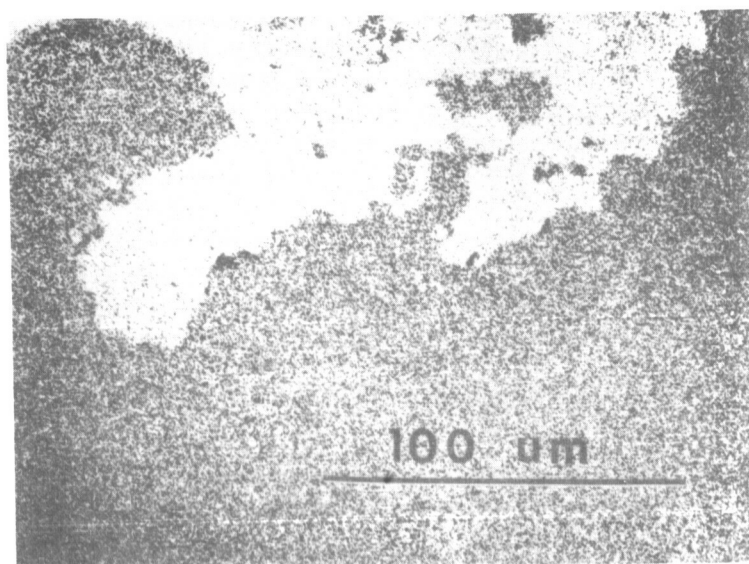
(C4) Al X-ray Map of (C1)
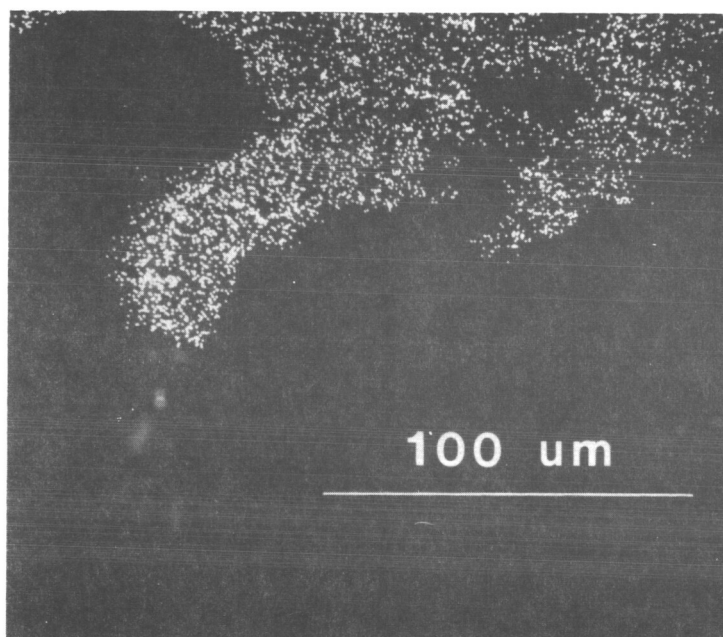
(C5) O X-ray Map of (C1)
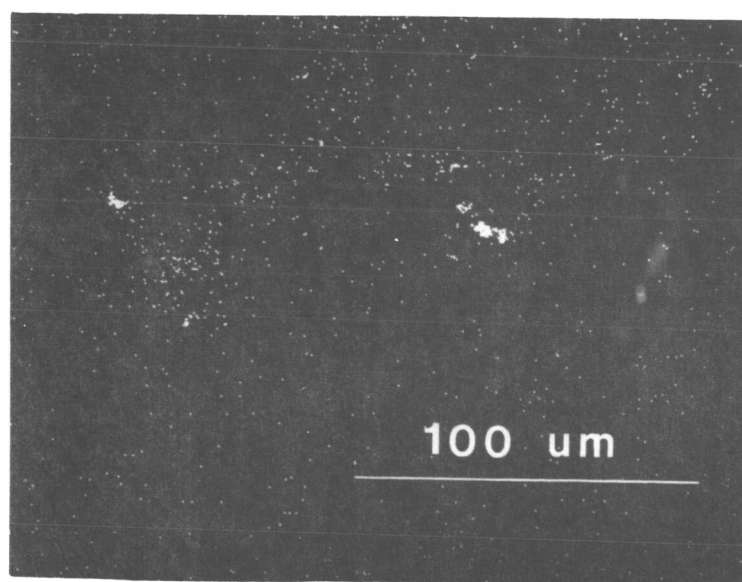
(C6) S X-ray Map of (C1)
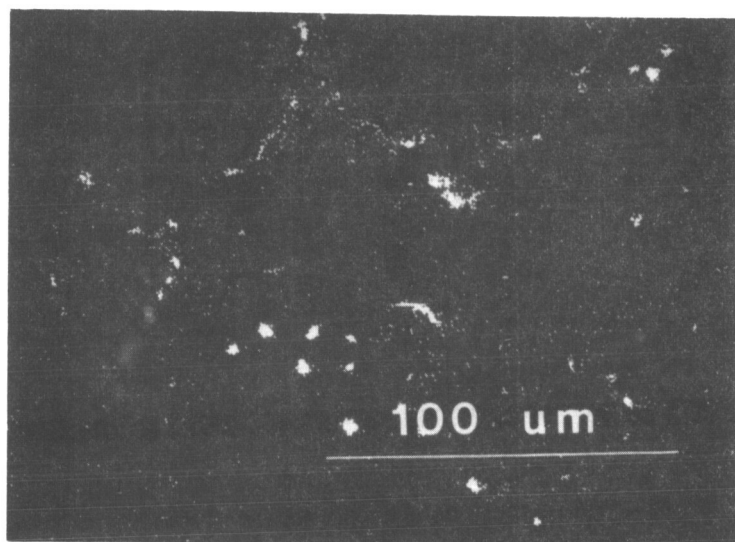
(C7) Na X-Ray Map of (C1)
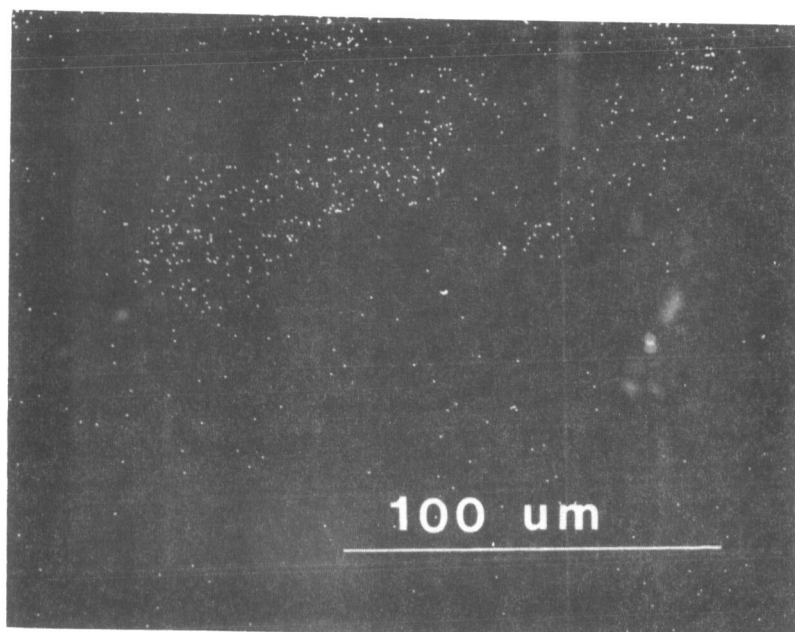
(C8) Zr X-ray Map of (C1)

Figure 37

SEM Macrograph of Ni-45 a/o Al-0.2 w/o Zr Sample

Showing Cracking and Lifting of Oxide Layer
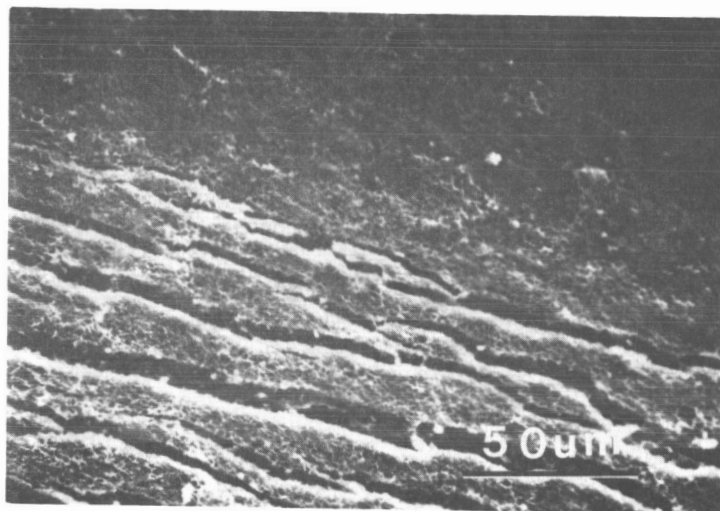
APPENDICES

APPENDIX A - Additional Weight Gain Curves

APPENDIX B - Additional Optical Macrophotographs

APPENDIX C - Additional Optical Micrographs

APPENDIX D - Additional Scanning Electron (SEM) Micrographs

APPENDIX E - Additional Optical Macrographs and Photomicrographs of Intermediate Time Exposure Samples

APPENDIX F - Oxidation of Nickel Aluminides

APPENDIX G - Hot Corrosion of the Iron Aluminides
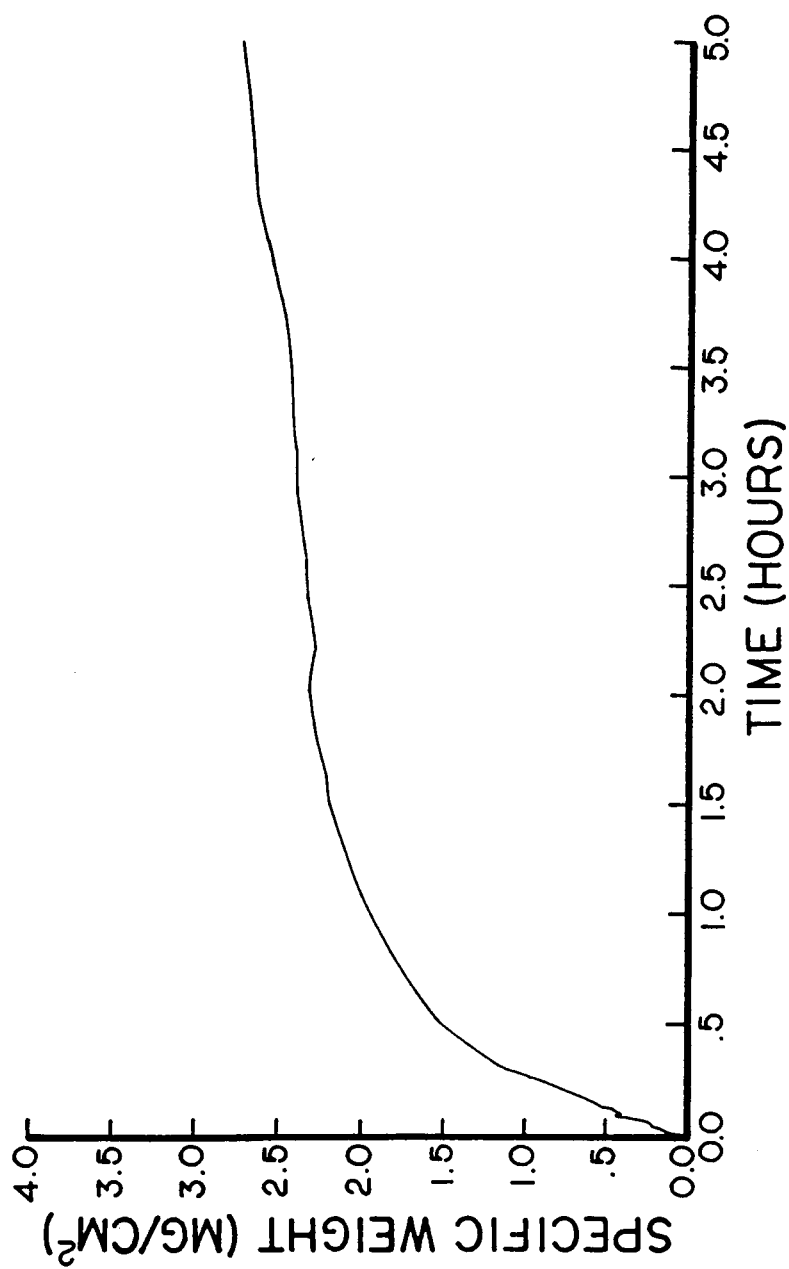
Figure A1

Ni - 45 a/o Al - 0.2 w/o Zr (P/M) Hot Corrosion Weight Gain Curve, Initial Stages
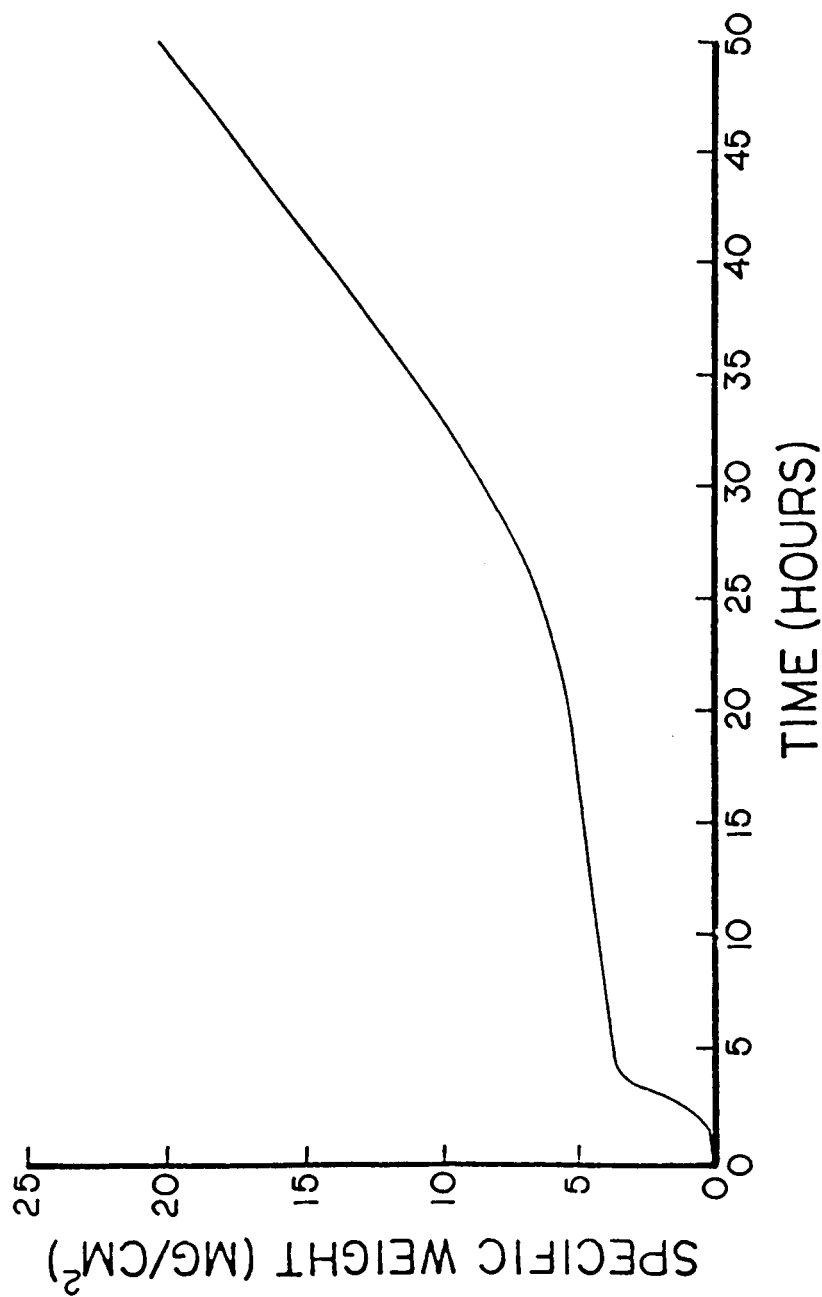
Figure A2 (a)

Ni – 45 a/o Al – 0.2 w/o Zr (P/M) Hot Corrosion Weight Gain Curve

For Sample Preoxidized at 900°C in O_2
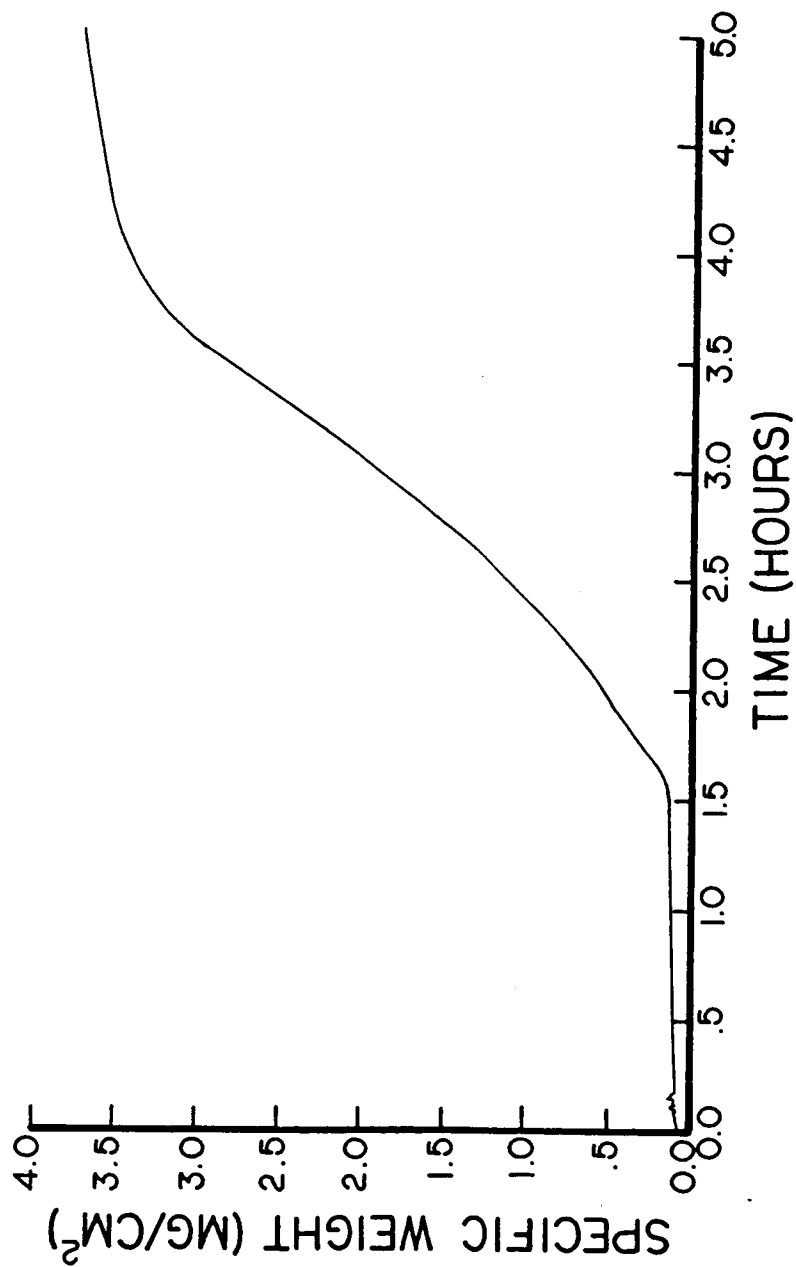
Figure A2 (b)

Ni – 45 a/o Al – 0.2 w/o Zr (P/M) Hot Corrosion Weight Gain Curve

For Sample Preoxidized at 900°C in O_2
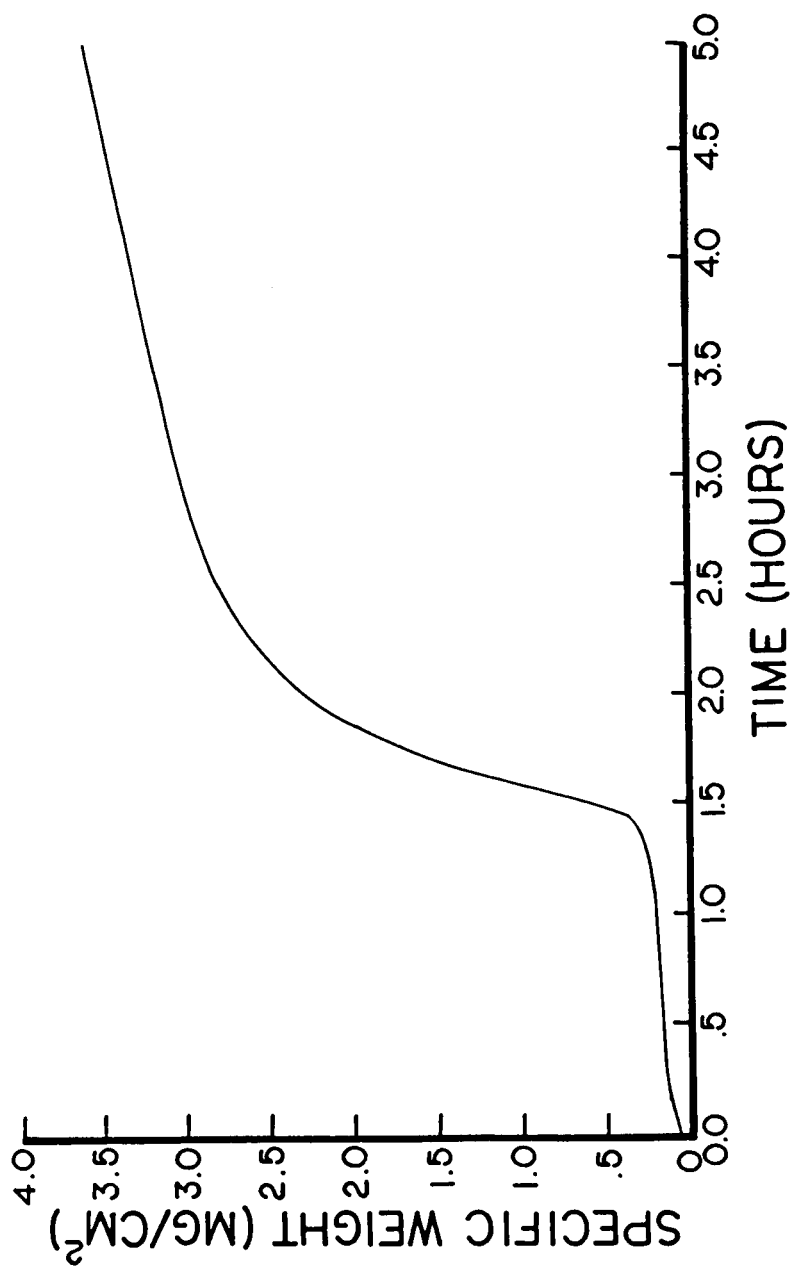
Figure A3 (a)

Ni - 45 a/o Al - 0.2 w/o Zr (P/M) Hot Corrosion Weight Gain Curve

for Sample Preoxidized at 1200°C in Air
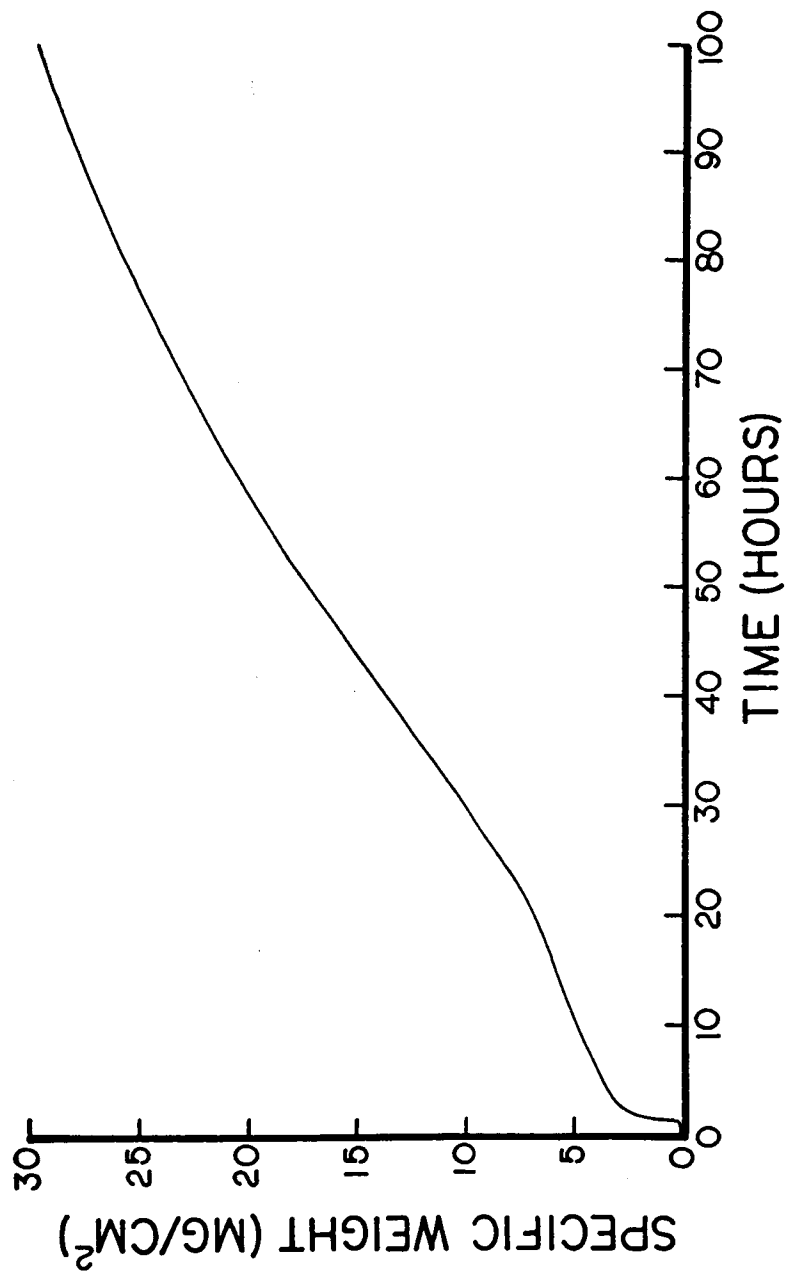
Figure A3 (b)

Ni – 45 a/o Al – 0.2 w/o Zr (P/M) Hot Corrosion Weight Gain Curve

for Sample Preoxidized at 1200°C in Air
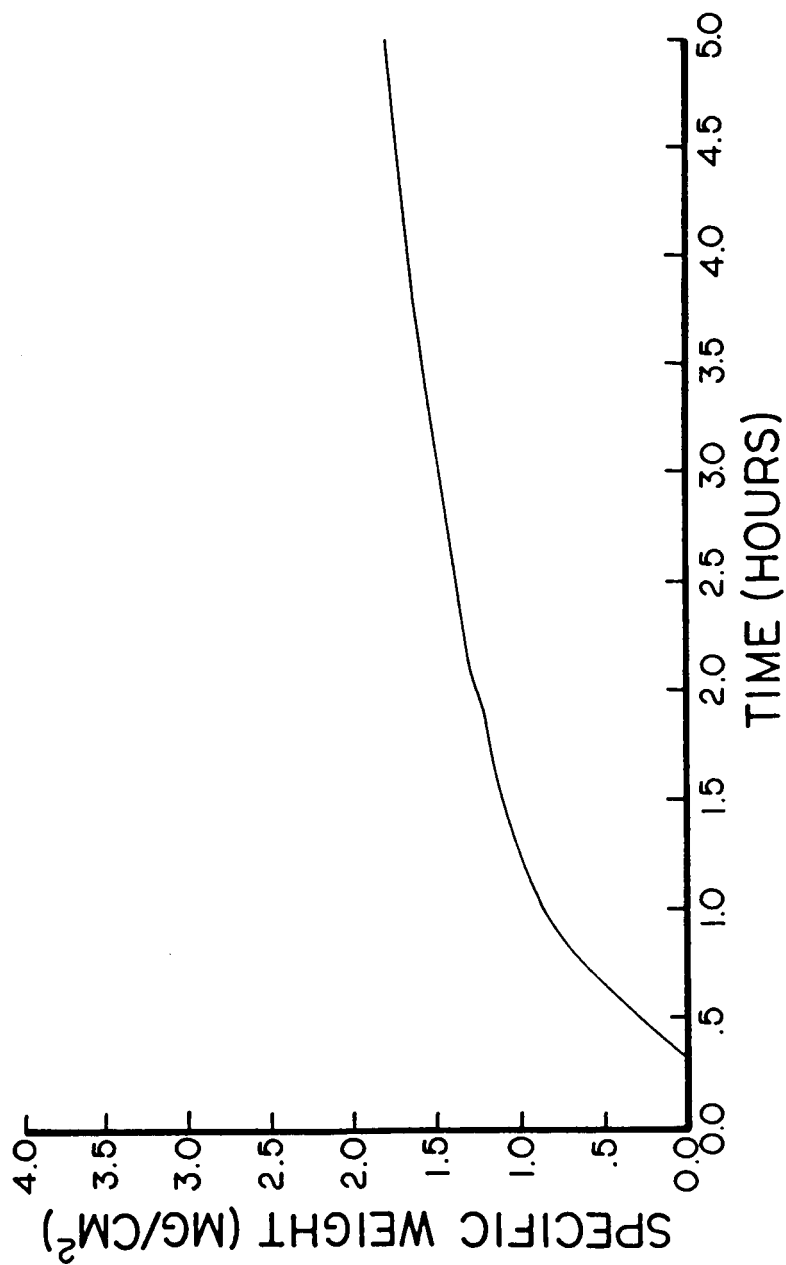
Figure A4

Ni – 45 a/o Al – 0.2 w/o Zr Hot Corrosion Weight Gain Curve
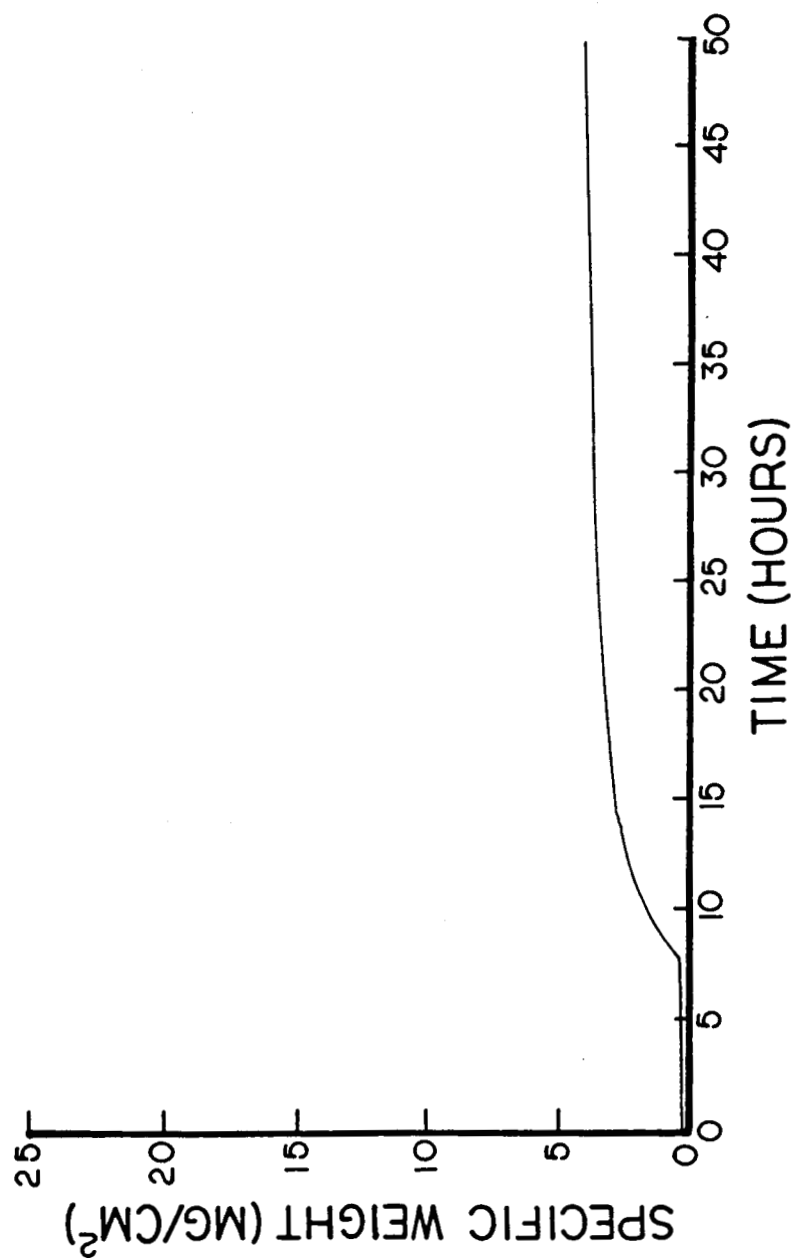
TIME (HOURS)

Figure A5

SPECIFIC WEIGHT (MG/CM²)

Ni – 50 a/o Al – 0.3 w/o Zr Hot Corrosion Weight Gain Curve for

Sample Preoxidized at 1200°C in Air

209
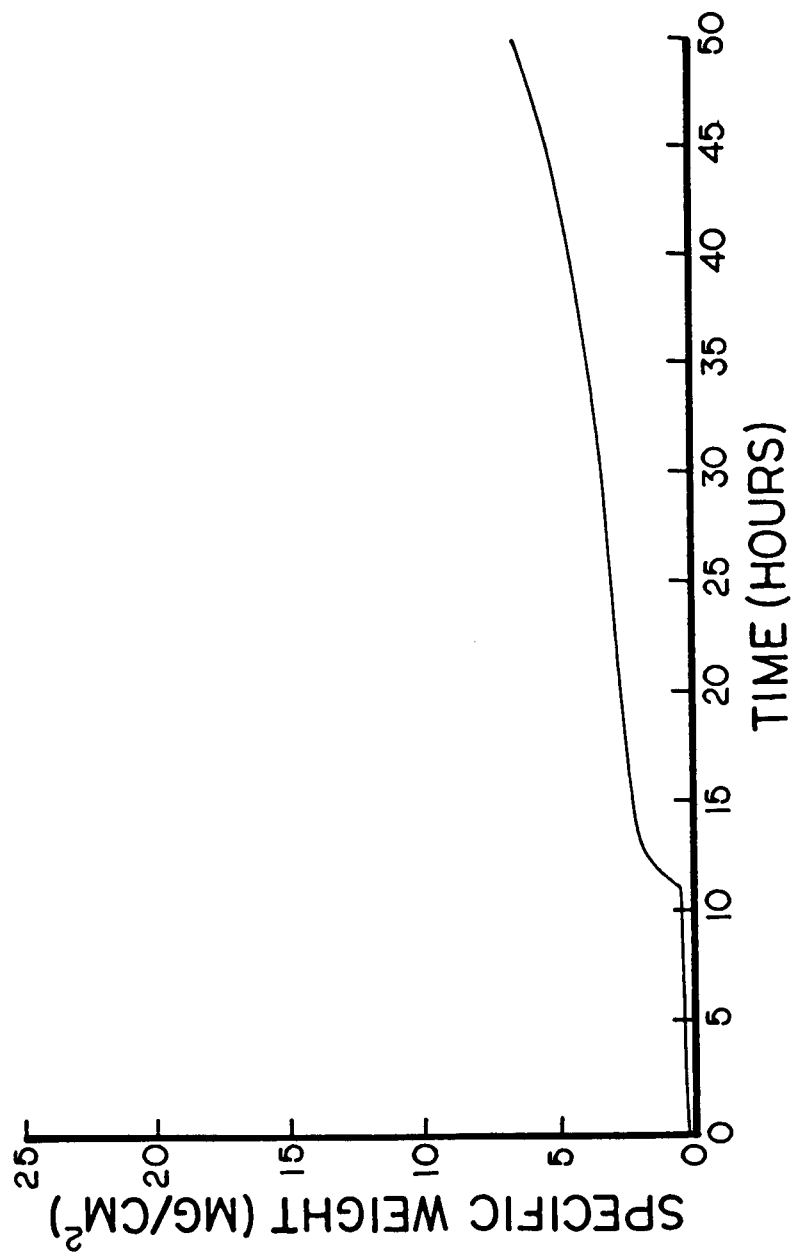
Figure A6

Ni – 50 a/o Al Hot Corrosion Weight Gain Curve
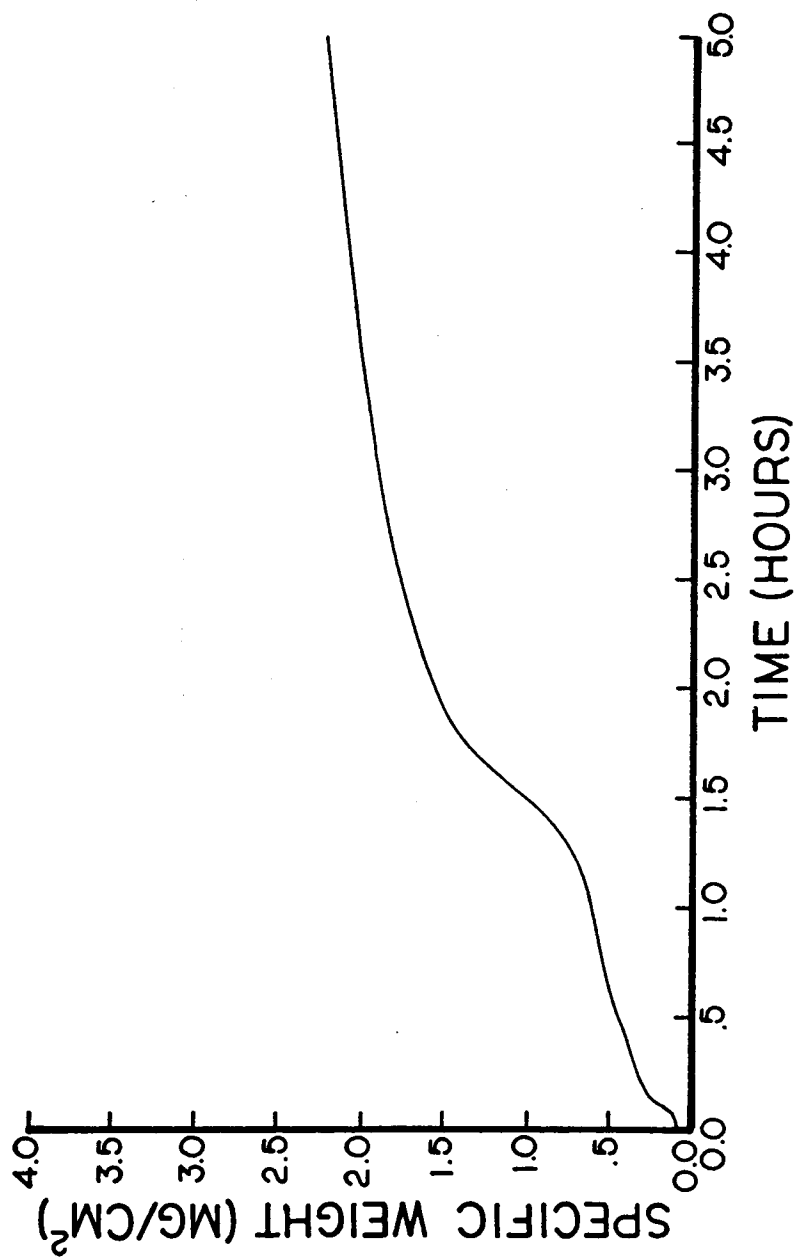
Figure A7 (a)

Ni – 50 a/o Al Hot Corrosion Weight Gain Curve for
Sample Preoxidized at 900°C in O_2
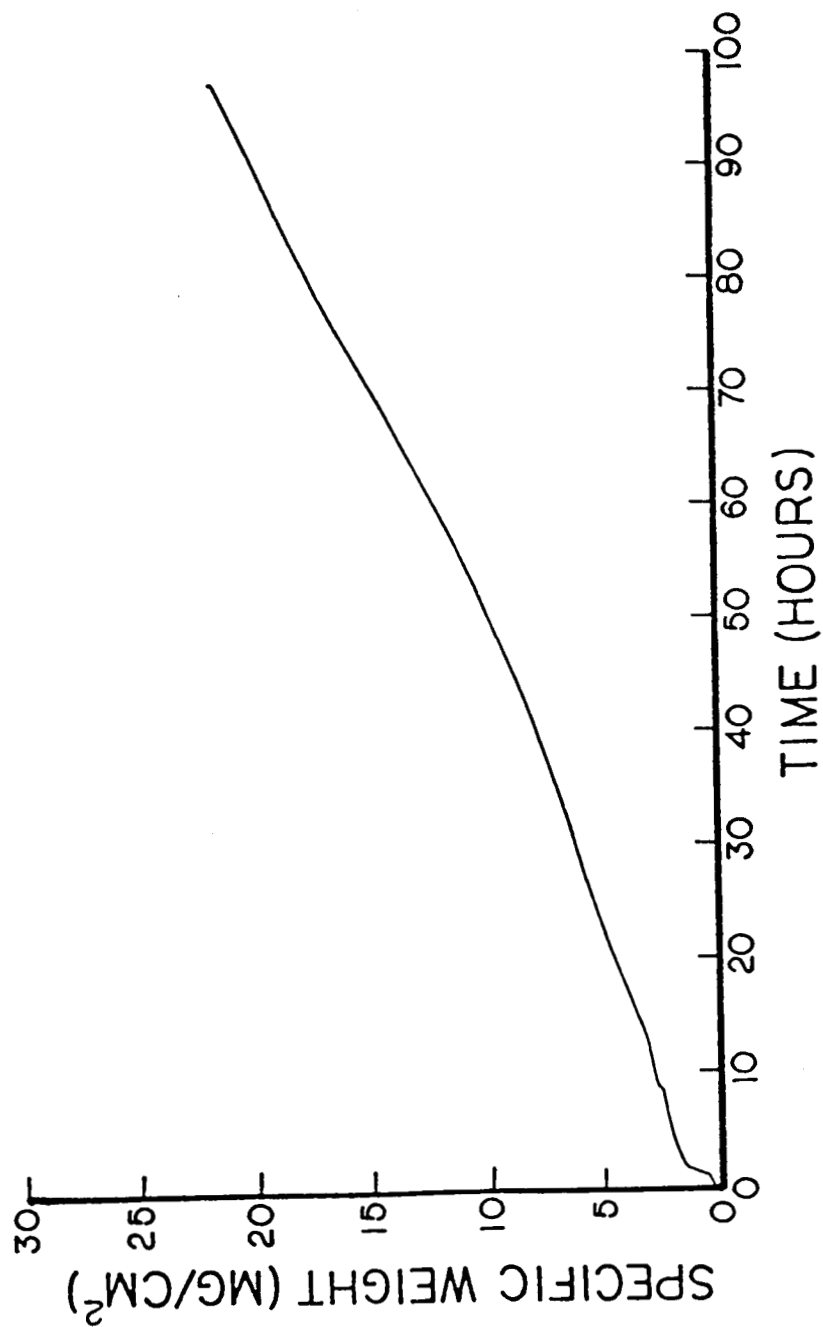
Figure A7 (b)

Ni - 50 a/o Al Hot Corrosion Weight Gain Curve for

Sample Preoxidized at 900°C in O_2
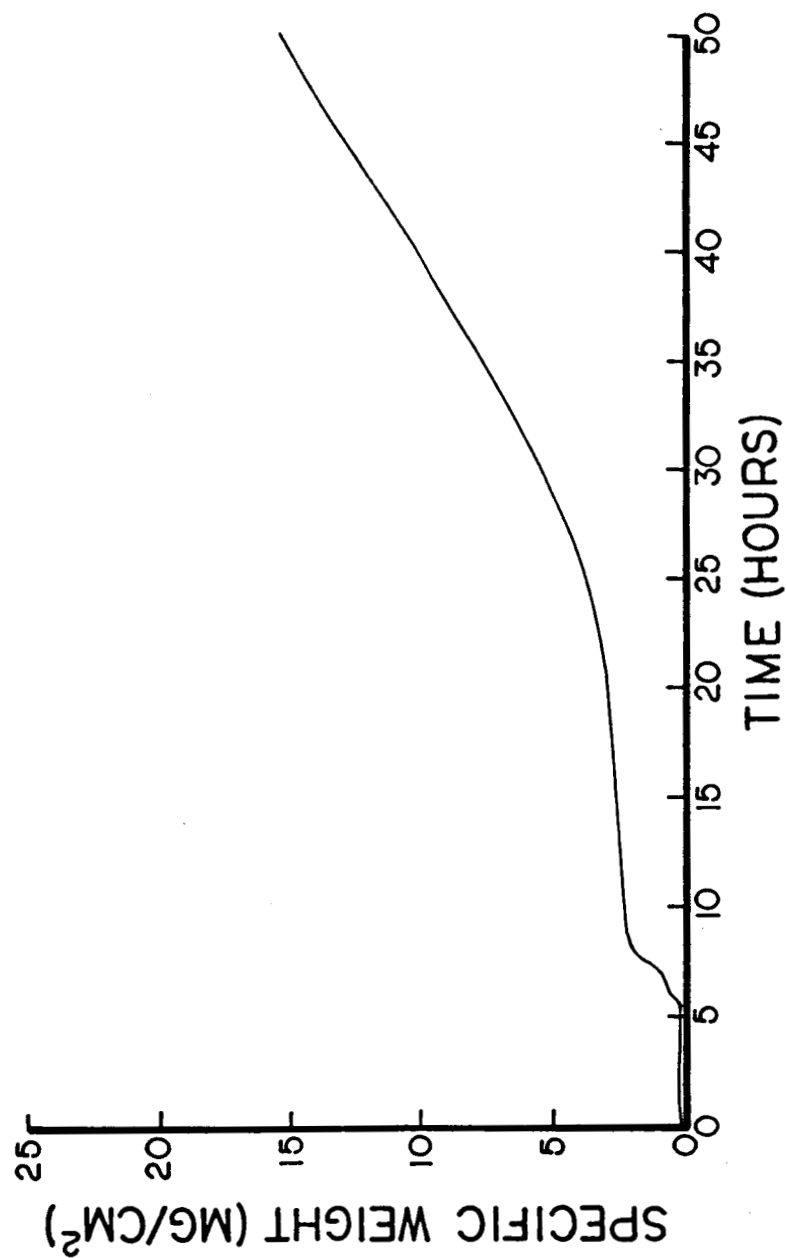
Figure A8 (a)

Ni – 50 a/o Al – 0.3 w/o Zr Hot Corrosion Weight Gain Curve for

Sample Preoxidized at 900°C in O_2

213
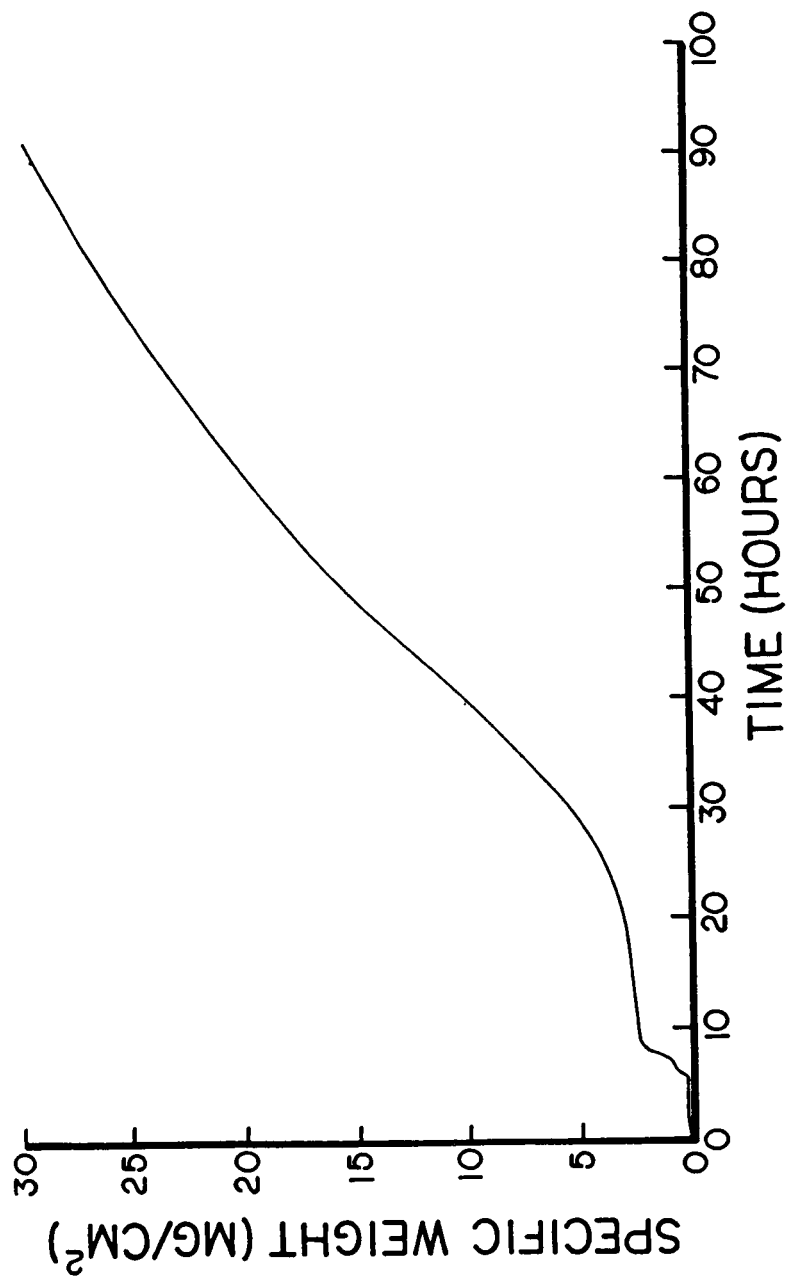
Figure A8 (b)

Ni – 50 a/o Al – 0.3 w/o Zr Hot Corrosion Weight Gain Curve for

Sample Preoxidized at 900°C in O_2
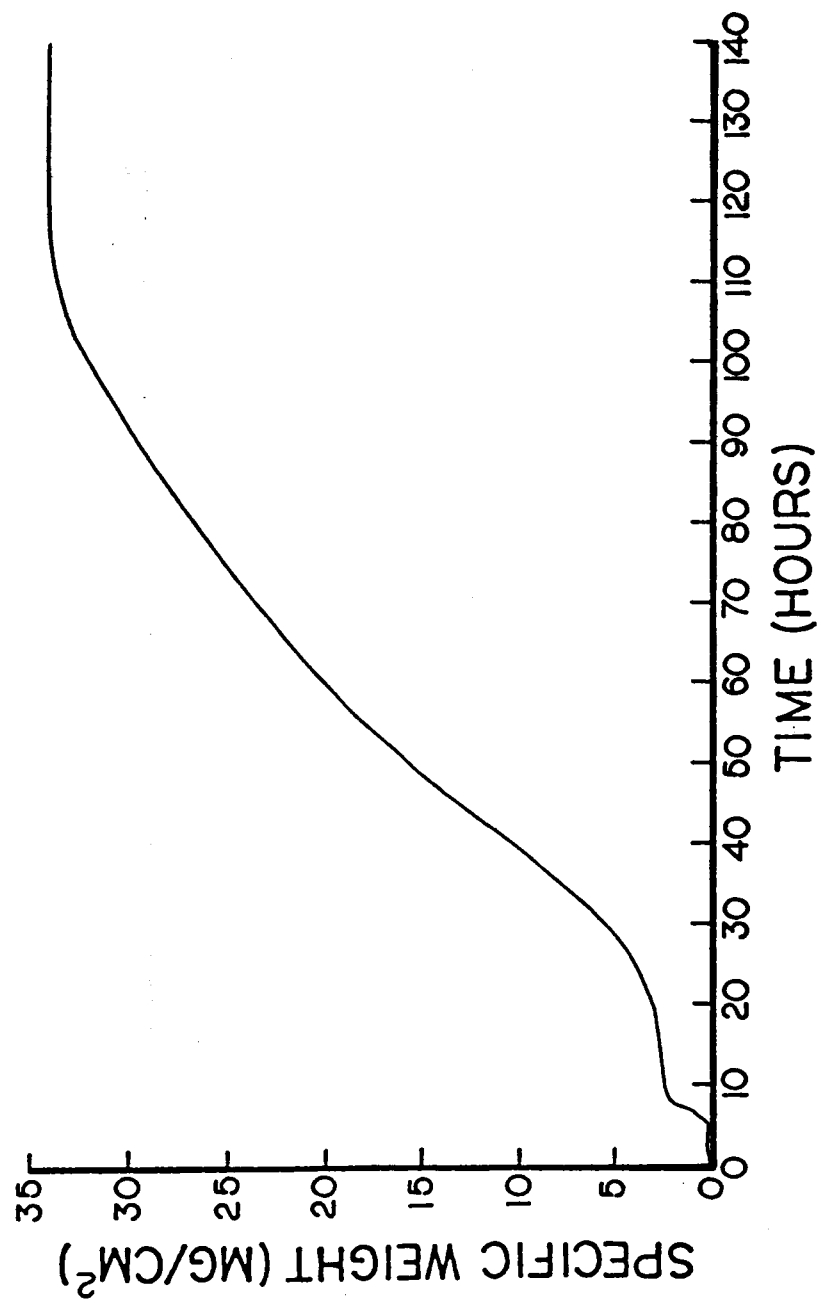
Figure A8 (c)

Ni - 50 a/o Al - 0.3 w/o Zr Hot Corrosion Weight Gain Curve for

Sample Preoxidized at 900°C in O_2
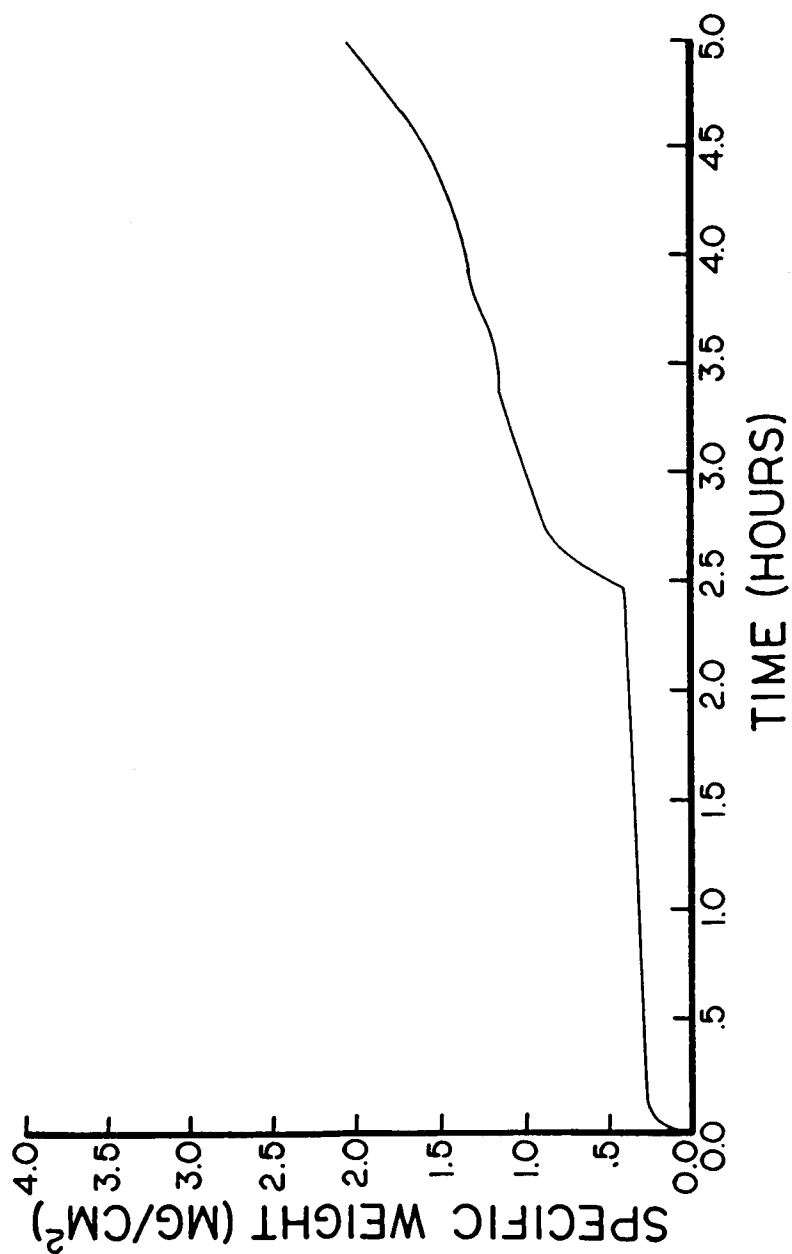
Figure A9 (a)

Ni – 50 a/o Al Hot Corrosion Weight Gain Curve for

Sample Preoxidized at 1200°C in Air
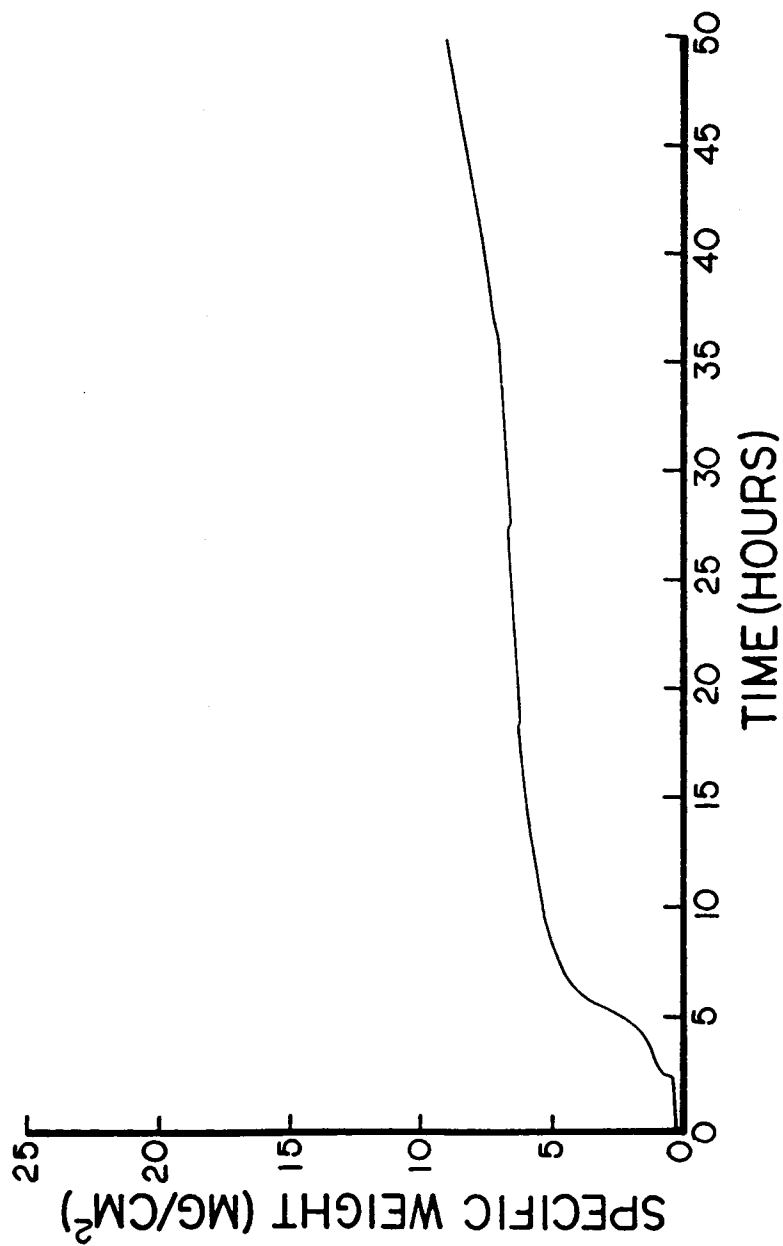
Figure A9 (b)

Ni – 50 a/o Al Hot Corrosion Weight Gain Curve for

Sample Preoxidized at 1200°C in Air

217
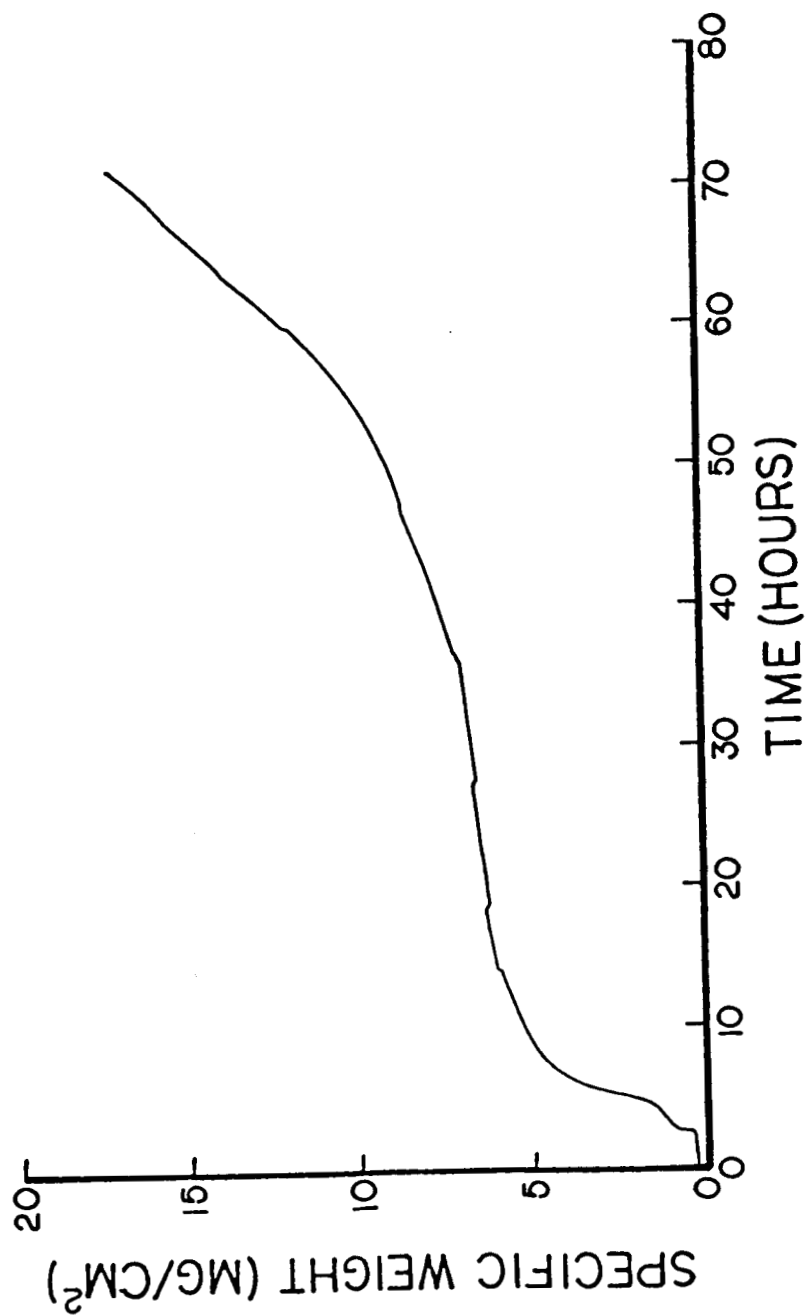
Figure A9 (c)

Ni – 50 a/o Al Hot Corrosion Weight Gain Curve for

Sample Preoxidized at 1200°C in Air

TIME (HOURS)
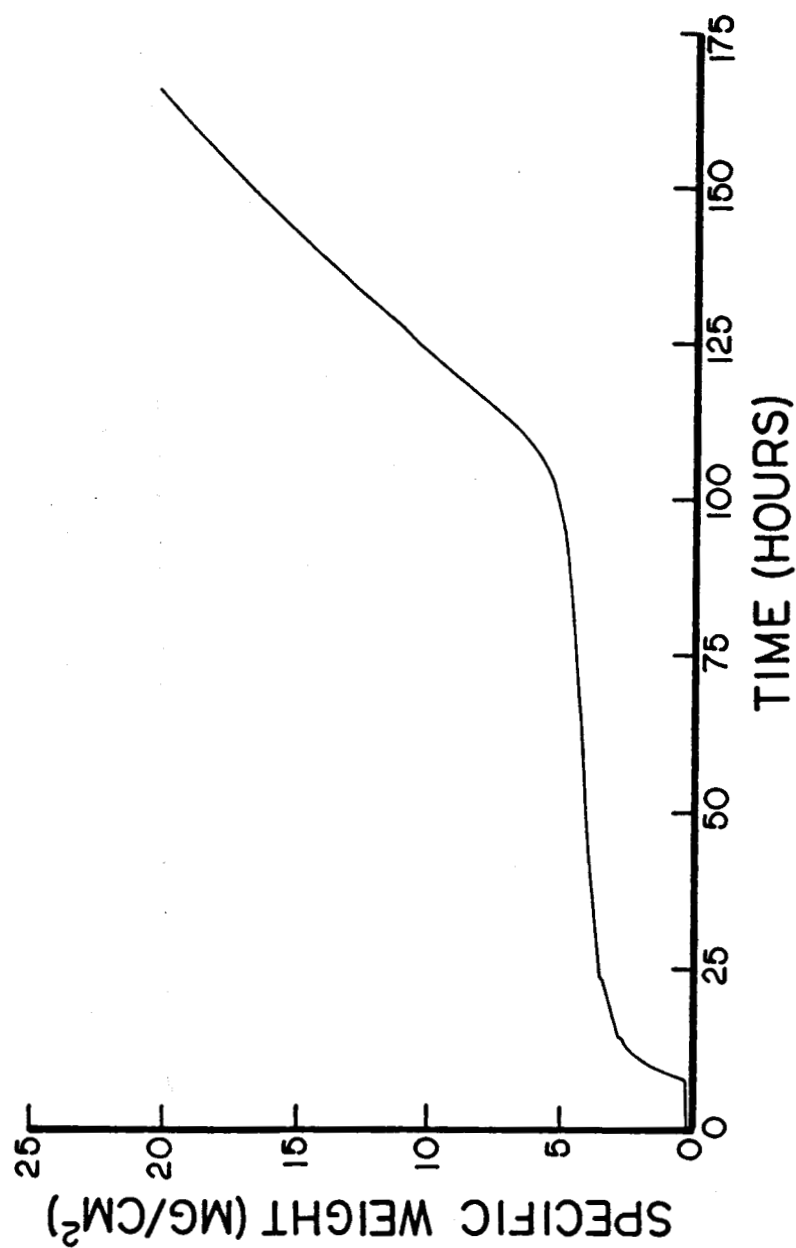
Figure A10

Ni – 50 a/o Al – 0.3 w/o Zr Hot Corrosion Weight Gain Curve for
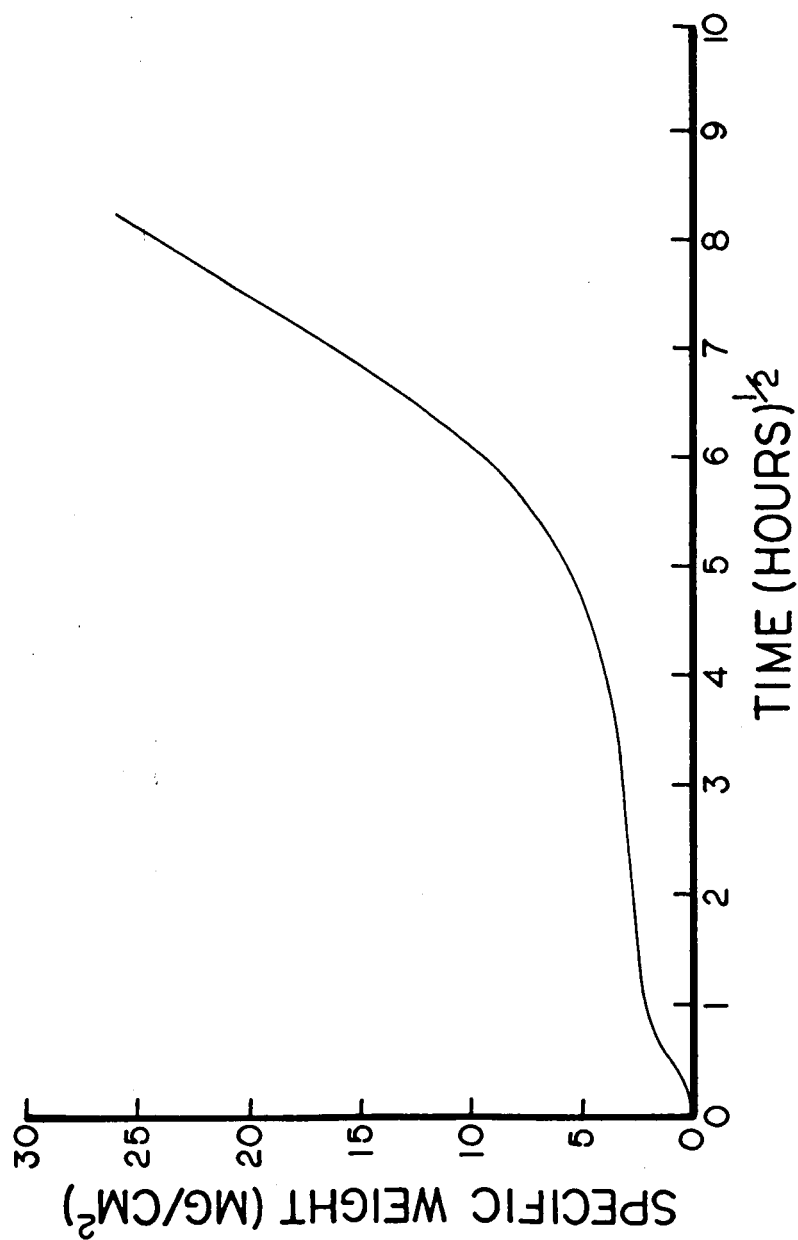
Sample Preoxidized at 1200°C in Air

Figure A11

Ni – 45 a/o Al 0.2 w/o Zr (P/M) Hot Corrosion Weight Gain Curve

Plotted on Parabolic Axes
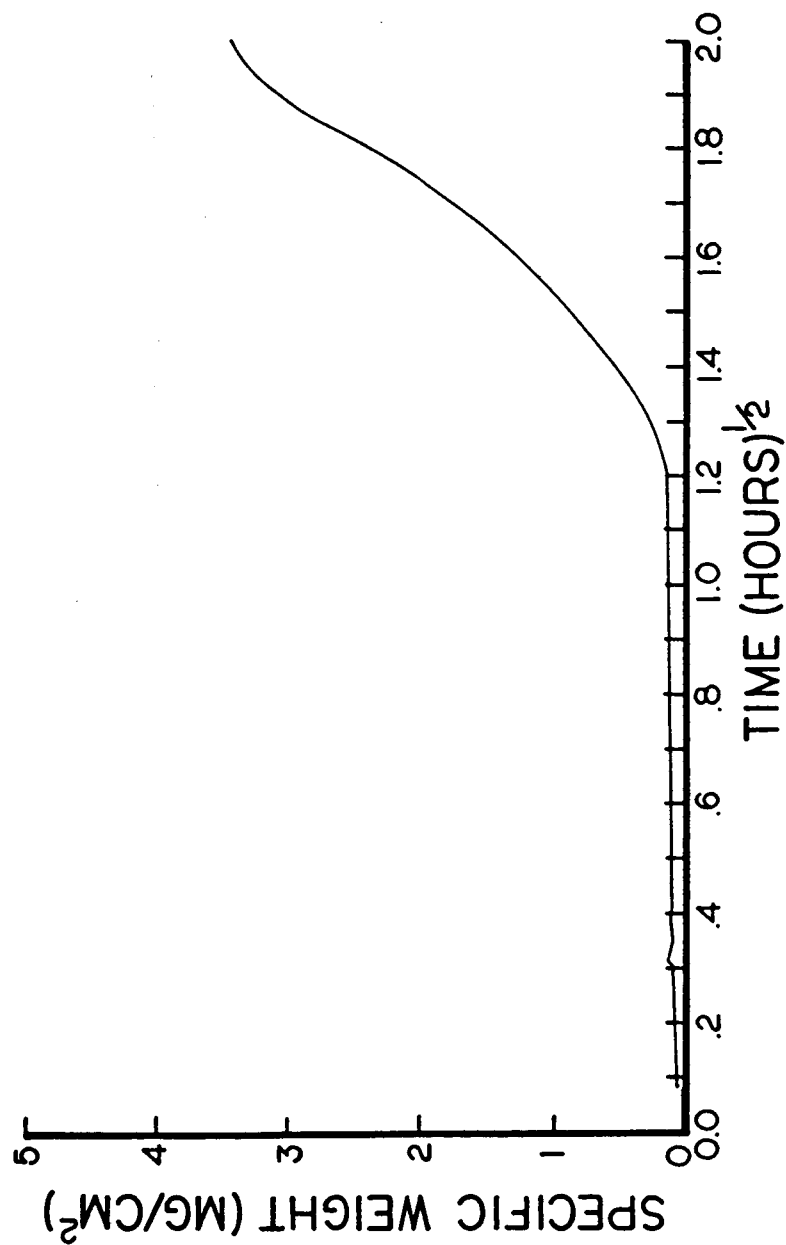
Figure A12 (a)

Ni – 45 a/o Al – 0.2 w/o Zr (P/M) Hot Corrosion Weight Gain Curve

Plotted on Parabolic Axes
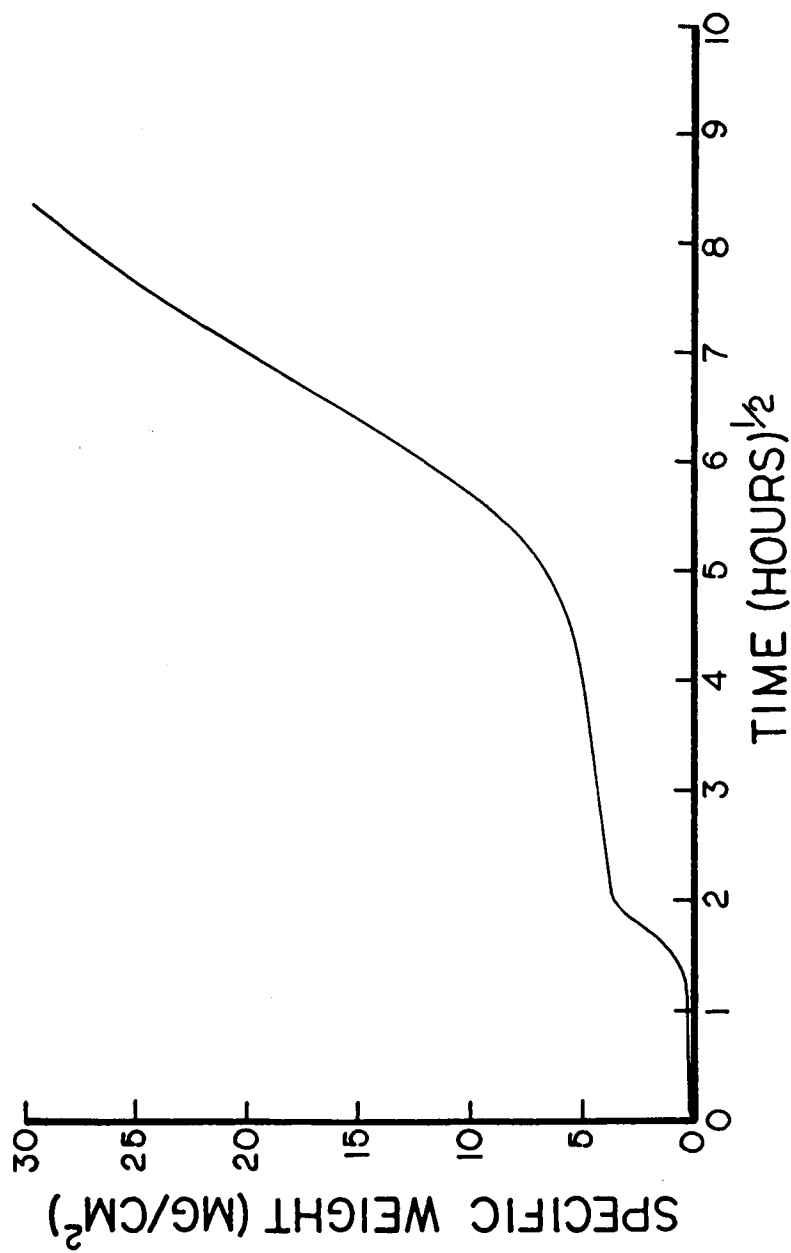
Figure A12 (b)

Ni – 45 a/o Al – 0.2 w/o Zr (P/M) Hot Corrosion Weight Gain Curve

Plotted on Parabolic Axes

222

APPENDIX B

Additional Macrographs of Oxidation and Hot Corrosion Samples
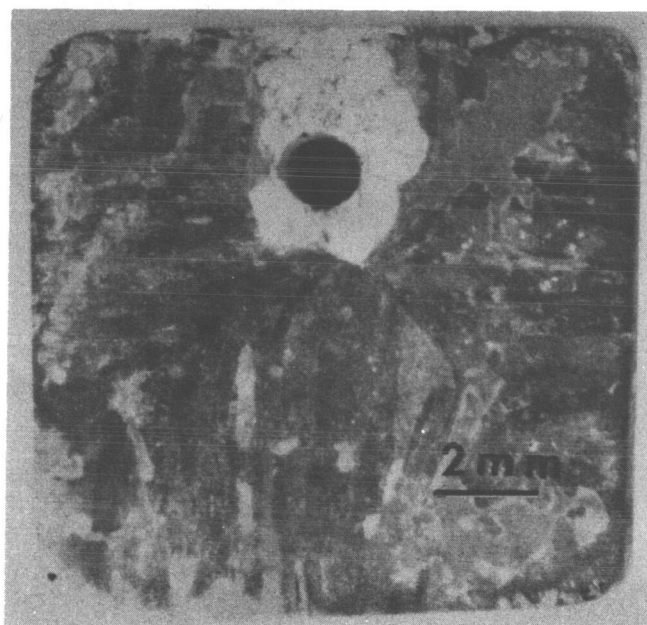
(a) Sample 18: Ni - 50 a/o Al
1200°C Preoxidation Sample Showing Spinel Near Hole
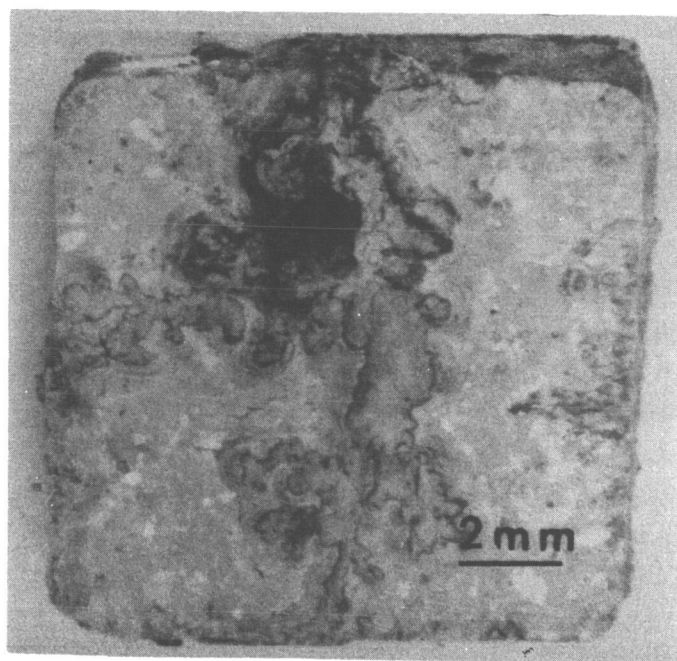
(b) Sample 22: Ni - 50 a/o Al.
Bare Metal Hot Corrosion Sample
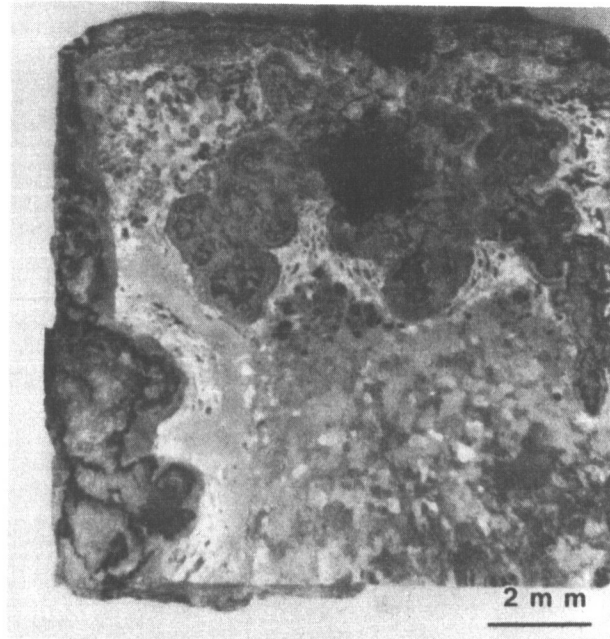
(c) Sample 23: Ni- 50 a/o Al
Bare Metal Hot Corrosion
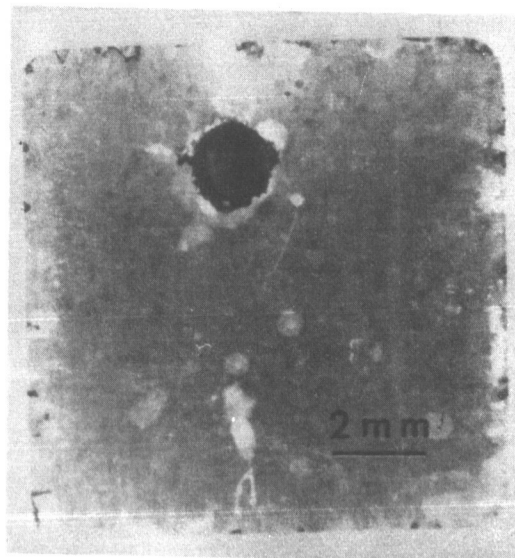
(d) Sample 23: Ni- 50 a/o Al
900°C Preoxidation
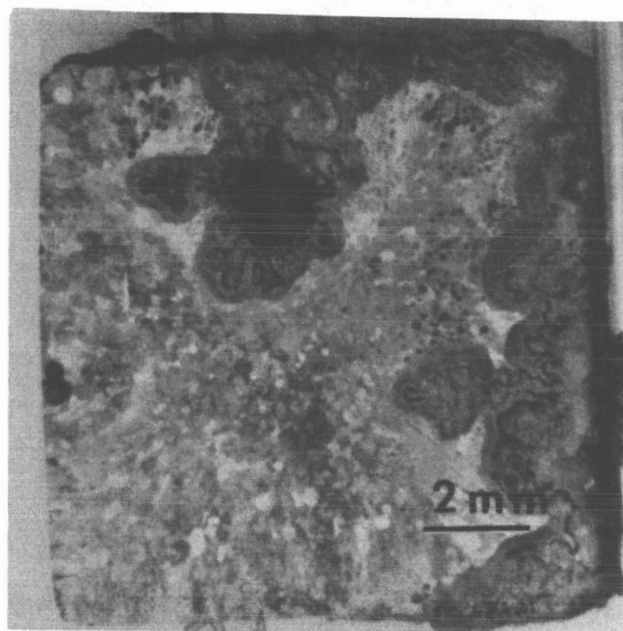
(e) Sample 23: Ni- 50 a/o Al
Same Side as (d) After Hot Corrosion
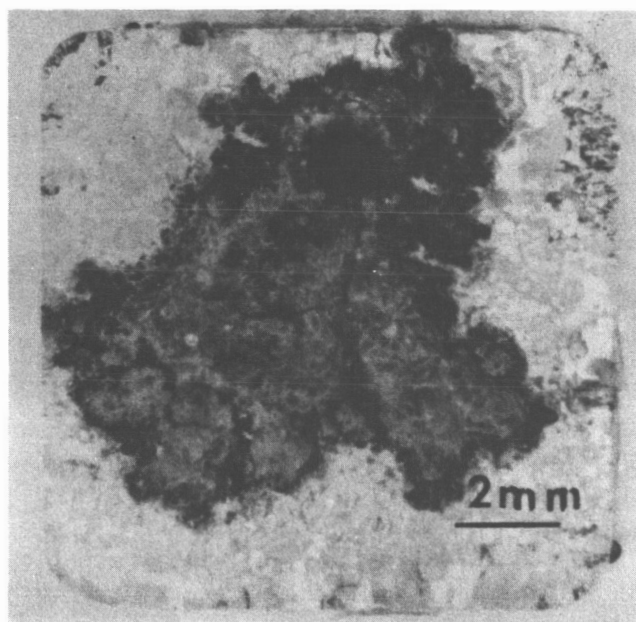
(f) Sample 26: Ni- 50 a/o Al
1200°C Preoxidation and Hot Corrosion
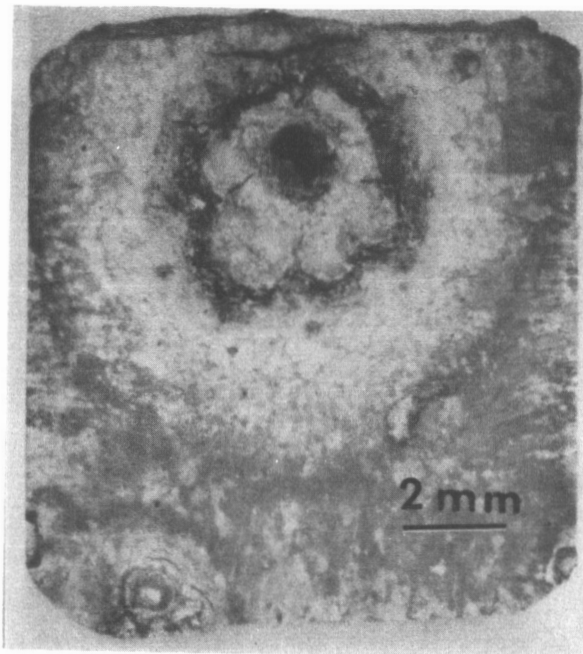
(g) Sample 16: Ni- 50 a/o Al - 0.3 w/o Zr
Bare Metal Hot Corrosion
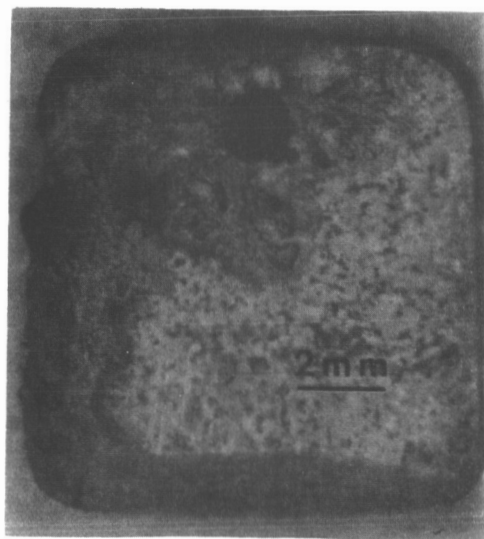
(h) Sample 35: Ni- 50 a/o Al - 0.3 Zr
Bare Metal Hot Corrosion
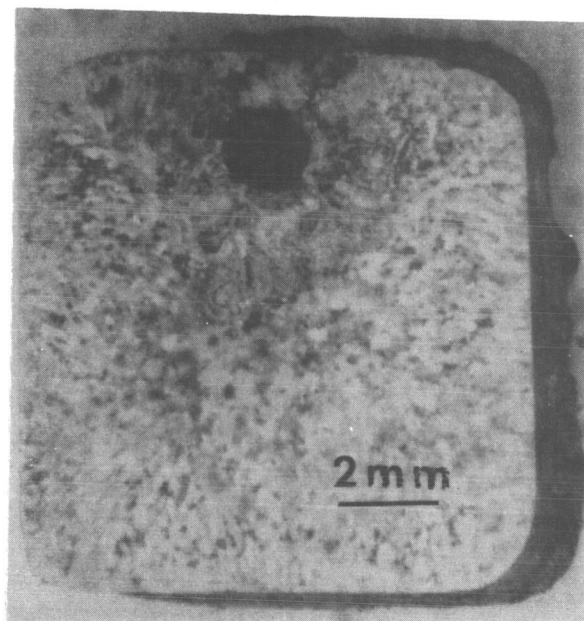
(i) Sample 35: Ni- 50 a/o Al - 0.3 Zr
Opposite Side of (h)
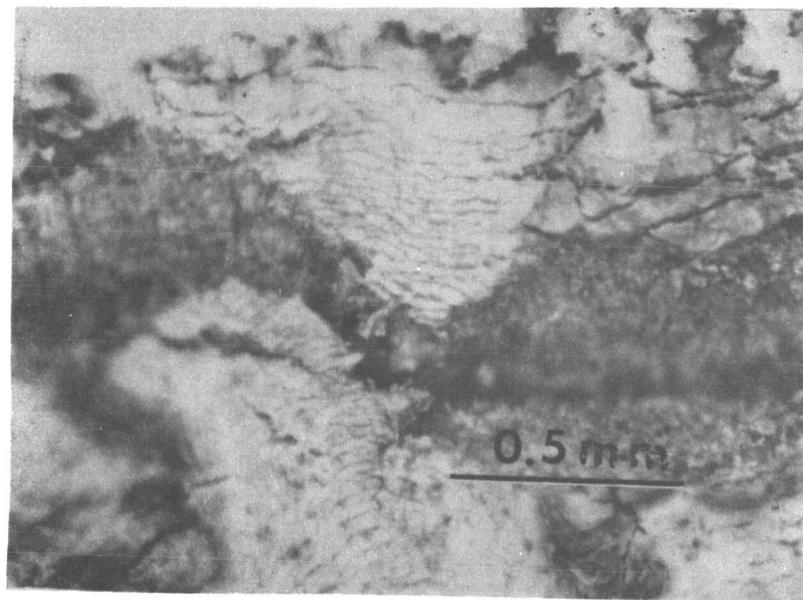
(j) Sample 35: Ni- 50 a/o Al - 0.3 Zr
Side View of (h)
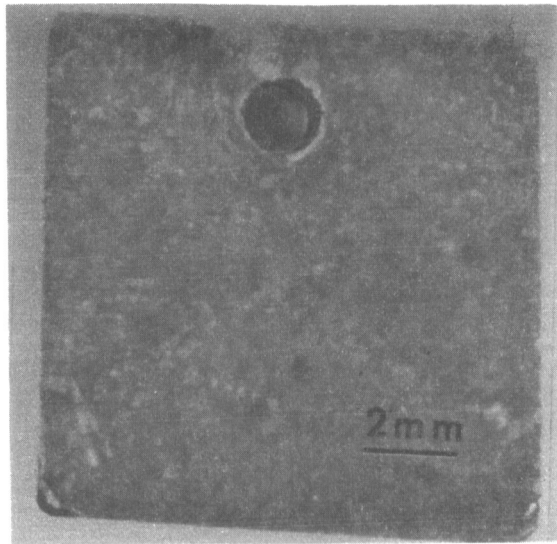
(k) Sample 24: Ni- 50 a/o Al - 0.3 Zr
900°C Preoxidation
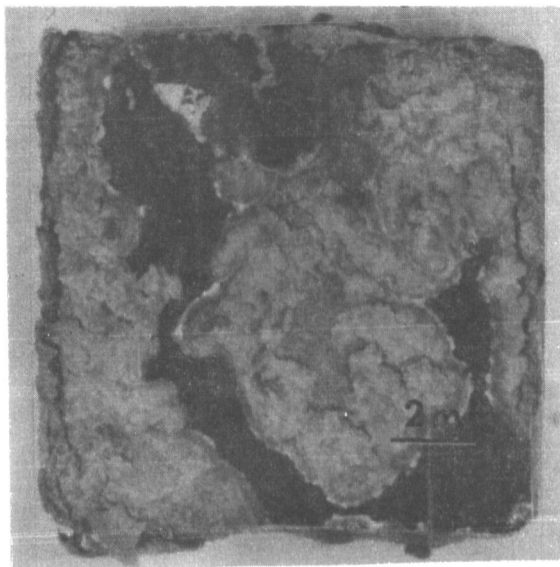
(1) Sample 24: Ni- 50 a/o Al - 0.3 Zr
Same Side as (k) After Hot Corrosion

229
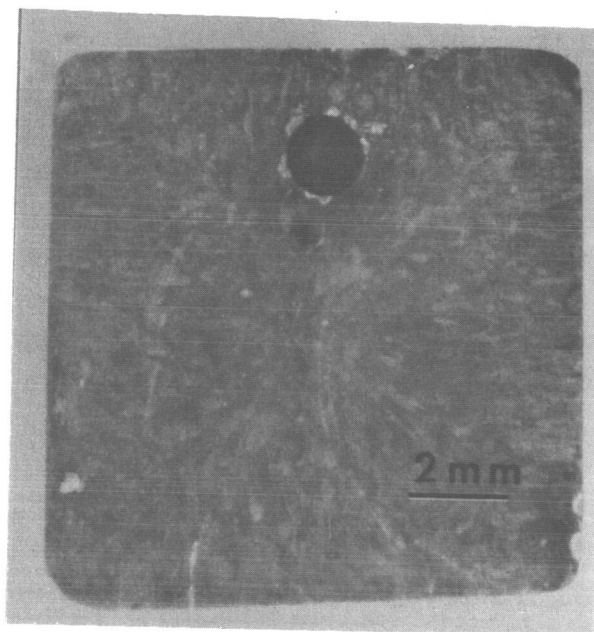
(m) Sample 24: Ni- 50 a/o Al - 0.3 Zr
900°C Preoxidation
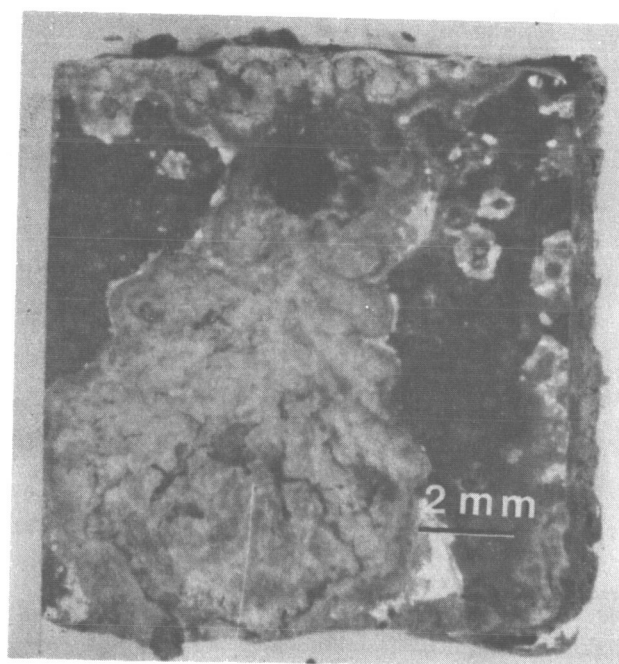
(n) Sample 24: Ni- 50 a/o Al - 0.3 Zr
Same Side As (m) After Hot Corrosion
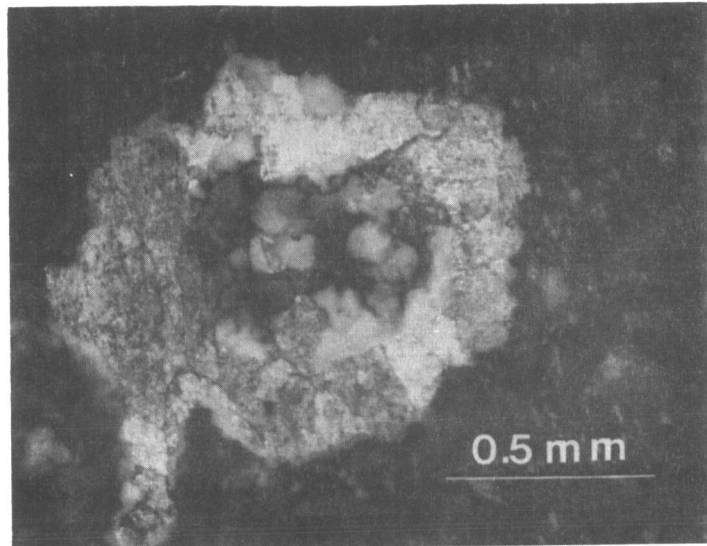
(o) Sample 24: Ni- 50 Al - 0.3 Zr
Close-up of Nodule in Upper Right Corner of (n)
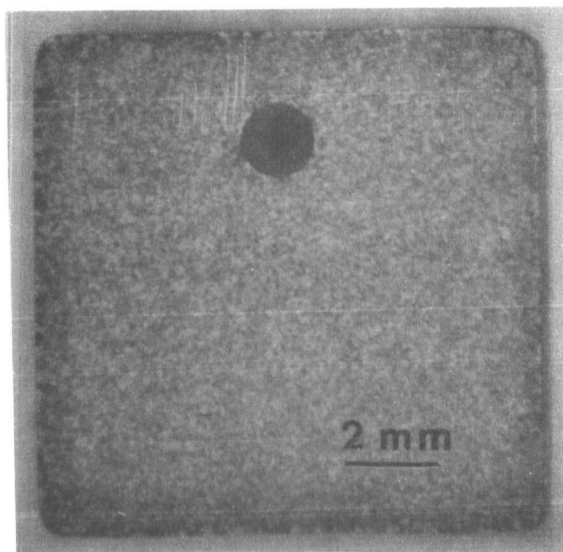
(p) Sample 15: Ni-24 a/o Al - 15 w/o Cr - 0.3 w/o Zr
1200°C Preoxidation Showing Extensive Spalling
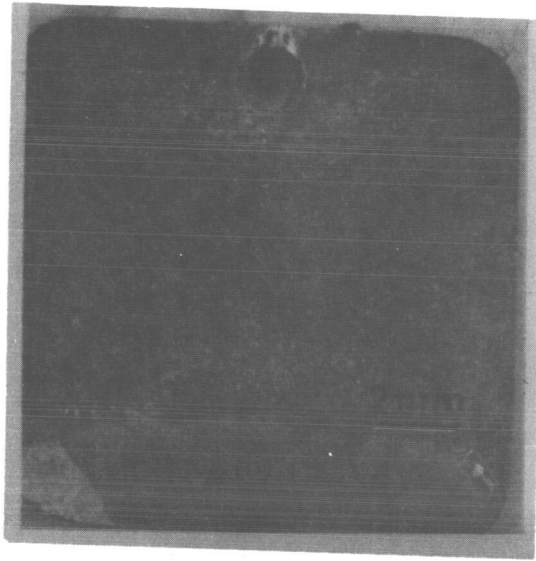
(q) Sample 29: Ni- 45 a/o Al - 5 w/o Cr
   Bare Metal Hot Corrosion Sample
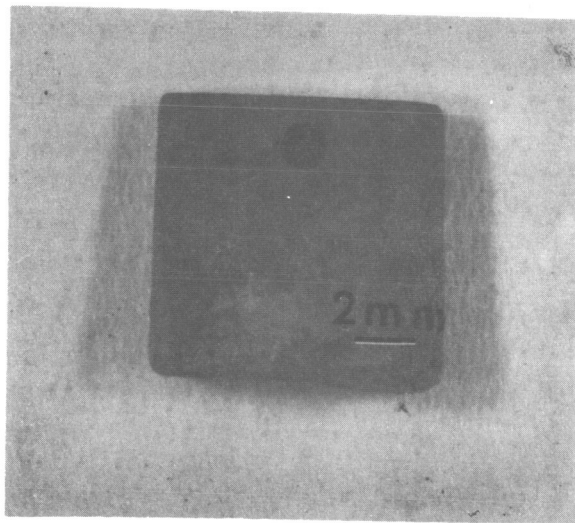
(r) Sample 14: Ni- 24 a/o Al - 15 w/o Cr - 0.3 w/o Zr
   Bare Metal Hot Corrosion. Worst Side.
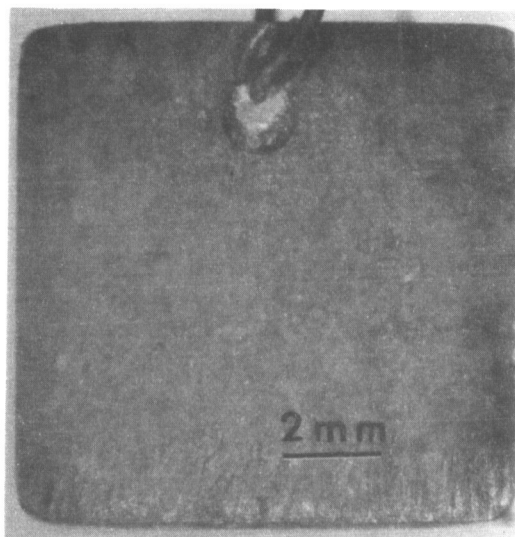
(s) Sample 13: Ni- 24 a/o Al - 15 w/o Cr - 0.3 w/o Zr
900°C Preoxidation and Hot Corrosion
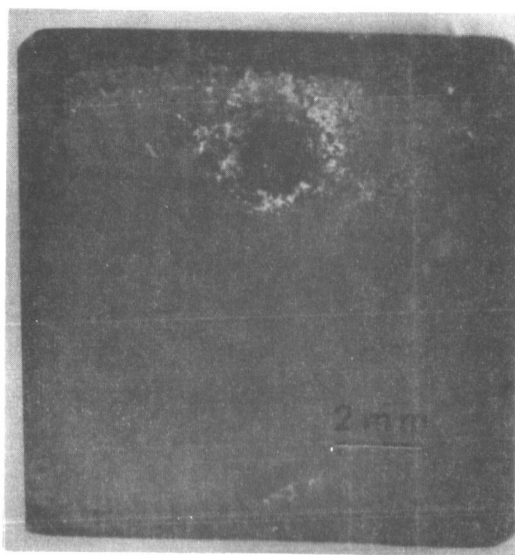
(t) Sample 28: Ni- 24 a/o Al - 15 w/o Cr - 0.3 w/o Zr
900°C Preoxidation and Hot Horrosion

APPENDIX C

Additional Optical Micrographs
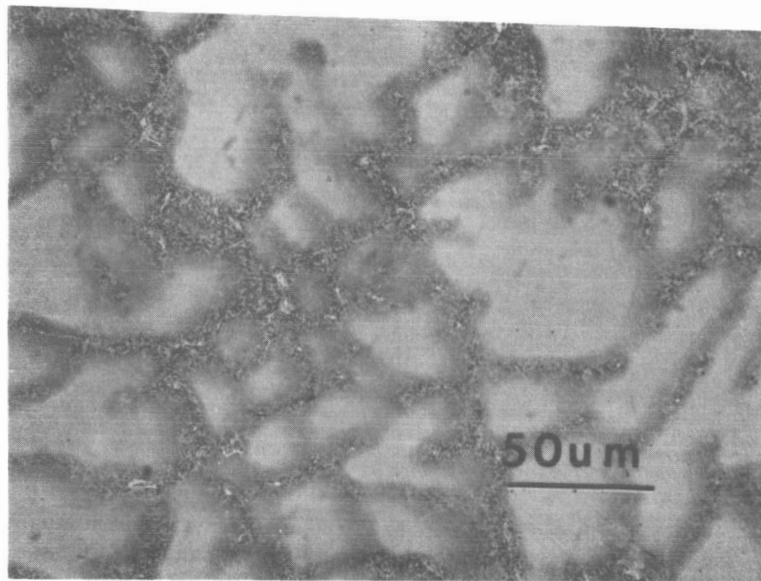
(a) As Received Ni- 45 a/o Al - 5 w/o Cr
Detail of Dendritic Microstructure
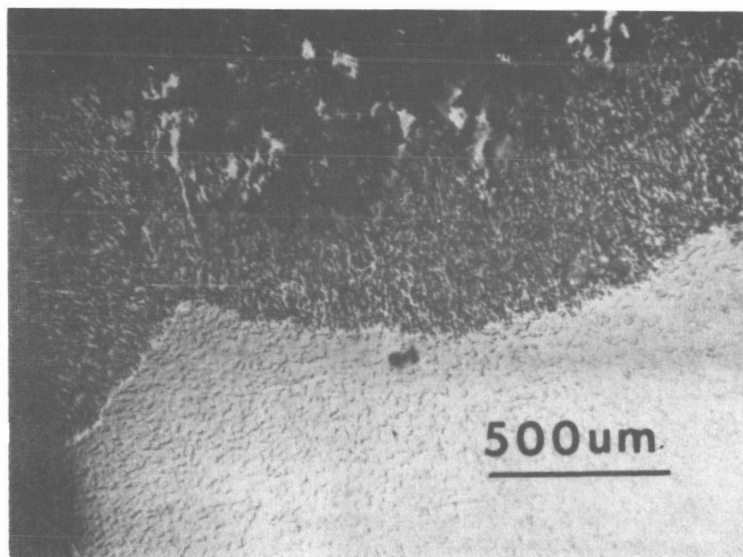
(b) Sample 2: Ni- 45 a/o Al - 0.2 w/o Zr (P/M)
Bare Metal Hot Corrosion

234
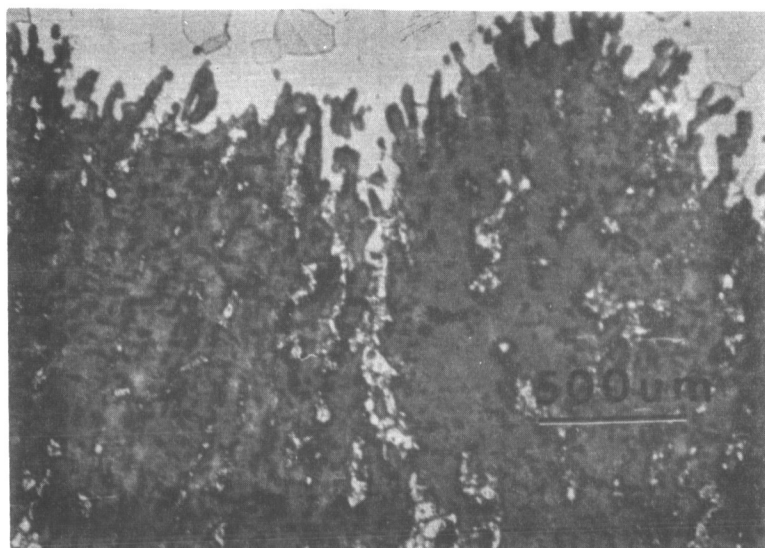
(c) Sample 3: Ni- 45 a/o Al - 0.2 w/o Zr (P/M)
Corrosion Interfacial Area Showing Incorporated Metal
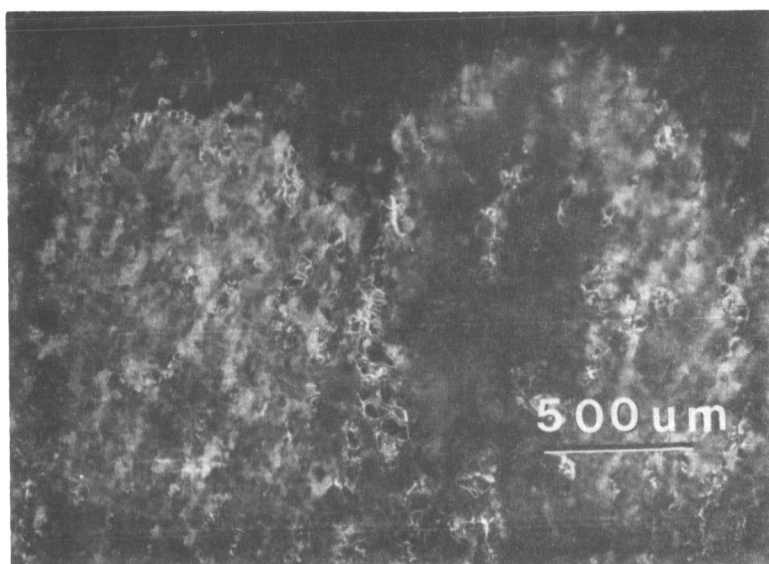
(d) Sample 3: Ni- 45 a/o Al - 0.2 w/o Zr (P/M)
Dark Field Micrograph of (c)
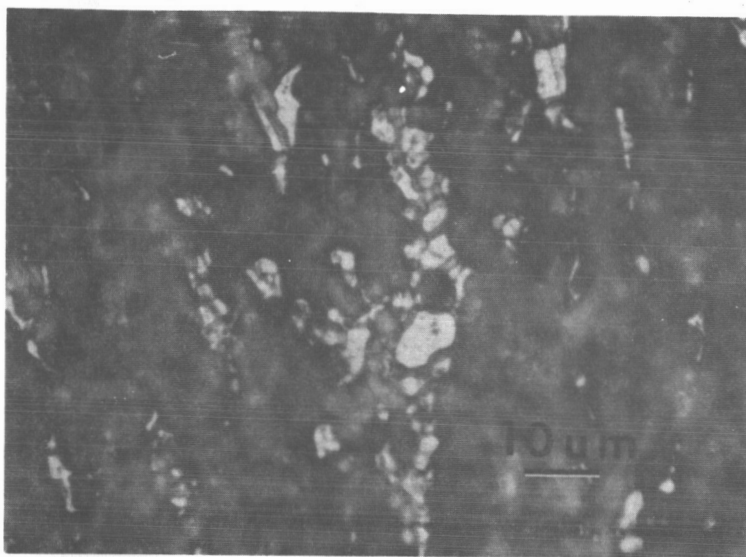
(e) Sample 3: Ni- 45 a/o Al - 0.2 w/o Zr (P/M)
Corrosion Scale and Incorporated Metal
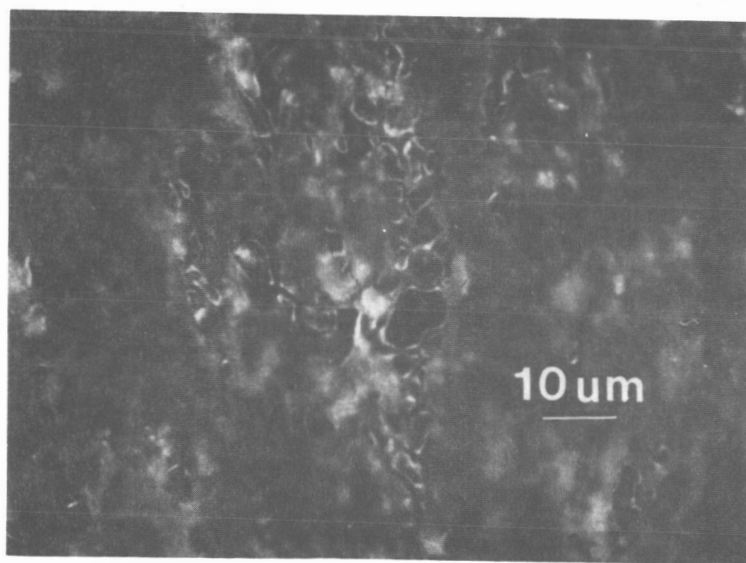
(f) Sample 3: Ni- 45 a/o Al - 0.2 w/o Zr
Dark Field Micrograph of (e)
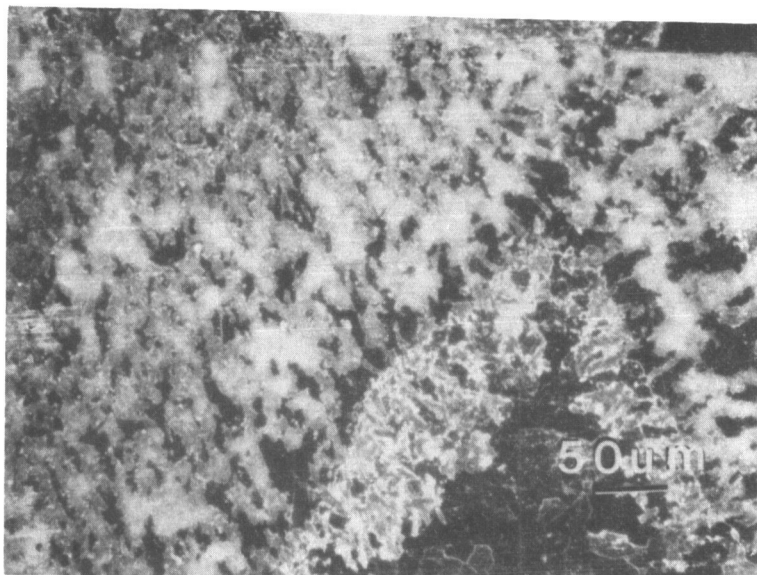
(g) Sample 2: Ni- 45 a/o Al - 0.2 w/o Zr (P/M)
Dark Field Micrograph Near a Corner
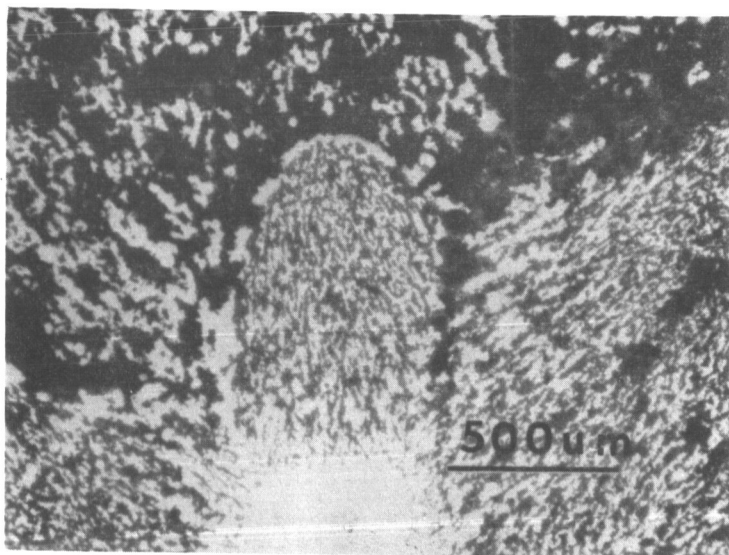
(h) Sample 5: Ni- 45 a/o Al - 0.3 w/o Zr (P/M)
Central Region of the Sample
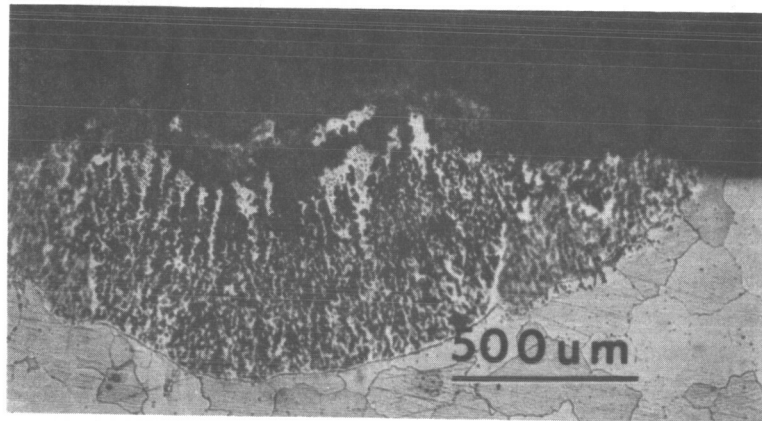
(i) Sample 10: Ni - 45 a/o Al - 0.2 w/o Zr
Corrosion Nodule
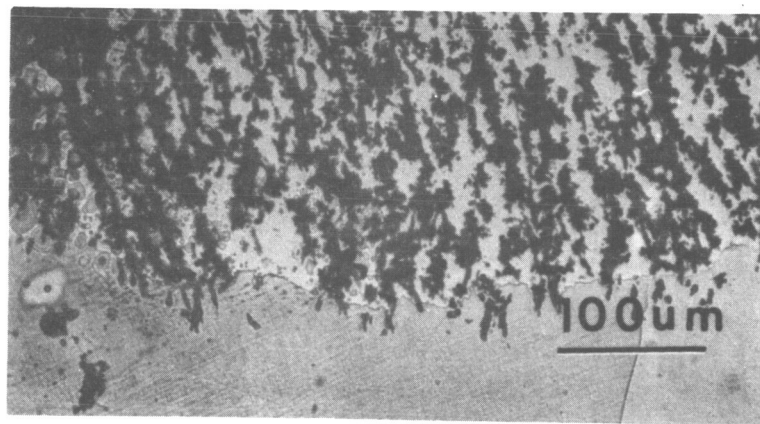
(j) Sample 11: Ni - 45 a/o Al - 0.2 w/o Zr
Corrosion Interface

(k) Sample 36: Ni- 50 a/o Al
Corrosion Scale
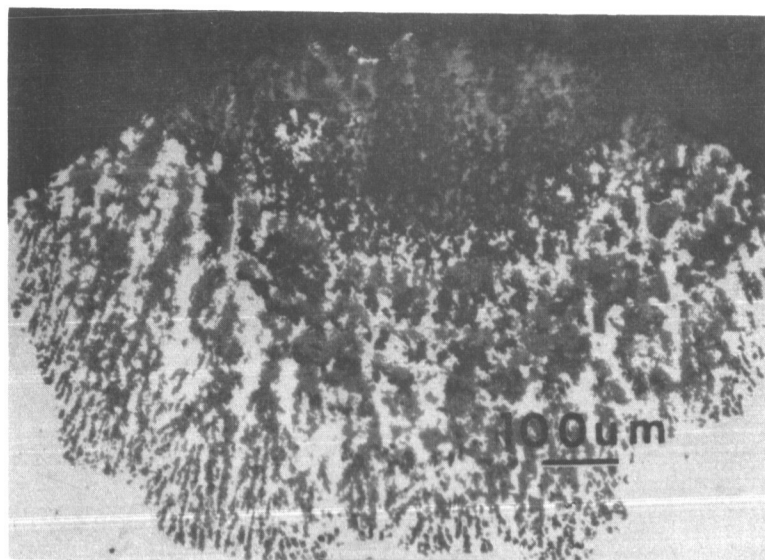
(1) Sample 23: Ni- 50 a/o Al
Corrosion Nodule

239
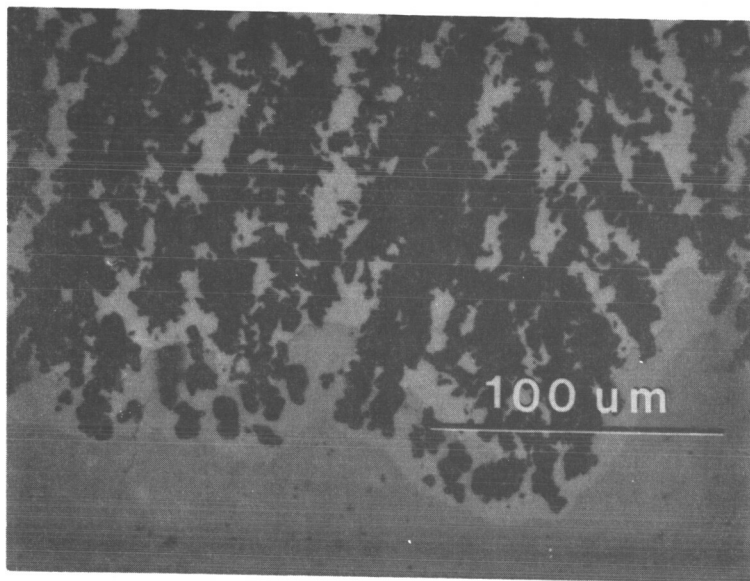
(m) Sample 22: Ni- 50 a/o Al
Detail of Corrosion Interface Showing Orange Layer
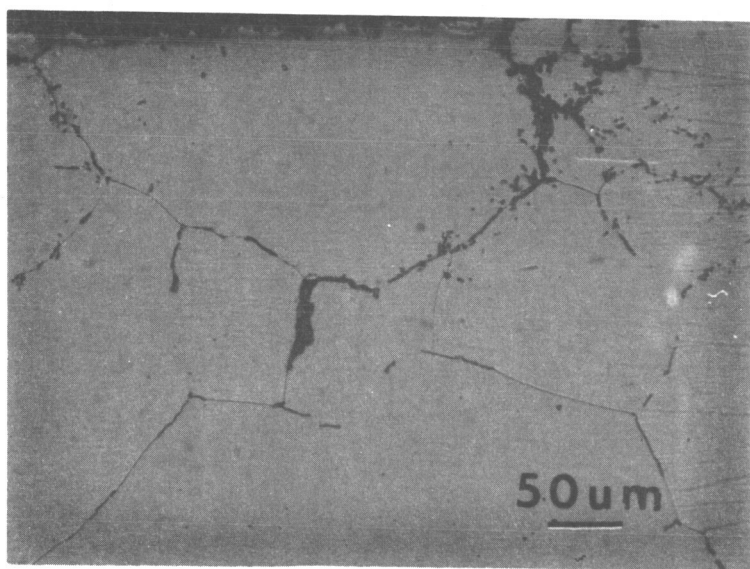
(n) Sample 17: Ni- 50 a/o Al - 0.3 w/o Zr
Detail Showing Some evidence of Grain Boundary Attack
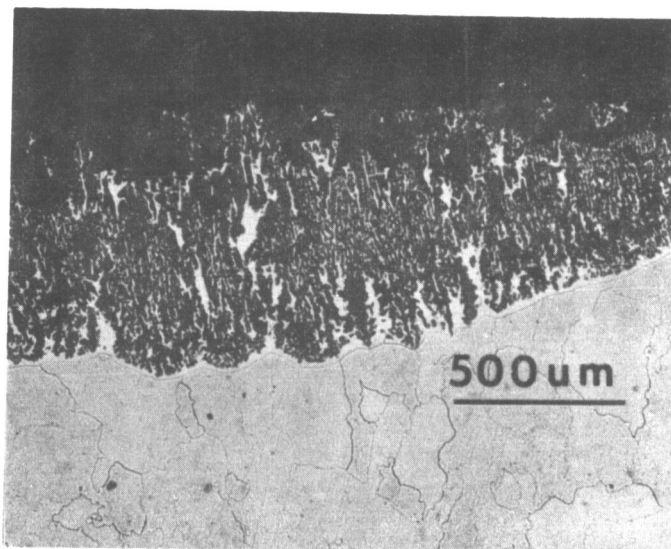
(o) Sample 24: Ni- 50 a/o Al - 0.3 w/o Zr
Corrosion Nodule
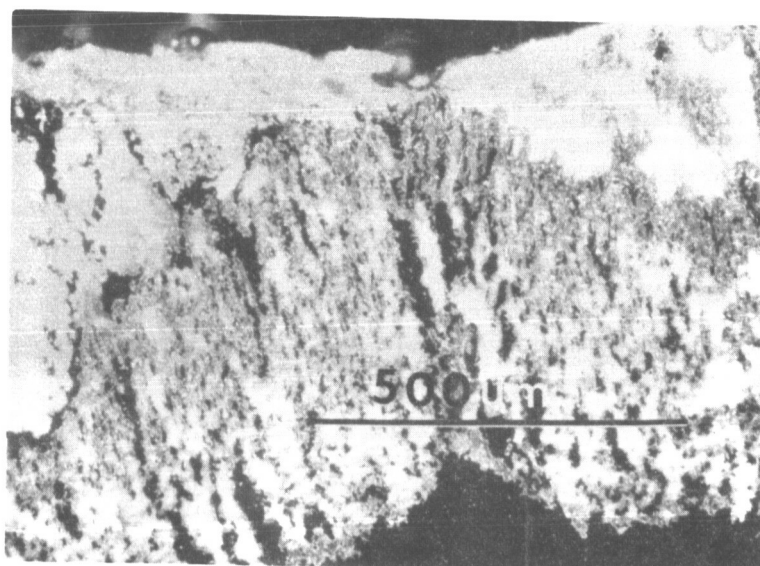
(p) Sample 24: Ni- 50 a/o Al - 0.3 w/o Zr
Dark Field optical Micrograph of Corrosion Scale
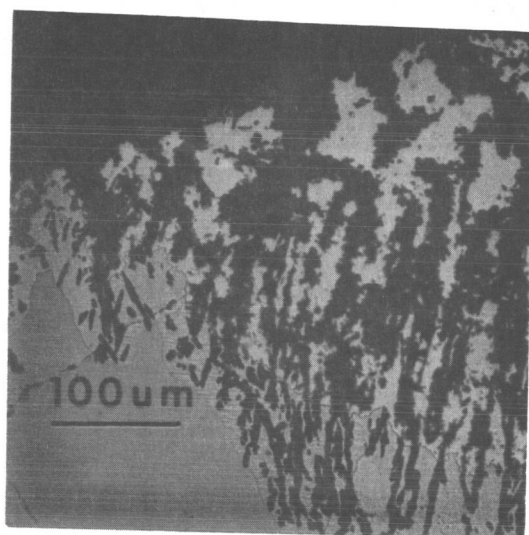
(q) Sample 17: Ni- 50 a/o Al - 0.3 w/o Zr
Corrosion nodule. Note Depleted Zone.
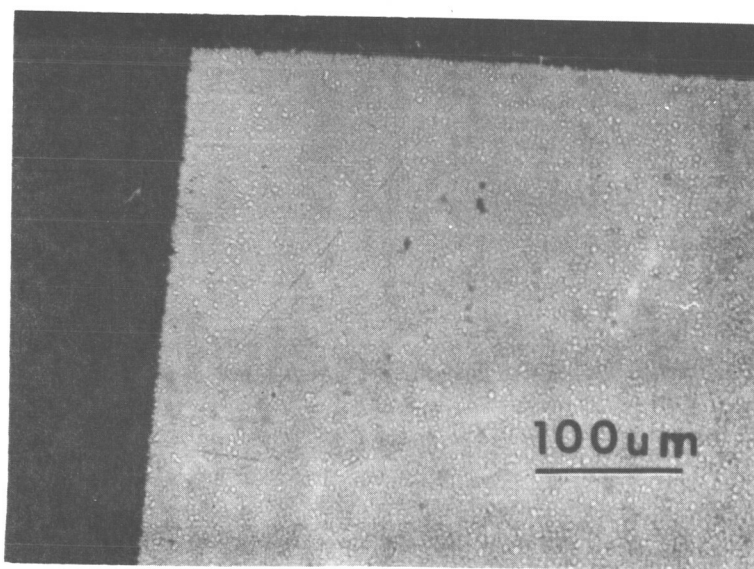
(r) Sample 13: Ni- 24 a/o Al - 15 w/o Cr - 0.3 w/o Zr
Corner of Exposed Sample
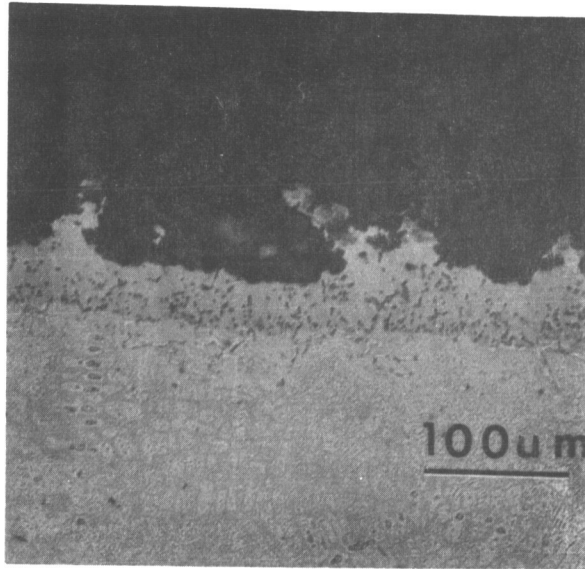
(s) Sample 14: Ni- 24 a/o Al - 15 w/o Cr - 0.3 w/o Zr
Corroded Region
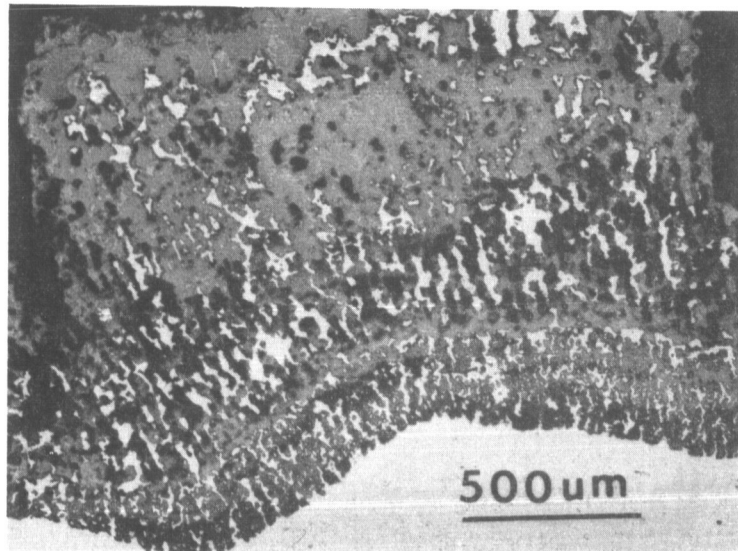

(t) Sample 25: Ni- 24 a/o Al - 15 w/o Cr - 0.3 w/o Zr
Corroded Region. Note Chromium Depletion At Interface.
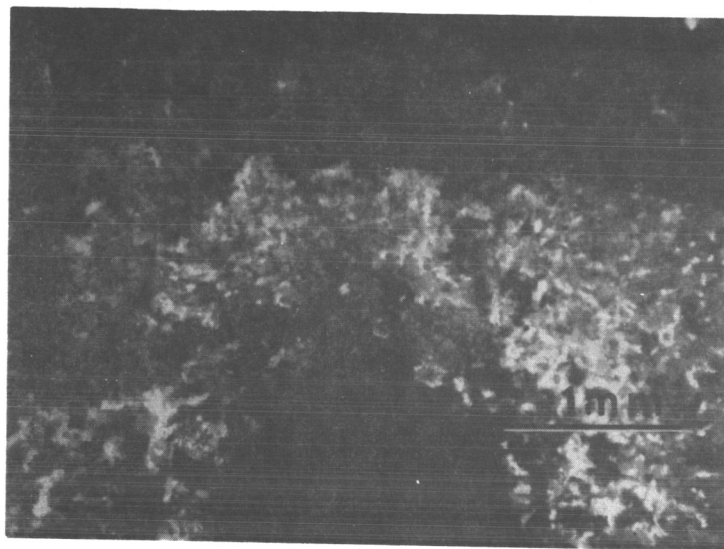
(u) Sample 28: Ni- 24 a/o Al - 15 w/o Cr - 0.3 w/o Zr
Dark Field Optical Micrograph of Corroded Region

Additional Scanning Electron Micrographs
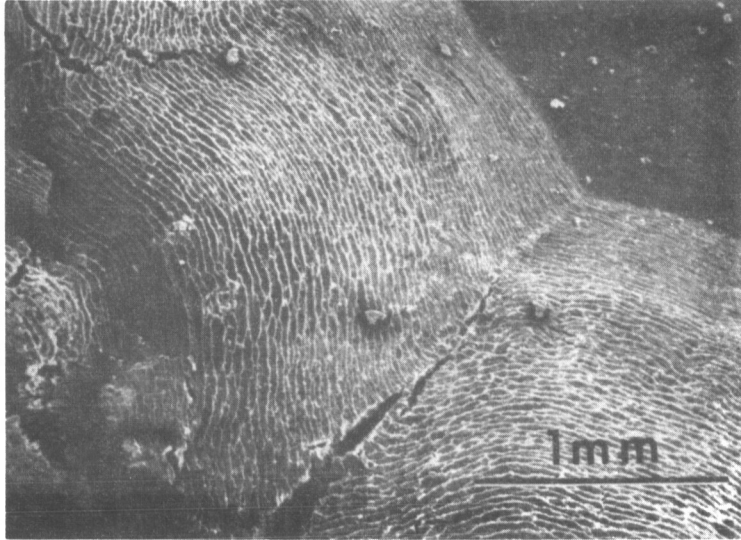
(a) Sample 5: Ni- 45 a/o Al – 0.2 w/o Zr (P/M)
Corroded Area at Outer Edge
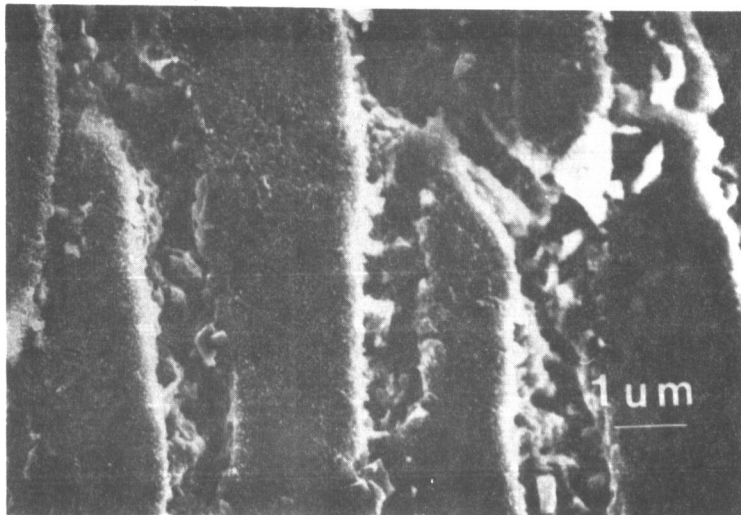
(b) Sample 5: Ni- 45 a/o Al – 0.2 w/o Zr (P/M)
Detail of Oxide Layer in (e) Being Lifted By Hot Corrosion
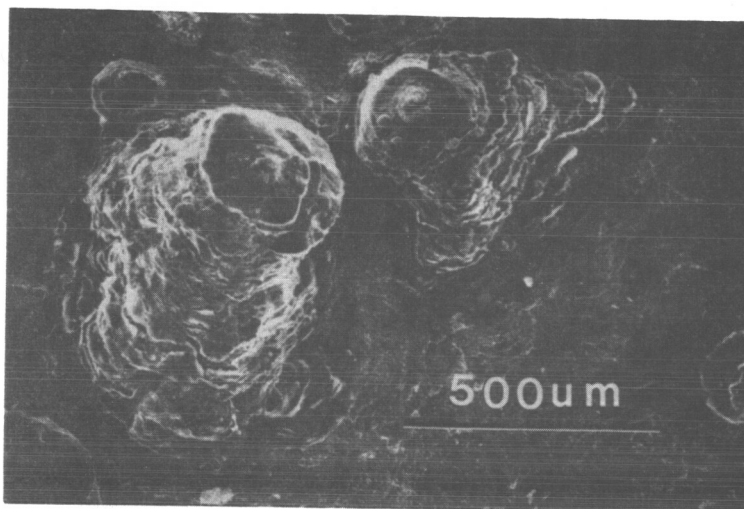
(c) Sample 2: Ni- 45 a/o Al - 0.2 w/o Zr (P/M)
Corrosion Nodules on Surface Near the Hanger Hole
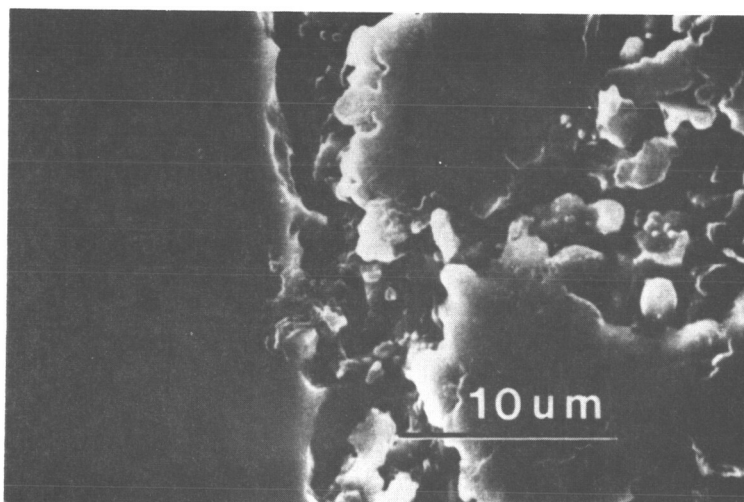
(d) Sample 3: Ni- 45 a/o Al - 0.2 w/o Zr (P/M)
Corrosion Interface
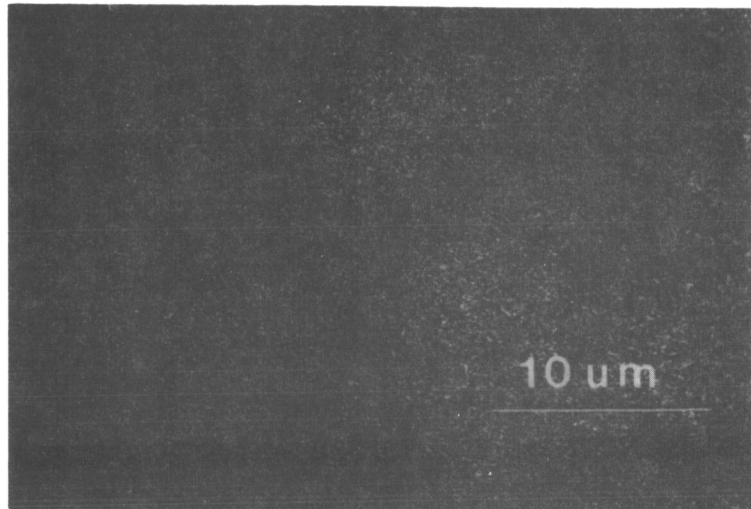
(e) Sample 3: Ni- 45 a/o Al - 0.2 w/o Zr (P/M)
Aluminum X-ray Map of (d)
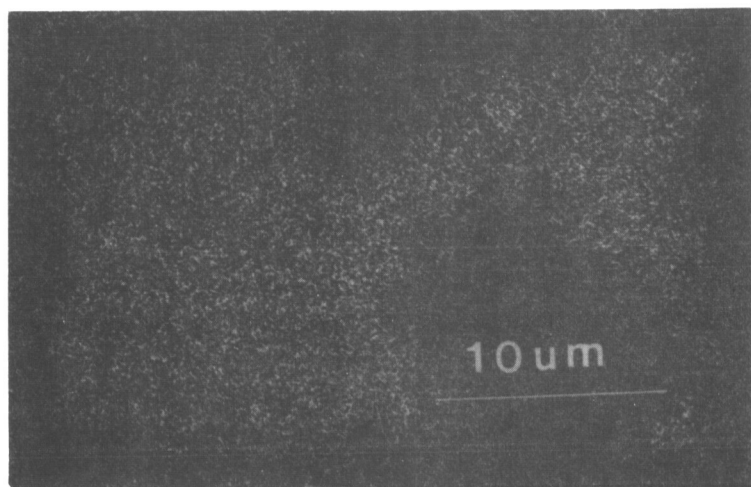
(f) Sample 3: Ni - 45 a/o Al - 0.2 w/o Zr (P/M)
Nickel X-Ray Map of (d)
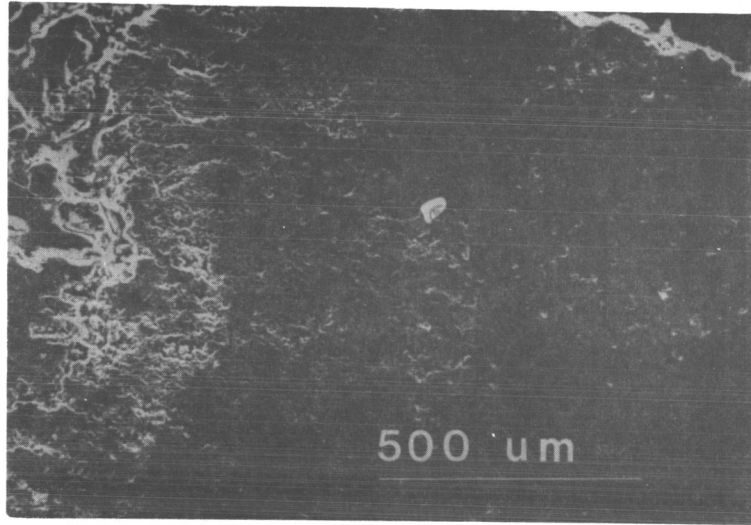
(g) Sample 11: Ni- 45 a/o Al - 0.2 w/o Zr
Corrosion Scale
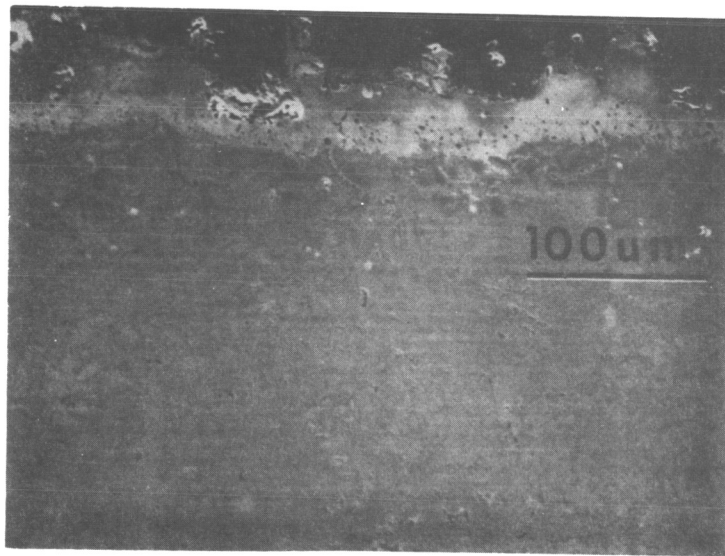
(h) Sample 14: Ni- 24 a/o Al - 15 w/o Cr - 0.3 w/o Zr
Corroded Surface
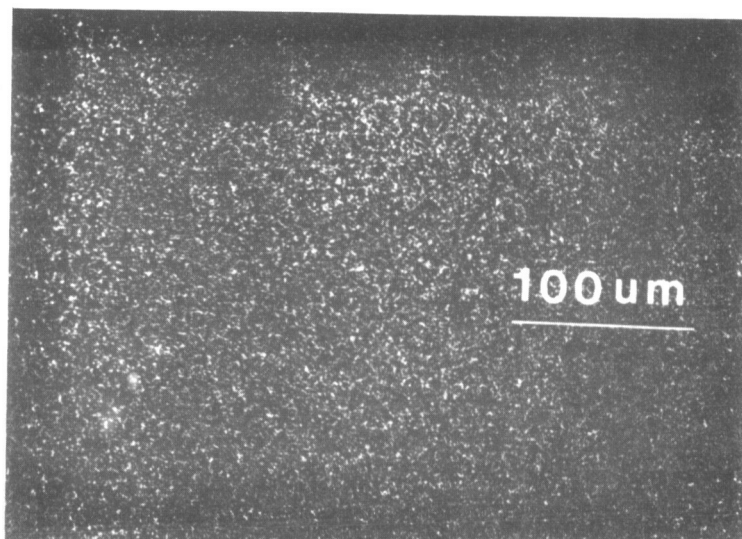
(i) Sample 14: Ni- 24 a/o Al - 15 w/o Cr - 0.3 w/o Zr
Nickel X-ray Map of (h)
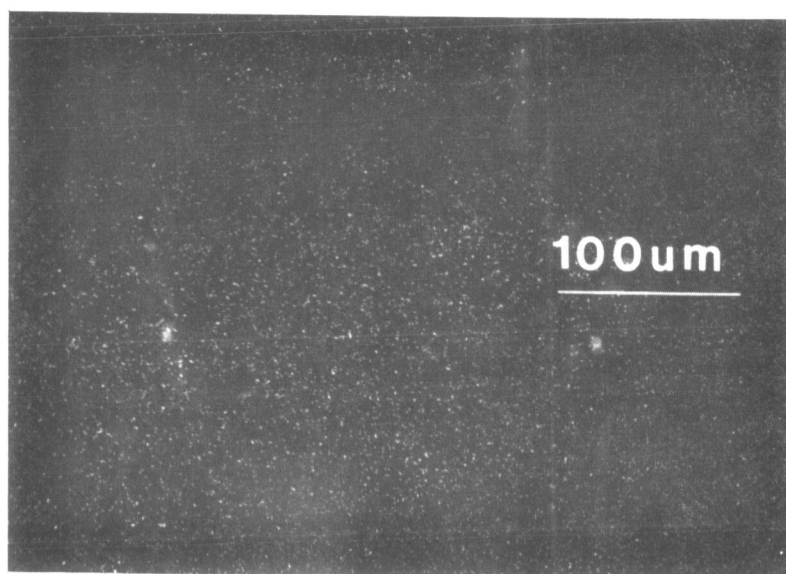
(j) Sample 14: Ni- 24 a/o Al - 15 w/o Cr - 0.3 w/o Zr
Chromium X-ray Map of (h)

249
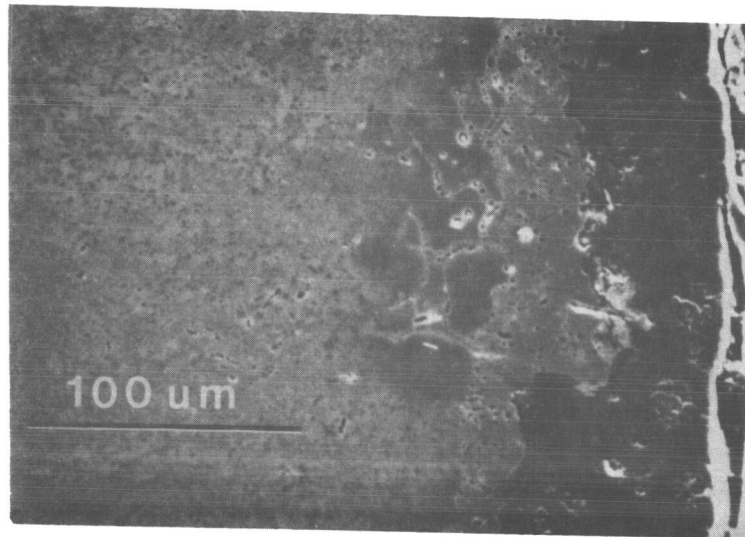
(k) Sample 14: Ni- 24 a/o Al - 15 w/o Cr - 0.3 w/o Zr
Corroded Area
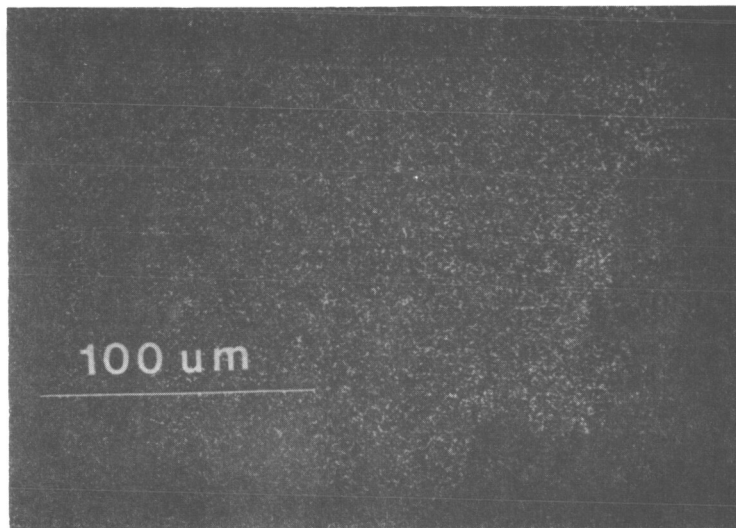
(1) Sample 14: Ni- 24 a/o Al - 15 w/o Cr - 0.3 w/o Zr
Nickel X-ray Map of (k)
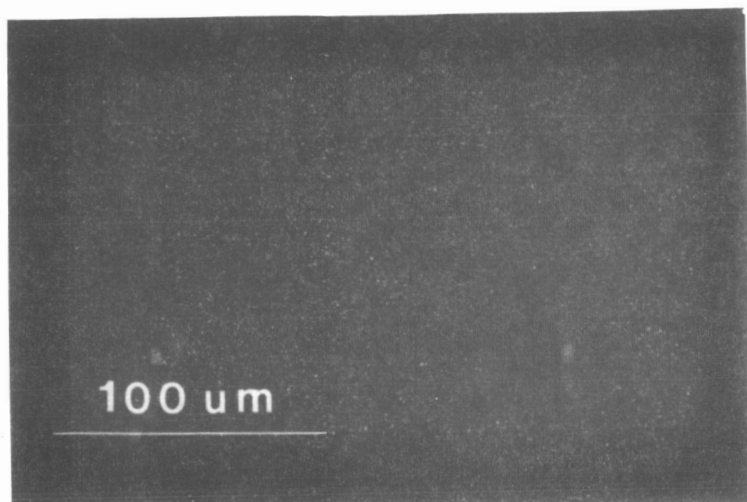
(m) Sample 14: Ni- 24 a/o Al - 15 w/o Cr - 0.3 w/o Zr
Chromium X-ray Map of (k)

APPENDIX E

Additional Macrographs and Photomicrographs
of Intermediate Time Exposures
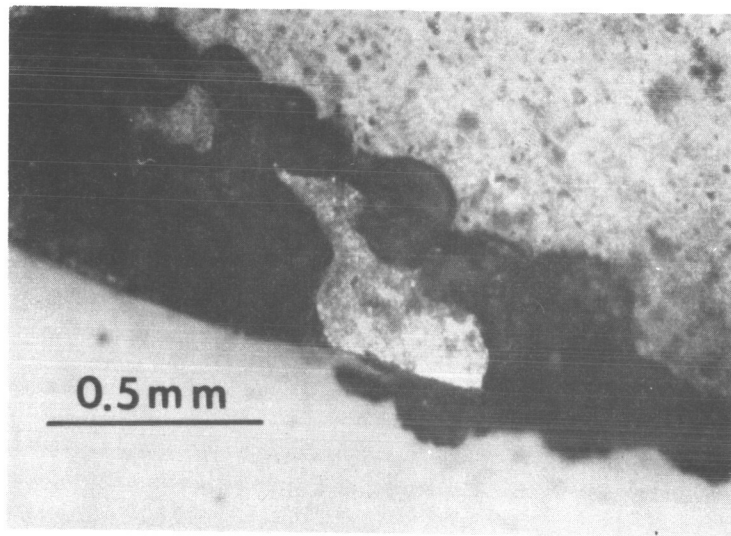
(a) Sample 30: 5 Minute Exposure
Corrosion at Edge
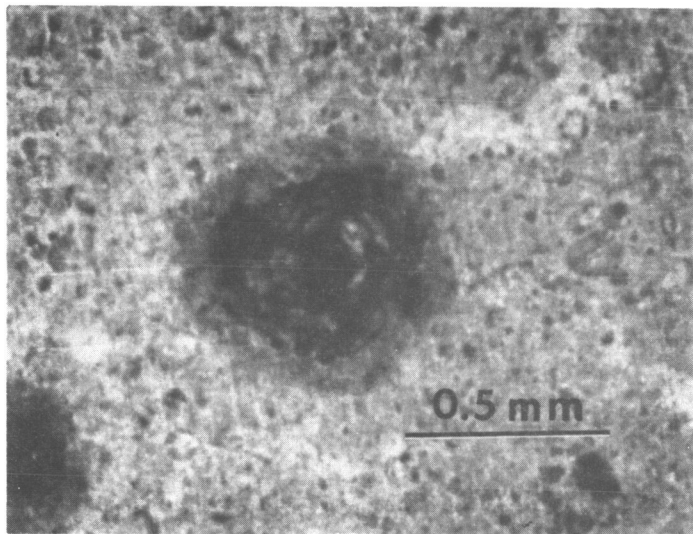
(b) Sample 30: 5 Minute Exposure
Corrosion Nodule
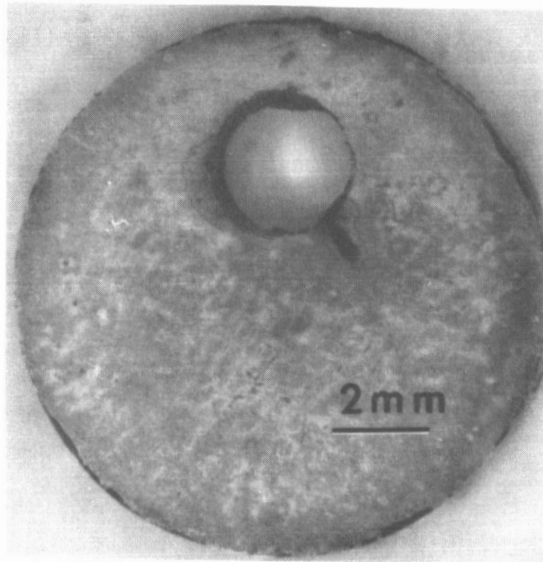
(c) Sample 31: 30 Minute Exposure
Opposite Side of Sample
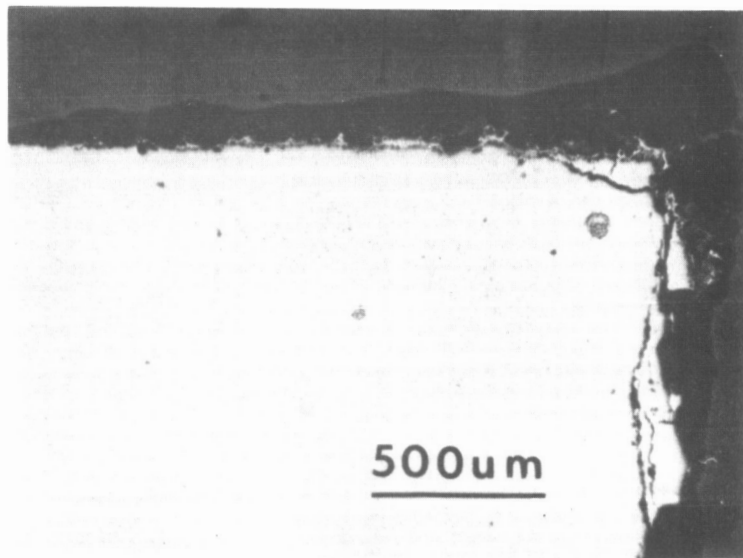
(d) Sample 31: 30 Minute Exposure
Transverse Section at Corner
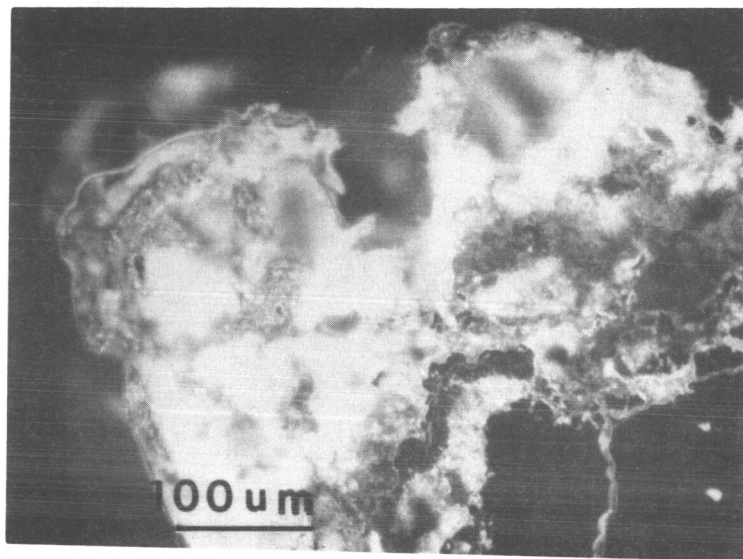
(e) Sample 31: 30 Minute Exposure
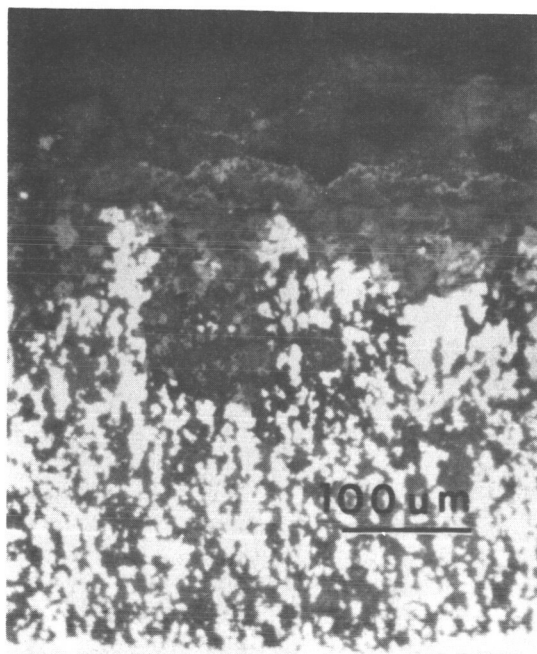Dark Field Optical Micrograph of Scale at Corner
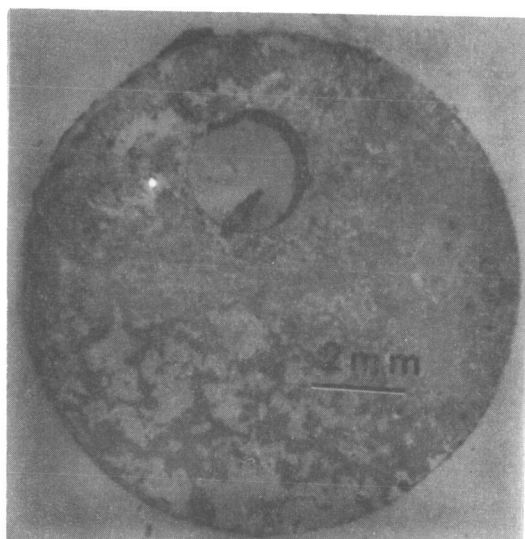
(f) Sample 34: 20 Hour Exposure
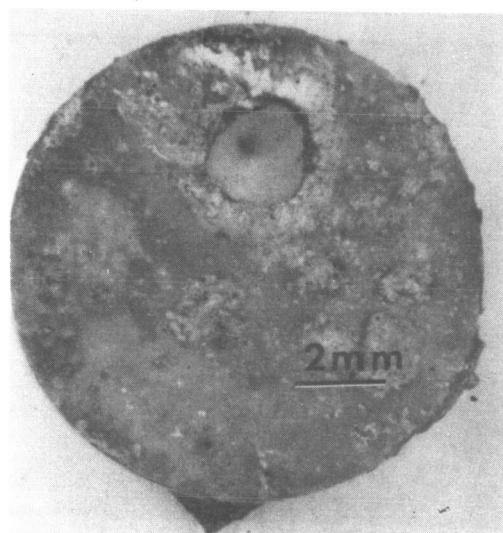Opposite Side of Sample

254
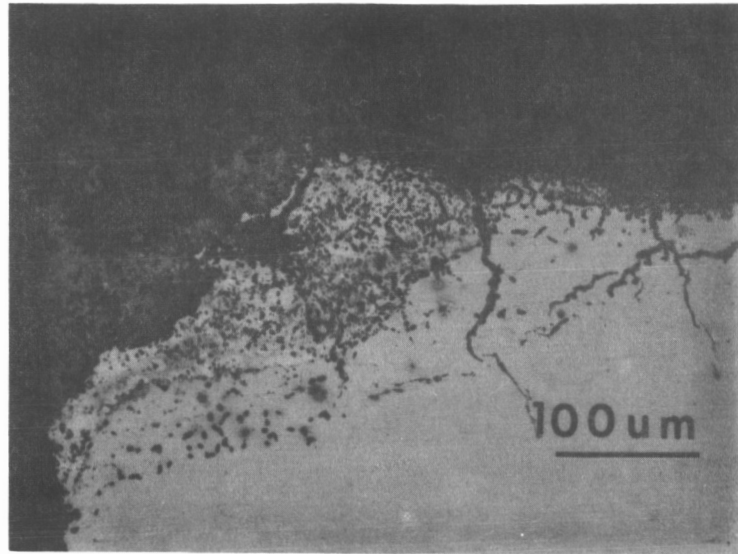
(g) Sample 34: 20 Hour Exposure
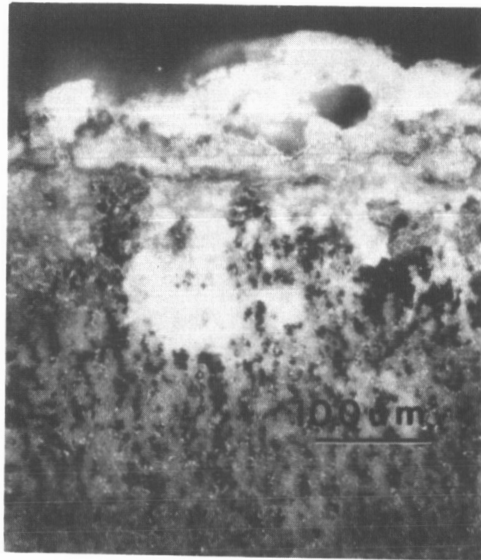Corrosion at Corner. Note Cracks.
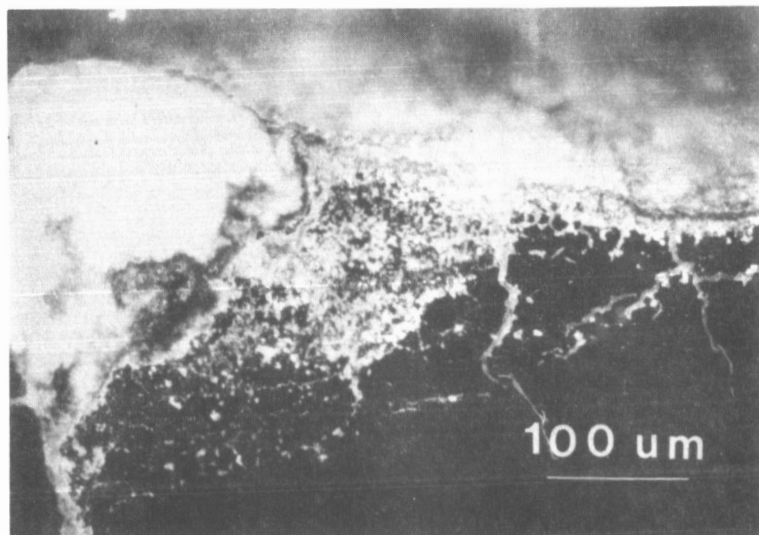
(h) Sample 34: 20 Hour Exposure
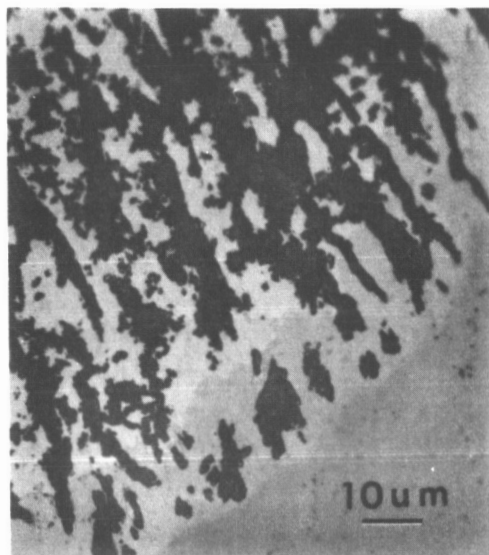Dark Field Optical Micrograph of (g)

(i) Sample 32: 30 Hour Exposure
Opposite Side of Sample

(j) Sample 32: 30 Hour Exposure
Badly Corroded Area

(k) Sample 32: 30 Hour Exposure
Dark Field Optical Micrograph of (j)

(l) Sample 32: 30 Hour Exposure
Corrosion Interface. Note Depleted Zones at Interface.

APPENDIX F

Oxidation of Beta Nickel Aluminides

Concurrent with this study selected samples were oxidized to provide a comparison for the hot corrosion samples.

Two types of oxidation tests were performed. Static oxidation test were done at 900°C in oxygen using the TGA furnace and 1200°C in air using a simple box furnace. In the hopes of getting a better oxide layer by removing surface contamination through spalling, cyclic oxidation tests were performed at 1200°C in air. Each cycle of these tests consisted of 1 hour at temperature followed by cooling to room temperature.

Only limited data was generated by these tests since they were not central to the program and more extensive work has been done by other researchers, notably Smialek (F1) and Doychak (F2). Weight gain curves for the 900°C static tests and 1200°C cyclic tests are presented in Figures F1 and F2. In addition, some SEM micrographs of the oxidized surfaces are shown in Figure F3. A macrophotograph of a Ni - 24 a/o Al - 15 w/o Cr - 0.3 w/o Zr sample is shown in Figure F4. It is typical in appearance for most of the samples. Additional macrophotographs of oxidized samples can be found in Appendix B.

The lacy structure of the oxide on the surface is typical of the beta nickel aluminides. The ridges are formed by the greater diffusivity of aluminum at the materials grain boundaries giving rise to greater transport of aluminum to the oxide layer in these regions. With more aluminum available to be oxidized the oxide layer grows more rapidly in these areas than in surrounding areas. This leads to a locally thicker layer and hence a ridge.

Of particular interest are the SEM micrographs of the Ni - 45

a/o Al - 0.2 w/o Zr P/M sample's edge shown in Figure F3(d). It shows significant spalling on the curved surface. The oxide on the flat surfaces was observed to be quite uniform with no observed spallation. Samples like this tested for hot corrosion resistance were corroded at the edges but showed little or no corrosion on the flat surfaces. This gives further credence to the concept that a complete oxide layer would give these alloys good hot corrosion resistance.

The cyclic oxidation results showed that the samples did not reach a steady state oxide thickness under the test conditions. This is in contrast to the expectations of J. Smialek who suggested the tests. His previous work indicated that a complete oxide layer would form that would stop further rapid weight changes in the samples. No explanation can be offered for this discrepancy from previous work since the phenomena was not studied in depth.

APPENDIX F REFERENCES

(F1) J. Smialek, <u>Proceedings of the 42nd Annual Meeting of the Electron Microscopy Soceity of America</u>, San Francisco Press, San Francisco, p. 594, (1984)
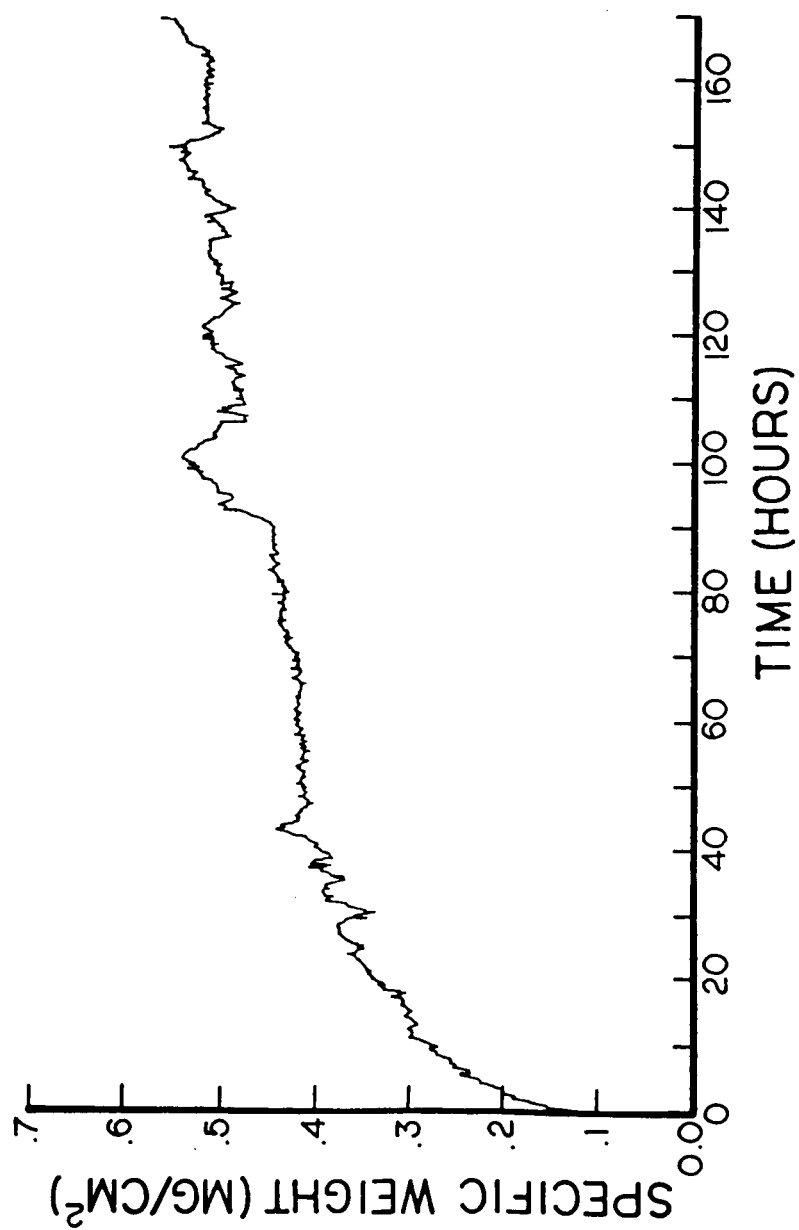
(F2) J.K. Doychak, NASA CR-174756, (Sept. 1984)

Figure F1

Typical Weight Gain Curve for 900°C Static Oxidation
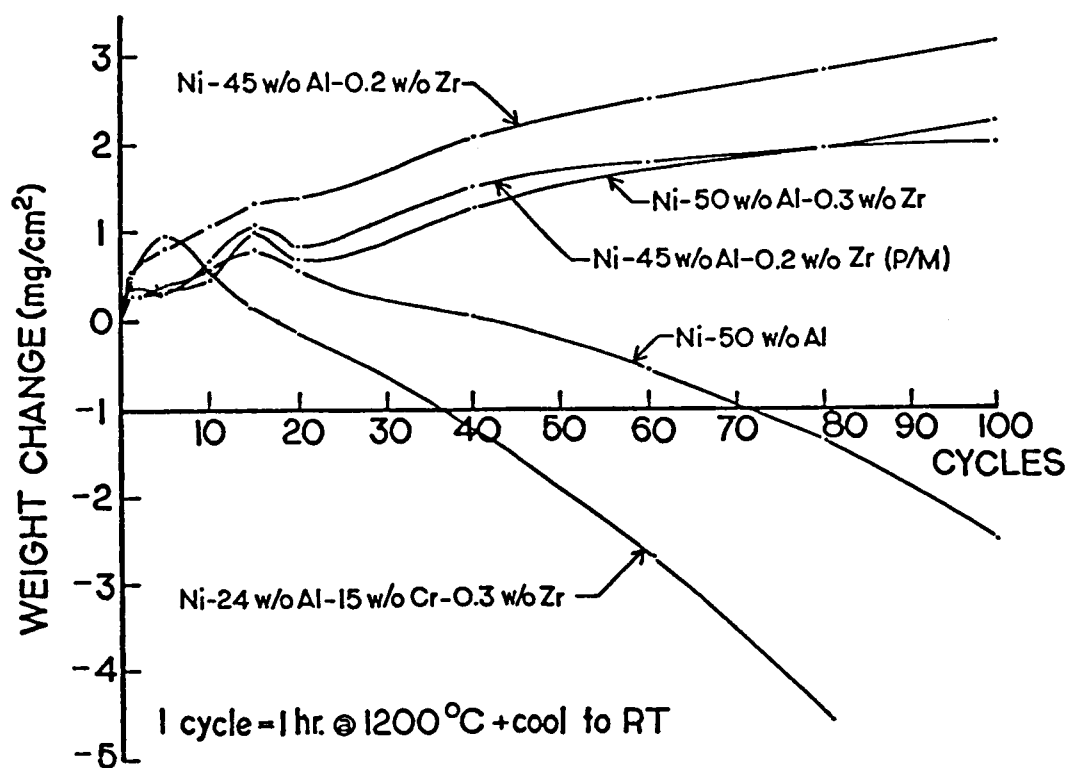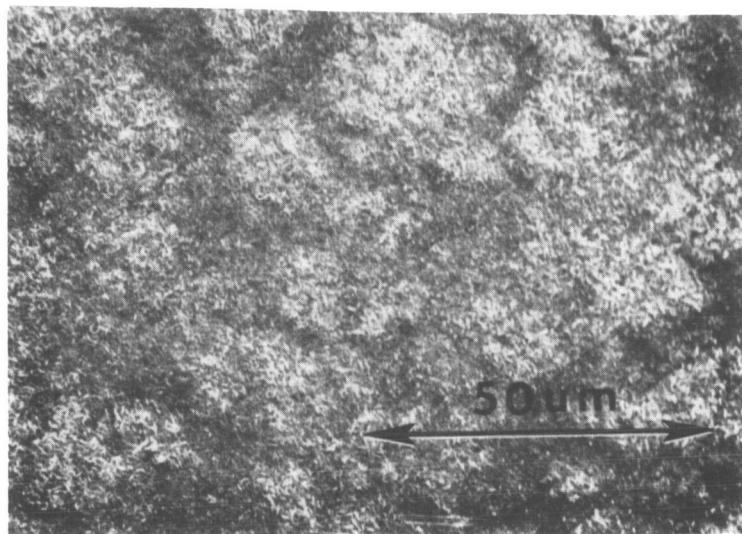
Weight Gain Curves for 900°C Cyclic Oxidation Samples

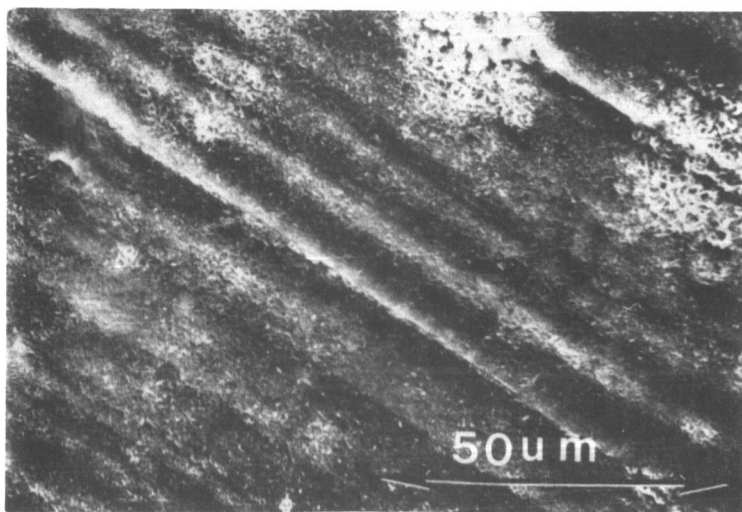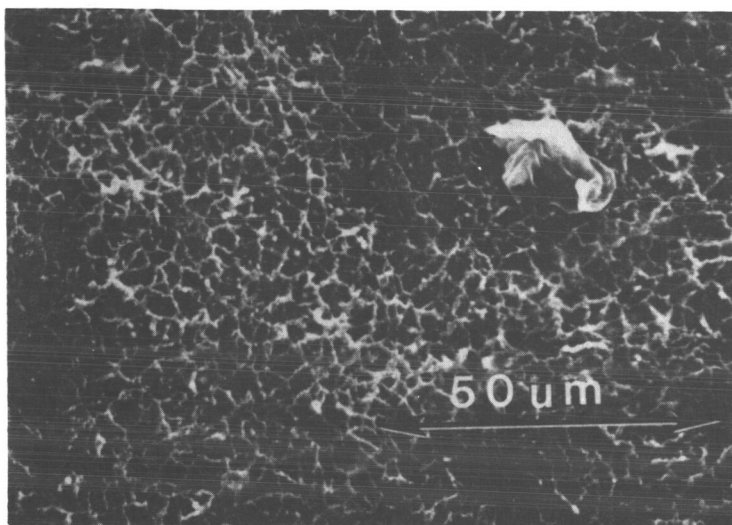Figure F2

Weight Gain Curves for 900°C Cyclic Oxidation Samples

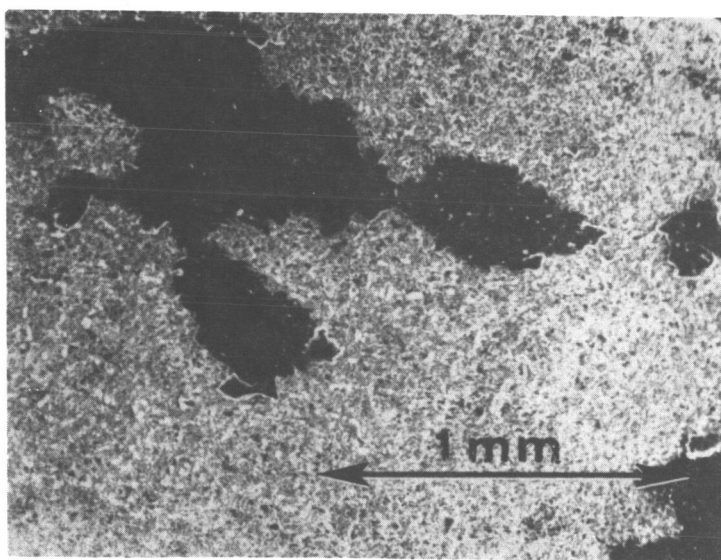Scanning Electron Micrographs of

Oxidized Sample Surfaces

(a) Sample 6: Ni - 45 a/o Al - 0.2 w/o Zr (P/M)
Flat Surface of Sample Oxidized at 900°C in Oxygen

(b) Sample 6: Ni - 45 a/o Al - 0.2 w/o Zr (P/M)
Edge of Sample Oxidized at 900°C in Oxygen

(c) Sample 7: Ni - 45 a/o Al - 0.2 w/o Zr (P/M)
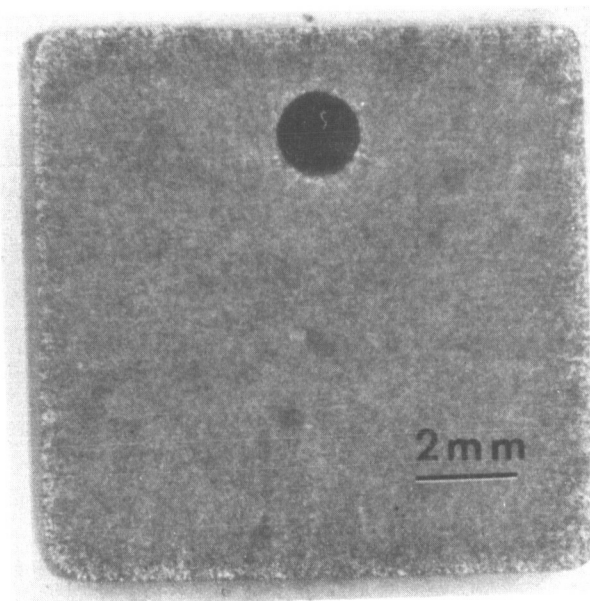Flat Surface of Sample Oxidized at 1200°C in Air

(d) Sample 7: Ni - 45 a/o Al - 0.2 w/o Zr (P/M)
Edge of Sample Oxidized at 1200°C in Air.
Note Large Areas of Spallation

Figure F4

Macrophotograph of Ni - 24 a/o Al - 15 w/o Cr - 0.3 w/o Zr

Sample After Cyclic Oxidation

APPENDIX G

Hot Corrosion of Iron Aluminides

Due to an error on the part of the melter, a sample of iron aluminide was cast by accident. This sample was tested for its hot corrosion resistance in the bare metal condition for a comparison with the nickel aluminide samples.

The composition for the iron aluminide is given in Table F1. Figure G1 shows the weight gain curve for the iron aluminide. In comparison to the nickel aluminide samples which showed a complex five stage hot corrosion process, the iron aluminides showed a parabolic weight gain over the 140 hours of the test. The absolute weight gain per unit area for the samples was also considerably less than for the nickel aluminides but more than would be expected for simple oxidation. Figure G2 shows a macrograph of the exposed sample's surface. Figures G2 to G5 show optical micrographs of the cross sections of the sample. As can be seen, the area seems to be similar to the Late Stage II nickel aluminide sample in morphology and extent except there is considerable intergranular attack along the grain boundaries beneath the corrosion nodule.

While no detailed mechanism was developed to explain these differences, the evidence suggests that the hot corrosion process for the iron aluminides is similar to that for nickel aluminides during Stage II. The primary difference is thought to be that a liquid sulphide phase is not formed for the iron aluminide while it can be formed for the nickel aluminide. The solid sulphide phase means that the oxidation of the sulphide is a solid state reaction that is most likely diffusion controlled. The lack of a liquid phase beneath the oxide layer also means that the oxide can not be fractured by pressure developed by the liquid, one possible method for compromising the protective oxide layer. The diffusion of oxygen

265

and sulphur through the solid phases is slower than through a liquid, so the kinetics are slowed considerably. The faster diffusion along grain boundaries leads to the more rapid attack in these areas, and the corrosion tends to proceed intergranularly into the sample. At the same time slower corrosion of the matrix is also occurring to give the observed surface attack.

Based on this single test, it appears that the iron aluminides are more hot corrosion resistant that the nickel aluminides. Some passing references to this effect have been made in the literature, but no detailed study was available.

Table G1

Composition of Iron Aluminide Sample

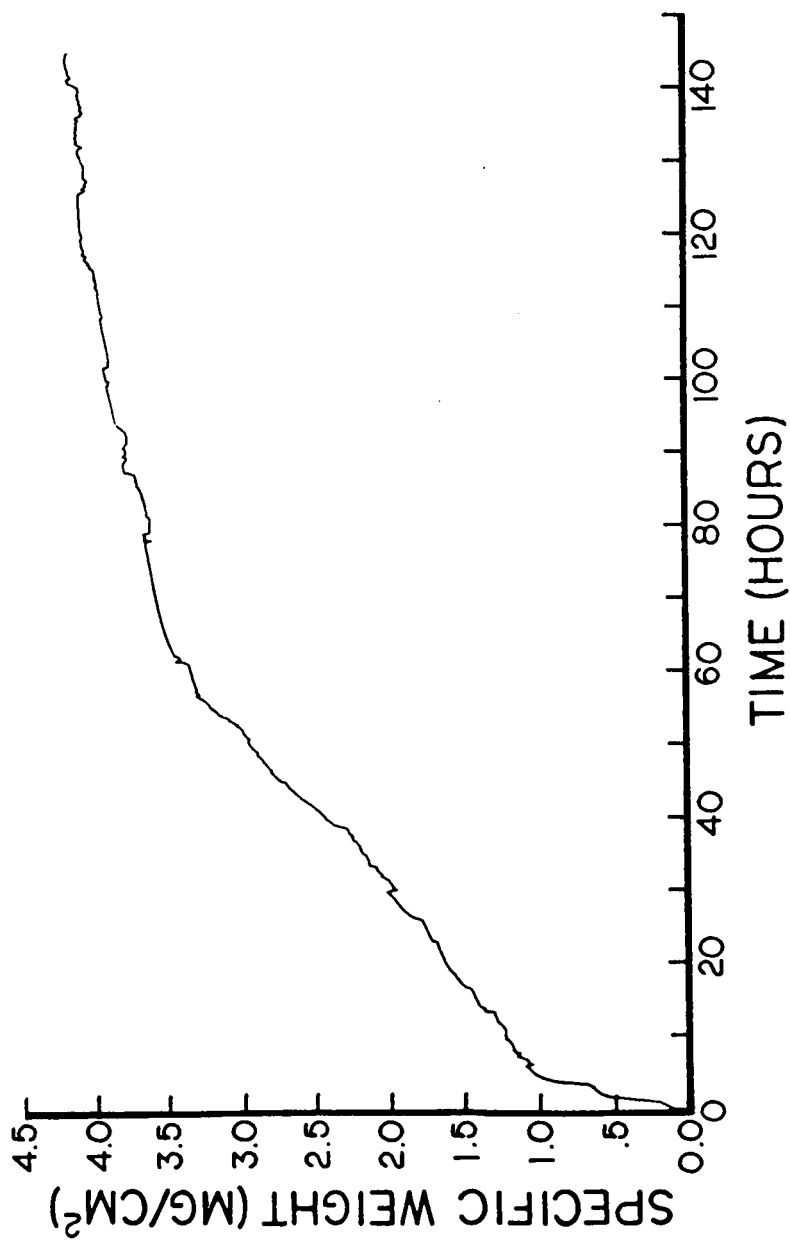|	Fe	Al	Zr
w/o	75.3	24.4	0.3
a/o	59.8	40.1	0.1

Figure G1

Fe – 40 a/o Al – 0.2 w/o Zr Hot Corrosion Weight Gain Curve

Figure G2

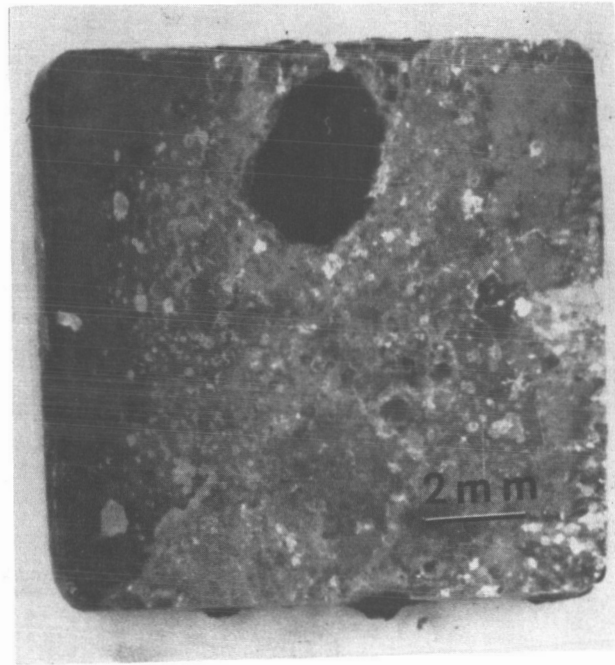## Macrophotograph of Exposed Sample Surface

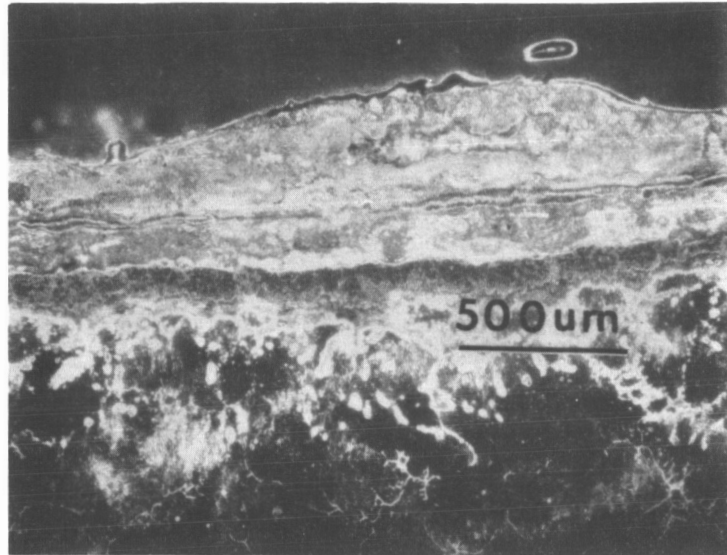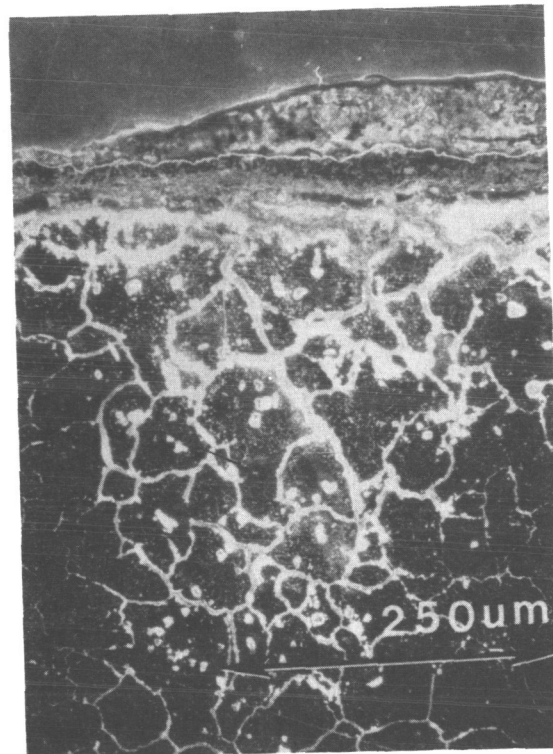Transverse Dark Field Optical Micrograph
of Corrosion Nodule

Figure G4
Transverse Dark Field Optical Micrograph of
Corroded Region Showing Extensive Intergranular Corrosion

REPORT DOCUMENTATION PAGE

Public reporting burden for this collection of information is estimated to average 1 hour per response, including the time for reviewing instructions, searching existing data sources, gathering and maintaining the data needed, and completing and reviewing the collection of information. Send comments regarding this burden estimate or any other aspect of this collection of information, including suggestions for reducing this burden, to Washington Headquarters Services, Directorate for information Operations and Reports, 1215 Jefferson Davis Highway, Suite 1204, Arlington, VA 22202-4302, and to the Office of Management and Budget, Paperwork Reduction Project (0704-0188), Washington, DC 20503.

1. AGENCY USE ONLY (Leave blank)	2. REPORT DATE	3. REPORT TYPE AND DATES COVERED
	March 1993	Final Contractor Report

4. TITLE AND SUBTITLE

Hot Corrosion of the B2 Nickel Aluminides

5. FUNDING NUMBERS

WU–505–63–40
NCC3–94

6. AUTHOR(S)

David L. Ellis

7. PERFORMING ORGANIZATION NAME(S) AND ADDRESS(ES)

Case Western Reserve University
Cleveland, Ohio 44106

8. PERFORMING ORGANIZATION REPORT NUMBER

E–7621

9. SPONSORING/MONITORING AGENCY NAMES(S) AND ADDRESS(ES)

National Aeronautics and Space Administration
Lewis Research Center
Cleveland, Ohio 44135–3191

10. SPONSORING/MONITORING AGENCY REPORT NUMBER

NASA CR–191082

11. SUPPLEMENTARY NOTES

Project Manager, Robert V. Miner, Advanced Metallics Branch, NASA Lewis Research Center, (216) 433–9515. This report was submitted by David L. Ellis as a thesis in partial fulfillment of the requirements for the degree Master of Science in Materials Engineering to Case Western Reserve University, Cleveland, Ohio.

12a. DISTRIBUTION/AVAILABILITY STATEMENT

Unclassified - Unlimited
Subject Category 26

12b. DISTRIBUTION CODE

13. ABSTRACT (Maximum 200 words)

The hot corrosion behavior of the B2 nickel aluminides was studied to determine the inherent hot corrosion resistance of the beta nickel aluminides and to develop a mechanism for the hot corrosion of the beta nickel aluminides. The effects of the prior processing of the material, small additions of zirconium, stoichiometry of the materials, and preoxidation of the samples were also examined. Additions of 2, 5, and 15 w/o chromium were used to determine the effect of chromium on the hot corrosion of the beta nickel aluminides and the minimum amount of chromium necessary for good hot corrosion resistance. The results indicate that the beta nickel aluminides have inferior inherent hot corrosion resistance despite their excellent oxidation resistance. Prior processing and zirconium additions had no discernible effect on the hot corrosion resistance of the alloys. Preoxidation extended the incubation period of the alloys only a few hours and was not considered to be an effective means of stopping hot corrosion. Stoichiometry was a major factor in determining the hot corrosion resistance of the alloys with the higher aluminum alloys having a definitely superior hot corrosion resistance. The addition of chromium to the alloys stopped the hot corrosion attack in the alloys tested. From a variety of experimental results, a complex hot corrosion mechanism was proposed. During the early stages of the hot corrosion of these alloys the corrosion is dominated by a local sulphidation/oxidation form of attack. During the intermediate stages of the hot corrosion, the aluminum depletion at the surface leads to a change in the oxidation mechanism from a protective external alumina layer to a mixed nickel-aluminum spinel and nickel oxide that can occur both externally and internally. The material undergoes extensive cracking during the later portions of the hot corrosion.

14. SUBJECT TERMS	15. NUMBER OF PAGES
Heat resistant alloys; Oxidation; Nickel alloys; Hot corrosion	273
	16. PRICE CODE A12

17. SECURITY CLASSIFICATION OF REPORT	18. SECURITY CLASSIFICATION OF THIS PAGE	19. SECURITY CLASSIFICATION OF ABSTRACT	20. LIMITATION OF ABSTRACT
Unclassified	Unclassified	Unclassified	

National Aeronautics and
Space Administration

Lewis Research Center
Cleveland, Ohio 44135

FOURTH CLASS MAIL

ADDRESS CORRECTION REQUESTED

NASA